PHASE 2 INITIAL BOREHOLE DRILLING AND TESTING, IGNACE AREA

WP04c Data Report – Porewater Extraction and Analysis and Petrographic Analysis for IG_BH02

APM-REP-01332-0245 **January 2022**

Golder Associates Ltd. and Hydroisotop

nwmo
NUCLEAR WASTE MANAGEMENT ORGANIZATION
SOCIÉTÉ DE GESTION DES DÉCHETS NUCLÉAIRES

Nuclear Waste Management Organization
22 St. Clair Avenue East, 4th Floor
Toronto, Ontario
M4T 2S3
Canada

Tel: 416-934-9814
Web: www.nwmo.ca

REPORT

PHASE 2 INITIAL BOREHOLE DRILLING AND TESTING, IGNACE AREA

WP4C Data Report – Porewater Extraction and Analysis and Petrographic Analysis for IG_BH02

Submitted to:

Nuclear Waste Management Organization

4th Floor

22 St. Clair Avenue East

Toronto, Ontario, M4T 2S3

Submitted by:

Golder Associates Ltd

6925 Century Avenue, Suite #100

Mississauga, Ontario

L5N 7K2

NWMO Document: APM-REP-01332-0245 R000



Distribution List

eCopy – Golder

eCopy – NWMO

eCopy – Hydroisotop

WP4C REPORT – POREWATER EXTRACTION AND ANALYSIS AND PETROGRAPHIC ANALYSIS FOR IG_BH02

CLIENT INFORMATION

Project Name:	Phase 2 Initial Borehole Drilling and Testing, Ignace Area
Project Number:	1671632
Client PO Number:	2000141
Document Name:	1671632(3401C) IG_BH02_WP04C_PW_Final_12Jan2022_R3a

Client:	Nuclear Waste Management Organization (NWMO)	
Address:	22 St. Clair Avenue East, 4th Floor	
City:	Toronto	
Province:	Ontario	
Postal Code:	M4T 2S3	
Client Contact:	Laura Kennell-Morrison	Maria Sánchez-Rico Castejón
Telephone:	647-259-3737	647-259-3720
Email:	lkennell@nwmo.ca	msanchez@nwmo.ca

Issue/Revision Index

Issue Code	Revision					Revision Details
	No.	By	Rev'd.	App.	Date	
RR	0	FE/JI	GWS	-	March 22, 2021	Draft released for review and comments
RR	1	FE/JI	GWS	JC	September 30, 2021	Revised draft for review and comments
RI	2	FE/JI	GWS	JC	December 20, 2021	Final report released for information
RI	3	FE/JI	GWS	JC	January 12, 2022	Revised final released for information

Issue Codes: RR = Released for Review and Comments, RI = Released for Information

SIGNATURES

Prepared by: _____

Dr. Florian Eichinger
Hydroisotop GmbH

Reviewed by: _____

George Schneider, M.Sc., P.Geo.
Project Director - Principal

Approved by: _____

Joe Carvalho, Ph.D., P.Eng.
Senior Geological Engineer - Principal

Table of Contents

1.0 INTRODUCTION 1

1.1 Geological Setting 2

1.2 Technical Objectives 4

2.0 SAMPLING AND SAMPLE PREPARATION 6

3.0 EXPERIMENTAL SET-UPS AND ANALYTICAL METHODS 9

3.1 Mineralogy and Petrography 9

3.2 Water content and water-loss porosity 9

3.3 Porewater extraction methods 10

3.3.1 Aqueous extraction experiments 10

3.3.2 Out-diffusion experiments 11

3.3.3 Isotope diffusive exchange technique 12

4.0 PETROGRAPHY AND MINERALOGY 14

5.0 WATER CONTENT AND WATER-LOSS POROSITY 52

5.1 Water contents 52

5.1.1 Gravimetric water contents determined on aqueous extraction core samples 52

5.1.2 Gravimetric water contents determined on porewater cores 54

5.1.3 Gravimetric water contents determined on out-diffusion cores 55

5.1.4 Water contents determined by isotope diffusive exchange 57

5.1.5 Summary and depth profiles of water content results 59

5.2 Bulk dry/wet density and water-loss porosity 60

6.0 CHEMICAL COMPOSITION OF EXPERIMENT SOLUTIONS OF AQUEOUS EXTRACTION AND OUT-DIFFUSION EXPERIMENTS 62

6.1 Chemical composition of aqueous extraction solutions 62

6.2 Chemical composition of out-diffusion experiment solutions 64

7.0 ELEMENTAL TIME SERIES AND PORE DIFFUSION COEFFICIENT OF CHLORIDE 68

7.1 Elemental elution curves 68

7.2 Modelling of pore diffusion coefficients 83

8.0 CHLORIDE, BROMIDE AND CHLORIDE ISOTOPES IN POREWATER OF BOREHOLE IG_BH02.....90

8.1 Porewater chloride concentrations estimated by aqueous extraction experiments.....90

8.2 Porewater chloride and bromide concentrations and $\delta^{37}Cl$ isotope ratios determined by out-diffusion experiments.....90

9.0 $\delta^{18}O$ AND $\delta^{2}H$ OF POREWATER OF CORE SAMPLES FROM BOREHOLE IG_BH02.....95

10.0 SUMMARY.....98

11.0 REFERENCES.....99

TABLES

Table 1: Overview of the core samples taken from IG_BH02 for porewater investigations (mbgs = mbgs down hole).....7

Table 2: Overview of the analytical porewater program conducted on core samples from borehole IG_BH02 (mbgs = mbgs down hole).....8

Table 3: Abbreviations of mineral names recommended by IUGS (Siivola & Schmid 2007).....14

Table 4: Definition of grain sizes recommended by IUGS (Schmid et al. 2007).....15

Table 5: Definition of alteration grades of rock forming minerals.....15

Table 6: Modal composition (Vol.%) of the occurring minerals obtained using point counting; Modal compositions of accessories were not determined (the modal percentage of accessories is <1 Vol.%).....17

Table 7: Normalized modal composition (Vol.%) of quartz, plagioclase and alkali feldspar obtained using point counting and classification of rock types.....17

Table 8: Gravimetric water contents of aliquots of AQ core samples from borehole IG_BH02 used for aqueous extraction experiments using wet (WC_{wet}) and dry masses (WC_{dry}) of the individual core pieces. The weighted values are calculated using the individual masses.....53

Table 9: Gravimetric water contents of head pieces of PW core samples from borehole IG_BH02 using wet (WC_{wet}) and dry masses (WC_{dry}) of the individual core pieces. The weighted values are calculated using the individual masses.....54

Table 10: Gravimetric water contents of out-diffusion core samples from borehole IG_BH02 calculated by the mass of cores determined before (b.e.) and after (a.e.) experiments using wet (WC_{wet}) and dry masses (WC_{dry}) of the individual core pieces; the error of the water content is determined by Gaussian error propagation (Appendix III).....55

Table 11: Gravimetric water contents determined on core samples from borehole IG_BH02 used for isotope diffusive exchange experiments ($WC_{IsoEx,grav}$); water contents are corrected for weight changes during the experiments (b.e.=before experiment, a.e. = after experiment); the gravimetric water contents determined on the rock pieces used in the experiments with LAB- and SSI-water are weighted; the error is determined by Gaussian error propagation (Appendix III).....57

Table 12: Water contents of core samples from borehole IG_BH02 calculated by the isotope diffusive exchange method (cf. eq. 7); the error of the water content is determined by Gaussian error propagation (Appendix III).....58

Table 13: Weighted gravimetric water contents of AQ- and PW-core samples in wt.% and Vol.% taken from borehole IG_BH02 and their corresponding total masses; the uncertainties of the water content values are the weighted standard deviations of the individual aliquots – showing the diversity of water contents in one entire core sample; the core volume is calculated using the bulk, wet density determined on the out-diffusion and aqueous extraction cores (Table 14) 59

Table 14: Bulk wet and dry density and water-loss (=WL-) porosity determined by water contents calculated for dry ($\Phi_{WL,dry}$) and wet ($\Phi_{WL,wet}$) core samples from borehole IG_BH02; the errors are calculated by Gaussian error propagation (Appendix III) 60

Table 15: Analytical results of the aqueous extraction solutions of crushed core samples from borehole IG_BH02; test solution types are classified after Jäckli (1970) 63

Table 16: Analytical results of test solutions of out-diffusion experiments using core samples from borehole IG_BH02 66

Table 17: Minimum (min), maximum (max) and average (ave) pore and effective diffusion coefficients determined by 1-dimensional modelling of Cl-elution curves of out-diffusion experiments conducted on core samples from borehole IG_BH02 at 45 °C and calculated by the Stoke-Einstein equation for 10 °C and 25°C 88

Table 18: Porewater Cl and Br concentrations and Br*1000/Cl mass ratios and $\delta^{37}Cl$ isotope signatures. Cl concentrations are determined by out-diffusion (o.d.) and estimated using aqueous extraction experiments (aq.ex.); the errors of porewater (o.d.) Br concentrations and Br*1000/Cl mass ratios are calculated by Gaussian error propagation (Appendix III); the errors of $\delta^{37}Cl$ values are the standard deviation of triplicate analyses 91

Table 19: $\delta^{18}O$ and $\delta^{2}H$ values of porewater of core samples from borehole IG_BH02; the errors are calculated by Gaussian error propagation 97

FIGURES

Figure 1: Location of IG_BH02 in relation to the Wabigoon / Ignace Area 1

Figure 2: Geological setting and location of boreholes IG_BH01, IG_BH02 and IG_BH03 in the northern portion of the Revell batholith 2

Figure 3: Classification/nomenclature according to the modal mineral content (Q + A + P = 100 Vol.%) of the individual core samples plotted in a simplified ternary Streckeisen diagram, after Bas & Streckeisen (1991). 18

Figure 4: Petrography of sample IG_BH02_PW001 (240.0 mbgs down hole) 20

Figure 5: Petrography of sample IG_BH02_PW003 (348.0 mbgs down hole) 23

Figure 6: Petrography of sample IG_BH02_PW005 (345.2 mbgs down hole) 26

Figure 7: Petrography of sample IG_BH02_PW006 (459.2 mbgs down hole) 29

Figure 8: Petrography of sample IG_BH02_PW008 (503.9 mbgs down hole) 32

Figure 9: Petrography of sample IG_BH02_PW012 (554.5 mbgs down hole) 35

Figure 10: Petrography of sample IG_BH02_PW014 (608.8 mbgs down hole) 38

Figure 11: Petrography of sample IG_BH02_PW016 (669.2 mbgs down hole) 41

Figure 12: Petrography of sample IG_BH02_PW018 (771.6 mbgs down hole) 44

Figure 13: Petrography of sample IG_BH02_PW020 (880.4 mbgs down hole).....47

Figure 14: Petrography of sample IG_BH02_PW022 (984.7 mbgs down hole).....50

Figure 15: Mass of core samples from borehole IG_BH02 before and after the out-diffusion experiments; the uncertainty of the core mass is ± 0.05 g 56

Figure 16: Water content calculated from the wet mass before and after the out-diffusion experiments of core sections from borehole IG_BH02; the error of the water content is determined by Gaussian error propagation (Appendix III) 56

Figure 17: Comparison of water contents determined by isotope diffusive exchange (WC_{IsoEx}) and gravimetrically ($WC_{IsoEx,grav}$, by wet weight, corrected for weight change during experiments) on the same core pieces; the error of the water content is determined by Gaussian error propagation.....58

Figure 18: Water content and water-loss porosity of core samples from borehole IG_BH02 (depths are mbgs (down hole).....61

Figure 19: Schoeller diagram of experiment solutions from aqueous extraction experiments conducted with core samples from borehole IG_BH02.....64

Figure 20: Schoeller diagram of experiment solutions from out-diffusion experiments 67

Figure 21: Elution curves of anions and cations set-up by the periodic sampling of test solutions from out-diffusion experiments using core samples from borehole IG_BH02; the errors are the analytical uncertainty of ± 5 %.....70

Figure 22: Maximum (Dp(max)) and minimum (Dp(min)) pore diffusion coefficients (45 °C) determined by a best fit of Cl elution curves in linear and logarithmic time and concentration scale; the solid lines mark the average diffusion coefficients (45 °C, Dp(ave)) 84

Figure 23: Average pore (left) and effective (middle) diffusion coefficients (10 °C) for chloride and the corresponding WL-porosity (right) of core samples from borehole IG_BH02 versus depth; the errors are the difference between the average and maximum/minimum values (depths are in mbgs (down hole)).....89

Figure 24: Porewater chloride and bromide concentrations (out-diffusion only), Br*1000/Cl mass ratios and $\delta^{37}Cl$ porewater signatures extracted from borehole IG_BH02 cores as function of depth (depth in mbgs (down hole)).....93

Figure 25: Chloride versus bromide concentrations of porewater from cores from borehole IG_BH02; the blue line indicates the seawater dilution line.....94

Figure 26: Porewater $\delta^{37}Cl$ isotope signatures versus porewater Cl-concentrations.....94

Figure 27: $\delta^{18}O$ and $\delta^{2}H$ porewater signatures as function of depth along borehole IG_BH02; errors are calculated by Gaussian error propagation (depth in mbgs (down hole)) 96

Figure 28: $\delta^{18}O$ versus $\delta^{2}H$ values of porewater; the blue line marks the global meteoric water line; the errors of the stable isotope ratios are calculated by Gaussian error propagation 97

APPENDICES

APPENDIX I

Photo Documentation

APPENDIX II

Analytical Raw Data

APPENDIX III

Error Calculations

1.0 INTRODUCTION

The Initial Borehole Drilling and Testing project in the Wabigoon and Ignace Area, Ontario is part of Phase 2 Geoscientific Preliminary Field Investigations of the NWMO's Adaptive Phased Management (APM) Site Selection Phase.

This project involves the drilling and testing of three deep boreholes within the northern portion of the Revell batholith. The third drilled borehole, IG_BH02, is located a direct distance of approximately 20 km southeast of the Wabigoon Lake Ojibway Nation and a direct distance of 42 km northwest of the Town of Ignace. Access to the IG_BH02 drill site is via Highway 17 and primary logging roads, as shown on Figure 1.

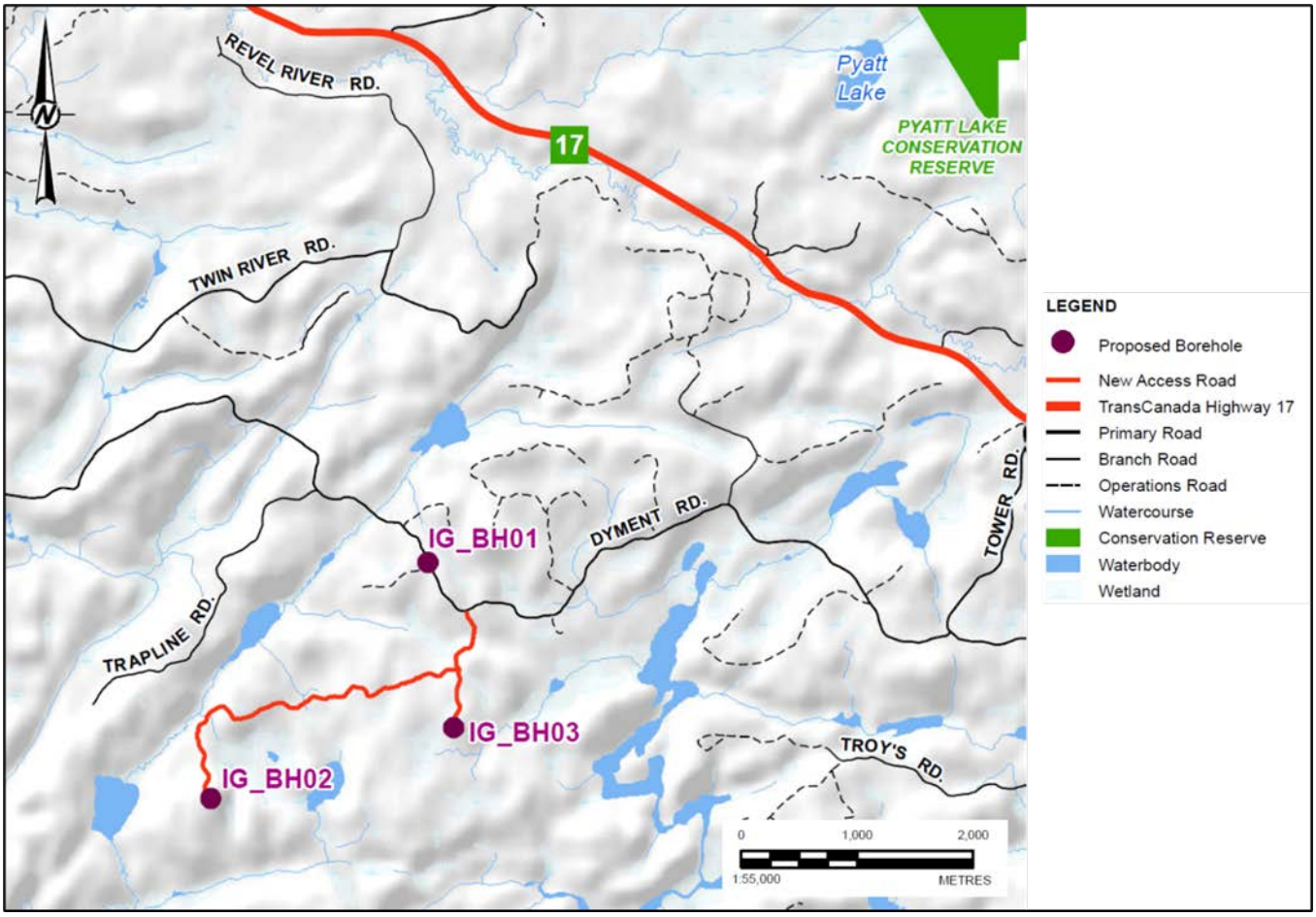


Figure 1: Location of IG_BH02 in relation to the Wabigoon / Ignace Area

The project was carried out by a team at Hydroisotop GmbH, subcontracted by Golder Associates Ltd. (Golder) on behalf of the NWMO. This report describes the testing methodology and results for Work Package 4C (WP4C): Porewater Extraction and Analysis and Petrographic Analysis for IG_BH02. IG_BH02 is an inclined borehole; all depths referred to in the text of this report are in metres below ground surface along the length of the borehole (mbgs (down hole)), or its equivalent metres borehole length (m BHL), rather than true vertical.

1.1 Geological Setting

The approximately 2.7 billion year old Revell batholith is located in the western part of the Wabigoon Subprovince of the Archean Superior Province. The batholith is roughly elliptical in shape trending northwest, is approximately 40 km in length, 15 km in width, and covers an area of approximately 455 km^2. Based on geophysical modelling, the batholith is approximately 2 km to 3 km thick through the center of the northern portion (SGL 2015). The batholith is surrounded by supracrustal rocks of the Raleigh Lake (to the north and east) and Bending Lake (to the southwest) greenstone belts (Figure 2).

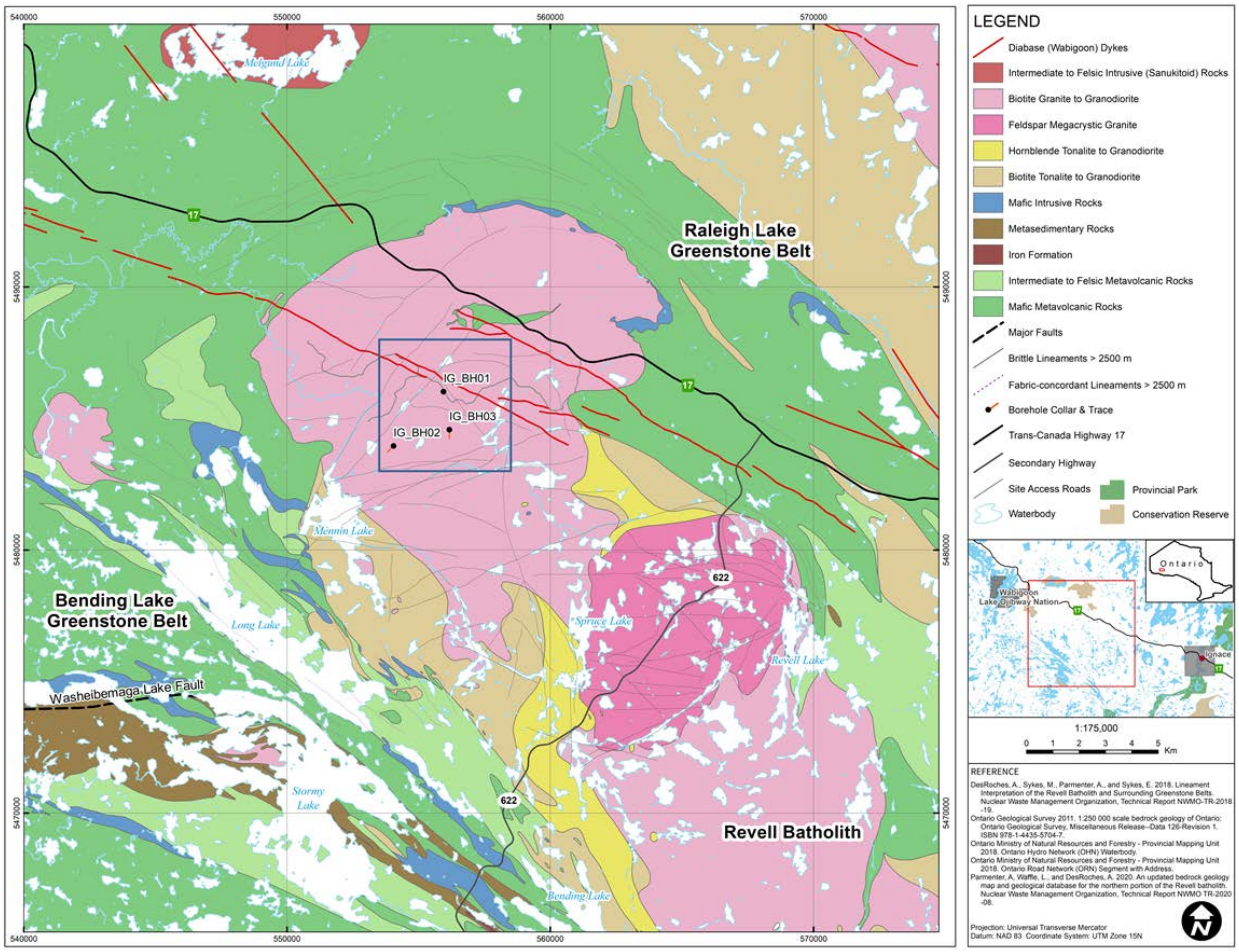


Figure 2: Geological setting and location of boreholes IG_BH01, IG_BH02 and IG_BH03 in the northern portion of the Revell batholith

Borehole IG_BH02 is located within an investigation area of approximately 19 km^2 in size, situated in the northern portion of the Revell batholith. Bedrock exposure in the area is generally very good due to minimal overburden, few water bodies, and relatively recent logging activities. Ground elevations generally range from 400 to 450 m above sea level. The ground surface broadly slopes towards the northwest as indicated by the flow direction of the main rivers in the area. Local water courses tend to flow to the southwest towards Mennin Lake (Figure 1).

Four main rock units are identified in the supracrustal rock group: mafic metavolcanic rocks, intermediate to felsic metavolcanic rocks, metasedimentary rocks, and mafic intrusive rocks (Figure 2). Sedimentation within the supracrustal rock assemblage was largely synvolcanic, although sediment deposition in the Bending Lake area may have continued past the volcanic period (Stone 2009; Stone 2010a; Stone 2010b). All supracrustal rocks are affected, to varying degrees, by penetrative brittle-ductile to ductile deformation under greenschist- to amphibolite-facies metamorphic conditions (Blackburn and Hinz 1996; Stone et al. 1998). In some locations, primary features, such as pillow basalt or bedding in sedimentary rocks are preserved, in other locations, primary relationships are completely masked by penetrative deformation. Uranium-lead (U-Pb) geochronological analysis of the supracrustal rocks produced ages that range between 2734.6 +/-1.1 Ma and 2725 +/-5 Ma (Stone et al. 2010).

Three main suites of plutonic rock are recognized in the Revell batholith, including, from oldest to youngest: a Biotite Tonalite to Granodiorite suite, a Hornblende Tonalite to Granodiorite suite, and a Biotite Granite to Granodiorite suite (Figure 2). Plutonic rocks of the Biotite Tonalite to Granodiorite suite occur along the southwestern and northeastern margins of the Revell batholith. The principal type of rock within this suite is a white to grey, medium-grained, variably massive to foliated or weakly gneissic, biotite tonalite to granodiorite. One sample of foliated and medium-grained biotite tonalite produced a U-Pb age of 2734.2+/-0.8 Ma (Stone et al. 2010). The Hornblende Tonalite to Granodiorite suite occurs in two irregularly-shaped zones surrounding the central core of the Revell batholith. Rocks of the Hornblende Tonalite to Granodiorite suite range compositionally from tonalite through granodiorite to granite and also include significant proportions of quartz diorite and quartz monzodiorite. One sample of coarse-grained grey mesocratic hornblende tonalite produced a U-Pb age of 2732.3+/-0.8 Ma (Stone et al. 2010). Rocks of the Biotite Granite to Granodiorite suite underlie most of the northern, central and southern portions of the Revell batholith. Rocks of this suite are typically coarse-grained, massive to weakly foliated, and white to pink in colour. The Biotite Granite to Granodiorite suite ranges compositionally from granite through granodiorite to tonalite. A distinct potassium (K)-Feldspar Megacrystic Granite phase of the Biotite Granite to Granodiorite suite occurs as an oval-shaped body in the central portion of the Revell batholith (Figure 2). One sample of coarse-grained, pink, massive K-feldspar megacrystic biotite granite produced a U-Pb age of 2694.0+/-0.9 Ma (Stone et al. 2010).

The bedrock surrounding IG_BH02 is composed mainly of massive to weakly foliated felsic intrusive rocks that vary in composition between granodiorite and tonalite, and together form a relatively homogeneous intrusive complex. Bedrock identified as tonalite transitions gradationally into granodiorite and no distinct contact relationships between these two rock types are typically observed (SRK and Golder 2015; Golder and PGW 2017). Massive to weakly foliated granite is identified at the ground surface to the northwest of the feldspar-megacrystic granite. The granite is observed to intrude into the granodiorite-tonalite bedrock, indicating it is distinct from, and younger than, the intrusive complex (Golder and PGW 2017).

West-northwest trending mafic dykes interpreted from aeromagnetic data extend across the northern portion of the Revell batholith and into the surrounding greenstone belts. One mafic dyke occurrence, located to the northwest of IG_BH01, is approximately 15-20 m wide (Figure 2). All of these mafic dykes have a similar character and are interpreted to be part of the Wabigoon dyke swarm. One sample from the same Wabigoon swarm produced a U-Pb age of 1887+/-13 Ma (Stone et al. 2010), indicating that these mafic dykes are Proterozoic in age. It is assumed based on surface measurements that these mafic dykes are sub-vertical (Golder and PGW 2017).

Long, narrow valleys are located along the western and southern limits of the investigation area (Figure 2). These local valleys host creeks and small lakes that drain to the southwest and may represent the surface expression of structural features that extend into the bedrock. A broad valley is located along the eastern limits of the investigation area and hosts a more continuous, un-named water body that flows to the south. The linear and segmented nature of this waterbody's shorelines may also represent the surface expression of structural features that extend into the bedrock.

Regional observations from mapping have indicated that structural features are widely spaced (typical 30 to 500 cm spacing range) and dominantly comprised of sub-vertical joints with two dominant orientations, northeast and northwest trending (Golder and PGW 2017). Interpreted bedrock lineaments generally follow these same dominant orientations in the northern portion of the Revell batholith (Figure 2; DesRoches et al. 2018). Minor sub-horizontal joints have been observed with minimal alteration, suggesting they are younger and perhaps related to glacial unloading. One mapped regional-scale fault, the Washeibemaga Lake fault, trends east and is located to the west of the Revell batholith (Figure 2). Ductile lineaments, also shown on Figure 2, follow the trend of foliation mapped in the surrounding greenstone belts. Additional details of the lithological units and structures found at surface within the investigation area are reported in Golder and PGW (2017).

1.2 Technical Objectives

The technical objectives of the porewater testing program are to assess the key chemical and transport properties of the crystalline host rock with depth and within the repository horizon (presently assumed to be between depths of approximately 400 and 600 m). The geochemical results will provide information about the palaeohydrogeological evolution of the bedrock system. Thin section petrographic analyses will be carried out at all sampling depths in order to characterize mineralogy and support the evaluation of the porewater chemistry (obtained by indirect extraction methods, which requires the determination of the in-situ water content and connected porosity). The evaluation of petrophysical parameters requires correlation with the petrographic and mineralogical characteristics of the rock samples.

The associated work tasks include:

- Aqueous extraction experiments to determine initial estimates of pore fluid composition and Total Dissolved Solids (TDS);
- Isotope diffusive exchange experiments, for the determination of stable water isotopes ($\delta^{18}O$ and $\delta^{2}H$);
- Out-diffusion experiments, for determination of porewater stable ion concentrations (Cl and Br), as well as the determination of pore and effective diffusion coefficients, D_p, D_e, for Cl;
- Compilation of elemental elution curves during out-diffusion experiments;
- $\delta^{37}Cl$ analyses;
- Bulk petrography; and
- Determination of density, water content and porosity for the various subsamples used in the above-listed analytical suites.

The characterization of the porewater composition and the solute transport processes in the rock matrix contribute important information for the long-term safety assessment of deep geological repositories for radioactive waste. Thus, knowledge of the porewater composition will allow better constraints on the processes affecting the near-

field of a repository. In designs where repository construction is restricted to bedrock of low permeability, the first water to interact with the repository barrier materials (e.g., bentonite, Cu-canister) will be the porewater. This interaction could result in changes of the physical and chemical properties of the various barrier materials. Knowledge of the porewater composition and its evolution over recent geological time – particularly during the last thousand to hundreds of thousands of years, in accordance with the expected lifespan of a geologic repository – is considered to be of high importance.

In combination with the knowledge gained about solute transport in the rock matrix, the characterization of porewater also contributes to a better understanding of processes related to the far-field environment around the repository. Thus, it provides valuable information about matrix diffusion as a potential retardation factor for radionuclides, and allows better constraints to be placed on the palaeohydrogeological history of a repository site. Due to the exchange by diffusion between fracture groundwater and matrix porewater, released radionuclides may be temporally immobilized by matrix diffusion, and possible subsequent sorption on mineral surfaces. For radionuclides susceptible to sorption, the accessible surface areas are greatly enhanced by matrix diffusion when compared to the accessible surface area on fracture surfaces alone. Matrix diffusion has the potential to increase solute transport times to the biosphere from the repository.

In contrast to fracture groundwater, porewater cannot be sampled by conventional groundwater sampling techniques. The chemical and isotopic composition of porewater has, therefore, to be derived by indirect extraction techniques based on rock material. In most of these indirect extraction techniques – especially in case of rocks of a porosity below about 2 vol.% – the original porewater concentrations are diluted and need to be back-calculated to in-situ concentrations. This requires a well-defined value for the connected porosity – accessible to different solutes under in-situ conditions. The derivation of such porosity values, as well as solute concentrations, is prone to various perturbations during drilling, core sampling, storage and experiments in the laboratory. The obtained data have to be carefully evaluated for potential perturbations induced by drilling activities, rock stress release and sample treatment in the laboratory in order to derive values that are representative of in-situ conditions. This requires detailed knowledge about the rock composition, the rock texture, and the local stress field, because porewater composition is dependent on these factors as well.

Matrix porewater of thirteen core samples taken from 240 m to 985 m below ground surface down hole (mbgs (down hole)) in the borehole IG_BH02, drilled as part of the Phase 2 Initial Borehole Drilling and Testing programme in the Ignace Area for the Nuclear Waste Management Organization (NWMO), was investigated for its chemical and isotopic composition using different methods. Additionally, the crystalline rock core samples were characterised for their petrophysical and mineralogical properties, including water content, water-loss porosity, bulk density, pore diffusion coefficient and mineralogical composition.

2.0 SAMPLING AND SAMPLE PREPARATION

A total of 35 samples from eleven depth intervals were taken from borehole IG_BH02 between October 16, 2019 and November 25, 2019 for the characterization of porewater (Table 1). Sampling was conducted by Golder Associates Ltd. (Golder) according to the instructions provided by Hydroisotop GmbH (Hydroisotop), which were applied and approved already during the investigations of core samples from borehole IG_BH01 and IG_BH03. After recovery from the borehole, the individual core sections were photographed and immediately packed in a plastic bag, evacuated and sealed airtight. This procedure was repeated for a second plastic bag and a final Al-coated plastic layer. The samples were stored in a refrigerator on site and then sent to Hydroisotop, Germany, in a cooler.

The samples arrived in the lab between October 28 and December 5, 2019. All samples were well packed and arrived in the lab with preserved vacuum in all three layers. At Hydroisotop the samples were stored in the refrigerator at 4°C and prepared between November 07 and December 11, 2019.

The assigned samples were unpacked and immediately wrapped into Parafilm™ and cut by dry-sawing into full-diameter sections. After sawing, the surfaces of the obtained pieces were cleaned with paper towels and again wrapped into Parafilm™. The entire sample preparation was conducted as rapidly as possible (within 10 minutes) after opening the sealed bags, in order to minimize evaporation.

One of the two core sections assigned for porewater investigations (PW0XX) taken from each depth interval was stored and sealed as a retained sample at 4°C in the refrigerator. The analytical program conducted on each sample is summarized in Table 2.

Table 1: Overview of the core samples taken from IG_BH02 for porewater investigations (mbgs = mbgs down hole)

		Depth							
Sample ID	Hydro Lab Nr.	from	to	ave	Length	Date sampled	Time sampled	Date sent	Date arrived
		mbgs	mbgs	mbgs	m		hh:mm		
IG_BH02_PW001	334070	239.79	240.14	240.0	0.35	16.10.19	23:57	22.10.19	28.10.19
IG_BH02_AQ001	334068	240.14	240.25	240.2	0.11	16.10.19	23:58	22.10.19	28.10.19
IG_BH02_PW002	334071	243.09	243.46	243.3	0.37	17.10.19	03:21	22.10.19	28.10.19
IG_BH02_PW003	334072	347.77	348.13	348.0	0.36	21.10.19	17:53	22.10.19	28.10.19
IG_BH02_AQ002	334069	348.44	348.60	348.5	0.16	21.10.19	17:56	22.10.19	28.10.19
IG_BH02_PW004	334073	351.52	351.90	351.7	0.38	22.10.19	02:36	22.10.19	28.10.19
IG_BH02_PW005	334457	377.96	378.31	378.1	0.35	27.10.19	13:28	31.10.19	06.11.19
IG_BH02_AQ003	334459	379.51	379.69	379.6	0.18	27.10.19	17:44	31.10.19	06.11.19
IG_BH02_PW006	334458	381.56	381.93	381.7	0.37	27.10.19	22:58	31.10.19	06.11.19
IG_BH02_AQ004	334460	381.93	382.06	382.0	0.13	27.10.19	22:55	31.10.19	06.11.19
IG_BH02_PW007	334461	382.76	383.16	383.0	0.40	29.10.19	17:57	31.10.19	06.11.19
IG_BH02_PW008	334916	454.98	455.39	455.2	0.41	04.11.19	05:35	06.11.19	12.11.19
IG_BH02_AQ005	334920	455.39	455.54	455.5	0.15	04.11.19	05:37	06.11.19	12.11.19
IG_BH02_PW009	334917	460.56	460.93	460.7	0.37	04.11.19	12:03	06.11.19	12.11.19
IG_BH02_PW010	334918	502.57	502.94	502.8	0.37	05.11.19	14:34	06.11.19	12.11.19
IG_BH02_AQ006	334921	503.76	503.89	503.8	0.13	05.11.19	14:36	06.11.19	12.11.19
IG_BH02_PW011	334919	507.54	507.88	507.7	0.34	05.11.19	16:08	06.11.19	12.11.19
IG_BH02_AQ007	335601	555.04	555.18	555.1	0.14	07.11.19	13:37	12.11.19	18.11.19
IG_BH02_PW012	335604	555.55	555.94	555.7	0.39	07.11.19	13:36	12.11.19	18.11.19
IG_BH02_PW013	335605	558.09	558.44	558.3	0.35	07.11.19	16:29	12.11.19	18.11.19
IG_BH02_PW014	335606	610.98	611.35	611.2	0.37	10.11.19	02:26	12.11.19	18.11.19
IG_BH02_AQ008	335602	611.35	611.48	611.4	0.13	10.11.19	02:28	12.11.19	18.11.19
IG_BH02_PW015	335607	613.66	614.04	613.9	0.38	10.11.19	04:56	12.11.19	18.11.19
IG_BH02_PW016	335608	665.64	666.01	665.8	0.37	12.11.19	04:01	12.11.19	18.11.19
IG_BH02_AQ009	335603	666.01	666.16	666.1	0.15	12.11.19	04:03	12.11.19	18.11.19
IG_BH02_PW017	335609	667.32	667.54	667.4	0.22	12.11.19	06:31	12.11.19	18.11.19
IG_BH02_PW018	336460	770.41	770.78	770.6	0.37	17.11.19	02:52	26.11.19	05.12.19
IG_BH02_AQ010	336457	771.38	771.51	771.4	0.13	17.11.19	02:54	26.11.19	05.12.19
IG_BH02_PW019	336461	772.88	773.29	773.1	0.41	17.11.19	05:13	26.11.19	05.12.19
IG_BH02_PW020	336462	878.60	878.96	878.8	0.36	21.11.19	06:40	26.11.19	05.12.19
IG_BH02_AQ011	336458	878.96	879.11	879.0	0.15	21.11.19	06:42	26.11.19	05.12.19
IG_BH02_PW021	336463	885.41	885.80	885.6	0.39	21.11.19	12:12	26.11.19	05.12.19
IG_BH02_PW022	336464	984.02	984.40	984.2	0.38	25.11.19	16:38	26.11.19	05.12.19
IG_BH02_AQ012	336459	984.40	984.53	984.5	0.13	25.11.19	16:41	26.11.19	05.12.19
IG_BH02_PW023	336465	985.74	986.12	985.9	0.38	25.11.19	20:50	26.11.19	05.12.19

Table 2: Overview of the analytical porewater program conducted on core samples from borehole IG_BH02 (mbgs = mbgs down hole)

				Experimental and analytical programme															
				Aqueous Extraction			Diffusive isotope exchange experiments			Out-diffusion experiments							Grav. WC	Thin section petrography	
Sample ID	Hydro Lab Nr.	Ave. Depth	Date prepared	Exp. Set-Up	Chemical analyses	Grav. WC	Exp. Set-Up	Isotope Analyses	Grav. WC	Exp. Set-Up	Time Series	Analyses ions	Analyses $\delta^{37}Cl$	Grav. WC	Density	Modelling D_p	Extra Pieces	Preparation	Microscopy
		mbgs																	
IG_BH02_PW001	334070	240.0	07.11.19				X	X	X	X	X	X	X	X	X	X	X	X	X
IG_BH02_AQ001	334068	240.2	07.11.19	X	X	X													
IG_BH02_PW002	334071	243.3	spare																
IG_BH02_PW003	334072	348.0	07.11.19				X	X	X	X	X	X	X	X	X	X	X	X	X
IG_BH02_AQ002	334069	348.5	07.11.19	X	X	X													
IG_BH02_PW004	334073	351.7	spare																
IG_BH02_PW005	334457	378.1	07.11.19				X	X	X	X	X	X	X	X	X	X	X	X	X
IG_BH02_AQ003	334459	379.6	07.11.19	X	X	X													
IG_BH02_PW006	334458	381.7	07.11.19				X	X	X	X	X	X	X	X	X	X	X	X	X
IG_BH02_AQ004	334460	382.0	07.11.19	X	X	X													
IG_BH02_PW007	334461	383.0	07.11.19				X	X	X	X	X	X	X	X	X	X	X		
IG_BH02_PW008	334916	455.2	07.11.19				X	X	X	X	X	X	X	X	X	X	X	X	X
IG_BH02_AQ005	334920	455.5	19.11.19	X	X	X													
IG_BH02_PW009	334917	460.7	spare																
IG_BH02_PW010	334918	502.8	19.11.19				X	X	X	X	X	X	X	X	X	X	X		
IG_BH02_AQ006	334921	503.8	19.11.19	X	X	X													
IG_BH02_PW011	334919	507.7	spare																
IG_BH02_AQ007	335601	555.1	19.11.19	X	X	X													
IG_BH02_PW012	335604	555.7	19.11.19				X	X	X	X	X	X	X	X	X	X	X	X	X
IG_BH02_PW013	335605	558.3	spare																
IG_BH02_PW014	335606	611.2	19.11.19				X	X	X	X	X	X	X	X	X	X	X	X	X
IG_BH02_AQ008	335602	611.4	19.11.19	X	X	X													
IG_BH02_PW015	335607	613.9	spare																
IG_BH02_PW016	335608	665.8	19.11.19				X	X	X	X	X	X	X	X	X	X	X	X	X
IG_BH02_AQ009	335603	666.1	19.11.19	X	X	X													
IG_BH02_PW017	335609	667.4	spare																
IG_BH02_PW018	336460	770.6	11.12.19				X	X	X	X	X	X	X	X	X	X	X	X	X
IG_BH02_AQ010	336457	771.4	11.12.19	X	X	X													
IG_BH02_PW019	336461	773.1	spare																
IG_BH02_PW020	336462	878.8	11.12.19				X	X	X	X	X	X	X	X	X	X	X	X	X
IG_BH02_AQ011	336458	879.0	11.12.19	X	X	X													
IG_BH02_PW021	336463	885.6	spare																
IG_BH02_PW022	336464	984.2	11.12.19				X	X	X	X	X	X	X	X	X	X	X	X	X
IG_BH02_AQ012	336459	984.5	11.12.19	X	X	X													
IG_BH02_PW023	336465	985.9	spare																

3.0 EXPERIMENTAL SET-UPS AND ANALYTICAL METHODS

Porewater investigations were performed on different types of samples that were subjected to different types of extraction and exchange experiments. This included aqueous extraction and out-diffusion experiments to characterise porewater using chemical tracers, isotope diffusive exchange experiments for the porewater $\delta^{18}O$ and $\delta^{2}H$ composition, and the determination of the water content and water-loss porosity on the respective samples.

Unless otherwise specified, the analytical work has been conducted at Hydroisotop GmbH, Germany.

3.1 Mineralogy and Petrography

Mineralogical and petrographic investigations were performed on rock material from thirteen PW samples taken along the borehole profile (Table 2). The samples were characterised using thin section microscopy. Modal mineralogy was determined by point counting.

End pieces of the core sections used for out-diffusion experiments (cf. Section 3.3.2) were first weighed and dried to determine the water content of the individual sections. After stable weight was reached (= ± 0.002 g for 14 days), thin sections (with a size of 32 x 20 mm) were produced by standard methods at Geotec Consult, Germany. Petrographic and mineralogical evaluation, description and documentation was performed using transmitted light microscopy.

3.2 Water content and water-loss porosity

The water content was determined on core material used for aqueous extraction experiments and out-diffusion experiments, as well as on the core pieces used for the isotope diffusive exchange technique. Water contents were also determined on extra pieces of core available from those used for the out-diffusion experiments.

The quality of sample preservation upon arrival in the laboratory was assessed by the condition of the sample bags and of the core surface (wet vs. dry).

For water content measurements, drill-core pieces were placed in a crystallization dish, weighed and subsequently dried at 105 °C until stable weight conditions were obtained. Before taking the initial wet weight of the full diameter core sections, the surface was allowed to dry on the balance until stable weight was achieved for ≈10 sec. During the following drying process, weighing was carried out weekly until the sample weight remained constant (± 0.002 g) for at least 14 days.

Water contents were determined on core samples used for aqueous extraction experiments (Table 2). Therefore, one half of the full core disc (234 – 419 g) was broken by a mortar to an edge length of approximately 1 cm, placed in a crystallization dish, weighed and put in the oven at 105 °C for drying. Additionally, the two cut uneven head pieces with weights between 84 and 209 g were also weighed and put in the oven to determine the water content. Drying times varied between 27 and 61 days for crushed pieces, and 21 to 49 days for full core discs.

Water contents also were determined on core pieces used for out-diffusion experiments, with weights between 1411 – 1477 g and on the two cut uneven head pieces with weights between 143 and 306 g. Drying times varied between 55 and 98 days for large sized out-diffusion cores and between 21 and 75 days for the head pieces.

Gravimetric water contents were further determined on crushed core sections used for the single isotope diffusive exchange experiments, after equilibration. Their masses varied between 275 and 410 g and drying times ranged between 26 and 67 days.

Finally, the gravimetric water content of the entire core sample (PW and AQ) was determined by using the values and weights of the individual pieces. The weighted water content values are scaled based on the masses of the sub-samples relative to the total sample weight. Additionally, the weighted water contents are calculated in Vol.% applying the bulk, wet density determined on out-diffusion cores and aliquots of aqueous extraction cores, assuming a water density of 1.0 g/cm^3.

The calculation of the water-loss porosity (i.e., the connected porosity) from the gravimetric water content requires a measure of the grain density. In rocks of low porosity, the bulk wet density can be used as a proxy for the grain density. A measure for the bulk wet density of the rocks used for out-diffusion and aqueous extraction experiments was obtained from volume and saturated mass of the core samples. The volume was calculated from measurements of height and diameter of the core samples using a Vernier Calliper, with an error of ± 0.01 mm.

Core lengths varied between 4.2 and 5.8 cm for aqueous extraction cores and between 18.4 and 19.4 cm for out-diffusion cores.

From known sample volume and wet mass, the bulk, wet and dry density is obtained by

$$\rho_{bulk,wet} = \frac{m_{rock,wet}}{V_{rock}}, \qquad \rho_{bulk,dry} = \frac{m_{rock,dry}}{V_{rock}} \qquad \text{eq. 1}$$

and the water-loss (connected) porosity, ϕ_{WL}, can be calculated according to

$$\phi_{WL} = WC_{wet} * \frac{\rho_{bulk,wet}}{\rho_{water}} \quad = \quad \phi_{WL} = \frac{m_{pw} \times 100}{r^2 \times h \times \pi \times \rho_{water}}, \qquad \text{eq. 2}$$

where WC_{wet} is the water content based on the wet weight of the rock sample and $\rho_{bulk,wet}$ the bulk wet density of the rock. In a first approximation, the density of water, ρ_{water}, is assumed to be 1 g/cm^3. Due to the low water content of the investigated crystalline rocks, the water content and water-loss porosity determined by the wet weight and bulk, wet density of the sample is essentially equal to those values calculated using the dry weight and bulk, dry density.

As shown by Gaussian error propagation, the error of the water content and the water-loss porosity depends predominately on the accuracy of the determination of the mass of porewater measured after unpacking (i.e., on the measured initial wet weight) and the final dry weight of the cores.

3.3 Porewater extraction methods

3.3.1 Aqueous extraction experiments

Aqueous extraction experiments were conducted prior to out-diffusion and isotope exchange experiments to estimate the salinity of the investigated porewaters.

Saturated full disc core sections were crushed by a mortar and sieved by an analytical sieve to a grain size of < 2 mm, and 78 to 103 g of rock material were put in a PE bottle, where 61 to 85 ml of deionized water were added. Subsequently, the bottle was gently shaken for 24 h. Afterward, the elution was decanted, filtered (0.45 µm) and immediately analysed for alkalinity, pH and sp. electrical conductivity (using a Metrohm Titrino 785 and WTW LF 325 system). Subsequently, the main anion and cation concentrations were analysed by IC using a Dionex ICS 1500 system. The analytical error of the ion concentration analyses is ± 5 %.

The porewater Cl-concentration was further calculated according to:

$$C_{i,pw} = \frac{C_{i,sol} \times V_{sol} \times 0.001}{m_{pw}}$$ eq. 3

where $C_{i,pw}$ = porewater elemental concentration, $C_{i,sol}$ = analyzed elemental concentration in the aqueous extraction solution, V_{sol} = Volume of aqueous extraction solution and m_{pw} = mass of porewater.

3.3.2 Out-diffusion experiments

Out-diffusion experiments were performed on intact full cores by immersion into ultrapure water. The volume of test water varied between 123 and 141 ml. During the experiments the two water reservoirs, i.e., porewater and test water, were allowed to exchange until equilibrium. Equilibrium with respect to chloride is considered achieved when the Cl concentration has been constant within the analytical error range (= ±5 %) over a minimum of 14 days.

After placing the core sample in the PE-vessel, the vessel was sealed and put in a vibrating water bath (40 rpm) at a constant temperature of 45 °C to accelerate diffusion. The PE-vessels were covered by a vapour-tight lid, which is equipped with two swagelock™ valves and PEEK™ sampling lines. The core, the experiment container and the test water were weighed before and after the experiment to ensure that no loss of test water occurred during the entire experiment. At specific time intervals of initially a few days, and later a few weeks, 0.5 ml of solution were sampled using a PVC-syringe to determine the chloride concentration as a function of time. The experimental time depended on the equilibration rate in the individual experiments. All out-diffusion experiments were ended between 127 and 152 days.

After equilibrium with respect to chloride was achieved, the vessels were removed from the water bath and cooled to room temperature. Subsequently, the cylinder, the core and the remaining test water was weighed and the supernatant solution was filtered (0.45 µm) and analysed immediately for pH, sp. el. conductivity (EC) and alkalinity (acid capacity 4.3 and base capacity 8.2), and later for major cations and anions and certain trace elements and isotopes.

The major cations (Na, K, Ca, Mg, Sr) and anions (F, Cl, NO_3, Br, SO_4) of the 0.5 ml time series and final test solutions of the out-diffusion experiments were analysed by ion chromatography using a Thermo Scientific Dionex Integrion HPIC. The relative analytical error of these analyses is ± 5 % based on multiple measurements of external check standard solutions (1σ). The final test solutions with a volume of approximately 100 ml were analysed undiluted and in different dilutions (1:10 and if necessary 1:20). The time series samples were analysed within days after sampling. Due to the low volume, the samples could only be measured once in a 1:10 dilution. Consequently, the detection limit is different for each element in the two different solutions.

The alkalinity titration, pH and EC measurements were performed using Metrohm titration systems and a WTW LF325 probe.

TOC and TIC concentrations were analysed on the final solutions using a Shimadzu VCSH analyser with a relative analytical error of ± 5 % based on multiple measurements of external check standard solutions (1σ).

Boron, aluminium, lithium and silica concentrations of out-diffusion test solutions were analysed at Görtler analytical services GmbH, Germany, using a Thermo Fischer ICP-MS system with a detection limit of 0.0001 mg/l and an analytical uncertainty of 5 %.

The $^{37}Cl/^{35}Cl$ isotope ratio, expressed as $\delta^{37}Cl$ relative to SMOC, was measured by a GC-MS-IRMS system (Thermo Fischer Delta S). Analytical errors were determined by the standard deviation of triplicate analyses of every sample.

Strontium isotope signatures were analysed at Iso Analysis UG, Germany, by a Thermo Fischer MC-ICP-MS system with an analytical uncertainty of 0.0005.

Chloride and bromide concentrations of the experiment solution can be converted to porewater concentrations by applying mass balance calculations if equilibrium between test water and porewater is achieved. With knowledge of the mass of porewater in the rock sample, the chloride and bromide concentration of the porewater can be calculated according to:

$$C_{pw} = \frac{(m_{pw} + m_{TWi} - \sum^{n} m_s) * C_{TW\infty} - (m_{TWi} * C_{TWi}) + \sum^{n} m_s * C_s}{m_{pw}} \qquad \text{eq. 4}$$

where C_{pw} = porewater concentration; m_{pw} = mass of porewater; m_{TWi} = initial mass of test water; C_{TWi} = initial Cl-concentration of test water; m_s = mass of sub sample used for time series; C_s = Cl concentration of sub sample used for time series.

The term $\sum m_s * C_s$ (Equation 4) describes the amount of Cl removed from the initial experiment solution for Cl time-series samples. A correction for chloride and bromide in the initial experiment solution ($m_{TWi} * C_{TWi}$) is necessary if this solution is not entirely free of chloride and bromide.

The unit for the porewater concentration is given in mg/kg_{H2O} (and not mg/l) because it is derived on a mass basis rather than a volumetric basis. This is due to the fact that the density of the porewater is not known beforehand, because it depends, in part, on the in-situ salinity of the water, which is unknown.

3.3.3 Isotope diffusive exchange technique

The isotope diffusive exchange technique to determine the water isotope composition, $\delta^{18}O$ and $\delta^{2}H$, of the porewater and the mass of porewater was originally developed by Rogge (1997) and Rübel et al. (2002) for sedimentary rocks and later adapted for crystalline rocks by Waber and Smellie (2005, 2006) and Eichinger et al. (2006). In this method, initially saturated rock material is placed into two vapour-tight containers together with different test waters of known isotope composition. The porewater and test water is then allowed to isotopically equilibrate via the vapour phase without any direct contact between the core material and the test water. The porewater isotope composition and the water content of the rock sample can then be derived by isotope mass balance relationships. It has been shown that the uncertainty of the derived isotope composition largely depends on the ratio of porewater to test water used in the experiments (e.g., Rübel et al. 2002). For crystalline rocks, this ratio was optimised by using larger volumes of rock and smaller volumes of test water in the experiments (e.g., Waber and Smellie 2005, 2006; Eichinger et al. 2006).

For the present samples, 1.8 ml of test water were placed in a Petri dish in the centre of a glass vessel and surrounded by hand crushed core pieces of 4 - 6 cm^3 in size and with a total mass of 275 to 431 g. After an equilibration time of 60 days, the two test waters were removed and analysed by Cavity Ring Down Spectroscopy using a Picarro L 2130-I Analyser. The results for the test waters are reported relative to the VSMOW standard with a precision of ± 0.15 ‰ for $\delta^{18}O$ and ± 1.5 ‰ for $\delta^{2}H$.

Test water and core material were weighed before and after the experiment to assess if test water was lost on the container walls and/or rock material due to evaporation and/or condensation. To minimise condensation, 0.3 mol of NaCl were dissolved in the test water to lower its water vapour pressure. For every sample, two experiments were performed: one using test water with an isotope composition close to that expected in the porewater ("LAB-

sample") and one using test water with an isotope composition far from that expected for the porewater ("ICE-sample").

The test water used for the LAB-sample was normal laboratory tap water ($\delta^{18}O$ = -10.15 to -10.30 ‰ V-SMOW; $\delta^{2}H$ = -73.3 to -72.6 ‰ V-SMOW), while that for the SSI-sample was water from an ice core drilled in Greenland ($\delta^{18}O$ = -31.77 to -31.62 ‰ V-SMOW; $\delta^{2}H$ = -246.1 to -245.1 ‰ V-SMOW). The equilibration time in the three reservoirs – rock porewater, test water and the air inside the container used as a diaphragm – depends on the volume of the container, the size of the rock pieces and the distance of the rock pieces to the test water (see Rogge 1997). Based on the estimations of the minimum time period required for complete isotopic equilibration (cf. Eichinger et al. 2006), an experimental time of 60 days was chosen.

The isotope diffusive exchange technique delivers the $\delta^{18}O$ and $\delta^{2}H$ values and the mass of the porewater present in the connected pore space of the rock sample. These parameters are calculated from the analytical results obtained for the two test water solutions using mass balance relationships according to:

$$m_{pw} * c_{pw}\Big|_{t=0} + m_{tw} * c_{tw}\Big|_{t=0} = (m_{pw} + m_{tw}) * c_{tw}\Big|_{t=\infty} \qquad \text{eq. 5}$$

where *m* = mass, *c* = isotope ratios expressed in the δ notation, *pw* = porewater, *tw* = test water; *t = 0* means the isotope concentrations at the beginning, and *t* = ∞ at the end of the experiment.

The water content of the applied samples is calculated by transformation of Equation 5 to

$$WC_{IsoEx} = \left[\frac{m_{TW(Std\,2)} \times m_{Rock(Std1)} \times (C_{TW^0(Std\,2)} - C_{TW\infty(Std\,2)}) + m_{TW(Std1)} \times m_{Rock(Std\,2)} \times (C_{TW\infty(Std1)} - C_{TW^0(Std1)})}{m_{Rock(Std1)} \times m_{Rock(Std\,2)} \times (C_{TW\infty(Std\,2)} - C_{TW\infty(Std1)})} \right] \times 100 \qquad \text{eq. 6}$$

where m_{Rock} = mass of rock, *Std 1* = test solution 1 and *Std 2* = test solution 2.

Equation 6 can be set up for oxygen and hydrogen isotope ratios of the test water, resulting in two independent values for the mass of porewater.

The $\delta^{18}O$- and $\delta^{2}H$- values of the porewater are calculated by transformation of Equation 5 to

$$C_{PW} = \frac{C_{TW\infty(Std1)} \times m_{TW(Std\,2)} \times m_{Rock(Std1)} \times (C_{TW\infty(Std\,2)} - C_{TW^0(Std\,2)}) - C_{TW\infty(Std\,2)} \times m_{TW(Std1)} \times m_{Rock(Std\,2)} \times (C_{TW\infty(Std1)} - C_{TW^0(Std1)})}{m_{TW(Std\,2)} \times m_{Rock(Std1)} \times (C_{TW\infty(Std\,2)} - C_{TW^0(Std\,2)}) - m_{TW(Std1)} \times m_{Rock(Std\,2)} \times (C_{TW\infty(Std1)} - C_{TW^0(Std1)})} \qquad \text{eq. 7.}$$

The errors of the calculated $\delta^{18}O$, $\delta^{2}H$ and the mass of porewater are computed for each sample using Gauss' law of error propagation.

4.0 PETROGRAPHY AND MINERALOGY

The interpretation of porewater derived by indirect methods using rock material requires knowledge about the rock composition and the physical properties of the rock. The petrographic and mineralogical investigations provide information about:

- The structure and texture of the rocks, which place constraints on pathways for solute migration.
- The type of pore space where porewater resides (intergranular versus intragranular), and a correlation of the experimentally determined petrophysical properties (porosity, density) with the petrography of the rocks.

Petrographic and mineralogical investigations were conducted on ten core samples taken from borehole IG_BH02 at depths between 240 and 984 mbgs (down hole). Additionally, thin section images of core sample IG_BH02_PW005 also were produced but the mineralogical composition by point counting was not determined on this sample due to a very fine to fine grained rock matrix. Thin sections were produced from the cut-off end pieces of core sections used for porewater out-diffusion experiments. The macroscopic and microscopic petrographic descriptions of the cores, minerals and rock textures were classified according to Bas & Streckeisen (1991) and Le Maitre et al. (2002). The nomenclature and mineral abbreviations, which are compiled in Table 3, were taken from Siivola & Schmid (2007). The mineral sizes are defined according to Schmid et al. (2007). The dimensions of the individual grain sizes are listed in Table 4. Alteration grades of rock forming minerals are defined based on the estimated altered area on individual grains (Table 5).

Table 3: Abbreviations of mineral names recommended by IUGS (Siivola & Schmid 2007)

Mineral Name	Abbreviation
Alkali feldspar	Afs
Apatite	Ap
Biotite	Bt
Clinozoisite	Czo
Epidote	Ep
Muscovite	Ms
Sericite	Ser
Opaque mineral	Op
Plagioclase	Pl
Quartz	Qtz
Titanite	Ttn
Zircon	Zrn

Table 4: Definition of grain sizes recommended by IUGS (Schmid et al. 2007)

Size	Description
>16 mm	Very coarse grained
4-16 mm	Coarse grained
1-4 mm	Medium grained
0.1-1 mm	Fine grained
0.01-0.1 mm	Very fine grained
<0.01 mm	Ultra-fine grained

Table 5: Definition of alteration grades of rock forming minerals

Proportion of crystal area	Degree of alteration
0 %	Unaltered
<40 %	Weakly altered
40-70 %	Moderately altered
>70 %	Highly altered

4.1 General macroscopic and microscopic description of core samples from borehole IG_BH02

The crystalline rock samples of borehole IG_BH02, which were sampled between 240 and 984 mbgs (down hole) and examined in this study, consist of macroscopically homogenous, unaltered granodiorite and tonalite. All samples, except core sample IG_BH02_PW005, show an equigranular and phaneritic structure. The core samples are not intersected by open fractures. No foliation is observed in any sample. Quartz, feldspars and biotite are distinguishable macroscopically. The red colour of five core samples (IG_BH02_PW001, IG_BH02_PW003, IG_BH02_PW006, IG_BH02_PW016 and IG_BH02_PW016) is caused by a red-staining of the plagioclase crystals, which is due to iron replacing calcium ions in the plagioclase crystal lattice. Core sample IG_BH02_PW005 is a porphyry consisting of a very fine grained matrix and medium to coarse grained plagioclase phenocrysts. Point counting was not performed on core sample IG_BH02_PW005 but the macroscopic appearance (texture, etc.) is described in Section 4.3.

Microscopically, the individual samples consist predominately of quartz, plagioclase, biotite and minor amounts of alkali feldspar in different modal compositions. Muscovite, sericite and epidote/clinozoisite are present as alteration products.

Alteration of alkali feldspar crystals could not be observed, and muscovite is only present in micro fissures of alkali feldspar in some samples. The individual core samples show variable degrees of alteration, mainly in plagioclase and biotite crystals. Plagioclase crystals are moderately to highly sericitized. Only few crystals are unaltered or weakly altered. Very fine to fine grained muscovite, sericite and epidote/clinozoisite are present as alteration products either in the core of sericitized plagioclase, or as alteration products over the entire plagioclase crystal. Fine grained muscovite and epidote/clinozoisite crystals are also present at the rim of weakly altered biotite crystals. It also seems that in some thin sections, biotite is partially replaced by epidote/clinozoisite. The

colour/pleochroism of biotite varies strongly within each thin section and ranges from dark brown to reddish-brownish and green. The light green(ish) biotite crystals frequently show sutural alteration at the rim, whereas dark brown biotite crystals show less alteration products. In all samples, the intergranular pore space between the individual rock-forming minerals is open and not filled with alteration products. In general, sutural altered biotite grains did not show clear grain boundaries in thin sections.

In samples IG_BH02_PW001, IG_BH02_PW012, IG_BH02_PW016. IG_BH02_PW018 alteration to chlorite could be observed in some biotite crystals whereas in samples IG_BH02_PW003, IG_BH002_PW006, IG_BH02_PW008, IG_BH02_PW014, IG_BH02_PW020, IG_BH02_PW022 biotite crystals were unaltered or weakly altered and showed no chloritization of biotite.

4.2 Modal composition of individual core samples from borehole IG_BH02

The modal composition of the individual samples was determined by point counting, which screened the entire thin section (about 35 x 20 mm).

The core samples consist mainly of quartz, plagioclase, alkali feldspar, biotite and muscovite + epidote/ clinozoisite in different modal compositions (Table 6). Opaque minerals, apatite, zircons and titanite are present as accessories (Table 6). The individual samples have varying proportions of altered plagioclase. The grade of alteration of plagioclase crystals also varies within the individual thin sections (Table 6).

Plagioclase is the most abundant mineral in all investigated rock samples with varying contents between 38 and 53 Vol.% (Table 6). The normalized proportion of altered plagioclase areas varies between 22 and 47 Vol.% of the detected plagioclase grains (Table 7). The proportion of quartz and alkali feldspar varies between 24 and 39 Vol.%, and between 5 and 25 Vol.%, respectively (Table 6). Alteration of alkali feldspar could not be observed in any sample. The proportion of biotite is between 2 and 10 Vol.% in the investigated samples (Table 6). Minerals showing abnormal (“vibrant”) or abnormal blue interference colours are summarized as muscovite and epidote/clinozoisite in Table 6 and are present in the range between 1 and 5 Vol.% in the investigated samples.

According to the modal composition determined by point counting, which is consistent with visual observations of the core in hand specimen, the individual core samples can be classified after Bas & Streckeisen (1991) and Streckeisen (1974) as phaneritic granodiorite to tonalite. The classification/nomenclature is specified by the modal mineral content of quartz (Q), plagioclase (P) and alkali feldspar (A) (Q + A + P = 100 Vol.%). After Streckeisen (1974), core samples containing 20 - 60 Vol.% quartz are defined as granodiorite with a proportion of 65 - 90 Vol% plagioclase of total feldspar (A + P = 100 Vol.%) and tonalite with a proportion of 90 - 100 Vol.% plagioclase of total feldspar (A + P = 100 Vol.%) (Table 7). The more current classification/nomenclature of Bas & Streckeisen (1991) used in this report differs from the classification/nomenclature of Streckeisen (1974). After Bas & Streckeisen (1991) the modal mineral contents of quartz, plagioclase and alkali feldspar of the individual core samples are plotted in a simplified ternary diagram (Figure 3). The percentage of alkali feldspar, determined by point counting is in the range of 8 - 27 Vol.% of the total proportion of quartz, plagioclase and alkali feldspar (Q + A + P = 100 Vol.%, Table 7) for all samples except IG_BH02_PW022. These samples lie within the classification field of granodiorite (Figure 3). For core sample IG_BH02_PW022 the percentage of alkali feldspar is 5 Vol.% of the entire proportion of quartz, plagioclase and alkali feldspar (Table 7). This sample plots within the classification field of tonalite (Figure 3). For the calculation of the proportions of quartz, plagioclase and alkali feldspar in the samples the sericitized portion of plagioclase was added to the unaltered plagioclase (i.e., Pl + altered Pl).

Table 6: Modal composition (Vol.%) of the occurring minerals obtained using point counting; Modal compositions of accessories were not determined (the modal percentage of accessories is <1 Vol.%)

Sample	Depth	Qtz	Pl	Altered Pl	Afs	Bt	Ms + Ep + Czo	Accessories
	mbgs (down hole)	Vol.%	Vol.%	Vol.%	Vol.%	Vol.%	Vol.%	Minerals
IG_BH02_PW001	240.0	34.3	23.6	14.1	15.0	9.7	3.3	Op, Ap, Zrn
IG_BH02_PW003	348.0	32.0	32.4	16.0	8.4	9.1	2.1	Op, Ap, Zrn, Ttn
IG_BH02_PW006	381.7	31.6	29.1	23.5	12.1	2.5	1.2	Op, Ap, Zrn
IG_BH02_PW008	454.98	28.3	28.0	18.4	21.2	3.1	1.0	Op, Ap, Zrn, Ttn
IG_BH02_PW012	555.7	27.1	31.7	14.1	14.1	8.8	4.2	Op, Ap, Zrn, Ttn
IG_BH02_PW014	611.2	30.3	26.3	15.1	21.1	5.2	2.0	Op, Ap, Zrn
IG_BH02_PW016	665.8	23.6	26.6	23.6	13.3	8.4	4.5	Op, Ap, Zrn
IG_BH02_PW018	770.6	25.2	34.0	9.6	25.5	3.2	2.5	Op, Ap, Zrn
IG_BH02_PW020	878.8	38.9	31.8	10.6	7.4	8.5	2.8	Op, Ap, Zrn
IG_BH02_PW022	984.2	33.6	40.1	12.1	4.9	6.5	2.8	Op, Ap, Zrn

Table 7: Normalized modal composition (Vol.%) of quartz, plagioclase and alkali feldspar obtained using point counting and classification of rock types

Sample	Depth	Qtz	Pl + altered Pl	Afs	Rock type[1)]	Proportion Afs of total feldspar	Rock type[2)]
	mbgs (down hole)	Vol.%	Vol.%	Vol.%		Vol.%	
IG_BH02_PW001	240.0	39.5	43.3	17.2	Granodiorite	28.4	Granodiorite
IG_BH02_PW003	348.0	36.1	54.5	9.4	Granodiorite	14.7	Granodiorite
IG_BH02_PW006	381.7	32.8	54.7	12.5	Granodiorite	18.7	Granodiorite
IG_BH02_PW008	454.98	29.5	48.4	22.1	Granodiorite	31.3	Granodiorite
IG_BH02_PW012	555.7	31.2	52.6	16.2	Granodiorite	23.6	Granodiorite
IG_BH02_PW014	611.2	32.6	44.7	22.7	Granodiorite	33.7	Granodiorite
IG_BH02_PW016	665.8	27.1	57.6	15.3	Granodiorite	21.0	Granodiorite
IG_BH02_PW018	770.6	26.7	46.3	27.0	Granodiorite	36.9	Granodiorite

Sample	Depth	Qtz	Pl + altered Pl	Afs	Rock type[1)]	Proportion Afs of total feldspar	Rock type[2)]
	mbgs (down hole)	Vol.%	Vol.%	Vol.%		Vol.%	
IG_BH02_PW020	878.8	43.8	47.8	8.4	Granodiorite	14.9	Granodiorite
IG_BH02_PW022	984.2	37.1	57.5	5.4	Tonalite	8.6	Tonalite

according to [1)]Bas & Streckeisen (1991) and [2)]Streckeisen (1974)

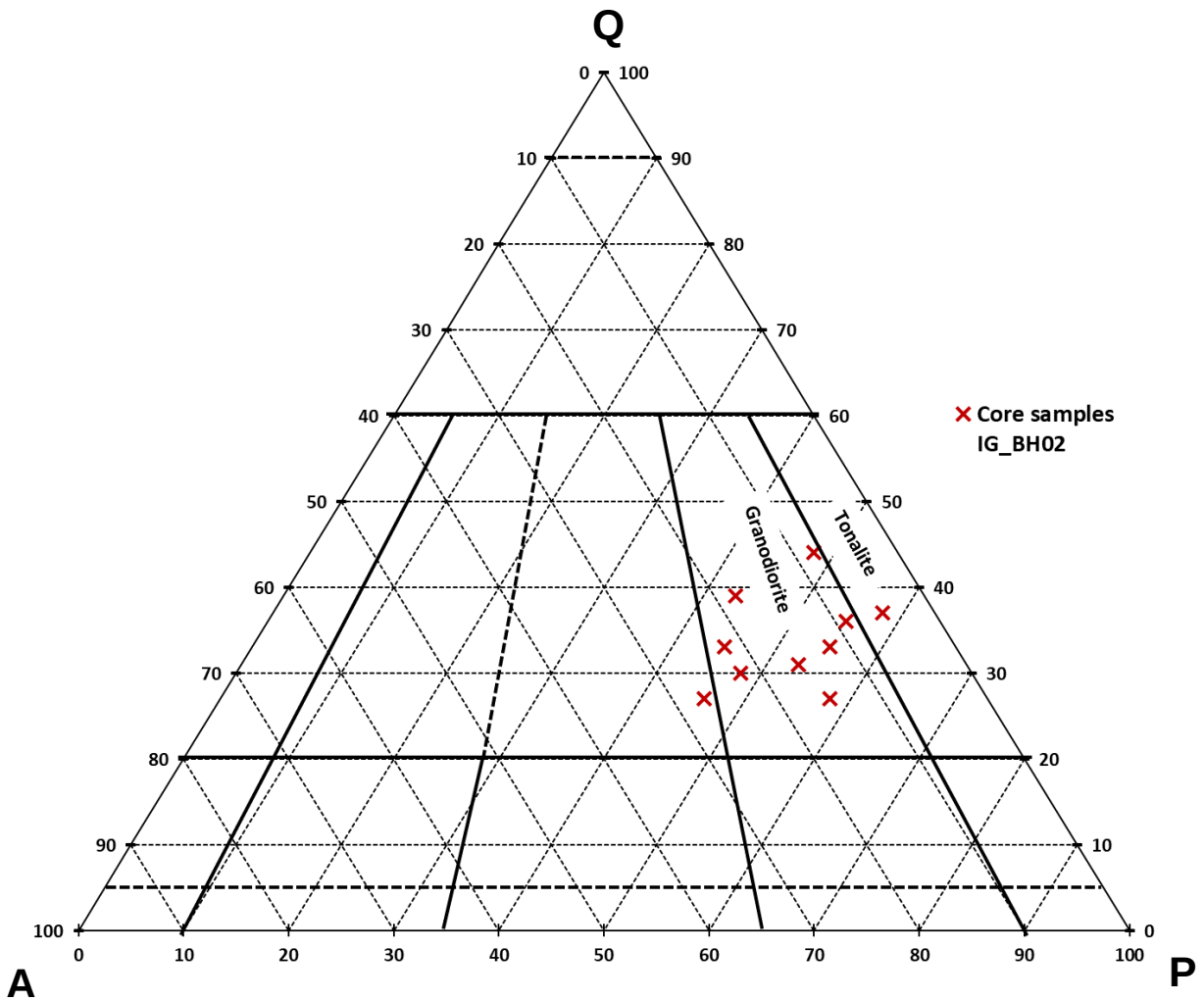


Figure 3: Classification/nomenclature according to the modal mineral content (Q + A + P = 100 Vol.%) of the individual core samples plotted in a simplified ternary Streckeisen diagram, after Bas & Streckeisen (1991)

4.3 Microscopic petrographic description of individual core samples from borehole IG_BH02

Sample IG_BH02_PW001 (240.0 mbgs down hole)

Macroscopically, sample IG_BH02_PW001 is a homogenous, equigranular and phaneritic granodiorite containing mainly fine to medium grained feldspar, quartz and biotite (Figure 8a, b). Microscopically, muscovite, sericite and epidote/clinozoisite are observed as alteration products (Figure 4c-k). Very fine grained zircon with pleochroic haloes, apatite crystals and opaque minerals are present as accessories.

Plagioclase (38 Vol.%) is mainly present as xenomorphic-hypidiomorphic fine to medium (few coarse) grained crystals showing a moderate to high degree of alteration. Moderately altered plagioclase crystals often contain very fine to fine grained needle like sericite, bladed or fibrous muscovite and granular epidote/clinozoisite, whereas the rim is free of alteration products (Figure 4g). Highly altered plagioclase contains alteration products in the whole crystal (Figure 4f). Few weakly altered plagioclase grains only contain epidote/clinozoisite in the core (Figure 4h).

Quartz (34 Vol.%) mainly occurs as xenomorphic-hypidiomorphic fine to medium grained crystals. Few quartz grains are coarse. Quartz is frequently arranged in the shape of clusters and no alteration products can be observed between quartz grains (Figure 4g and h).

Biotite (10 Vol.%) is mainly present as xenomorphic, fine to medium grained crystals showing colours/pleochroism in the range of dark brown(ish) to light green(ish) (Figure 4d). Some crystals show alteration to chlorite and are associated with very fine to fine grained epidote/clinozoisite and fine-grained needle like muscovite (Figure 4f, i and k). Frequently very fine to fine grained granular epidote/clinozoisite and stalky muscovite is observed at grain boundaries of sericitized plagioclase and also in the vicinity of unaltered quartz and alkali feldspar and weakly altered plagioclase. Few biotite crystals are partially replaced by epidote/clinozoisite (Figure 4f). Very fine grained zircons with pleochroitic haloes and apatite crystals are observed as inclusions in a small proportion of weakly altered biotite crystals.

Alkali feldspar (15 Vol.%) are present as xenomorphic fine to medium grained crystals. Few crystals are coarse grained. Alkali feldspar is unaltered and frequently shows microcline twining or lamellae of albite (Figure 4e-g, i).

Bladed, stalky or fibrous muscovite and granular epidote/clinozoisite (3 Vol.%) are present as very fine to fine grained inclusions in sericitized plagioclase and in association with weakly altered or chloritized biotite (Figure 8e-k). Fine grained xenomorphic-hypidiomorphic epidote/clinozoisite with abnormal blue/yellow and colourful interferences also partially replaces some weakly or chloritized biotite crystals (Figure 4e and f).

The pore space between quartz and feldspar grains is open and no alteration products are observed (Figure 4f, g and h). In the presence of alteration products at the grain boundaries of altered or chloritized biotite grains, a clear grain boundary generally is not observed (Figure 8e, i and k).



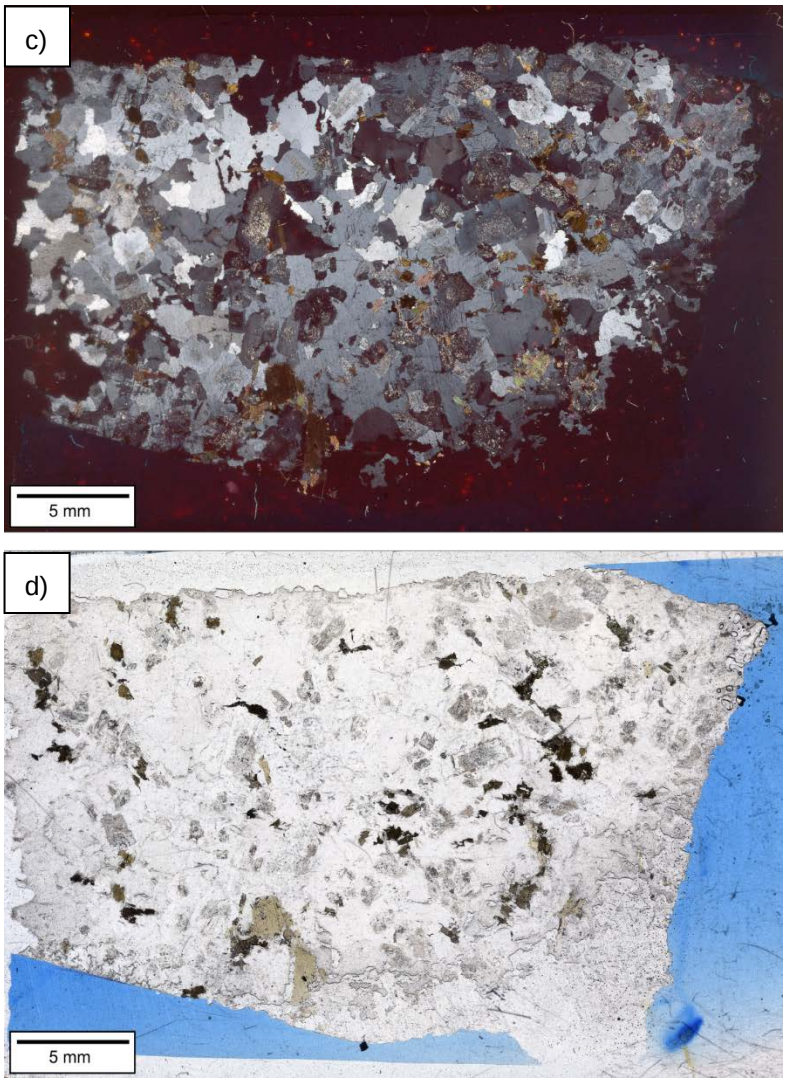
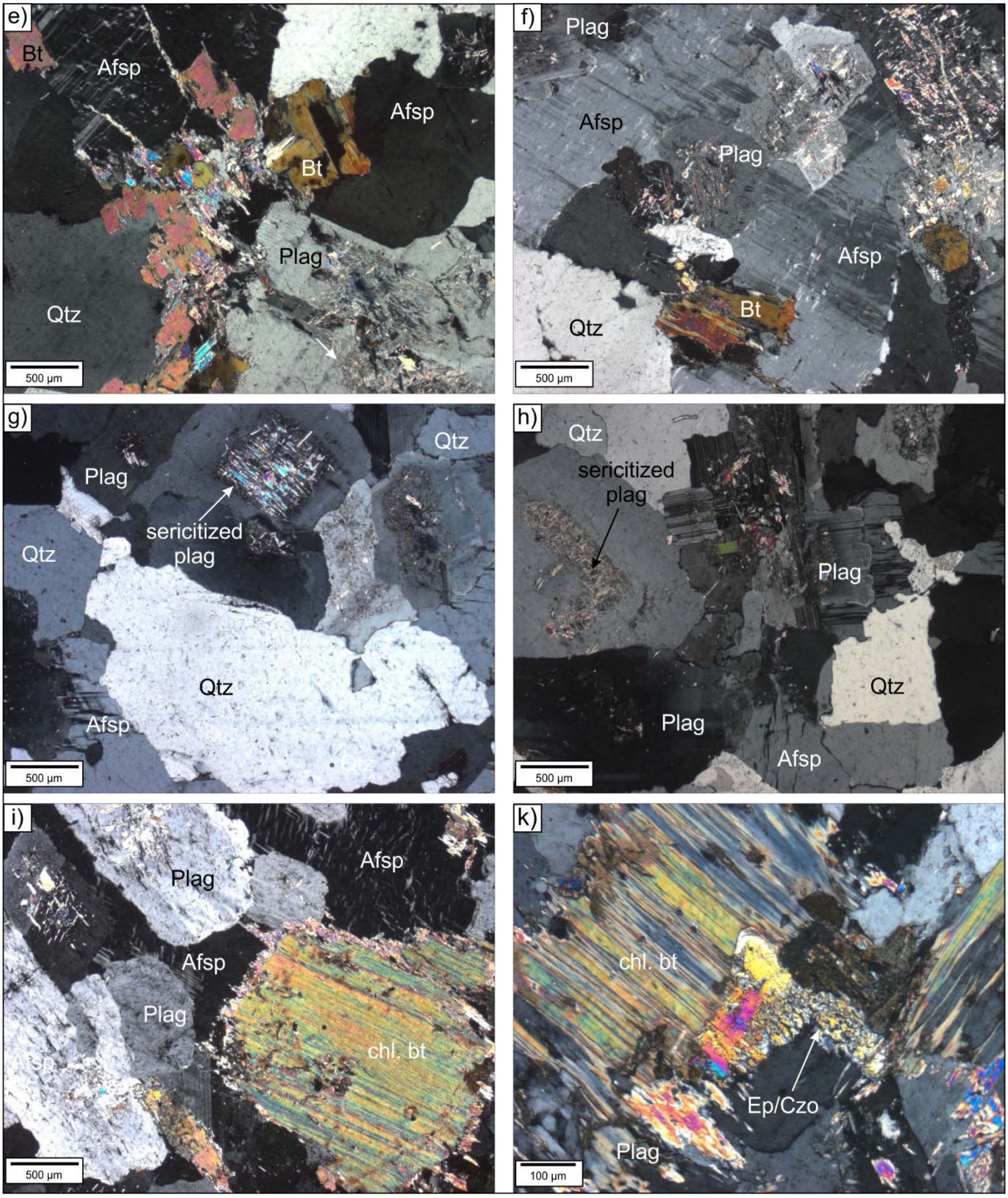


Figure 4: Petrography of sample IG_BH02_PW001 (240.0 mbgs down hole)

Notes: a) Macroscopic appearance of the core, b) Macroscopic appearance of the core section PW001 used for thin section production, c) Overview of the mineral assemblage under transmitted, cross-polarized light, d) Overview of the mineral assemblage under transmitted plane-polarized light, e) Sericitized plagioclase, weakly altered biotite and unaltered alkali feldspar and quartz under transmitted cross-polarized light, f) Sericitized plagioclase and weakly chloritized biotite partially replaced by epidote/clinozoisite embedded in unaltered alkali feldspar under transmitted cross-polarized light, g) Quartz cluster without alteration products and sericitization of plagioclase core under transmitted cross-polarized light, h) Plagioclase sericitized in the core and unaltered quartz and alkali feldspar under transmitted cross-polarized light, i) Chloritized biotite and highly altered plagioclase embedded in unaltered alkali feldspar under transmitted cross-polarized light, k) Chloritized biotite and epidote/clinozoisite under transmitted cross-polarized light.


e)
Bt
Afsp
Afsp
Bt
Plag
Qtz
500 µm
f)
Plag
Afsp
Plag
Afsp
Bt
Qtz
500 µm
g)
Qtz
Plag
sericitized
plag
Qtz
Qtz
Afsp
500 µm
h)
Qtz
sericitized
plag
Plag
Qtz
Plag
Afsp
500 µm
i)
Plag
Afsp
Afsp
Plag
chl. bt
500 µm
k)
chl. bt
Ep/Czo
Plag
100 µm

Sample IG_BH02_PW003 (348.0 mbgs down hole)

Sample IG_BH02_PW003 is a homogenous, equigranular, phaneritic granodiorite. Macroscopically, medium to coarse grained feldspars, and fine to medium grained quartz and biotite can be distinguished (Figure 5a, b). Fine grained sericite, muscovite and epidote/clinozoisite are observed microscopically as alteration products in plagioclase (Figure 5c-k) and around undefined grain boundaries of biotite (Figure 5e and h). Quartz and alkali feldspar are free from alteration products (Figure 5h-i). Very fine grained apatite, zircon, titanite and opaque minerals are present as accessories.

Plagioclase makes up to 48 Vol.% and occurs as xenomorphic-hypidiomorphic fine to medium grained and weakly to moderately altered crystals. Only few crystals show a high degree of alteration. Weakly altered plagioclase crystals contain very fine grained sericite and few bladed muscovite and granular epidote/clinozoisite mainly in the core of the crystal, whereas the rim is free of alteration products (Figure 5g and i). Moderately to highly altered plagioclase is associated with weakly altered biotite (Figure 5e, f and h) and shows very fine grained sericite and very fine to fine grained needle like and bladed muscovite and granular epidote/clinozoisite inclusions (Figure 5k).

Quartz (32 Vol.%) mainly occurs as xenomorphic fine to medium grained crystals. Few quartz crystals are coarse grained. Quartz is frequently arranged in the shape of clusters and no alteration products can be observed between quartz grains (Figure 5i).

Biotite (9 Vol.%) occurs in minor amounts in the sample. Biotite is present as xenomorphic-hypidiomorphic fine to medium grained crystals showing no or a low degree of alteration (Figure 5c, e and h). Weakly altered crystals are associated with granular epidote/clinozoisite and fine grained needle-like muscovite which is present as a margin around weakly altered biotite and at sutural grain boundaries (Figure 5e and h). Few weakly altered biotite grains are associated with hypidiomorphic to idiomorphic epidote/clinozoisite inclusions and few biotite crystals are partially replaced by epidote/clinozoisite (Figure 5f and h). Very fine grained zircons with pleochroic haloes and apatite crystals are observed as inclusions in unaltered and weakly altered biotite.

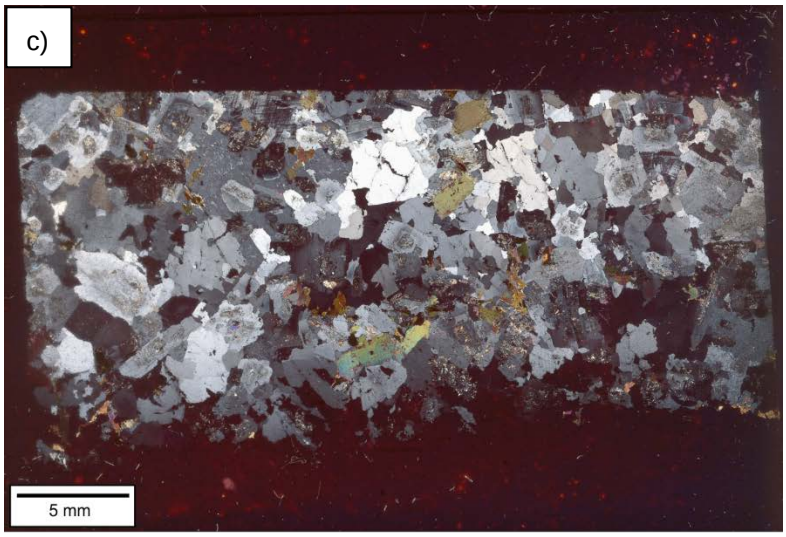
Alkali feldspar (8 Vol.%) occurs as xenomorphic fine to medium (few coarse) grained crystals. They are free from alteration products and are mainly associated with unaltered quartz and unaltered to weakly altered plagioclase. Few crystals show microcline twinning or lamellae of albite (Figure 5g and i).

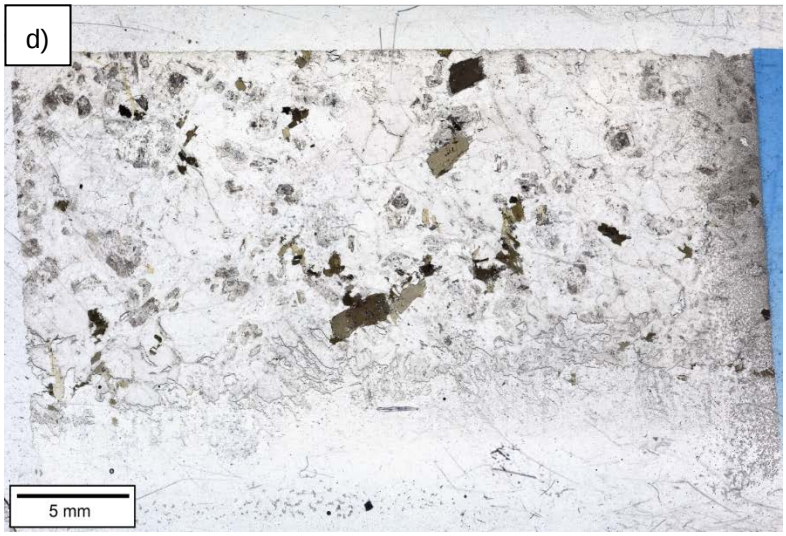
Minor amounts of very fine grained sericite, and very fine to fine grained bladed or stalky muscovite and granular epidote/clinozoisite (5 Vol.%) occur as alteration products in weakly to moderately sericitized plagioclase and in association with weakly altered biotite (Figure 5e-k). In association with weakly altered biotite, muscovite is present at sutural grain boundaries of biotite (Figure 5e and h). Few fine grained epidote/clinozoisite crystals show a hypidiomorphic-idiomorphic shape (Figure 5h and k).

The pore space between quartz grains is open and not filled with alteration products (Figure 5g-i). In association with weakly altered biotite, the grain boundaries are not defined due to a margin of fine grained needle-like muscovite (Figure 5e and h).

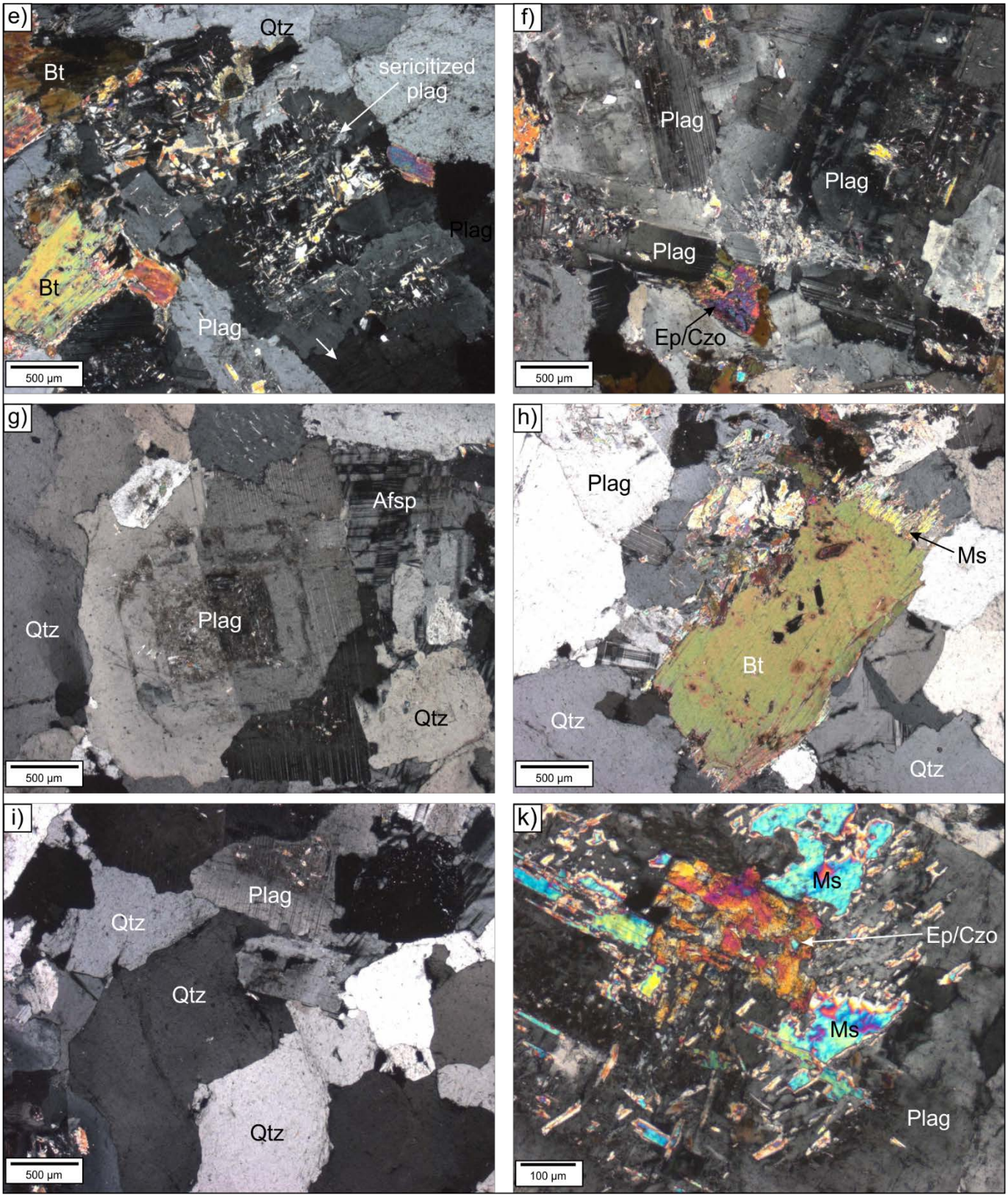


Figure 5: Petrography of sample IG_BH02_PW003 (348.0 mbgs down hole)





Notes: a) Macroscopic appearance of the core, b) Macroscopic appearance of the core section PW003 used for thin section production, c) Overview of the mineral assemblage under transmitted cross-polarized light, d) Overview of the mineral assemblage under transmitted plane-polarized light, e) Weakly altered biotite with sutural grain boundary and chloritized biotite in association with moderately to highly altered plagioclase containing bladed muscovite and granular epidote/clinozoisite under transmitted cross-polarized light, f) Weakly to moderately altered plagioclase and biotite mainly replaced by epidote/clinozoisite under transmitted cross-polarized light, g) Sericitized core of zoned plagioclase and unaltered alkali feldspar and quartz under transmitted cross-polarized light, h) Biotite with sutural grain boundary and inclusions of pleochroic haloes and hypidiomorphic epidote in association with alteration products surrounded by unaltered quartz and alkali feldspar under transmitted cross-polarized light, i) Weakly altered plagioclase and unaltered quartz and alkali feldspar under transmitted cross-polarized light, k) Sericitized plagioclase containing epidote/clinozoisite and muscovite under transmitted cross-polarized light.


e)
Qtz
Bt
sericitized plag
Plag
Bt
Plag
500 µm
f)
Plag
Plag
Plag
Ep/Czo
500 µm
g)
Afsp
Qtz
Plag
Qtz
500 µm
h)
Plag
Ms
Bt
Qtz
Qtz
500 µm
i)
Plag
Qtz
Qtz
Qtz
500 µm
k)
Ms
Ep/Czo
Ms
Plag
100 µm

Sample IG_BH02_PW005 (345.2 mbgs down hole)

Macroscopically sample IG_BH02_PW005 consists of fine to medium grained plagioclase phenocrysts embedded in a very fine to fine grained matrix (Figure 6a, b). Microscopically, quartz, feldspar, muscovite and epidote/ clinozoisite are observed (Figure 6c-k). In contrast to the other investigated rock samples no biotite is present in this sample.

Plagioclase occurs as xenomorphic-hypidiomorphic fine to medium grained phenocrysts. Some crystals are highly sericitized (Figure 6e and h), whereas some crystals are weakly to moderately altered and show zonation or lamellar twinning (Figure 6f and g). Some phenocrysts are associated with fibrous muscovite and granular epidote/clinozoisite as alteration products (Figure 6k). Very fine to fine grained plagioclase is also present in the matrix of the rock sample.

The matrix consists mainly of xenomorphic very fine to fine grained quartz and feldspars which are not distinguishable. Also, minor amounts of fibrous muscovite and granular epidote/clinozoisite are present as alteration products (Figure 6e-k).



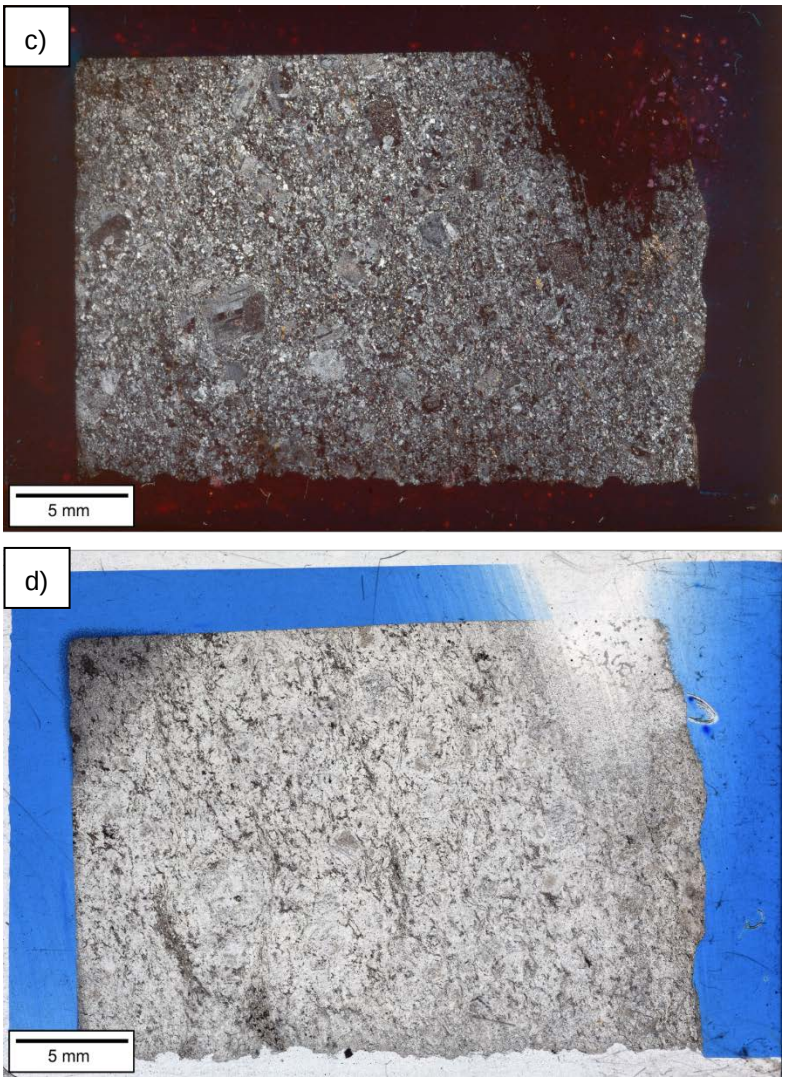
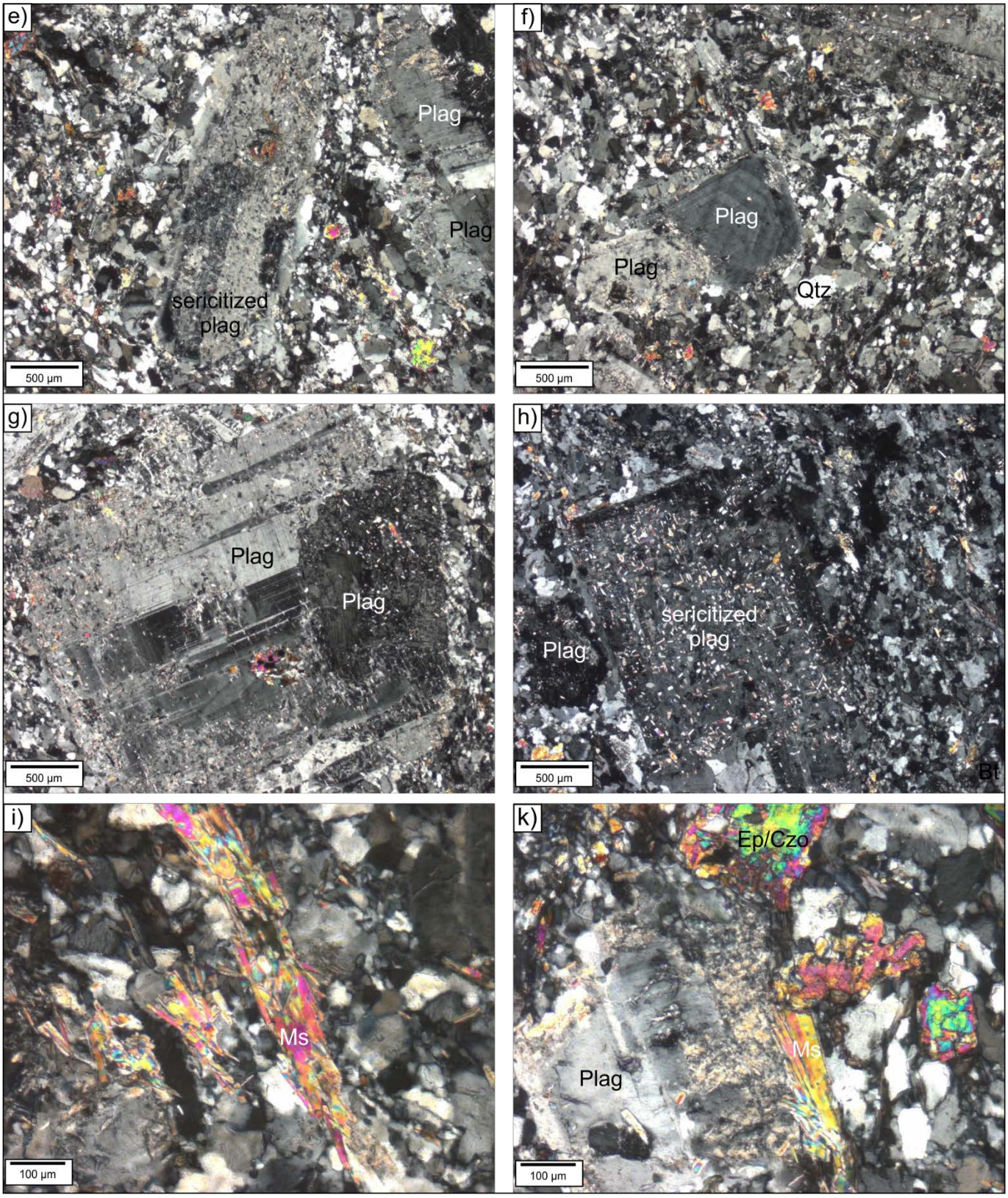


Figure 6: Petrography of sample IG_BH02_PW005 (345.2 mbgs down hole)

Notes: a) Macroscopic appearance of the core, b) Macroscopic appearance of the core section PW005 used for thin section production, c) Overview of the mineral assemblage under transmitted cross-polarized light, d) Overview of the mineral assemblage under transmitted plane-polarized light, e) Medium grained sericitized plagioclase embedded in very fine to fine grained matrix of feldspar and quartz and alteration products under transmitted cross-polarized light, f) Zoned plagioclase phenocryst partially sericitized and embedded in very fine to fine grained matrix under transmitted cross-polarized light, g) Medium grained moderately altered plagioclase phenocryst showing lamellar twinning and very fine to fine grained matrix under transmitted cross-polarized light, h) Highly sericitized medium grained plagioclase and very fine to fine grained matrix under transmitted cross-polarized light, i) Fine grained fibrous muscovite and very fine to fine grained quartz and feldspars under transmitted cross-polarized light, k) Fine grained moderately altered plagioclase in association with fibrous muscovite and granular epidote/clinozoisite under transmitted cross-polarized light.


e)
Plag
Plag
sericitized plag
500 µm
f)
Plag
Plag
Qtz
500 µm
g)
Plag
Plag
500 µm
h)
sericitized plag
Plag
500 µm
Bt
i)
Ms
100 µm
k)
Ep/Czo
Ms
Plag
100 µm

Sample IG_BH02_PW06 (459.2 mbgs down hole)

The texture of the granodiorite sample IG_BH02_PW006 is homogenous, equigranular and phaneritic (Figure 7a, b). Macroscopically, fine to medium grained feldspar, quartz and minor amounts of biotite can be distinguished (Figure 7b). The red colour of some plagioclase in this rock sample might be due to iron replacing some calcium ions in the plagioclase crystal lattice (staining of plagioclase crystals). Minor amounts of muscovite, sericite and epidote/clinozoisite are observed microscopically as alteration products (Figure 7c-k). Apatite, zircon and opaque minerals are present as accessories.

Plagioclase (53 Vol.%) occurs as xenomorphic-hypidiomorphic fine to medium grained crystals, which show varying degrees of alteration. Weakly and moderately altered crystals contain very fine grained needle-like sericite and stalky or bladed muscovite mainly in the core of the crystal (Figure 7f-h). Also, stalky and bladed very fine and fine grained muscovite and granular epidote/clinozoisite appear as inclusions in moderately to highly altered plagioclase crystals (Figure 7e, g and k). The few highly sericitized plagioclase crystals are associated primarily with granular epidote/clinozoisite.

Quartz (32 Vol.%) is present as xenomorphic, fine to medium grained crystals. Quartz crystals are frequently arranged in the shape of medium grained clusters surrounded by fine grained crystals (Figure 7f and g).

The amount of biotite (2 Vol.%) is very low compared to the other rock samples. Biotite is present as xenomorphic-hypidiomorphic fine (few medium) grained crystals showing no, or a low degree of, alteration (Figure 7c and e). Few weakly altered crystals are associated with granular epidote/clinozoisite, which partially replaces the biotite, and fine grained needle-like muscovite which is present as a margin around weakly altered biotite and at sutural grain boundaries (Figure 7e). Very fine grained zircons with pleochroic haloes and apatite crystals are observed as inclusions in unaltered and weakly altered biotite.

Alkali feldspar (12 Vol.%) occurs as xenomorphic-hypidiomorphic medium (few coarse) grained mainly unaltered crystals. Few crystals show microfissures filled with very fine grained needle-like muscovite and granular epidote/clinozoisite. Microcline twinning and lamellae of albite are observed in some alkali feldspar crystals (Figure 7e, f and h-k).

The low amount of biotite is associated with a very low amount of very fine to fine grained inclusions of bladed to stalky muscovite, granular epidote/clinozoisite and sericite (1 Vol.%) in sericitized plagioclase (Figure 7e-k). Few biotite crystals are partially replaced by epidote/clinozoisite. Very fine grained needle-like muscovite is also present at sutural grain boundaries of weakly altered biotite crystals (Figure 7e).

The grain boundaries between quartz and feldspar crystals are open and no alteration product is present in the pore space (Figure 7f-h and k). Along weakly altered biotite, a clear grain boundary is not observed (Figure 7e). In the vicinity of altered minerals, the intergranular pore space is also open. Only a small proportion of micro-fissures in alkali feldspar are filled with alteration products (Figure 7e).

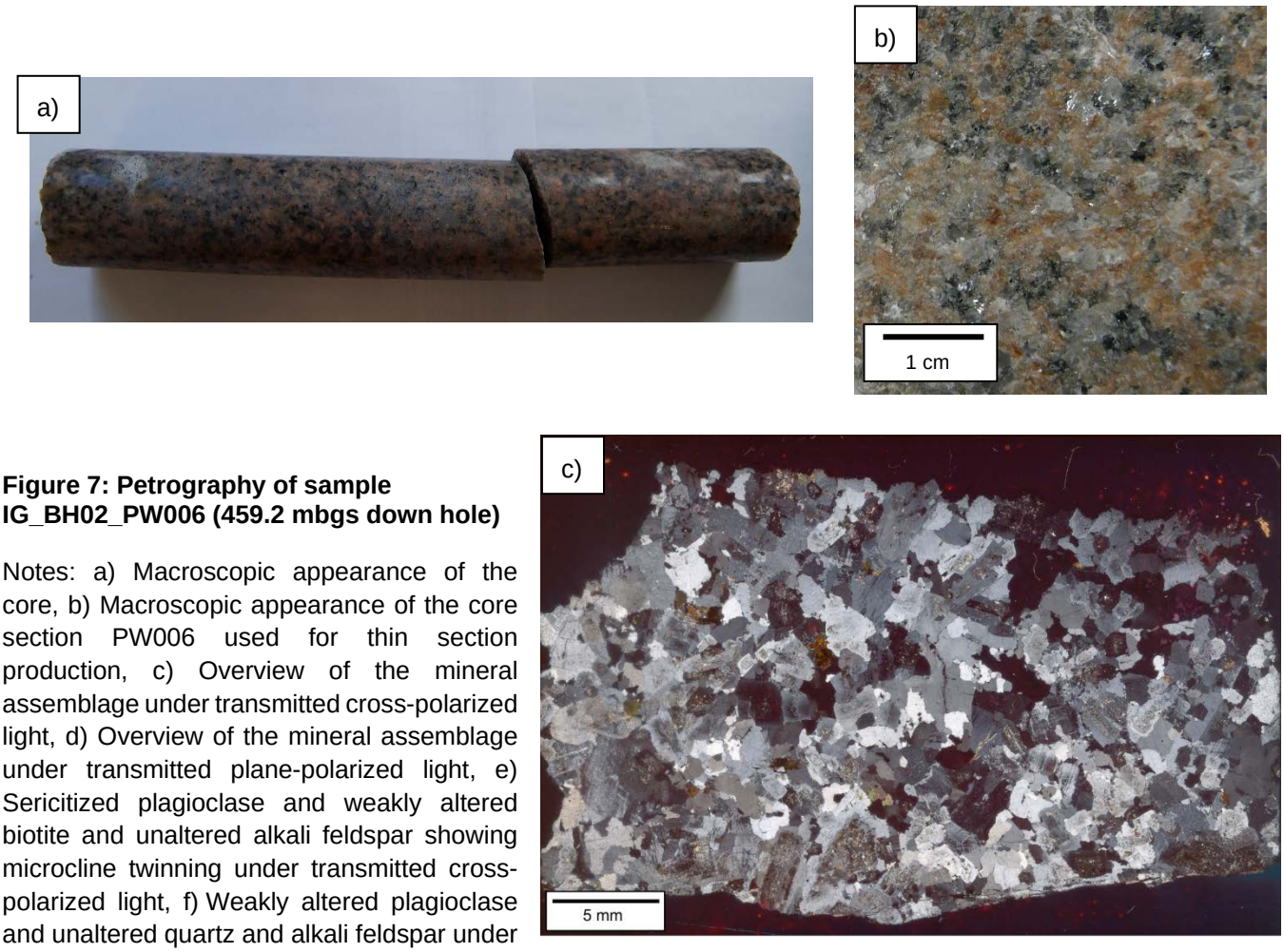
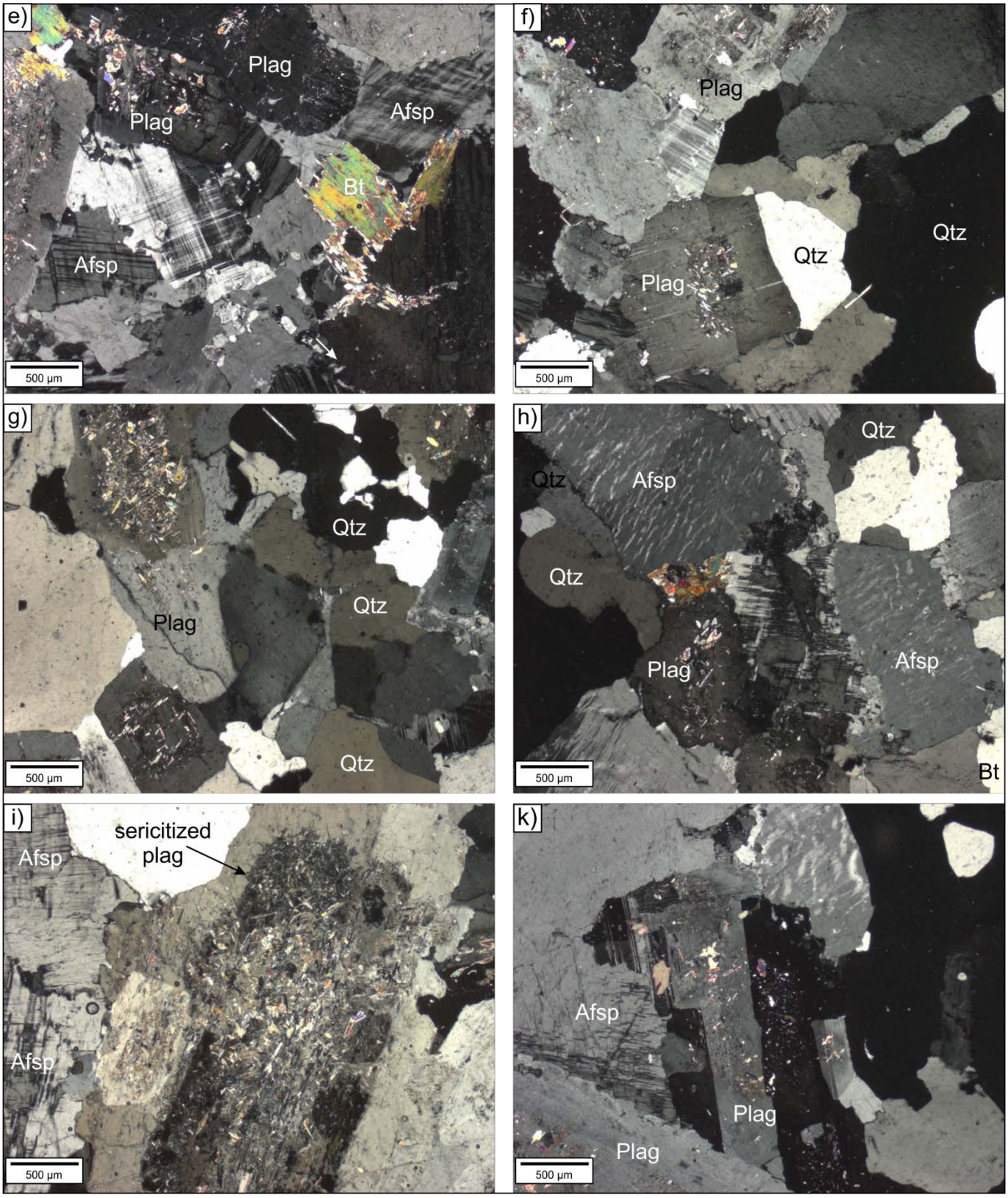


Figure 7: Petrography of sample IG_BH02_PW006 (459.2 mbgs down hole)

Notes: a) Macroscopic appearance of the core, b) Macroscopic appearance of the core section PW006 used for thin section production, c) Overview of the mineral assemblage under transmitted cross-polarized light, d) Overview of the mineral assemblage under transmitted plane-polarized light, e) Sericitized plagioclase and weakly altered biotite and unaltered alkali feldspar showing microcline twinning under transmitted cross-polarized light, f) Weakly altered plagioclase and unaltered quartz and alkali feldspar under transmitted cross-polarized light, g) Weakly to moderately altered plagioclase with alteration products mainly in the core and unaltered alkali feldspar under transmitted cross-polarized light, h) Weakly altered plagioclase and unaltered alkali feldspar and quartz under transmitted cross-polarized light, i) Highly sericitized coarse grained plagioclase and unaltered alkali feldspar under transmitted cross-polarized light, k) Weakly altered plagioclase and unaltered alkali feldspar and quartz under transmitted cross-polarized light.


e)
Plag
Plag
Afsp
Bt
Afsp
500 µm
f)
Plag
Qtz
Qtz
Plag
500 µm
g)
Qtz
Qtz
Plag
Qtz
500 µm
h)
Qtz
Qtz
Afsp
Qtz
Plag
Afsp
Bt
500 µm
i)
sericitized
plag
Afsp
Afsp
500 µm
k)
Afsp
Plag
Plag
500 µm

Sample IG_BH02_PW008 (503.9 mbgs down hole)

Macroscopically, sample IG_BH02_PW008 is a homogenous, equigranular and phaneritic granodiorite containing mainly fine to medium grained feldspar, quartz and biotite (Figure 8a, b). Microscopically, muscovite, sericite and epidote/clinozoisite are observed as alteration products (Figure 8c-k). Very fine grained zircon with pleochroic haloes, apatite crystals, titanite and opaque minerals are present as accessories.

Plagioclase (46 Vol.%) occurs as xenomorphic-hypidiomorphic fine to medium grained crystals, which show variable degrees of alteration. Few unaltered and weakly altered crystals show a strong zonation (Figure 8e), and frequently a zonation with alteration products only occurring in the core of the grain can be observed in sericitized plagioclase (Figure 8e). In moderately to highly altered plagioclase, very fine grained sericite, bladed and stalky muscovite and/or granular epidote/clinozoisite are present (Figure 8e-k). Some plagioclase grains show micro-fissures filled with very fine grained needle-like muscovite (Figure 8k).

Quartz (28 Vol.%) is present as xenomorphic, fine to medium grained crystals, which are frequently arranged in the shape of clusters (Figure 8h). No alteration products are observed between quartz grains.

The amount of biotite is very low like in sample IG_BH02_PW008 (3 Vol.%). Biotite appears as xenomorphic-hypidiomorphic fine to medium grained bladed crystals which are unaltered or weakly altered and show varying colours/pleochroism (Figure 8c, d, e-g). In association with quartz, alkali feldspar and unaltered to weakly altered plagioclase, a small proportion of biotite grains show sutural grain boundaries with a margin of very fine grained needle like muscovite (Figure 8f). In the vicinity to altered plagioclase, fine grained granular epidote/clinozoisite also is present (Figure 8f). Few very fine grained titanite crystals, zircons with pleochroic haloes and apatite crystals are observed as inclusions in unaltered and weakly altered biotite.

Alkali feldspar makes up to 21 Vol.% and occurs as xenomorphic, fine to coarse grained crystals frequently showing microcline twinning or lamellae of albite (Figure 8f, g). Alteration of alkali feldspar is typically not observed, but in association with weakly altered biotite some micro-fissures are filled with very fine grained needle-like muscovite (Figure 8f).

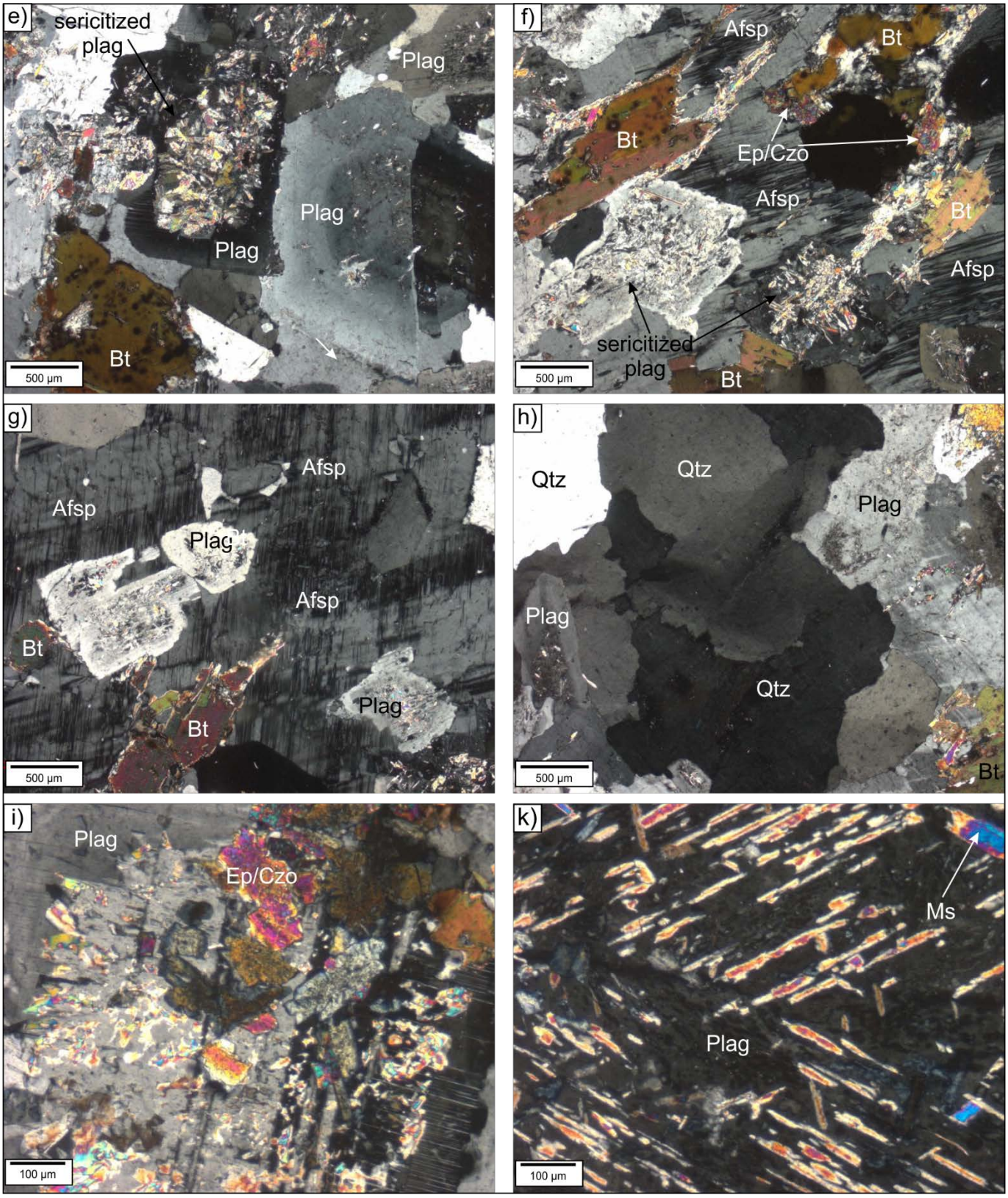
Minor amounts of sericite, muscovite and epidote/clinozoisite (1 Vol.%) occur as very fine to fine grained inclusions in weakly to highly sericitized plagioclase (Figure 8c-k). In association with weakly altered biotite, muscovite frequently forms a sutural texture at the grain boundaries (Figure 8f). In few plagioclase crystals micro-fissures are filled by very fine grained needle-like muscovite (Figure 8k). As observed in rock sample IG_BH02_PW006, the amount of alteration products is relatively low in this sample, which may correlate with the low proportion of biotite.

The pore space between grain boundaries of quartz and feldspar is open and not filled with alteration products (Figure 8g and h). Along sutural altered biotite grains, no clear grain boundary can be observed (Figure 8f). The pore space also is open when no alteration minerals are observed to be present.



Figure 8: Petrography of sample IG_BH02_PW008 (503.9 mbgs down hole)

Notes: a) Macroscopic appearance of the core, b) Macroscopic appearance of the core section PW008 used for thin section production, c) Overview of the mineral assemblage under transmitted, cross-polarized light, d) Overview of the mineral assemblage under transmitted plane-polarized light, e) Highly sericitized plagioclase containing very fine grained needle-like and bladed muscovite and xenomorphic to hypidiomorphic epidote/clinozoisite and weakly altered zoned plagioclase and weakly altered biotite under transmitted cross-polarized light, f) Weakly altered biotite partially replaced by epidote/clinozoisite and highly sericitized plagioclase embedded in unaltered alkali feldspar under transmitted cross-polarized light, g) Sericitized plagioclase and biotite embedded in xenomorphic, coarse grained and unaltered alkali feldspar under transmitted cross-polarized light, h) Quartz cluster with open grain boundaries under transmitted cross-polarized light, i) Sercitized core of a plagioclase crystal with very fine to fine grained epidote/clinozoisite and very fine grained muscovite inclusions under transmitted cross-polarized light, k) Needle-like fine grained sericite and granular fine grained epidote/clinozoisite in micro-fissures of plagioclase under transmitted cross-polarized light.


e)
sericitized plag
Plag
Plag
Plag
Bt
500 µm
f)
Afsp
Bt
Bt
Ep/Czo
Afsp
Bt
Afsp
sericitized plag
Bt
500 µm
g)
Afsp
Afsp
Plag
Afsp
Bt
Plag
Bt
500 µm
h)
Qtz
Qtz
Plag
Plag
Qtz
Bt
500 µm
i)
Plag
Ep/Czo
100 µm
k)
Ms
Plag
100 µm

Sample IG_BH02_PW012 (554.5 mbgs down hole)

Sample IG_BH02_PW012 is a homogenous, equigranular, phaneritic granodiorite (Figure 9a, b). Macroscopically, fine to medium grained feldspar, quartz and biotite can be distinguished (Figure 9b). Minor amounts of muscovite, sericite and epidote/clinozoisite are observed microscopically as alteration products (Figure 9c-k). Apatite, zircon, titanite and opaque minerals are present as accessories.

Plagioclase makes up to 46 Vol.% and occurs as xenomorphic-hypidiomorphic fine to medium grained crystals with varying degrees of alteration. Moderately to highly altered plagioclase is frequently associated with weakly altered biotite and contains very fine to fine grained sericite, bladed or stalky muscovite and granular epidote/clinozoisite (Figure 9e-h). Weakly altered plagioclase shows alteration products mainly in the core of the crystal and few weakly altered plagioclase crystals show lamellar twinning (Figure 9f).

Quartz (27 Vol.%) mainly occurs as xenomorphic-hypidiomorphic fine to medium grained crystals. Few quartz grains are coarse. Quartz is frequently arranged in the shape of clusters and no alteration products can be observed between quartz grains (Figure 9).

About 9 vol.% of biotite is present in this rock sample. Biotite occurs as xenomorphic-hypidiomorphic fine to medium grained crystals showing a dark brown to greenish pleochroism (Figure 9d) and no, or a low degree of, alteration (Figure 9c, e-g, k). Only few crystals show alteration to chlorite. Weakly altered crystals are frequently associated with hypidiomorphic-idiomorphic granular epidote/clinozoisite and some biotite crystals are partially replaced by epidote/clinozoisite (Figure 9f, k). Few biotite crystals show a sutural grain boundary of very fine grained muscovite (Figure 9f). Very fine grained zircons with pleochroic haloes and apatite crystals are observed as inclusions in unaltered and weakly altered biotite.

Alkali feldspar (14 Vol.%) occurs as xenomorphic fine to coarse grained crystals showing mainly no alteration products (Figure 9e, f, h), but in association with biotite, a small proportion of crystals show muscovite and epidote/clinozoisite in micro-fissures. Microcline twinning or lamellae of albite are frequently observed in alkali feldspar (Figure 9e, f, h).

Very fine grained sericite, and very fine to fine grained stalky, fibrous and bladed muscovite and granular epidote/clinozoisite (4 Vol.%) occur as alteration products in weakly to highly sericitized plagioclase and in association with weakly altered biotite (Figure 9e-k). Few fine grained epidote/clinozoisite crystals show a hypidiomorphic-idiomorphic shape.

The pore space between quartz and feldspar grains is open and free from alteration products (Figure 9h, i). For a small proportion of biotite sutural grain boundaries, a clear grain boundary cannot be observed for the crystals (Figure 9h).



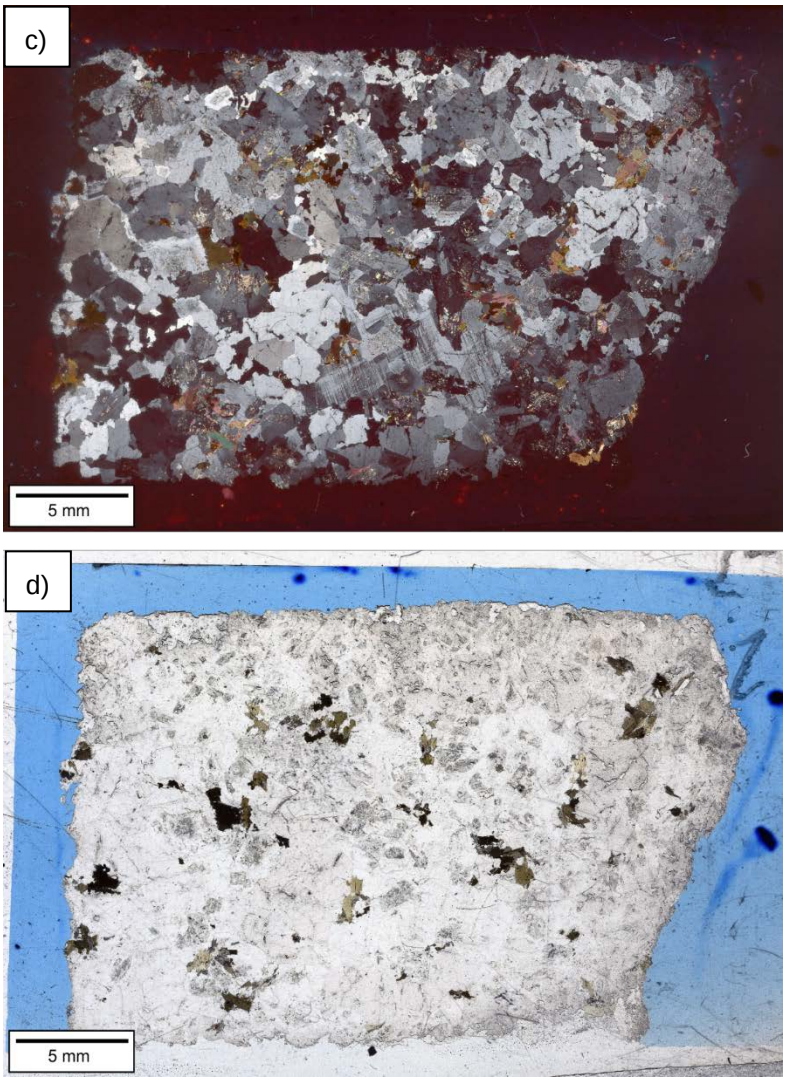
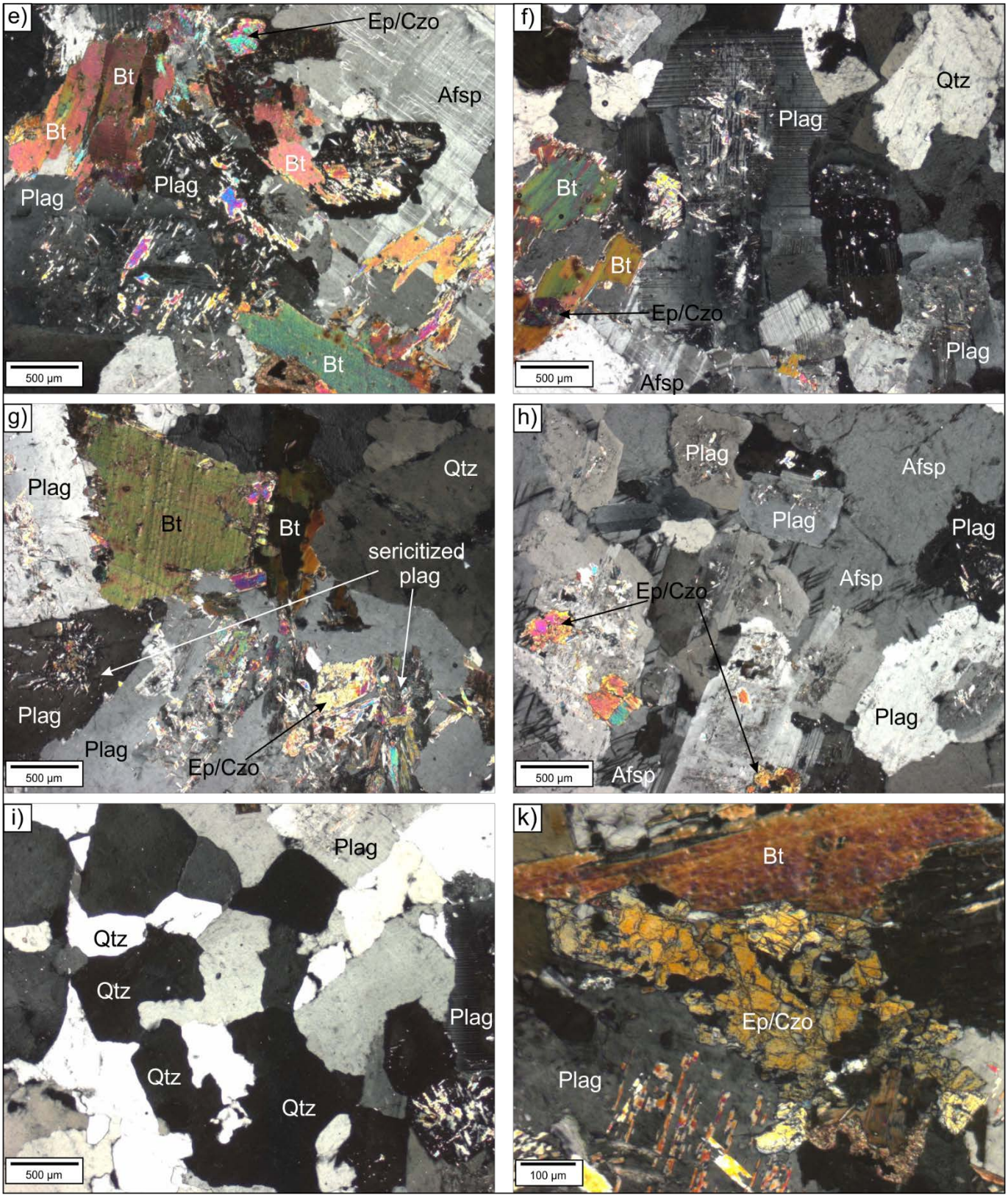


Figure 9: Petrography of sample IG_BH02_PW012 (554.5 mbgs down hole)

Notes: a) Macroscopic appearance of the core, b) Macroscopic appearance of the core section PW012 used for thin section production, c) Overview of the mineral assemblage under transmitted cross-polarized light, d) Overview of the mineral assemblage under transmitted plane-polarized light, e) Weakly altered biotite partially replaced by epidote/clinozoisite and altered plagioclase embedded in unaltered alkali feldspar under transmitted cross-polarized light, f) Weakly altered plagioclase showing lamellar twinning and weakly altered biotite partially replaced by epidote/clinozoisite under transmitted cross-polarized light, g) Sericitized plagioclase and weakly altered biotite and unaltered quartz under transmitted cross-polarized light, h) Fine grained granular epidote/clinozoisite in association with sericitized plagioclase and unaltered alkali feldspar under transmitted cross-polarized light, i) Cluster of unaltered quartz under transmitted cross-polarized light, k) Weakly altered biotite partially replaced by epidote/clinozoisite under transmitted cross-polarized light.


e)
Ep/Czo
Bt
Afsp
Bt
Bt
Plag
Plag
Bt
500 µm
f)
Qtz
Plag
Bt
Bt
Ep/Czo
Plag
500 µm
Afsp
g)
Plag
Qtz
Bt
Bt
sericitized plag
Plag
Plag
500 µm
Ep/Czo
h)
Plag
Afsp
Plag
Plag
Ep/Czo
Afsp
Plag
500 µm
Afsp
i)
Plag
Qtz
Qtz
Plag
Qtz
Qtz
500 µm
k)
Bt
Ep/Czo
Plag
100 µm

Sample IG_BH02_PW014 (608.8 mbgs down hole)

Sample IG_BH02_PW014 consists of a homogenous, equigranular, phaneritic tonalite (Figure 10a, b). Macroscopically, no alteration is observed and fine to medium grained feldspar, quartz and biotite can be distinguished. Minor amounts of muscovite, epidote/clinozoisite and sericite are observed microscopically as alteration products (Figure 10c-i). Apatite, zircon and opaque minerals are present as accessories.

Plagioclase (41 Vol.%) occurs as xenomorphic-hypidiomorphic fine to medium grained crystals, which show variable degrees of alteration. Unaltered plagioclase crystals were not observed. In some weakly to moderately altered plagioclase crystals a strong zonation, with alteration products only occurring in the core of the grain, can be observed (Figure 10i). Few weakly to moderately altered crystals show lamellar twinning (Figure 10i). In moderately to highly altered plagioclase, very fine grained sericite, bladed and stalky muscovite and/or granular epidote/clinozoisite are present (Figure 10e-h). Few plagioclase crystals only contain fine grained granular epidote/clinozoisite as alteration products.

Quartz (30 Vol.%) is present as xenomorphic, fine to medium grained crystals, which are frequently arranged in the shape of clusters (Figure 10k). No alteration products are observed between quartz grains.

Biotite (5 Vol.%) appears as xenomorphic-hypidiomorphic fine to medium grained bladed crystals which are unaltered or weakly altered and show varying colours/pleochroism (Figure 10c, d, f, g). In association with quartz, alkali feldspar and unaltered to weakly altered plagioclase, the biotite grains show sutural grain boundaries with a margin of very fine grained needle-like muscovite (Figure 10f, g). In the vicinity of altered plagioclase, very fine to fine grained granular epidote/clinozoisite also is present (Figure 10f, g). Few fine grained and very fine grained zircons with pleochroic haloes and apatite crystals are observed as inclusions in unaltered and weakly altered biotite.

About 21 Vol.% of alkali feldspar is present as unaltered xenomorphic-hypidiomorphic fine to medium (few coarse) grained crystals. Frequently, alkali feldspar crystals show microcline twinning or lamellae of albite (Figure 10e, h, I, k).

Minor amounts of sericite, muscovite and epidote/clinozoisite (2 Vol.%) occur as very fine to fine grained inclusions in weakly to highly sericitized plagioclase (Figure 10e-i). In association with weakly altered biotite, muscovite frequently forms a sutural texture at the grain boundaries (Figure 10f, g). Granular epidote/clinozoisite is also present in association with weakly altered biotite and sericitized plagioclase (Figure 10f, g, h).

The pore space between grain boundaries of quartz and feldspar is open and not filled with alteration products (Figure 10e, i, k). Along sutural altered biotite grains, no clear grain boundary can be observed (Figure 10f, g). The pore space also is open when no alteration minerals are present.



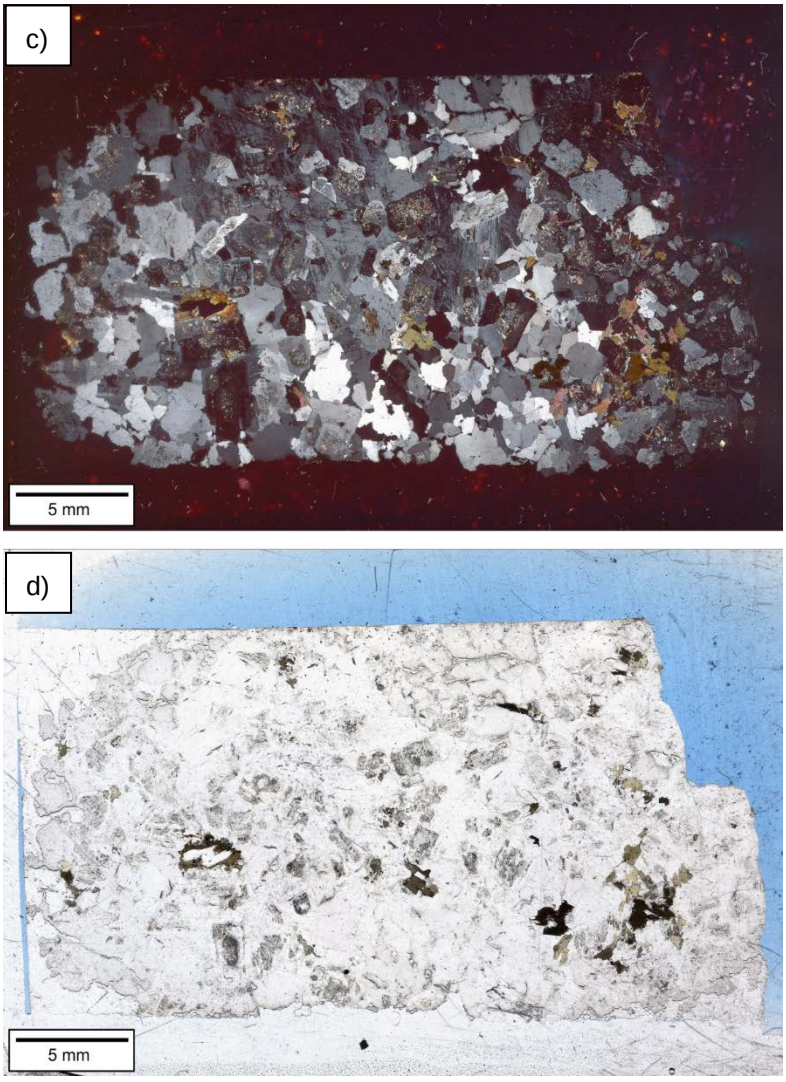
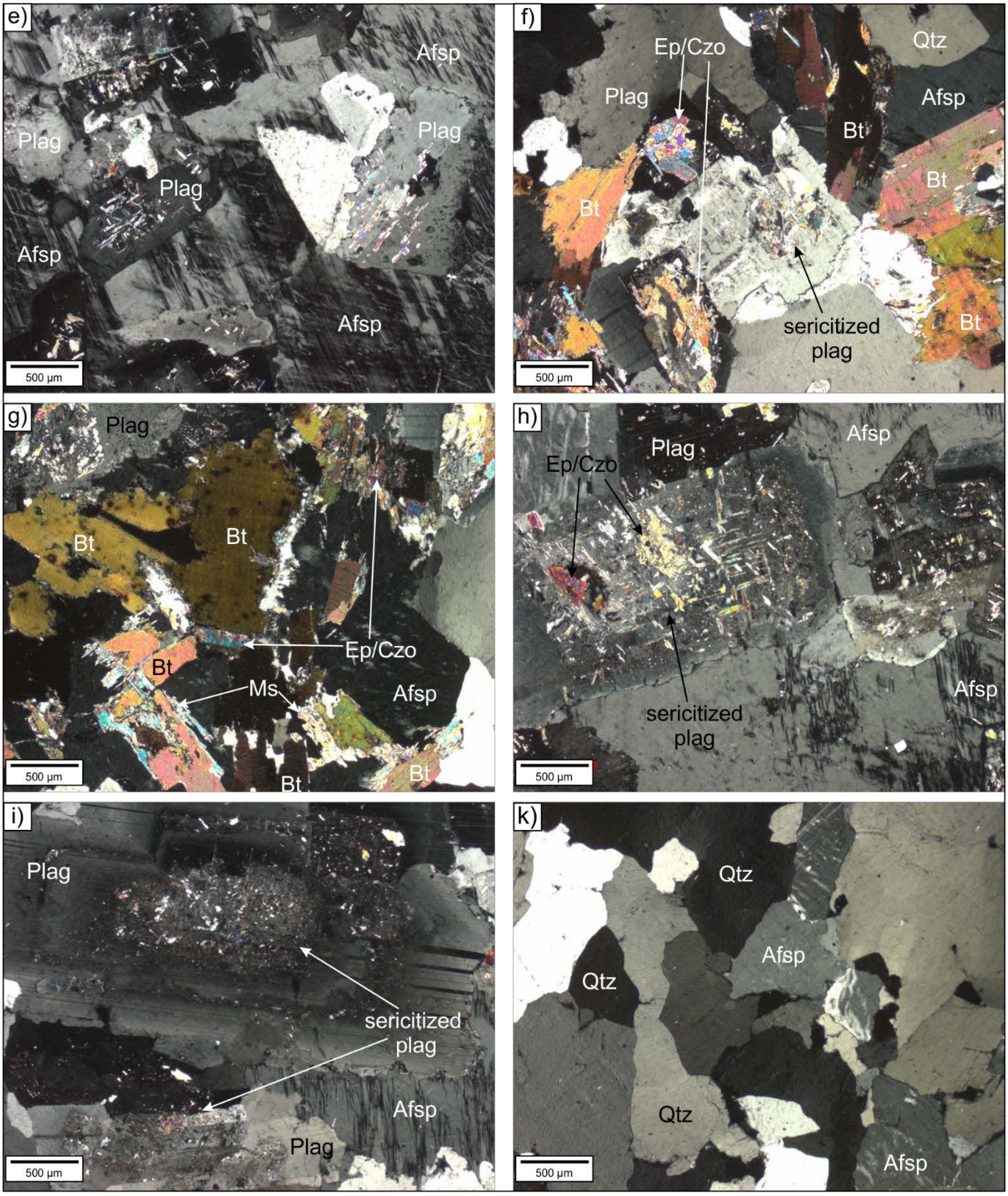


Figure 10: Petrography of sample IG_BH02_PW014 (608.8 mbgs down hole)

Notes: a) Macroscopic appearance of the core, b) Macroscopic appearance of the core section PW014 used for thin section production, c) Overview of the mineral assemblage under transmitted cross-polarized light, d) Overview of the mineral assemblage under transmitted plane-polarized light, e) Quartz cluster with open grain boundaries and unaltered biotite under transmitted cross-polarized light, f) Weakly altered plagioclase and unaltered quartz under transmitted cross-polarized light, g) Unaltered quartz and moderately altered plagioclase containing granular epidote/clinozoisite under transmitted cross-polarized light, h) Moderately altered plagioclase in association with weakly altered biotite and epidote/clinozoisite under transmitted cross-polarized light, i) Weakly altered plagioclase and weakly chloritized biotite and epidote/clinozoisite under transmitted cross-polarized light, k) Weakly altered biotite and margin of muscovite at sutural grain boundaries under transmitted cross-polarized light.


e)
Afsp
Plag
Plag
Plag
Afsp
Afsp
500 µm
f)
Ep/Czo
Qtz
Plag
Afsp
Bt
Bt
Bt
sericitized
plag
Bt
500 µm
g)
Plag
Bt
Bt
Ep/Czo
Bt
Ms
Afsp
Bt
Bt
500 µm
h)
Plag
Afsp
Ep/Czo
sericitized
plag
Afsp
500 µm
i)
Plag
sericitized
plag
Afsp
Plag
500 µm
k)
Qtz
Afsp
Qtz
Qtz
Afsp
500 µm

Sample IG_BH02_PW016 (669.2 mbgs down hole)

Sample IG_BH02_PW016 is a homogenous, equigranular, phaneritic granodiorite. Macroscopically, medium to coarse grained feldspars, and fine to medium grained quartz and biotite can be distinguished (Figure 11a, b). Fine grained sericite, muscovite and epidote/clinozoisite are observed microscopically as alteration products in plagioclase and around undefined grain boundaries of plagioclase and biotite (Figure 11c-k). Quartz and alkali feldspar are free from alteration products (Figure 11e, f, i). Very fine to fine grained apatite, zircon, titanite and opaque minerals are present as accessories.

Plagioclase (51 Vol.%) occurs as xenomorphic-hypidiomorphic fine to medium grained crystals, which are mainly weakly to moderately altered. Only few crystals are highly altered. Most plagioclase crystals contain fine grained sericite, bladed and stalky muscovite crystals and/or epidote/clinozoisite (Figure 11e-h) and few plagioclase crystals contain only fine grained bladed muscovite in the core of the crystal (Figure 11e). Lamellar twinning can be observed in a small proportion of weakly altered crystals (Figure 11e, h, i).

Quartz (24 Vol.%) is present as fine to medium grained crystals and mainly occurs as clusters. Fine grained quartz is mainly present at grain boundaries to plagioclase and biotite, whereas medium grained crystals occur primarily within clusters (Figure 11f, i). Medium grained quartz is frequently surrounded by fine grained quartz (Figure 11c).

Biotite (8 Vol.%) is present as xenomorphic, fine to medium grained bladed crystals showing mainly brown and greenish colours/pleochroism and no, or a low degree of, alteration (Figure 11c-g, k). Only very few biotite crystals show alteration to chlorite. In association with sericitized plagioclase, it seems that some biotite crystals are partially replaced by epidote/clinozoisite (Figure 11h). Sutural grain boundaries of very fine grained muscovite and/or granular epidote/clinozoisite also frequently occur together with sericitized plagioclase (Figure 11f, k). Very fine grained opaque apatite and zircon minerals can be observed as inclusions in some unaltered and weakly altered biotite crystals.

Alkali feldspar (13 Vol.%) occurs as xenomorphic fine to medium grained crystals, frequently showing lamellae of albite (Figure 11e, f). Alteration of alkali feldspar is not observed.

Muscovite and epidote/clinozoisite make up to 5 Vol.%. Muscovite is mainly present as very fine to fine grained needle-like inclusions (sericite) or fine grained bladed crystals in weakly to highly sericitized plagioclase (Figure 11e-k). At a small proportion of biotite grain boundaries, muscovite replaces biotite as a sutural grain boundary or in the shape of fine grained bladed crystals. Epidote/clinozoisite showing abnormal yellow/blue interference colours occurs mainly as very fine to fine grained granular crystals in the core of sericitized plagioclase and adjacent to weakly altered biotite (Figure 11g, k). Epidote/clinozoisite partially replaces some biotite crystals (Figure 11h).

The intergranular pore space between quartz and feldspar minerals is open and not filled with alteration products (Figure 11e, f, i), which appears to reflect natural conditions. Along sutural weakly altered biotite grains, a clear grain boundary is not observed. In the vicinity of altered minerals, the intergranular pore space is open.



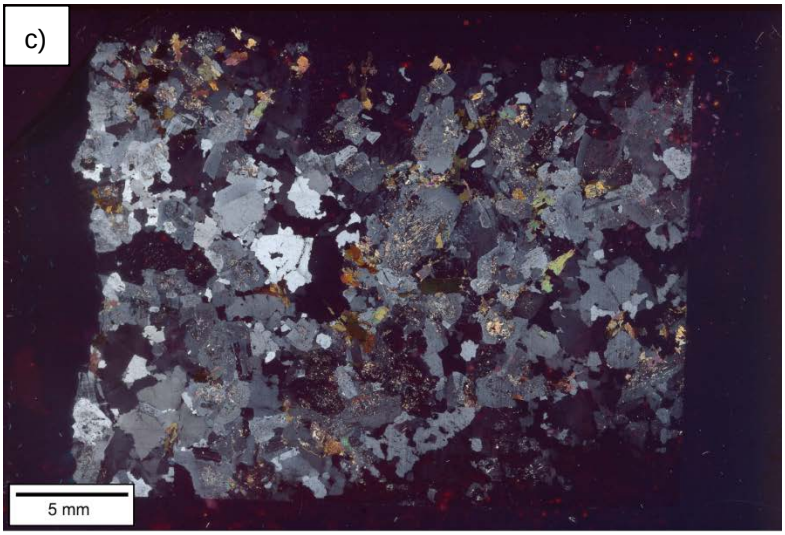
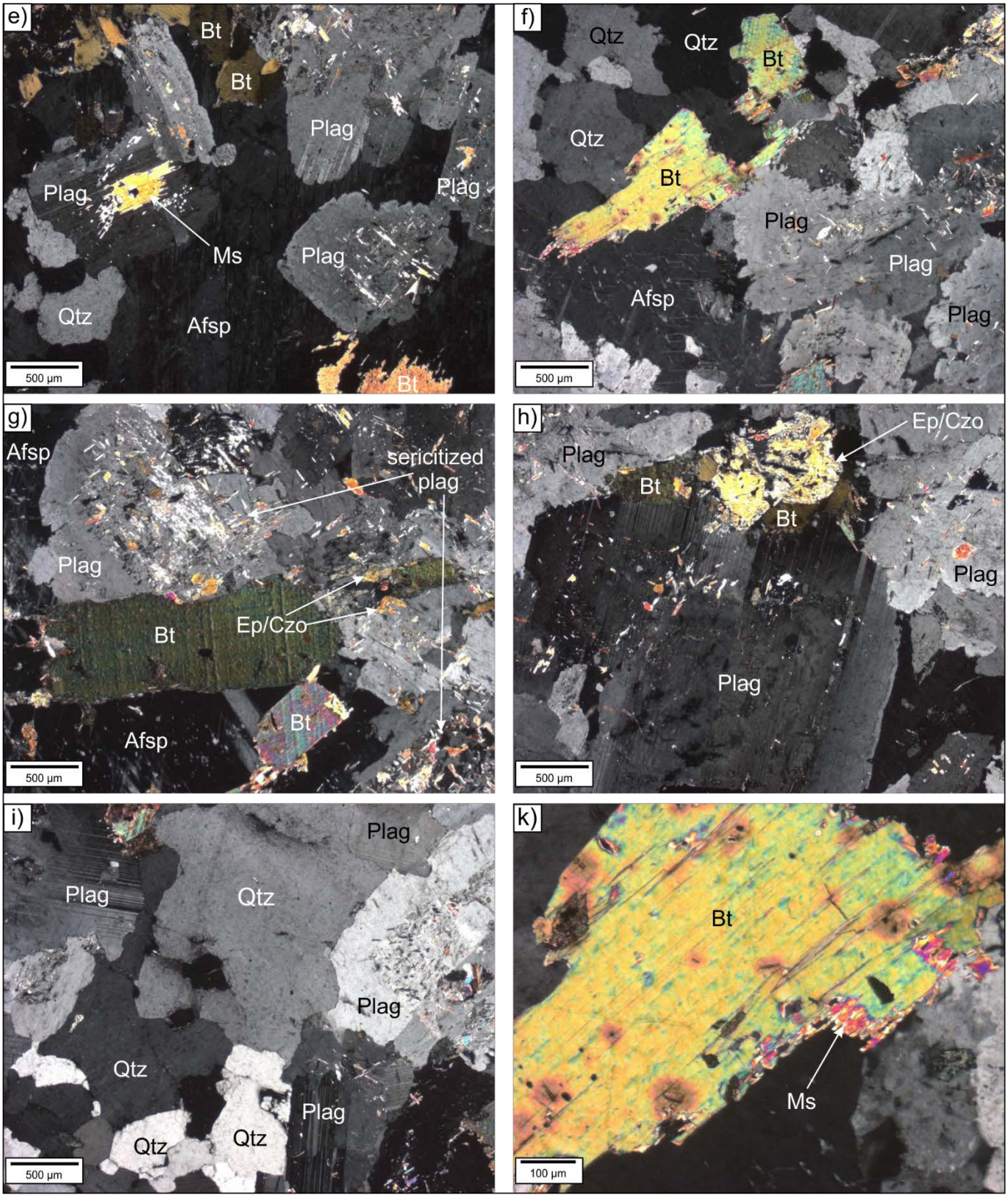




Figure 11: Petrography of sample IG_BH02_PW016 (669.2 mbgs down hole)

Notes: a) Macroscopic appearance of the core, b) Macroscopic appearance of the core section PW0016 used for thin section production, c) Overview of the mineral assemblage under transmitted cross-polarized light, d) Overview of the mineral assemblage under transmitted plane-polarized light, e) Weakly altered plagioclase containing fine grained bladed muscovite and unaltered biotite and alkali feldspar and quartz under transmitted cross-polarized light, f) Weakly altered plagioclase and biotite, and unaltered alkali feldspar and quartz under transmitted cross-polarized light, g) Weakly altered biotite in association with moderately altered plagioclase and epidote/clinozoisite under transmitted cross-polarized light, h) Weakly altered plagioclase and biotite partially replaced by epidote/clinozoisite under transmitted cross-polarized light, i) Cluster of unaltered quartz and weakly to moderately altered plagioclase under transmitted cross-polarized light, k) Weakly altered plagioclase with sutural grain boundary and inclusions of zircon with pleochroic haloes under transmitted cross-polarized light.


e)
Bt
Bt
Plag
Plag
Plag
Ms
Plag
Qtz
Afsp
Bt
500 µm
f)
Qtz
Qtz
Bt
Qtz
Bt
Plag
Plag
Afsp
Plag
500 µm
g)
Afsp
sericitized plag
Plag
Bt
Ep/Czo
Bt
Afsp
500 µm
h)
Ep/Czo
Plag
Bt
Bt
Plag
Plag
500 µm
i)
Plag
Plag
Qtz
Plag
Qtz
Qtz
Qtz
Plag
500 µm
k)
Bt
Ms
100 µm

Sample IG_BH02_PW018 (771.6 mbgs down hole)

Sample IG_BH02_PW018 is a homogenous, equigranular and phaneritic tonalite. Macroscopically, medium to coarse grained feldspar and fine to medium grained quartz and biotite form the bulk of the rock (Figure 12a, b). Microscopically, minor amounts of muscovite, sericite and epidote/clinozoisite are observed as alteration products (Figure 12c-h, k). Very fine grained, opaque minerals, zircon crystals with pleochroic haloes and apatite appear as accessories. The degree of alteration of plagioclase seems to be very low in this rock sample compared to the other rock samples. This might be due to the relatively low biotite content.

Plagioclase (44 Vol.%) is present as xenomorphic-hypidiomorphic fine and medium grained crystals. The main group of plagioclase is unaltered or weakly to moderately altered. Very fine grained sericite and fine grained stalky and bladed muscovite and/or fine grained granular epidote/clinozoisite are present mainly in the core of weakly to moderately altered plagioclase (Figure 12e, f, h). In association with weakly altered or chloritized biotite, muscovite is present in micro-fissures of some plagioclase crystals (Figure 12k).

Quartz makes up to 25 Vol.% of the rock. Xenomorphic, fine to medium grained crystals frequently appear as clusters (Figure 12i). Few fine grained opaque minerals are present as accessories between quartz grains.

The amount of biotite is relatively low in this rock sample (3 Vol.%). Biotite is mainly present as xenomorphic, fine to medium grained crystals showing colours/pleochroism in the range of dark brown(ish) to light green(ish) (Figure 12c, d, g, h). Some biotite crystals show alteration to chlorite and are frequently associated with fine grained granular epidote/clinozoisite (Figure 12e, k). In the vicinity of unaltered alkali feldspar and plagioclase, chloritized biotite is observed (Figure 12e, g). Very fine grained zircons with pleochroic haloes and apatite crystals are observed as inclusions in weakly altered biotite.

The alkali feldspar content is high compared to the other rock samples (25 Vol.%). Alkali feldspar is present as xenomorphic medium to coarse grained crystals showing microcline twinning or a microperthite texture (Figure 12f-h). In association with alkali feldspar no alteration products are present, but some micro-fissures are filled with very fine grained needle-like muscovite (Figure 12g).

The content of muscovite and epidote/clinozoisite in this sample is about 3 Vol.%. Muscovite occurs as fine grained needle-like inclusions (sericite) or as stalky and bladed crystals in weakly to moderately sericitized plagioclase (Figure 12e, f, k). Some biotite crystals seem to be replaced partially by epidote/clinozoisite (Figure 12k).

The pore space between quartz and feldspar crystals is open and not filled with alteration products (Figure 12e-i). Along sutural altered/chloritized biotite grains and next to alteration products, a clear grain boundary is generally not observed (Figure 12e, g, k). In the vicinity of altered minerals, the intergranular pore space is open.



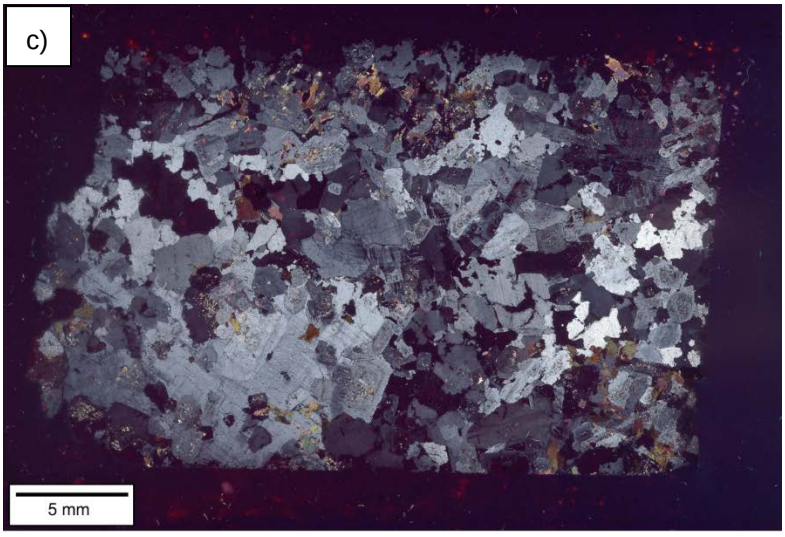
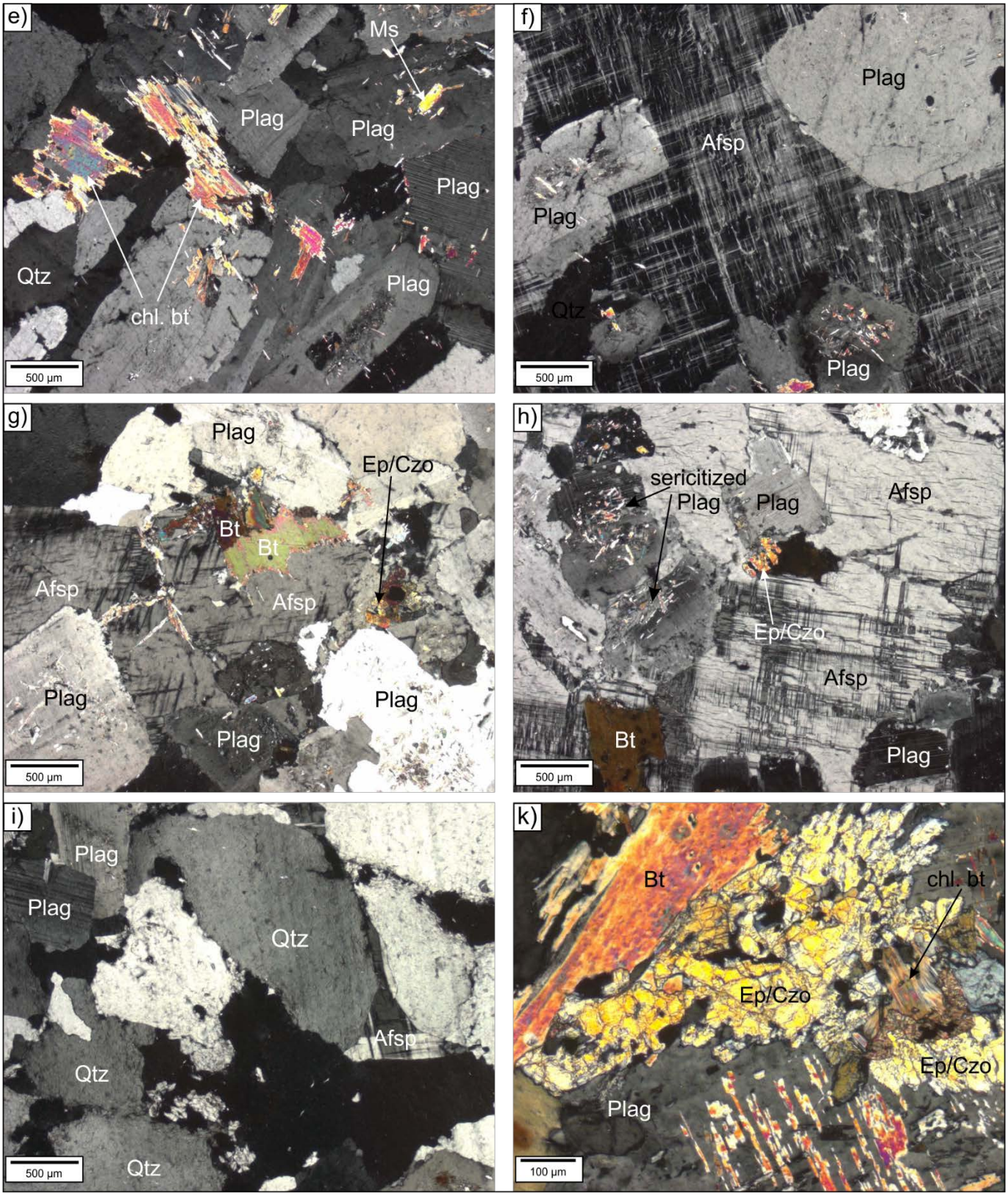




Figure 12: Petrography of sample IG_BH02_PW018 (771.6 mbgs down hole)

Notes: a) Macroscopic appearance of the core, b) Macroscopic appearance of the core section PW0018 used for thin section production, c) Overview of the mineral assemblage under transmitted cross-polarized light, d) Overview of the mineral assemblage under transmitted plane-polarized light, e) Highly altered plagioclase in association with biotite and epidote/clinozoisite under transmitted cross-polarized light, f) Moderately altered plagioclase with mainly granular epidote/clinozoisite in the core and unaltered biotite and epidote/clinzoisite under transmitted cross-polarized light, g) Unaltered quartz and alkali feldspar with microcline twining and altered plagioclase under transmitted cross-polarized light, h) Altered plagioclase in association with weakly altered biotite and epidote/clinozoisite under transmitted cross-polarized light, i) Unaltered biotite and quartz with open grain boundaries under transmitted cross-polarized light, k) Chloritized biotite partially replaced by epidote/clinozoisite under transmitted cross-polarized light.


e)
Ms
Plag
Plag
Plag
Qtz
chl. bt
Plag
500 µm
f)
Plag
Afsp
Plag
Qtz
Plag
500 µm
g)
Plag
Ep/Czo
Bt
Bt
Afsp
Afsp
Plag
Plag
Plag
500 µm
h)
sericitized
Plag
Plag
Afsp
Ep/Czo
Afsp
Bt
Plag
500 µm
i)
Plag
Plag
Qtz
Afsp
Qtz
Qtz
500 µm
k)
Bt
chl. bt
Ep/Czo
Ep/Czo
Plag
100 µm

Sample IG_BH02_PW020 (880.4 mbgs down hole)

Sample IG_BH02_PW020 is a homogenous, equigranular, phaneritic granodiorite (Figure 13a, b). Macroscopically, fine to medium grained feldspar, quartz and biotite can be distinguished (Figure 13b). Minor amounts of muscovite, sericite and epidote/clinozoisite are observed microscopically as alteration products (Figure 13c-f, h, k). Apatite, zircon and opaque minerals are present as accessories.

Plagioclase (43 Vol.%) is present as xenomorphic-hypidiomorphic fine to medium grained crystals showing variable degrees of alteration. In moderately to highly altered plagioclase micro-fissures are often filled with fine grained needle-like sericite and/or very fine granular epidote/clinozoisite (Figure 13h). Unaltered or weakly altered plagioclase crystals that are not associated with biotite contain fine grained fibrous or needle-like muscovite as inclusions and frequently show lamellar twinning (Figure 13f, g).

The quartz content is high compared to the other rock samples (39 Vol.%). Quartz mainly occurs as xenomorphic-hypidiomorphic fine to medium (few coarse) grained crystals. Quartz is frequently arranged in the shape of clusters and no alteration products can be observed between quartz grains (Figure 13i). Few fine grained opaque minerals are observed as accessories between quartz grains.

Biotite (8 Vol.%) is present as xenomorphic-hypidiomorphic fine to medium grained crystals showing no, or a low degree of, alteration (Figure 13e, f, k). Some weakly altered crystals are associated with granular epidote/clinozoisite (Figure 13f, k) and fine grained needle-like muscovite, which is present as a margin around weakly altered biotite and at sutural grain boundaries (Figure 13e). Very fine grained zircons with pleochroic haloes and apatite crystals are observed as inclusions in weakly altered biotite.

Alkali feldspar (7 Vol.%) occurs as xenomorphic fine to medium grained crystals showing no alteration products. The main group of alkali feldspar shows microcline twinning or lamellae of albite (Figure 13g, h).

Very fine grained sericite, and very fine to fine grained muscovite and epidote/clinozoisite (2 Vol.%) occur as alteration products in weakly to highly sericitized plagioclase and in association with weakly altered biotite (Figure 13c-f, h, k). In association with weakly altered biotite, muscovite is present at sutural grain boundaries of biotite (Figure 13e). Epidote/clinozoisite is also present in the vicinity of weakly altered biotite (Figure 13f, k).

The pore space between quartz grains is open and not filled with alteration products (Figure 13f, i). In association with weakly altered biotite, the grain boundaries are not defined due to a margin of fine grained needle-like muscovite (Figure 13e).



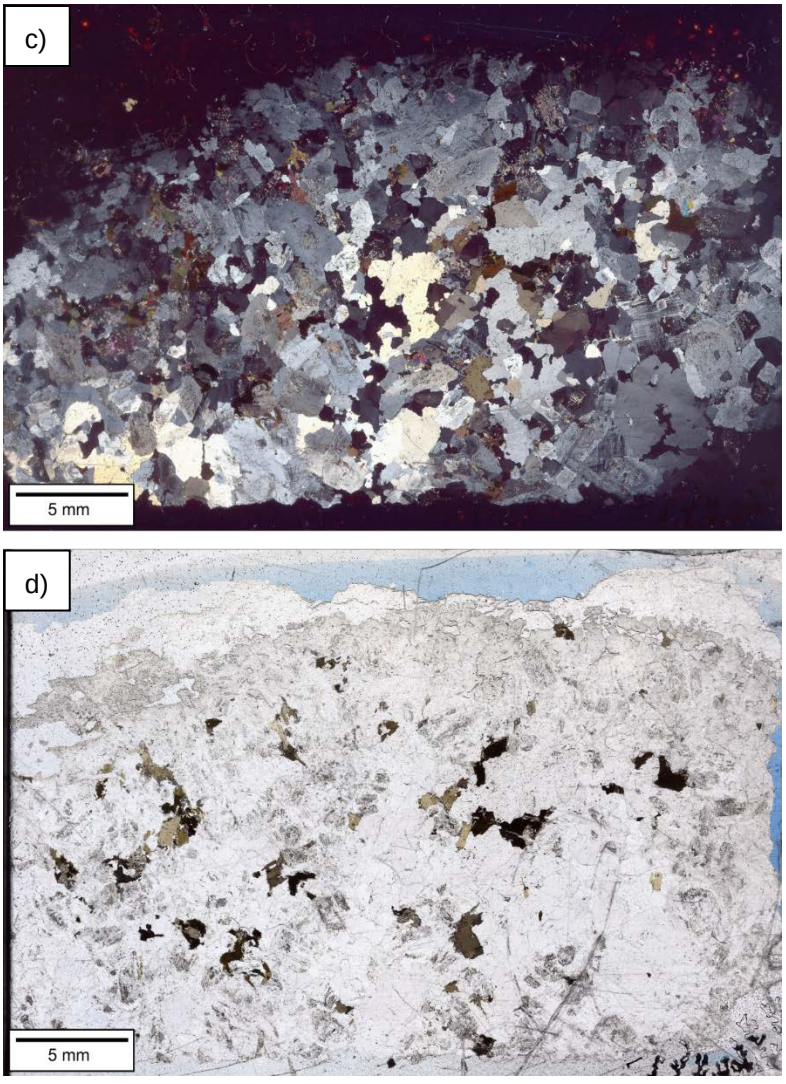
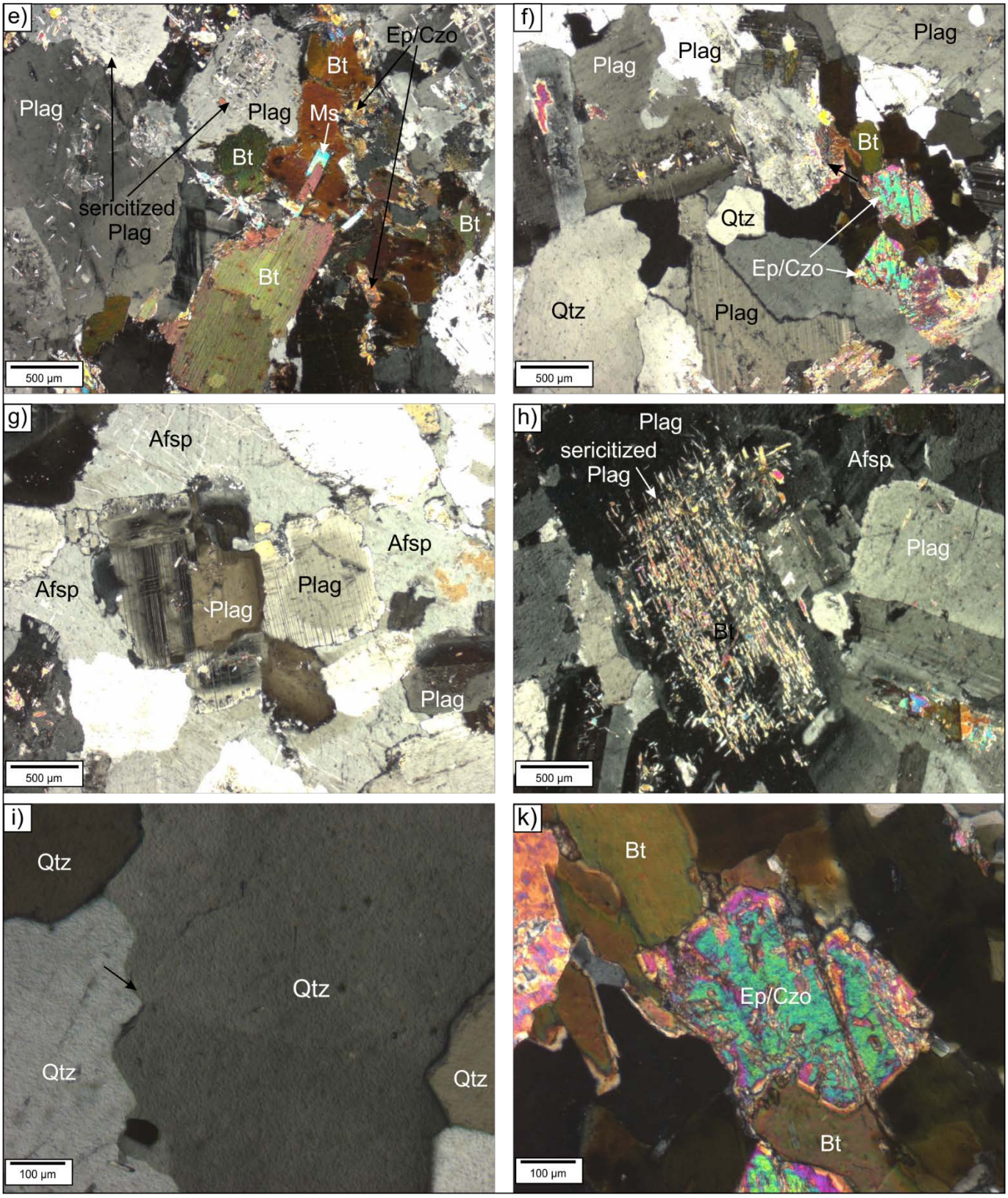


Figure 13: Petrography of sample IG_BH02_PW020 (880.4 mbgs down hole)

Notes: a) Macroscopic appearance of the core, b) Macroscopic appearance of the core section PW020 used for thin section production, c) Overview of the mineral assemblage under transmitted cross-polarized light, d) Overview of the mineral assemblage under transmitted plane-polarized light, e) Weakly altered biotite associated with epidote/clinozoisite and sericitized plagioclase under transmitted cross-polarized light, f) Non altered to weakly altered plagioclase and biotite partially replaced by epidote/clinozoisite under transmitted cross-polarized light, g) Plagioclase and alkali feldspar without alteration products under transmitted cross-polarized light, h) Highly sericitized plagioclase in the vicinity of unaltered plagioclase and alkali feldspar under transmitted cross-polarized light, i) Cluster of quartz crystals under transmitted cross-polarized light, k) Biotite and epidote/clinozoisite under transmitted cross-polarized light.


e)
Ep/Czo
Bt
Plag
Plag
Ms
Bt
sericitized
Plag
Bt
Bt
500 µm
f)
Plag
Plag
Plag
Bt
Qtz
Ep/Czo
Qtz
Plag
500 µm
g)
Afsp
Afsp
Afsp
Plag
Plag
Plag
500 µm
h)
Plag
sericitized
Plag
Afsp
Plag
Bt
500 µm
i)
Qtz
Qtz
Qtz
Qtz
100 µm
k)
Bt
Ep/Czo
Bt
100 µm

Sample IG_BH02_PW022 (984.7 mbgs down hole)

Sample IG_BH02_PW022 is a homogenous, equigranular, phaneritic tonalite. It is mainly composed of fine to medium grained feldspar, quartz and biotite (Figure 14a, b). The proportion of alkali feldspar which can be distinguished microscopically from plagioclase is very low in this thin section (Figure 14d). Minor amounts of muscovite, sericite and epidote/clinozoisite occur as alteration products (Figure 14c-f, i, k). Apatite, zircon, and opaque minerals are present as accessories.

Plagioclase makes up to 52 Vol.% and occurs as xenomorphic–hypidiomorphic, fine to medium grained crystals. In this rock sample, plagioclase shows varying degrees of alteration. Some plagioclase crystals are unaltered or weakly altered and show lamellar twinning or a strong zonation (Figure 14e, f). Moderately altered plagioclase contains fine grained sericite, fine grained stalky and bladed muscovite and/or fine grained granular epidote/clinozoisite (Figure 14i, k). Only a small proportion of crystals show a high degree of alteration. In association with weakly altered biotite, epidote/clinozoisite is frequently present (Figure 14e, k).

Quartz (34 Vol.%) occurs as xenomorphic and mainly fine to medium grained crystals, and frequently occurs in the form of clusters (Figure 14g). Few crystals are coarse grained. No alteration products are observed between quartz grains.

Biotite (6 Vol.%) is present as xenomorphic, fine to medium grained bladed crystals showing mainly brown and greenish colours/pleochroism (Figure 14c). In this rock sample, no alteration of biotite to chlorite is observed. Weakly altered crystals seem to be partially replaced by fine grained epidote/clinozoisite. In association with altered plagioclase, epidote/clinozoisite is frequently present at biotite grain boundaries (Figure 14e, f, k). Very fine grained opaque minerals, apatite and zircons can be observed as inclusions in some unaltered or weakly altered biotite crystals.

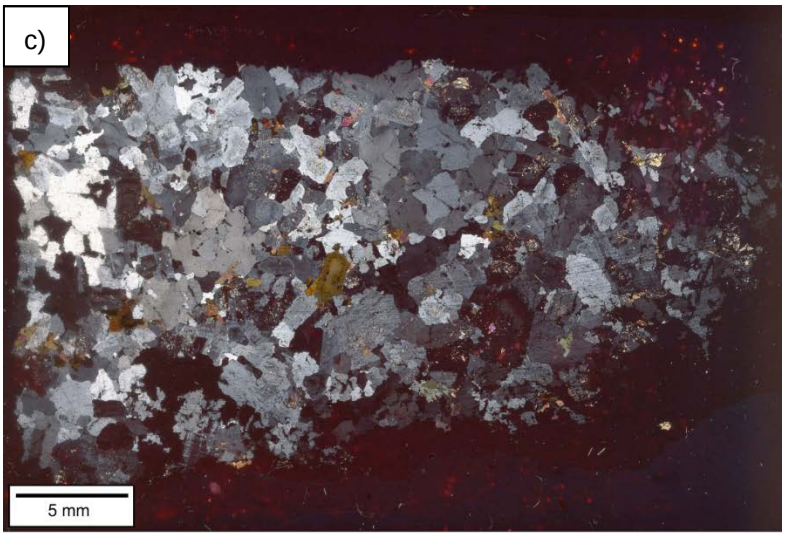
The alkali feldspar content is very low compared to the other thin sections (5 Vol.%). Alkali feldspar is present as xenomorphic fine grained crystals, which are unaltered. Some crystals show lamellae of albite (microcline-perthite) or microcline twinning (Figure 14h, i).

Sericite, muscovite and epidote/clinozoisite (3 Vol.%) occur as very fine to fine grained needle-like, bladed or granular inclusions in weakly to moderately altered plagioclase (Figure 14c-f, h, k). In association with weakly altered biotite and altered plagioclase, epidote/clinozoisite is also frequently present and appears to partially replace some biotite crystals (Figure 14e).

The pore space between quartz and feldspar grains is open and free from alteration products (Figure 14g). In association with some weakly altered biotite, the grain boundaries are not defined due to a margin of fine grained needle-like muscovite or granular epidote/clinozoisite (Figure 14e, k).

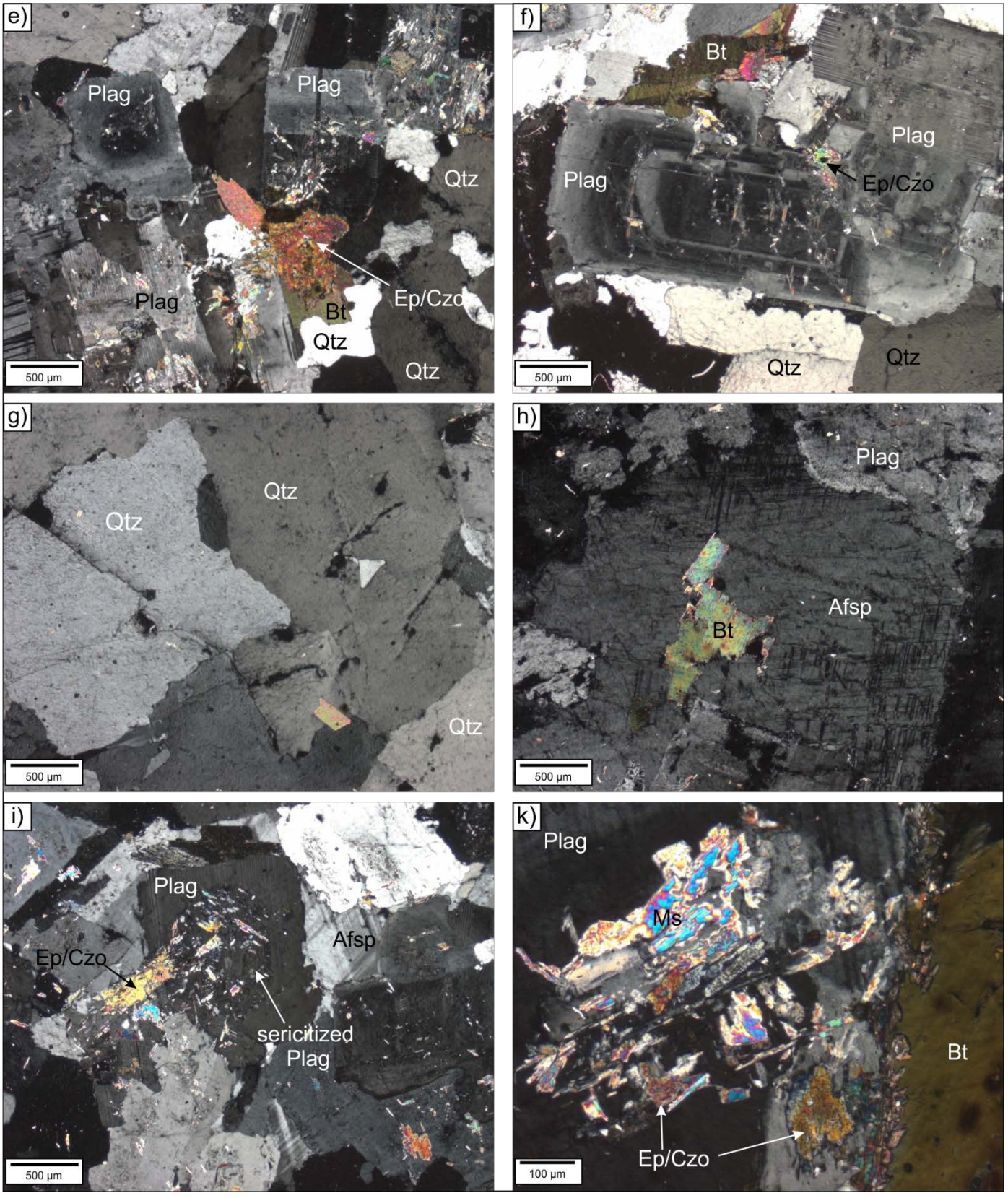


Figure 14: Petrography of sample IG_BH02_PW022 (984.7 mbgs down hole)





Notes: a) Macroscopic appearance of the core, b) Macroscopic appearance of the core section PW0022 used for thin section production, c) Overview of the mineral assemblage under transmitted cross-polarized light, d) Overview of the mineral assemblage under transmitted plane-polarized light, e) Epidote/clinozoisite in association with biotite and unaltered to weakly altered plagioclase under transmitted cross-polarized light, f) Unaltered plagioclase showing strong zonation and unaltered quartz under transmitted cross-polarized light, g) Cluster of quartz crystals under transmitted cross-polarized light, h) Unaltered plagioclase containing fine grained unaltered biotite under transmitted cross-polarized light, i) Weakly altered plagioclase in association with epidote/clinozoisite under transmitted cross-polarized light, k) Muscovite and epidote/clinozoisite inclusions in plagioclase in vicinity to biotite under transmitted cross-polarized light.


e)
Plag
Plag
Qtz
Ep/Czo
Plag
Bt
Qtz
Qtz
500 µm
f)
Bt
Plag
Plag
Ep/Czo
Qtz
Qtz
500 µm
g)
Qtz
Qtz
Qtz
500 µm
h)
Plag
Afsp
Bt
500 µm
i)
Plag
Afsp
Ep/Czo
sericitized
Plag
500 µm
k)
Plag
Ms
Bt
Ep/Czo
100 µm

5.0 WATER CONTENT AND WATER-LOSS POROSITY

Water content, bulk density and water-loss porosity were determined on originally saturated segments of the core samples from borehole IG_BH02. The water content was determined by two independent methods, i.e., gravimetrically by drying rock sections at 105 °C to stable weight conditions, and by using the isotope diffusive exchange technique (see Section 3). The gravimetric water content (WC_{grav}) was determined on different segments of the core samples (i.e., on those pieces used for the individual experiments). The initial saturated weight of all these samples was recorded directly after unpacking and preparation of the samples in the laboratory. This ensures that the calculation of the porewater mass is not affected by any possible changes induced during the experiments. Such possible changes were monitored as well by recording the sample weight right after termination of the experiment and before the drying process began. The water loss was calculated using the initial wet weight measured in the lab and the final weight after drying.

The exact determination of the in-situ mass of porewater is of particular importance when using indirect extraction methods, because porewater tracer concentrations are calculated by mass balance equations using the mass of porewater (cf. Section 3). Knowledge of the water-loss porosity (calculated from the water content and density) is further required for the derivation of diffusion coefficients (cf. Section 7).

5.1 Water contents

Gravimetric water contents were determined on the individual core segments used for the specific experiments (cf. Section 3).

5.1.1 Gravimetric water contents determined on aqueous extraction core samples

The gravimetric water contents were determined on different aliquots, with weights between 84 g and 419 g, of the twelve AQ samples taken between 240 and 985 mbgs (down hole). These values were further used for the estimation of porewater Cl- and Br-concentrations determined by aqueous extraction experiments (cf. Chapter 6.1).

The gravimetric water contents determined on individual aliquots of the AQ samples vary between 0.15 wt.% and 0.34 wt.%, with weighted values ranging between 0.16 ± 0.01 and 0.29 ± 0.04 wt.% (Table 8).

The water contents determined by taking the wet (WC_{wet}) and dry weight (WC_{dry}) are similar within the first two decimal places due to the low water masses in the investigated cores.

The water contents determined on the individual aliquots of the different AQ samples vary significantly, probably due to mineralogical heterogeneities.

Table 8: Gravimetric water contents of aliquots of AQ core samples from borehole IG_BH02 used for aqueous extraction experiments using wet (WC_{wet}) and dry masses (WC_{dry}) of the individual core pieces. The weighted values are calculated using the individual masses

		Aq.ex. subsample A			Aq.ex. subsample B			Aq.ex. subsample C			WC weighted		
Sample	Depth	mass	WC_{wet}	WC_{dry}	mass	WC_{wet}	WC_{dry}	mass	WC_{wet}	WC_{dry}	WC_{wet}	WC_{dry}	Stdev
	mbgs	g	wt.%	wt.%	g	wt.%	wt.%	g	wt.%	wt.%	wt.%	wt.%	wt.%
IG_BH02_AQ001	240.2	325.84	0.17	0.17	87.40	0.26	0.26	84.55	0.21	0.21	0.19	0.19	0.04
IG_BH02_AQ002	348.5	356.78	0.17	0.17	102.63	0.16	0.16	187.24	0.17	0.17	0.17	0.17	0.01
IG_BH02_AQ003	379.6	419.46	0.28	0.28	209.45	0.27	0.27	161.92	0.34	0.34	0.29	0.29	0.04
IG_BH02_AQ004	382.0	317.55	0.17	0.17	120.94	0.18	0.18	126.18	0.19	0.20	0.18	0.18	0.01
IG_BH02_AQ005	455.5	383.98	0.23	0.23	121.26	0.26	0.26	136.26	0.32	0.32	0.25	0.25	0.05
IG_BH02_AQ006	530.8	306.69	0.22	0.22	126.12	0.24	0.24	131.69	0.27	0.27	0.24	0.24	0.02
IG_BH02_AQ007	555.1	334.45	0.20	0.20	176.31	0.20	0.21	170.67	0.21	0.21	0.20	0.20	0.01
IG_BH02_AQ008	611.4	282.64	0.17	0.17	116.82	0.19	0.19	171.80	0.18	0.18	0.18	0.18	0.01
IG_BH02_AQ009	666.1	313.24	0.17	0.17	137.37	0.23	0.23	166.30	0.20	0.20	0.19	0.19	0.03
IG_BH02_AQ010	771.4	234.05	0.15	0.15	137.38	0.17	0.17	132.79	0.16	0.17	0.16	0.16	0.01
IG_BH02_AQ011	879.0	361.47	0.17	0.17	146.04	0.17	0.17	155.51	0.17	0.17	0.17	0.17	0.01
IG_BH02_AQ012	984.5	293.66	0.17	0.17	112.01	0.19	0.19	125.18	0.20	0.20	0.18	0.18	0.02

* mbgs (down hole)

5.1.2 Gravimetric water contents determined on porewater cores

Gravimetric water contents were determined on different aliquots of the thirteen large sized PW samples taken between 240 mbgs and 984 mbgs (down hole).

Gravimetric water contents determined on head pieces

During sample preparation, the head pieces with weights between 143 g and 323 g were cut, weighed and dried at 105 °C to obtain a first estimate about the water contents of the investigated core samples.

The gravimetric water contents determined on the head pieces of the PW core samples vary between 0.16 wt.% and 0.34 wt.%, with weighted WC_{grav} values between 0.16 ± 0.01 wt.% and 0.29 ± 0.09 wt.% (Table 9).

The water contents determined by taking the wet (WC_{wet}) and dry weight (WC_{dry}) are similar within the first two decimal places due to the low water masses in the investigated cores.

The water contents determined on the two head pieces of the different PW samples vary, which is most likely due to mineralogical heterogeneities.

Table 9: Gravimetric water contents of head pieces of PW core samples from borehole IG_BH02 using wet (WC_{wet}) and dry masses (WC_{dry}) of the individual core pieces. The weighted values are calculated using the individual masses

		Subsample A			Subsample B			WC weighted		
Sample	Depth	mass	WCwet	WCdry	mass	WCwet	WCdry	WCwet	WCdry	Stdev
	mbgs	g	wt.%	wt.%	g	wt.%	wt.%	wt.%	wt.%	wt.%
IG_BH02_PW001	240.0	151.8	0.23	0.23	183.6	0.22	0.22	0.22	0.22	0.01
IG_BH02_PW003	348.0	154.1	0.17	0.17	283.3	0.18	0.18	0.18	0.18	0.01
IG_BH02_PW005	378.1	228.2	0.25	0.25	306.7	0.30	0.30	0.28	0.28	0.04
IG_BH02_PW006	381.7	181.8	0.24	0.24	170.0	0.17	0.17	0.20	0.21	0.05
IG_BH02_PW007	383.0	143.2	0.21	0.21	218.1	0.34	0.34	0.29	0.29	0.09
IG_BH02_PW008	455.2	176.4	0.32	0.33	150.4	0.22	0.22	0.28	0.28	0.07
IG_BH02_PW010	502.8	167.3	0.20	0.20	323.7	0.23	0.23	0.22	0.22	0.02
IG_BH02_PW012	555.7	229.8	0.21	0.21	198.8	0.21	0.21	0.21	0.21	0.01
IG_BH02_PW014	611.2	203.3	0.23	0.23	249.6	0.20	0.20	0.21	0.21	0.02
IG_BH02_PW016	665.8	244.4	0.19	0.19	190.5	0.20	0.20	0.20	0.20	0.01
IG_BH02_PW018	770.6	242.7	0.17	0.17	174.0	0.16	0.16	0.17	0.17	0.01
IG_BH02_PW020	878.8	182.9	0.16	0.16	158.7	0.16	0.16	0.16	0.16	0.01
IG_BH02_PW022	984.2	162.4	0.22	0.22	282.6	0.21	0.21	0.21	0.21	0.01

* mbgs (down hole)

5.1.3 Gravimetric water contents determined on out-diffusion cores

Gravimetric water contents on large sized 1,411 g to 1,477 g core pieces were determined by the weights taken before and after their long-term immersion in deionised water during out-diffusion experiments. The weight differences of cores before and after out-diffusion experiments are between 0.002 g and 0.270 g (Table 10, Figure 15). Seven of the 13 samples have weights between 0.002 g to 0.062 g lower after the experiments than before the experiments. These differences, resulting from the determination of the initial weight after surface drying of the cores (as defined in Section 3.2), have only a very minor influence on the water contents at the given accuracy (Table 5). Five samples have weights between 0.099 g and 0.270 g higher than before the experiments. The weight gain might indicate 1) the influence of stress release and the saturation of newly created pore space or 2) evaporation during the time between recovery and sealing.

The gravimetric water contents determined on the out-diffusion cores vary between 0.17 wt.% and 0.24 wt.% with weighted WC_{grav} values ranging between 0.15 ± 0.01 wt.% and 0.22 ± 0.01 wt.% (Table 10). The weight differences of the core samples determined before (b.e.) and after the experiments (a.e.) result in water content variations of 0.02 wt.% or less for all thirteen samples (Table 10, Figure 16). These differences are within the error ranges determined by Gaussian error propagation (Table 10, Figure 16). The water contents determined by taking the wet (WC_{wet}) and dry weight (WC_{dry}) are similar within the first two decimal places due to the low water masses in the investigated cores (Table 10).

Table 10: Gravimetric water contents of out-diffusion core samples from borehole IG_BH02 calculated by the mass of cores determined before (b.e.) and after (a.e.) experiments using wet (WC_{wet}) and dry masses (WC_{dry}) of the individual core pieces; the error of the water content is determined by Gaussian error propagation (Appendix III)

		mass core			mass porewater		$WC_{grav,wet}$		$WC_{grav,dry}$		error WC_{grav}
Sample	Depth	wet b.e.	wet a.e.	Δm_{core}	m_{core} b.e.	m_{core} a.e.	m_{core} b.e.	m_{core} a.e.	m_{core} b.e.	m_{core} a.e.	
	mbgs*	G	G	g	g	g	wt.%	wt.%	wt.%	wt.%	wt.%
IG_BH02_PW001	240.0	1477.468	1477.466	-0.002	2.930	2.928	0.20	0.20	0.20	0.20	0.01
IG_BH02_PW003	348.0	1473.575	1473.680	0.105	2.278	2.383	0.15	0.16	0.15	0.16	0.01
IG_BH02_PW005	378.1	1450.139	1450.077	-0.062	1.550	1.488	0.11	0.10	0.11	0.10	0.01
IG_BH02_PW006	381.7	1428.741	1428.665	-0.076	2.453	2.377	0.17	0.17	0.17	0.17	0.01
IG_BH02_PW007	383.0	1437.323	1437.312	-0.011	2.489	2.478	0.17	0.17	0.17	0.17	0.01
IG_BH02_PW008	455.2	1407.760	1407.724	-0.036	3.048	3.012	0.22	0.21	0.22	0.21	0.01
IG_BH02_PW010	502.8	1460.395	1460.505	0.110	3.031	3.141	0.21	0.22	0.21	0.22	0.01
IG_BH02_PW012	555.7	1411.850	1411.845	-0.005	2.744	2.739	0.19	0.19	0.19	0.19	0.01
IG_BH02_PW014	611.2	1450.400	1450.344	-0.056	2.478	2.422	0.17	0.17	0.17	0.17	0.01
IG_BH02_PW016	665.8	1462.393	1462.355	-0.038	2.904	2.866	0.20	0.20	0.20	0.20	0.01
IG_BH02_PW018	770.6	1450.160	1450.430	0.270	2.413	2.683	0.17	0.18	0.17	0.19	0.02
IG_BH02_PW020	878.8	1448.892	1449.060	0.168	2.428	2.596	0.17	0.18	0.17	0.18	0.02
IG_BH02_PW022	984.2	1441.711	1441.810	0.099	2.743	2.842	0.19	0.20	0.19	0.20	0.01

***** mbgs (down hole)

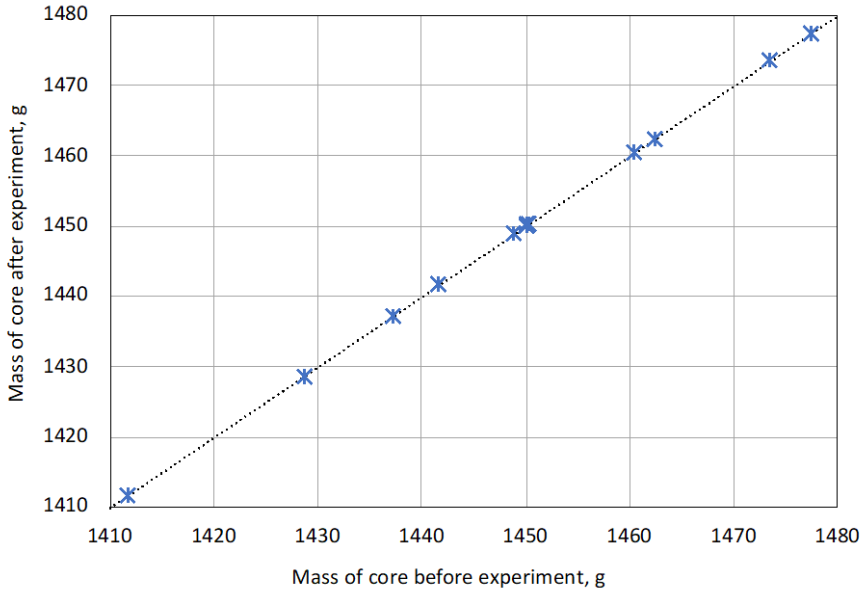


Figure 15: Mass of core samples from borehole IG_BH02 before and after the out-diffusion experiments; the uncertainty of the core mass is ± 0.05 g

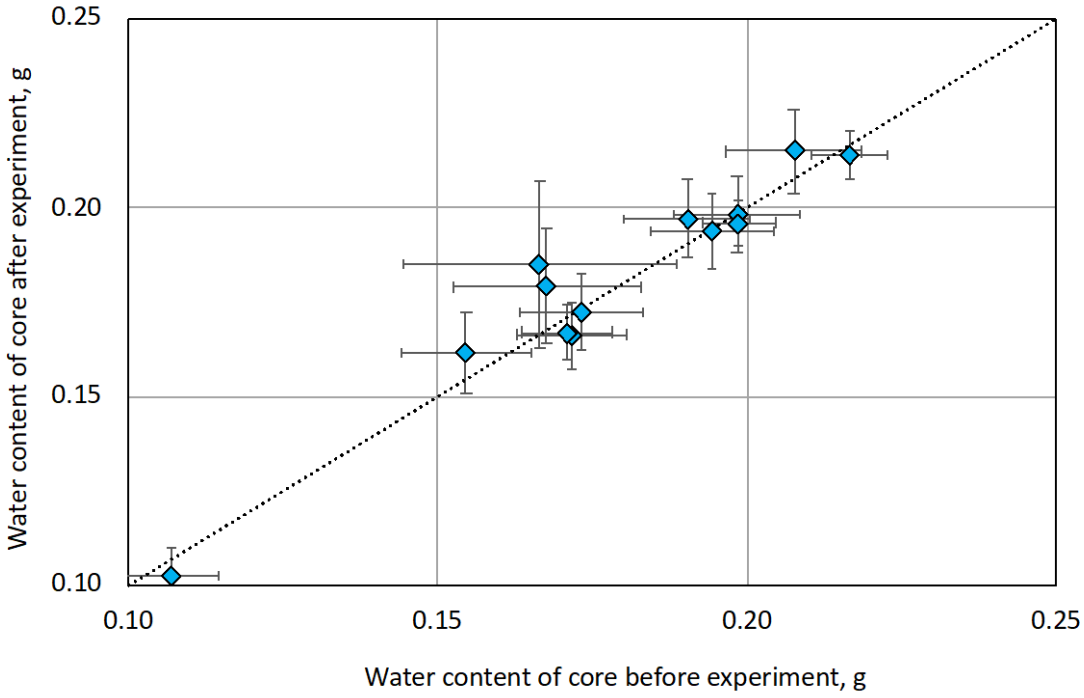


Figure 16: Water content calculated from the wet mass before and after the out-diffusion experiments of core sections from borehole IG_BH02; the error of the water content is determined by Gaussian error propagation (Appendix III)

5.1.4 Water contents determined by isotope diffusive exchange

Gravimetric water contents were determined on crushed core pieces used for the isotope diffusive exchange experiments. The masses of the used rock material are measured before and after the experiments. During the experiments the rocks remain saturated. A weight change of the rocks above the analytical uncertainty of ± 0.05 g (constant total weight) was observed in 14 experiments (Table 11). Therefore, the water contents were corrected for the weight loss or gain.

The gravimetric water contents determined on rock pieces used for isotope diffusive exchange experiments ($WC_{IsoEx,grav,corr.}$) vary between 0.11 wt.% and 0.18 wt.% with weighted $WC_{IsoEx,grav}$ values ranging from 0.11 ± 0.01 wt.% to 0.17 ± 0.01 wt.% (Table 11).

The water contents determined by the isotope diffusive exchange technique (WC_{IsoEx}) for core samples from borehole IG_BH02 vary between 0.16 ± 0.01 wt.% and 0.22 ± 0.02 wt.% (Table 12). The water contents determined by isotope diffusive exchange are slightly higher than those determined gravimetrically (Table 11 and Table 10, Figure 17).

Table 11: Gravimetric water contents determined on core samples from borehole IG_BH02 used for isotope diffusive exchange experiments ($WC_{IsoEx,grav}$); water contents are corrected for weight changes during the experiments (b.e.=before experiment, a.e. = after experiment); the gravimetric water contents determined on the rock pieces used in the experiments with LAB- and SSI-water are weighted; the error is determined by Gaussian error propagation (Appendix III)

	LAB				SSI				$WC_{IsoEx,grav.}$ weighted,corr.
	mass	Δm (a.e.-b.e.)	$WC_{IsoEx,grav}$	$WC_{IsoEx,grav,corr.}$	mass	Δm (a.e.-b.e.)	$WC_{IsoEx,grav}$	$WC_{IsoEx,grav,corr.}$	
	G	g	wt.%	wt.%	g	g	wt.%	wt.%	wt. %
IG_BH02_PW001	334.3	0.043	0.15	0.16	334.6	0.060	0.15	0.17	0.17±0.01
IG_BH02_PW003	369.9	0.093	0.12	0.14	372.5	0.110	0.11	0.14	0.14±0.01
IG_BH02_PW005	275.2	-0.052	0.13	0.11	275.4	-0.060	0.13	0.11	0.11±0.01
IG_BH02_PW006	303.5	-0.025	0.16	0.15	307.5	-0.020	0.14	0.14	0.14±0.01
IG_BH02_PW007	398.0	-0.013	0.15	0.15	396.3	-0.003	0.16	0.16	0.15±0.01
IG_BH02_PW008	383.8	-0.010	0.16	0.16	376.8	-0.028	0.18	0.17	0.17±0.01
IG_BH02_PW010	389.5	0.048	0.15	0.16	385.8	0.095	0.15	0.18	0.17±0.01
IG_BH02_PW012	410.3	0.031	0.13	0.14	430.5	0.005	0.15	0.15	0.15±0.01
IG_BH02_PW014	380.6	-0.043	0.15	0.14	381.7	-0.025	0.14	0.14	0.14±0.01
IG_BH02_PW016	368.6	-0.151	0.20	0.16	364.4	-0.160	0.20	0.15	0.16±0.01
IG_BH02_PW018	374.9	-0.069	0.16	0.15	354.2	-0.070	0.16	0.14	0.14±0.01
IG_BH02_PW020	401.1	-0.122	0.18	0.14	388.2	-0.158	0.18	0.14	0.14±0.01
IG_BH02_PW022	383.1	-0.155	0.21	0.16	361.5	-0.152	0.20	0.16	0.16±0.01

Table 12: Water contents of core samples from borehole IG_BH02 calculated by the isotope diffusive exchange method (cf. eq. 7); the error of the water content is determined by Gaussian error propagation (Appendix III)

	WC_{IsoEx} ($\delta^{18}O$)	WC_{IsoEx} ($\delta^{2}H$)	WC_{IsoEx} average
	wt.%	wt.%	wt.%
IG_BH02_PW001	0.19±0.01	0.19±0.02	0.19±0.02
IG_BH02_PW003	0.18±0.01	0.18±0.01	0.18±0.01
IG_BH02_PW005	0.16±0.01	0.17±0.02	0.17±0.02
IG_BH02_PW006	0.18±0.01	0.18±0.02	0.18±0.02
IG_BH02_PW007	0.19±0.01	0.19±0.01	0.19±0.01
IG_BH02_PW008	0.20±0.01	0.19±0.01	0.19±0.01
IG_BH02_PW010	0.22±0.01	0.21±0.02	0.22±0.02
IG_BH02_PW012	0.18±0.01	0.17±0.01	0.17±0.01
IG_BH02_PW014	0.18±0.01	0.17±0.01	0.18±0.01
IG_BH02_PW016	0.20±0.01	0.19±0.01	0.20±0.01
IG_BH02_PW018	0.17±0.01	0.18±0.01	0.18±0.01
IG_BH02_PW020	0.16±0.01	0.16±0.01	0.16±0.01
IG_BH02_PW022	0.18±0.01	0.19±0.01	0.18±0.01

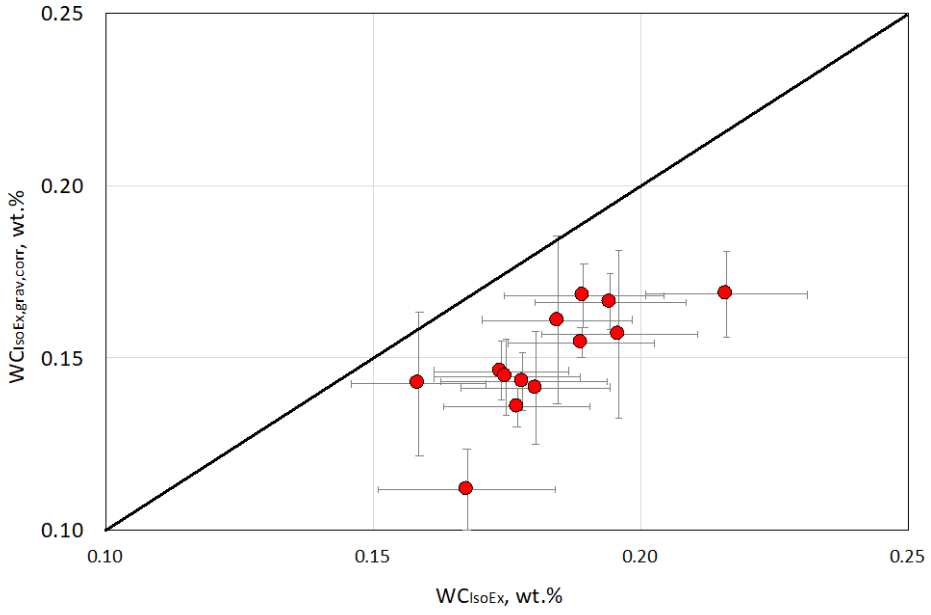


Figure 17: Comparison of water contents determined by isotope diffusive exchange (WC_{IsoEx}) and gravimetrically ($WC_{IsoEx,grav}$, by wet weight, corrected for weight change during experiments) on the same core pieces; the error of the water content is determined by Gaussian error propagation

5.1.5 Summary and depth profiles of water content results

The gravimetric water contents determined on the AQ and PW cores are weighted by the masses of the individual rock pieces (Table 13). The weighted water content represents the entire core, with masses between 497 g and 790 g for AQ cores and between 2,391 g and 2,726 g for PW cores. As noted, the water contents of the individual aliquots vary, which is presumed to be caused by mineralogical heterogeneities. This indicates that water content values cannot be extrapolated.

The weighted gravimetric water contents of the AQ- and PW-core samples taken between 240 mbgs and 984 mbgs vary between 0.15±0.09 wt.% and 0.25±0.05 wt.% (=0.39±0.08 Vol.% - 0.67±0.0.13 Vol.%, Table 13). The water contents of the individual sub-samples and of the AQ and PW samples, which are generally collected close, or adjacent, to one another (e.g. AQ001 and PW001), can differ significantly. This is demonstrated by the large error bars associated with the weighted water content values (Table 8, Figure 6). A clear trend in the water content values with depth cannot be observed.

Table 13: Weighted gravimetric water contents of AQ- and PW-core samples in wt.% and Vol.% taken from borehole IG_BH02 and their corresponding total masses; the uncertainties of the water content values are the weighted standard deviations of the individual aliquots – showing the diversity of water contents in one entire core sample; the core volume is calculated using the bulk, wet density determined on the out-diffusion and aqueous extraction cores (Table 14)

Sample	Depth	$m_{rock,tot}$	$WC_{grav,weighted}$	Bulk,wet density	$Vol._{core}$	$WC_{grav,\ weighted}$
	mbgs	g	wt. %	g/cm³	cm³	Vol.%
IG_BH02_AQ001	240.2	497.8	0.19±0.04	2.63	189.5	0.51±0.12
IG_BH02_AQ002	348.5	646.6	0.17±0.01	2.64	245.0	0.44±0.01
IG_BH02_AQ003	379.6	790.8	0.29±0.04	2.66	297.1	0.77±0.10
IG_BH02_AQ004	382.0	564.7	0.18±0.01	2.66	212.6	0.47±0.04
IG_BH02_AQ005	455.5	641.5	0.25±0.05	2.65	242.0	0.67±0.13
IG_BH02_AQ006	530.8	564.5	0.24±0.02	2.59	217.7	0.61±0.06
IG_BH02_AQ007	555.1	681.4	0.20±0.01	2.66	256.3	0.54±0.01
IG_BH02_AQ008	611.4	571.3	0.18±0.01	2.64	216.6	0.47±0.04
IG_BH02_AQ009	666.1	616.9	0.19±0.03	2.65	233.2	0.51±0.08
IG_BH02_AQ010	771.4	504.2	0.16±0.01	2.63	191.9	0.41±0.03
IG_BH02_AQ011	879.0	663.0	0.17±0.01	2.65	250.0	0.45±0.01
IG_BH02_AQ012	984.5	530.9	0.18±0.02	2.63	201.9	0.47±0.05
IG_BH02_PW001	240.0	2481.8	0.19±0.04	2.65	937.3	0.50±0.09
IG_BH02_PW003	348.0	2653.4	0.15±0.03	2.65	1001.7	0.39±0.08
IG_BH02_PW005	378.1	2535.6	0.15±0.09	2.70	940.8	0.40±0.25
IG_BH02_PW006	381.7	2391.7	0.17±0.03	2.62	913.5	0.45±0.07
IG_BH02_PW007	383.0	2592.9	0.18±0.07	2.64	982.2	0.49±0.19
IG_BH02_PW008	455.2	2495.1	0.21±0.05	2.62	951.3	0.55±0.14
IG_BH02_PW010	502.8	2726.8	0.19±0.04	2.62	1042.0	0.51±0.10
IG_BH02_PW012	555.7	2681.3	0.18±0.03	2.62	1022.8	0.47±0.09

Sample	Depth mbgs	$m_{rock,tot}$ g	$WC_{grav,weighted}$ wt. %	Bulk,wet density g/cm³	$Vol._{core}$ cm³	$WC_{grav,\ weighted}$ Vol.%
IG_BH02_PW014	611.2	2665.5	0.17±0.03	2.64	1010.4	0.45±0.09
IG_BH02_PW016	665.8	2630.2	0.20±0.01	2.64	996.7	0.52±0.01
IG_BH02_PW018	770.6	2596.0	0.17±0.01	2.63	987.2	0.44±0.01
IG_BH02_PW020	878.8	2579.9	0.17±0.01	2.64	976.7	0.45±0.02
IG_BH02_PW022	984.2	2631.3	0.20±0.01	2.67	987.1	0.53±0.03

* mbgs (down hole)

5.2 Bulk dry/wet density and water-loss porosity

The bulk dry and wet density is calculated according to Equation 1 (Section 3.2) using the dry and wet mass of the full diameter cylindrical cores and the volume of the core samples determined by measuring the height and core diameter by a Vernier Calliper. Bulk wet densities were determined for the cores used for out-diffusion and aqueous extraction experiments before crushing, and bulk dry density was determined only for out-diffusion cores.

Bulk dry and wet density values of the core samples from borehole IG_BH02 are similar, differing by a maximum of 0.01 g/cm³, due to the low water content of the samples, and vary between 2.61 and 2.69 g/cm³ (Table 14).

The water-loss (connected) porosity was calculated according to Equation 2 (Section 3.2) using the water content calculated by the dry and wet weight and the bulk dry/wet density of the samples. Water-loss porosities are calculated for core sections used for the out-diffusion and aqueous extraction experiments, for which the water content and the bulk dry/wet density were determined. Water-loss porosities calculated using the wet mass and density differ by a maximum of 0.01 Vol.% from those determined by the dry mass and density (Table 14).

Water-loss porosity values of core samples taken between 240 and 984 mbgs (down hole) from borehole IG_BH02 vary between 0.39 ± 0.03 Vol.% and 0.77 ± 0.11 Vol.% (Table 14, Figure 18). The porosity values and water contents for the samples follow the same trends with depth (Figure 18).

Table 14: Bulk wet and dry density and water-loss (=WL-) porosity determined by water contents calculated for dry ($\Phi_{WL,dry}$) and wet ($\Phi_{WL,wet}$) core samples from borehole IG_BH02; the errors are calculated by Gaussian error propagation (Appendix III)

Sample	Depth mbgs*	bulk, wet density g/cm³	bulk, dry density g/cm³	water-loss porosity $\Phi_{WL,wet}$ Vol.%	water-loss porosity $\Phi_{WL,dry}$ Vol.%
IG_BH02_AQ001	240.2	2.63		0.51±0.08	
IG_BH02_AQ002	348.5	2.64		0.44±0.08	
IG_BH02_AQ003	379.6	2.66		0.77±0.11	
IG_BH02_AQ004	382.0	2.66		0.47±0.09	
IG_BH02_AQ005	455.5	2.65		0.67±0.08	
IG_BH02_AQ006	530.8	2.59		0.61±0.11	
IG_BH02_AQ007	555.1	2.66		0.54±0.13	
IG_BH02_AQ008	611.4	2.64		0.47±0.09	
IG_BH02_AQ009	666.1	2.65		0.51±0.08	

Sample	Depth mbgs*	bulk, wet density g/cm³	bulk, dry density g/cm³	water-loss porosity $\Phi_{WL,wet}$ Vol.%	water-loss porosity $\Phi_{WL,dry}$ Vol.%
IG_BH02_AQ010	771.4	2.63		0.41±0.07	
IG_BH02_AQ011	879.0	2.65		0.45±0.08	
IG_BH02_AQ012	984.5	2.63		0.47±0.06	
IG_BH02_PW001	240.0	2.65	2.64	0.50±0.02	0.50±0.02
IG_BH02_PW003	348.0	2.65	2.64	0.39±0.03	0.39±0.03
IG_BH02_PW005	378.1	2.70	2.69	0.40±0.02	0.40±0.02
IG_BH02_PW006	381.7	2.62	2.61	0.45±0.03	0.45±0.03
IG_BH02_PW007	383.0	2.64	2.64	0.49±0.02	0.49±0.02
IG_BH02_PW008	455.2	2.62	2.62	0.55±0.03	0.55±0.03
IG_BH02_PW010	502.8	2.62	2.61	0.51±0.04	0.51±0.04
IG_BH02_PW012	555.7	2.62	2.62	0.47±0.02	0.47±0.02
IG_BH02_PW014	611.2	2.64	2.63	0.45±0.03	0.45±0.03
IG_BH02_PW016	665.8	2.64	2.63	0.52±0.03	0.52±0.03
IG_BH02_PW018	770.6	2.63	2.62	0.44±0.06	0.44±0.06
IG_BH02_PW020	878.8	2.64	2.64	0.45±0.04	0.45±0.04
IG_BH02_PW022	984.2	2.67	2.66	0.53±0.03	0.52±0.03

* mbgs (down hole)

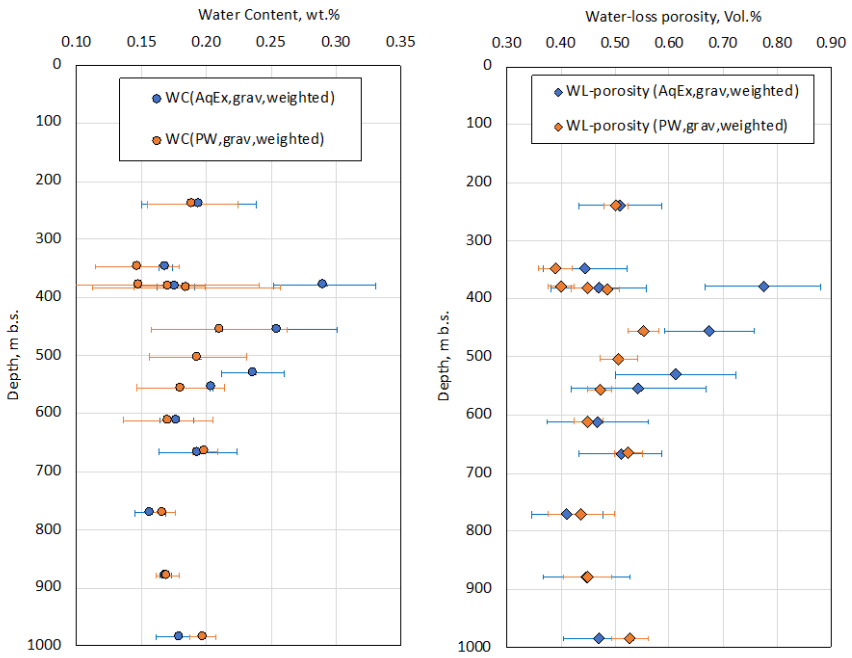


Figure 18: Water content and water-loss porosity of core samples from borehole IG_BH02 (depths are mbgs (down hole)

6.0 CHEMICAL COMPOSITION OF EXPERIMENT SOLUTIONS OF AQUEOUS EXTRACTION AND OUT-DIFFUSION EXPERIMENTS

Out-diffusion and aqueous extraction experiments were performed on thirteen PW- and twelve AQ core samples taken from borehole IG_BH02, respectively. In both experiments the investigated rock samples were immersed in test water. The concentrations of dissolved constituents in the test solutions originate from:

a) porewater, which exchanges and mixes with test water;

b) water-rock interactions, releasing reactive elements in the test water; and

c) fluid inclusions (only aqueous extractions), which are liberated during crushing of the rocks.

6.1 Chemical composition of aqueous extraction solutions

The purpose of aqueous extraction experiments is to obtain an initial estimate of the porewater salinity, which is necessary for the adjustment of the ion concentration in the test waters for the indirect porewater extraction methods.

Crushing and grinding of the rock material liberates fluid trapped in mineral fluid inclusions. During leaching, all salts will become dissolved, in addition to the limited dissolution of the original mineral assemblage. The mineralization of a leach solution is therefore the sum of: (i) the constituents originally dissolved in the porewater, (ii) the constituents present in fluid inclusions, and (iii) water-rock interactions during the leaching process. Thus, aqueous leach solutions represent a complex composition in rocks with abundant fluid inclusions and/or rapidly reacting mineral phases.

The aqueous extraction solutions produced by the immersion of crushed cores from borehole IG_BH02 in deionized water (procedure cf. Section 3.3.1) have pH values between 8.8 and 9.8, and a mineralization between 65 and 123 mg/L (sp. electrical conductivity = 89 – 217 µS/cm, Table 15). The dissolved constituents consist predominately of Na, K, Ca, HCO_3, Cl and SO_4 in different concentrations and proportions (Table 15, Figure 19). Minor concentrations of Mg, F and Br could be detected. Concentrations of Sr were below detection limit (Table 15). Silicon and aluminium could be detected in concentrations between 4.6 and 10.0 mg/L (Si) and between 0.06 and 7.4 mg/L (Al).

The estimated porewater Cl-concentrations of core samples from IG_BH02, extracted by aqueous extraction experiments using the weighted water contents of the AQ samples (cf. Table 8), vary between 2,048 mg/kg_{PW} and 14,941 mg/kg_{PW} (Table 18).

Table 15: Analytical results of the aqueous extraction solutions of crushed core samples from borehole IG_BH02; test solution types are classified after Jäckli (1970)

Sample		IG_BH02_AQ001	IG_BH02_AQ002	IG_BH02_AQ003	IG_BH02_AQ004	IG_BH02_AQ005	IG_BH02_AQ006	IG_BH02_AQ007	IG_BH02_AQ008	IG_BH02_AQ009	IG_BH02_AQ010	IG_BH02_AQ011	IG_BH02_AQ012
Interval	mbgs	240.2	348.5	379.6	382.0	455.5	530.8	555.1	611.4	666.1	771.4	879.0	984.5
Hydroisotop No.		334573	334574	334575	334576	335730	335731	335732	335733	335734	337083	337084	337085
MISCELLANEOUS PROPERTIES													
pH (lab)	-log(H+)	9.8	9.7	9.3	9.4	9.8	9.5	9.5	9.4	9.3	9.3	9.1	8.8
Electr. Conductivity	µS/cm	117	89	136	109	138	120	111	95	130	181	217	196
Sample Temperature	ºC	23.8	23.9	23.9	23.8	23.9	24	24.1	24.1	23.9	22.8	22.8	22.9
Alkalinity (pH 4,3) Lab.	mmol/l	0.83	0.66	0.8	0.67	1.13	0.85	0.78	0.49	0.65	0.76	0.68	0.56
Alkalinity (pH 8,2) Lab.	mmol/l	0.43	0.61	0.61	0.61	0.43	0.61	0.29	0.21	0.21	0.26	0.28	0.16
DOC	mg/l	2.6	1.5	1.6	1.1	3.2	2.6	3.1	2.8	2.4	3.3	2.8	2.7
DISSOLVED CONSTITUENTS													
CATIONS	mg/l												
Sodium (Na+)	mg/l	15.0	12.3	22.5	14.8	24.7	19.4	19.6	16.4	16.3	18.1	16.7	14.1
Potassium (K+)	mg/l	8.2	5.1	2.6	6.6	10.3	11.3	10.5	5.5	5.5	12.2	12.3	10.0
Magnesium (Mg+2)	mg/l	<0.2	<0.2	<0.2	<0.2	0.27	<0.2	0.22	<0.2	<0.2	0.64	0.49	0.29
Calcium (Ca+2)	mg/l	3.1	2.4	4.4	3.2	4.0	2.2	2.1	2.5	2.0	8.5	12.9	13.4
Strontium (Sr+2)	mg/l	<0.1	<0.1	<0.1	<0.1	<0.1	<0.1	<0.1	<0.1	<0.1	<0.1	<0.1	<0.1
Silicon (Si+4)	mg/l	8.1	7.9	5.6	8.6	9.2	7.9	10.0	7.1	6.8	5.2	4.9	4.6
Aluminium (Al+3)	mg/l	0.64	0.71	0.53	0.67	2.6	3.6	7.4	2.8	1.2	0.26	0.07	0.06
ANIONS													
Fluoride (F-)	mg/l	0.10	<0.1	0.69	0.11	0.22	0.17	0.14	<0.1	<0.1	0.12	0.11	<0.1
Chloride (Cl-)	mg/l	4.80	4.30	14.9	10.2	13.1	13.2	13.5	14.7	9.0	27.0	36.7	34.2
Bromide (Br-)	mg/l	3.1	0.35	0.23	0.14	0.20	0.40	0.17	0.20	0.12	0.86	0.96	1.2
Sulfate (SO4-2)	mg/l	0.75	<0.5	1.00	0.58	1.6	1.2	3.5	2.8	1.8	1.8	1.3	1.9
Nitrate (NO3-)	mg/l	<0.2	<0.2	0.22	<0.2	<0.2	<0.2	<0.2	<0.2	<0.2	<0.2	<0.2	<0.2
Total Alkalinity	meq/l	0.83	0.66	0.80	0.67	1.1	0.85	0.78	0.49	0.65	0.76	0.68	0.56
Total Alkalinity as HCO3	mg/l	50.8	40.5	48.7	41.1	69.1	51.7	47.8	29.8	39.5	46.4	41.5	34.2
PARAMETERS CALCULATED FROM ANALYTICAL DATA													
Sum of Analysed Constituents	mg/l	83	65	95	77	123	100	97	72	74	116	123	109
Charge Balance	%	1.33%	-0.03%	-0.75%	-0.26%	0.41%	-0.74%	0.03%	0.69%	0.35%	0.001%	-1.00%	-0.56%
ION-ION RATIOS													
Br*1000/Cl weight	mg/mg	64.6	81.4	15.4	13.7	15.3	30.3	12.6	13.6	13.3	31.9	26.2	35.1
Water type*		Na-K-(Ca)-HCO3-(Cl)	Na-(K)-(Ca)-HCO3-(Cl)	Na-(Ca)-HCO3-Cl	Na-(K)-(Ca)-HCO3-Cl	Na-(K)-(Ca)-HCO3-Cl	Na-K-HCO3-Cl	Na-K-HCO3-Cl	Na-(K)-(Ca)-HCO3-Cl	Na-(K)-(Ca)-HCO3-Cl	Na-Ca-(K)-Cl-HCO3	Na-Ca-(K)-Cl-HCO3	Ca-Na-(K)-Cl-HCO3

*according to Jäckli (1979): XX = > 50 eq.%, XX = 50-20 eq.% (XX) = 20-10 eq.%

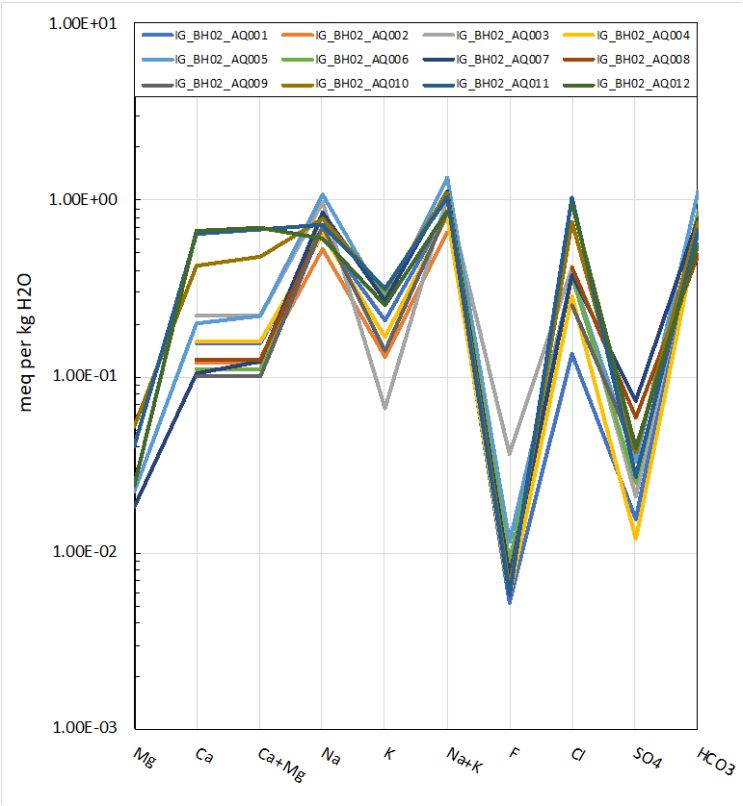


Figure 19: Schoeller diagram of experiment solutions from aqueous extraction experiments conducted with core samples from borehole IG_BH02

6.2 Chemical composition of out-diffusion experiment solutions

Out-diffusion experiments were performed on 13 core samples from borehole IG_BH02 to derive the porewater chloride and bromide concentrations, porewater $\delta^{37}Cl$ isotope ratios, and chemical composition of the test solutions - which are the basis for the hydrogeochemical modelling of porewater chemical compositions. The core sections varied in diameter between 60.5 mm and 61.3 mm, with lengths between 184 mm and 194 mm. The corresponding volume of the sections varied between 538 cm^3 and 558 cm^3 and the saturated mass was between 1,407 g and 1,477 g. In the out-diffusion experiments, the mass ratio of experiment solution to rock samples was between 0.084 and 0.101 (Table 16).

During the out-diffusion experiments, a continuous exchange between porewater and test water takes place until equilibrium conditions with respect to conservative, non-reactive compounds are achieved. The exchange appears to occur primarily by diffusion (cf. Section 7). For chemically conservative elements, such as chloride and bromide, for which the porewater is the only source, the porewater concentration can be calculated using the gravimetrically determined porewater mass of the rock sample. For reactive elements and compounds, such as Ca, Mg, Na, K, Sr, Si, Al, SO_4^{2-} and HCO_3^-, the contribution of mineral dissolution reactions during the experiment has to be taken into account. Those reactions are evaluated by the determination of the concentrations of the non-conservative elements taken in time-series (cf. Section 7.1).

The pH of the experiment solutions varies between 7.3 and 8.2, with a total mineralization between 134 mg/L and 506 mg/L (EC = 171 - 997 µS/cm, Table 16). It should be noted that the total mineralization obtained for the

experiment solutions depends on the water content of the sample and the water/rock ratio used in the experiment (Table 10) and does not directly reflect differences in porewater salinity.

The experimental solutions contain Na (22.0 – 40.4 mg/L), Ca (8.2 – 144 mg/L), K (2.0 – 7.7 mg/L), HCO_3 (34.8 – 133 mg/L), Cl (2.2 – 279 mg/L) and SO_4 (3.3 – 11.6 mg/L) in varying proportions and concentrations (Table 16, Figure 20).

Based on the out-diffusion test solutions, samples are characterized by Na- and HCO_3- dominated water between 242 and 383 mbgs (down hole), and transition to a Na-Cl dominated water between 455 and 611 mbgs (down hole) and further to a Ca- and Cl- dominated water between 665 and 984 mbgs (down hole), with similar mineralogical composition throughout (Table 16, Figure 20)

Silicon (expressed as Si) is present in concentrations between 7.5 and 9.7 mg/L. Lithium, magnesium, strontium, aluminium, boron, fluoride, bromide and nitrate are below detection limit or present in low or trace concentrations (Table 16).

The concentrations of dissolved organic carbon (DOC) vary between 7.6 and 12.6 mg/L.

The DIC/TIC concentrations (DIC = TIC, because analysed on filtered samples) determined by TIC-analyser vary between 6.8 and 26.2 mg/L. The comparison of the TIC concentrations determined by direct analyses with those determined by acid titration (AC4.3) shows that the total alkalinity is almost exclusively determined by HCO_3. The differences between the TIC values determined by the two methods are very low, ranging between 0.1 and 0.8 %.

In the experiment, the carbon system of the test water – porewater system is influenced by in- and/or out-gassing of atmospheric CO_2. For all out-diffusion solutions, the CO_2 partial pressure was estimated using the TIC concentrations determined by titration and pH-values of the out-diffusion solutions. The estimated log pCO_2 range between -5.5 and -3.8 and are lower than that of the atmosphere (log pCO_2 ~ -3.5). The low CO_2 concentration and undersaturation with respect to the atmosphere is caused by the high pH values (7.3 – 8.2), which lead to formation of HCO_3 instead of CO_2.

The strontium $^{87}Sr/^{86}Sr$ isotope ratios of the out-diffusion test solutions vary between 0.721609 and 0.741507, with Sr-concentrations varying between 0.05 and 1.6 mg/L (Table 16).

Table 16: Analytical results of test solutions of out-diffusion experiments using core samples from borehole IG_BH02

Sample		IG_BH02_PW001	IG_BH02_PW003	IG_BH02_PW005	IG_BH02_PW006	IG_BH02_PW007	IG_BH02_PW008	IG_BH02_PW010	IG_BH02_PW012	IG_BH02_PW014	IG_BH02_PW016	IG_BH02_PW018	IG_BH02_PW020	IG_BH02_PW022
Hydroisotop Nr.		342485	342486	342487	342488	342489	342490	342491	342492	342493	342494	343751	343752	344146
Interval	m.b.s.	240.0	348.0	378.1	381.7	383.0	455.2	502.8	555.7	611.2	665.8	770.6	878.8	984.2
Ratio Exp.Water : Rock	g/g	0.085	0.084	0.085	0.086	0.088	0.096	0.092	0.101	0.086	0.087	0.087	0.090	0.090
Ratio TW:PW	g/g	42.7	54.3	79.7	50.1	50.7	44.4	44.5	51.7	50.6	44.0	52.0	53.6	47.5
MISCELLANEOUS PROPERTIES														
pH	-log(H+)	8.2	8.0	7.5	7.5	7.9	7.6	7.6	7.4	7.8	7.6	7.4	7.4	7.3
Spec.Electr. Conductivity	µS/cm	171	215	363	340	260	320	381	385	378	768	600	997	973
Acid Capacity (4.3)	mmol	1.45	1.46	2.16	2.18	1.18	0.99	1.02	1.11	0.72	0.96	0.63	0.57	0.79
Base Capacity (8.2)	mmol	0.003	0.018	0.14	0.169	0.025	0.046	0.053	0.09	0.022	0.058	0.062	0.057	0.091
Sample Temperature	°C	20.3	20.0	19.7	19.5	19.4	20.6	20.9	21.0	19.9	21.8	24.3	24.2	24.8
DOC	mg/l	10.8	9.6	10.7	12.6	9.1	9.5	7.7	7.6	10.6	8.2	8.5	7	11.4
TIC	mg/l	17.3	17.5	25.9	26.2	14.2	11.8	12.2	13.3	8.7	11.6	7.6	6.8	9.4
TIC (AC4.3)	mg/l	17.4	17.5	25.9	26.2	14.2	11.9	12.2	13.3	8.6	11.5	7.6	6.8	9.5
Δ(TIC)	mg/l	0.10	0.02	0.02	-0.04	-0.04	0.08	0.04	0.02	-0.06	-0.08	-0.04	0.04	0.08
DISSOLVED CONSTITUENTS														
CATIONS	mg/l													
Sodium (Na+)	mg/l	26.8	30.0	32.7	27.0	22.0	31.5	32.8	32.7	29.6	40.4	23.3	25.9	28.5
Potassium (K+)	mg/l	2.0	2.3	6.2	6.0	3.0	4.0	4.7	4.6	4.4	7.7	5.4	7.1	7.4
Lithium (Li+)	mg/l	0.036	0.076	0.043	0.052	0.043	0.066	0.071	0.040	0.083	0.061	0.052	0.075	0.084
Calcium (Ca+2)	mg/l	8.2	12.6	34.9	36.0	22.8	27.7	36.2	38.4	37.9	96.0	79.5	144	139
Magnesium (Mg+2)	mg/l	<0.2	<0.2	0.85	1.5	0.61	0.40	0.38	0.33	0.21	0.41	0.31	0.37	0.24
Strontium (Sr+2)	mg/l	0.05	0.19	0.75	0.77	0.42	0.44	0.60	0.64	0.79	1.6	1.0	1.5	0.96
Aluminium (Al+3)	mg/l	0.52	0.24	0.070	0.060	0.23	0.18	0.14	0.11	0.13	0.07	0.048	0.053	0.020
Silicium (Si+4)	mg/l	8.1	7.5	9.3	9.7	8.7	7.7	8.0	9.7	8.6	8.5	9.1	7.6	9.2
Boron (B)	mg/l	0.57	0.65	0.75	0.80	0.67	0.39	0.39	0.32	0.37	0.40	0.045	0.084	0.047
ANIONS														
Fluoride (F-)	mg/l	2.0	2.6	1.0	0.92	1.4	1.9	2.1	1.7	1.2	1.4	1.3	0.85	0.86
Chloride (Cl-)	mg/l	2.2	12.3	40.1	31.2	30.9	56.4	74.5	72.0	80.9	194	157	279	262
Bromide (Br-)	mg/l	0.75	1.5	0.74	0.59	0.59	1.2	1.4	1.3	1.4	3.4	4.1	5.4	6.6
Nitrate (NO3-)	mg/l	<0.2	<0.2	<0.2	<0.2	0.3	<0.2	<0.2	<0.2	<0.2	0.21	<0.2	<0.2	<0.2
Sulphate (SO4-2)	mg/l	4.0	5.8	6.2	7.4	5.9	3.3	3.8	6.9	5.6	6.1	5.5	7.2	11.6
Total Alkalinity as HCO3	mg/l	88.2	88.8	132	133	72.2	60.2	62.1	67.6	44.2	58.8	38.6	34.8	48.0
PARAMETERS CALCULATED FROM ANALYTICAL DATA														
Sum of Analysed Constituents	mg/l	134	156	255	244	160	187	219	226	206	410	316	506	505
Charge Balance:	%	-2.5	-2.1	-1.1	-0.1	-0.5	2.4	1.0	1.6	2.0	1.0	-1.2	-0.83	-0.84
WATER TYPE		Na-(Ca)-HCO3	Na-(Ca)-HCO3-(Cl)	Na-Ca-HCO3-Cl	Na-Ca-HCO3-Cl	Na-Ca-HCO3-Cl	Na-Ca-Cl-HCO3	Na-Ca-Cl-HCO3	Na-Ca-Cl-HCO3	Na-Ca-Cl-HCO3	Ca-Na-Cl-(HCO3)	Ca-Na-Cl-(HCO3)	Ca-Na-Cl	Ca-Na-Cl
ION-ION RATIOS														
Br*1000/Cl weight		341	122	18.5	18.9	19.1	21.3	18.8	18.1	17.3	17.5	26.1	19.4	25.2
Br*1000/Cl molal	mol/mol	151	54.1	8.2	8.4	8.5	9.4	8.3	8.0	7.7	7.8	11.6	8.6	11.2
Na/Cl molal	mol/mol	18.8	3.8	1.3	1.3	1.1	0.9	0.7	0.7	0.6	0.3	0.2	0.1	0.2
K/Na molal	mol/mol	0.04	0.05	0.11	0.13	0.08	0.07	0.08	0.08	0.09	0.11	0.14	0.16	0.15
SO4/Cl molal	mol/mol	0.67	0.17	0.06	0.09	0.07	0.02	0.02	0.04	0.03	0.01	0.01	0.01	0.02
Na/(Cl+SO4)	mol/mol	11.2	3.2	1.2	1.2	1.0	0.8	0.7	0.7	0.6	0.3	0.2	0.1	0.2
ISOTOPE RATIOS														
δ37Cl	pm SMOC	Cl too low	-0.20	0.12	0.03	0.09	0.81	0.04	0.23	0.13	0.04	0.41	0.60	0.09
error δ37Cl	pm SMOC		0.20	0.20	0.33	0.50	0.44	0.49	0.22	0.20	0.20	0.29	0.20	0.31
87Sr/86Sr		0.741507	0.735749	0.721609	0.725064	0.724294	0.737073	0.737913	0.734107	0.727686	0.723057	0.737279	0.734765	0.740251
error 87Sr/86Sr		0.00005	0.00005	0.00005	0.00005	0.00005	0.00005	0.00005	0.00005	0.00005	0.00005	0.00005	0.00005	0.00005

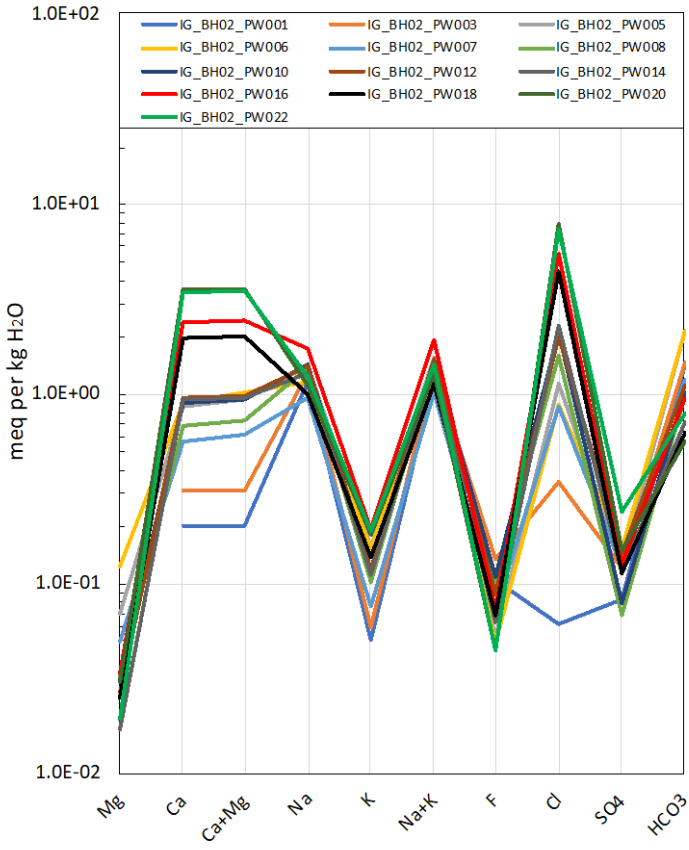


Figure 20: Schoeller diagram of experiment solutions from out-diffusion experiments

7.0 ELEMENTAL TIME SERIES AND PORE DIFFUSION COEFFICIENT OF CHLORIDE

7.1 Elemental elution curves

Non-destructive out-diffusion experiments are performed based on the concept of chemical exchange between porewater residing in the rock matrix and a test solution of known composition surrounding the rock sample. The experimental setup is maintained until specific conditions between the two solution reservoirs are attained. Because of the closed system character of out-diffusion experiments, the specific conditions to be achieved between the two solution reservoirs are equilibrium for any solutes for which the porewater is the only source, and which are only subjected to transport processes (i.e., Cl and Br).

For the present study, improved analytical techniques allowed continuous monitoring of all major solute concentrations in the eluate solutions during out-diffusion. This allows definition of mineral reactions and – at a later stage – possible determination of solute specific transport (e.g., ion-specific accessible porosity) in the matrix of crystalline rocks.

Porewater chloride and bromide concentrations are calculated based on the final concentrations in the out-diffusion test solutions and the water content of the individual core samples (cf. Section 3). The approach to equilibrium was monitored by periodically taking sub-samples and analysing them for their Cl and Br concentrations. The criterion for attainment of equilibrium conditions is defined by a difference of less than 5 % in Cl- and Br-concentrations between the last sub-sample and the final test solution at the end of the experiment. This corresponds to the analytical uncertainty of the Cl and Br measurements. Sub-samples were collected as a function of time for all out-diffusion experiments.

Out-diffusion experiments were run for 127 to 152 days. Equilibrium with respect to Cl and Br was attained for all samples with respect to the above mentioned criteria after 44 – 62 days for Cl, and 29 – 62 days for Br, respectively (Figure 21).

The calculated Br*1000/Cl mass ratios (expressed as Br/Cl-ratio) of the individual out-diffusion experiments either increase within the first days or weeks of elution or are constant over the entire period of elution (Figure 21). This indicates that there is no significant influence of a diffusional fractionation between bromide and chloride.

Sodium shows a heterogeneous elution behaviour. For the samples IG_BH02_PW001, PW003, PW008, PW010, PW012 and PW016, the Na-concentration in the individual test waters shows a steep increase in the first 5-10 days, followed by a flattening of the curve and an achieved equilibrium after app. 60-100 days (Figure 21). The Na-concentrations in the test solutions of the samples IG_BH02_PW005, PW006, PW007 and PW0014 show also a steep increase in the first days of the experiments, followed by a flattening of the curve and a continuous increase, which becomes less with ongoing experimental time (Figure 21), not reaching a full equilibrium after the experimental time. The Na elution curves of the samples IG_BH02_PW018, PW020 and PW022 show a diffusion like shape and equilibrium after 50 to 60 days.

Potassium, in contrast, reaches equilibrium in all conducted out-diffusion experiments, although the elution curves are different. The K-concentrations in the test solutions of the samples IG_BH02_PW001, PW003, PW007, PW008, PW010, PW012, PW014 and PW016 show a sharp increase within the first one to two days of the experiments, followed by flattening and achievement of equilibrium after app 15-20 days. The K-concentrations in the test solutions emerging the core samples IG_BH02_PW005 and PW006 show also a sharp concentration increase in the first days, followed by flattening of the curve and equilibrium after 30-40 days (PW005) and 75-90

days (PW006), respectively (Figure 21). The K-elution curves of the samples IG_BH02_PW018, PW020 and PW022 show diffusion like shape with equilibrium after 15-20 days (Figure 21).

Calcium shows heterogeneous elution behaviour in the individual out-diffusion experiments. All samples, except of core sample IG_BH02_PW018, reach equilibrium between 75 to 120 days (Figure 21).

For all samples, the sulphate concentrations display a steady increase during the entire elution period (Figure 21). This is reasoned to be caused by the oxidation and elution of sulphide minerals, which are present in the rock as accessories (cf. Chapter 4.3).

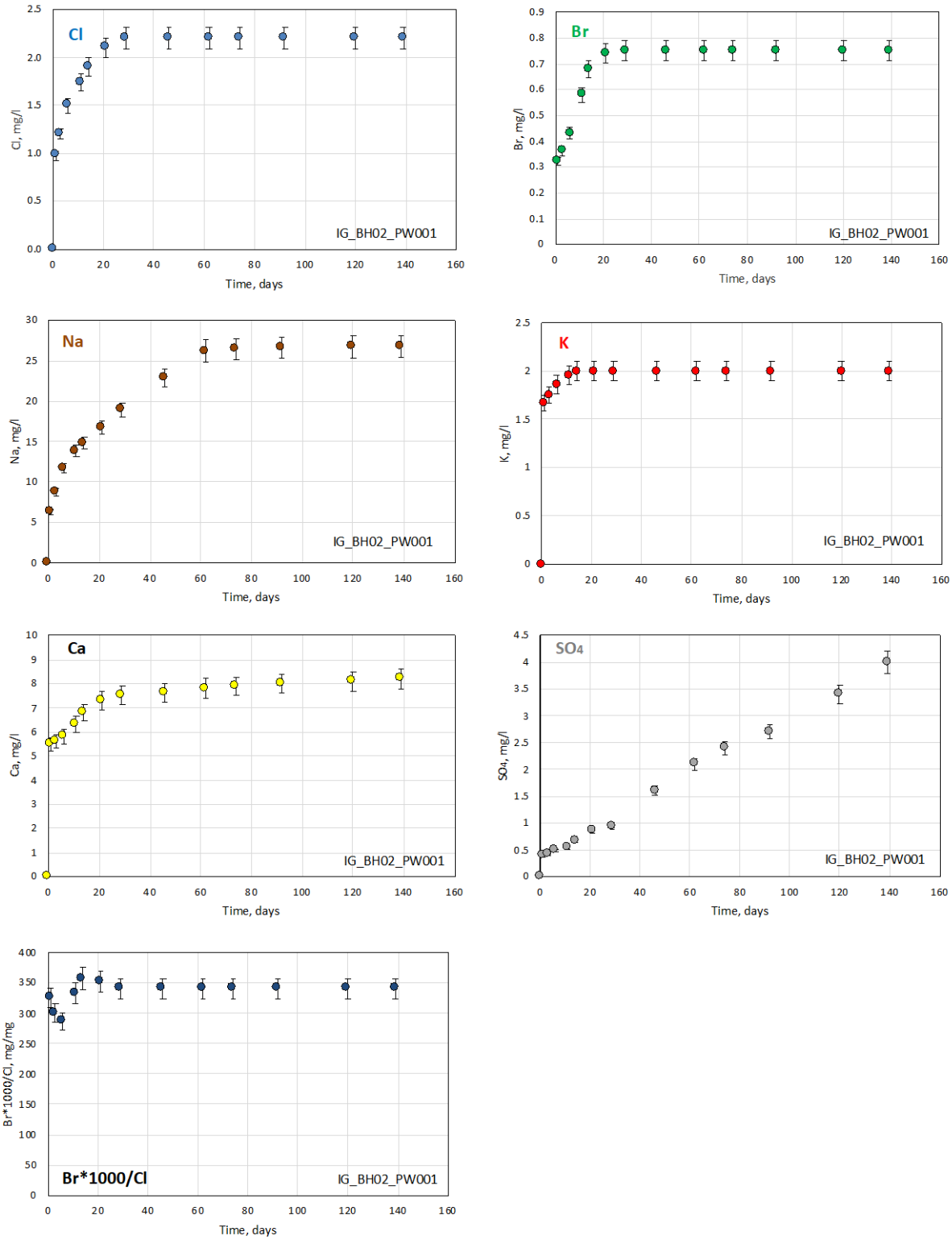


Figure 21: Elution curves of anions and cations set-up by the periodic sampling of test solutions from out-diffusion experiments using core samples from borehole IG_BH02; the errors are the analytical uncertainty of ± 5 %

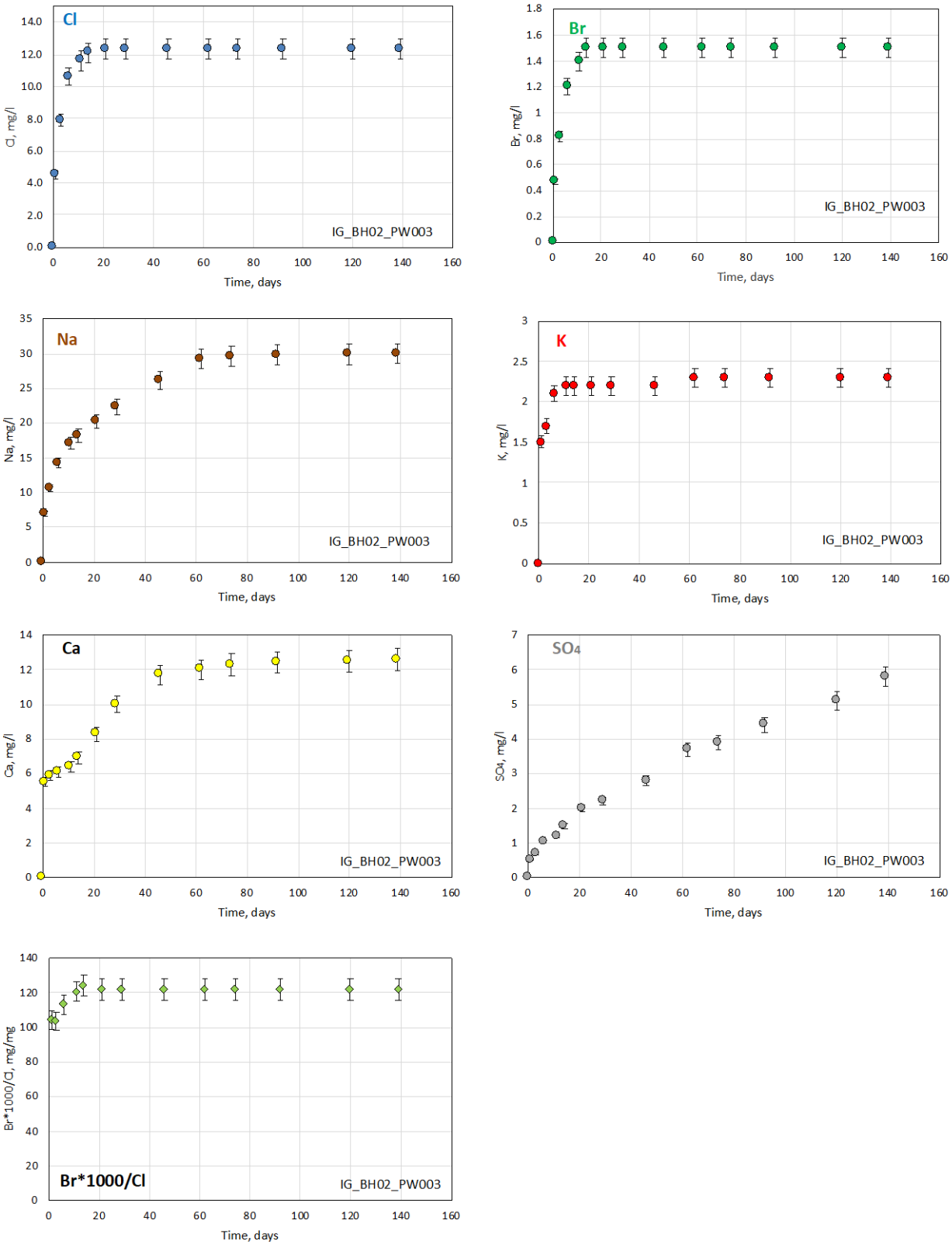


Figure 21 continued

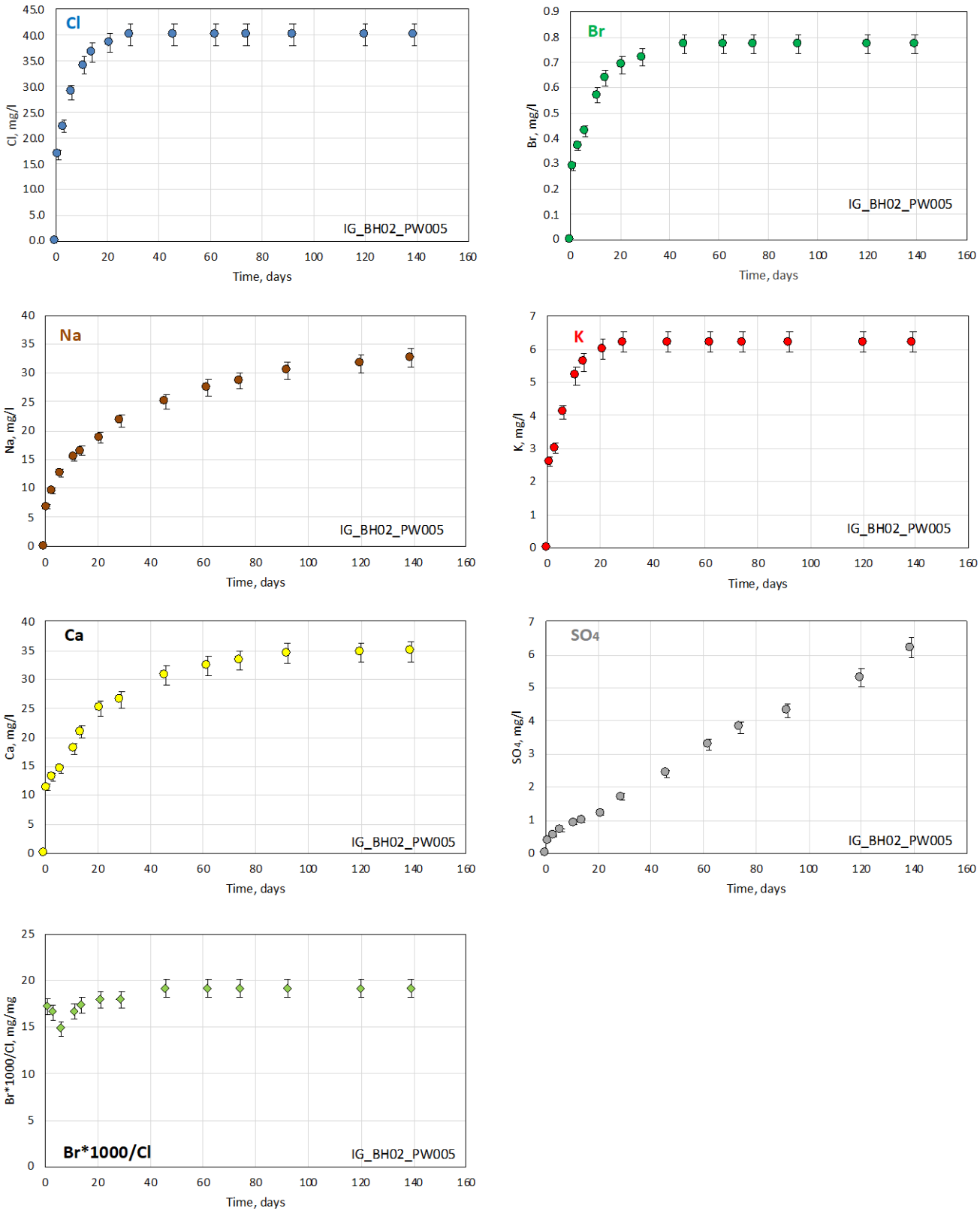


Figure 21 continued

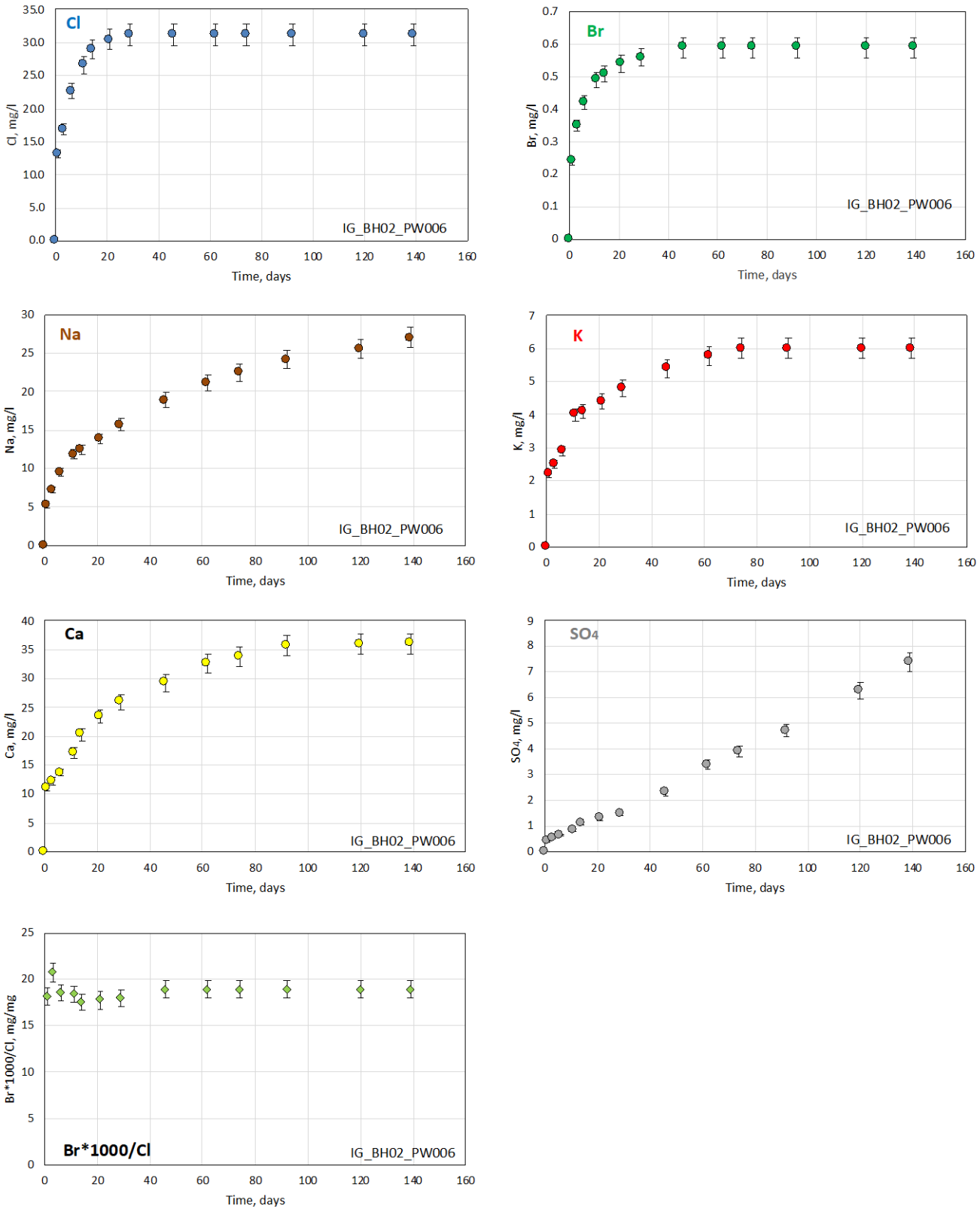


Figure 21 continued

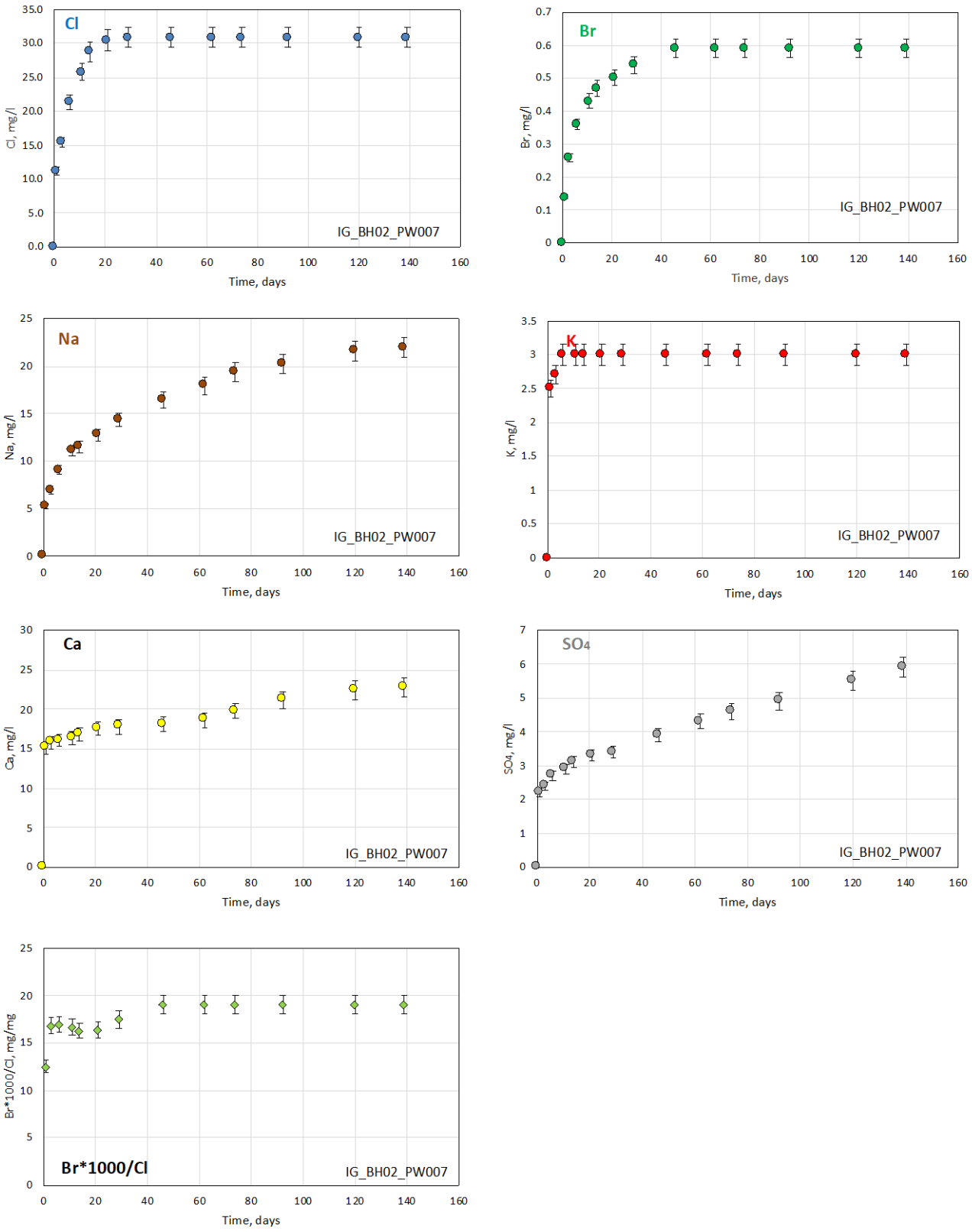


Figure 21 continued

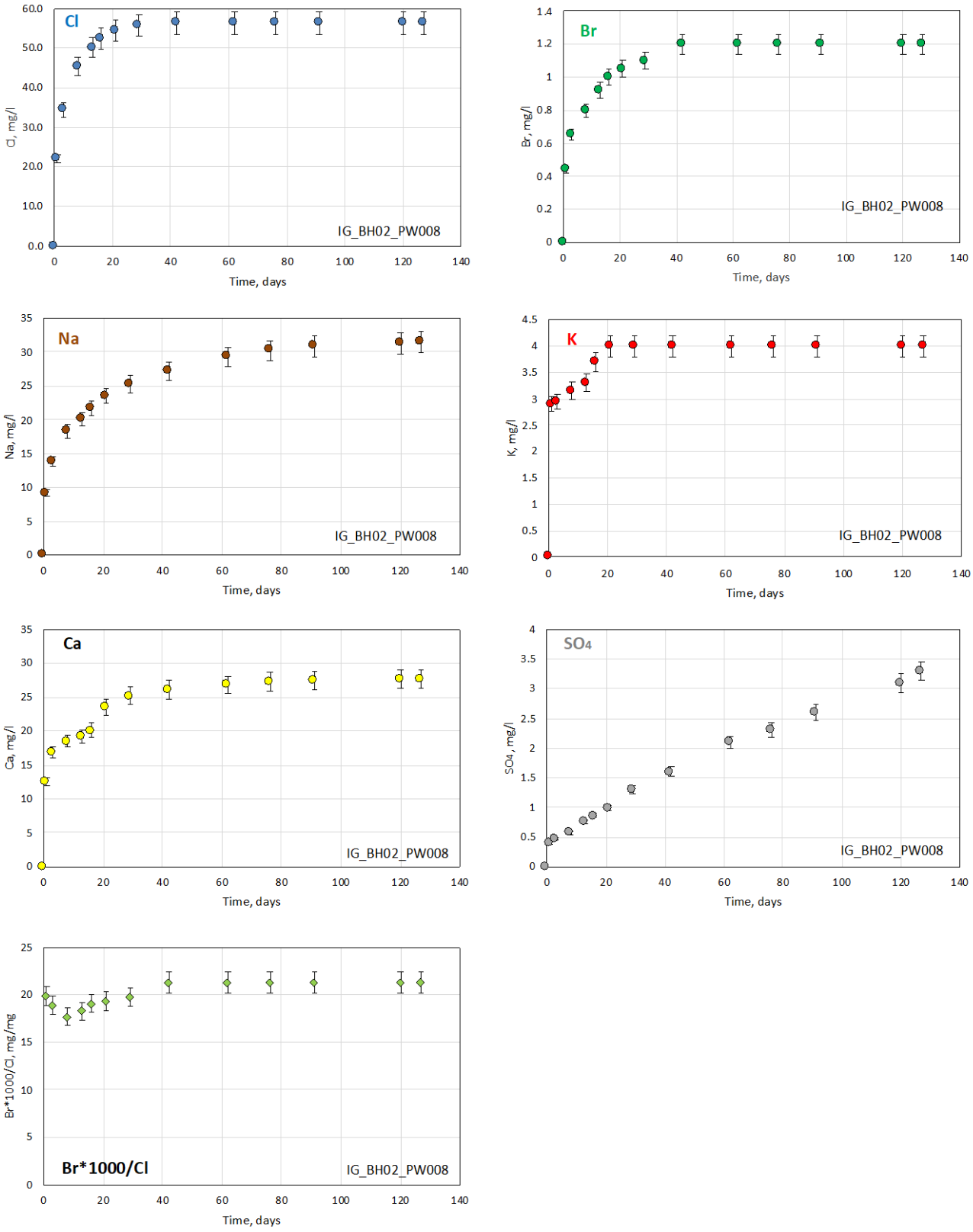


Figure 21 continued

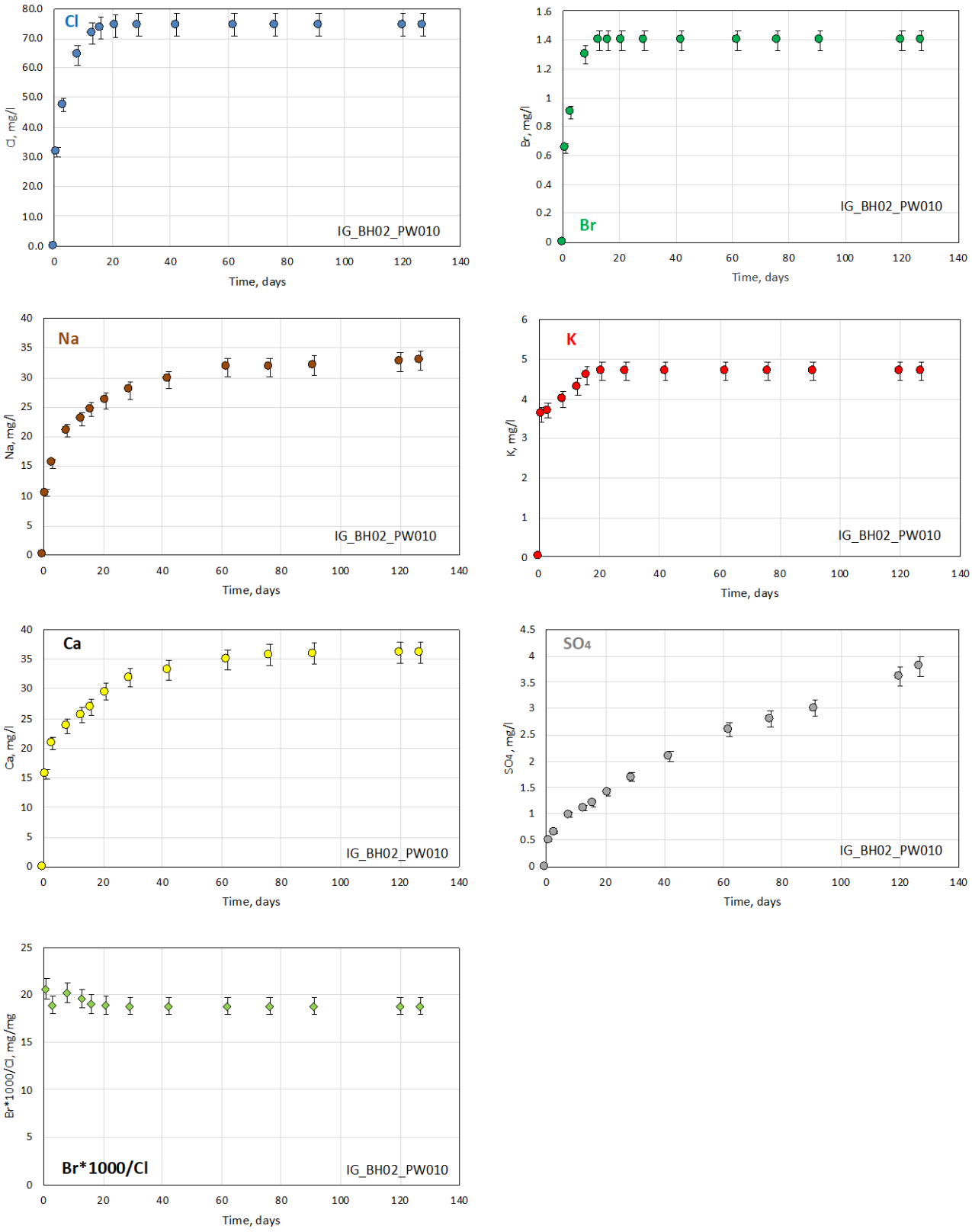


Figure 21 continued

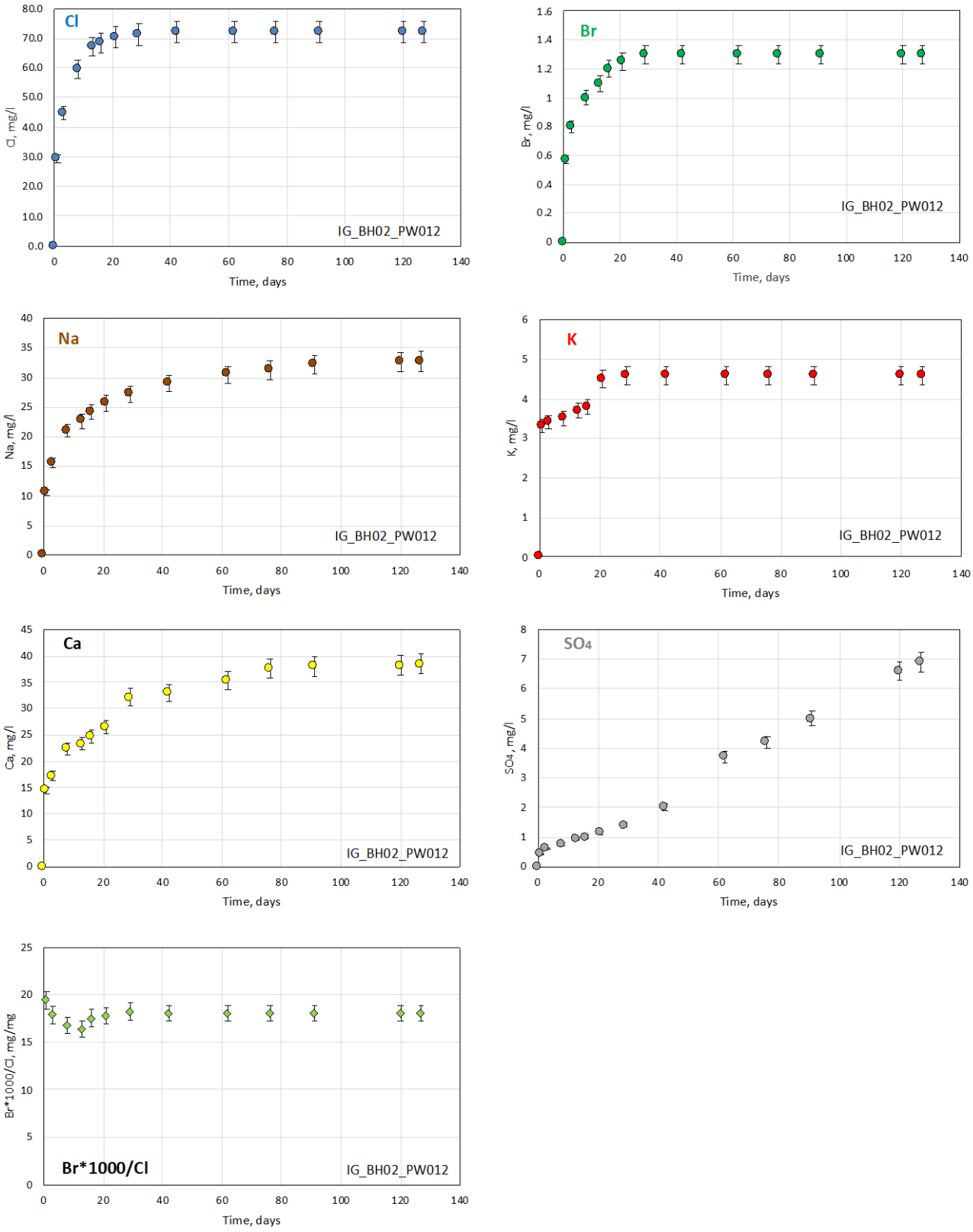


Figure 21 continued

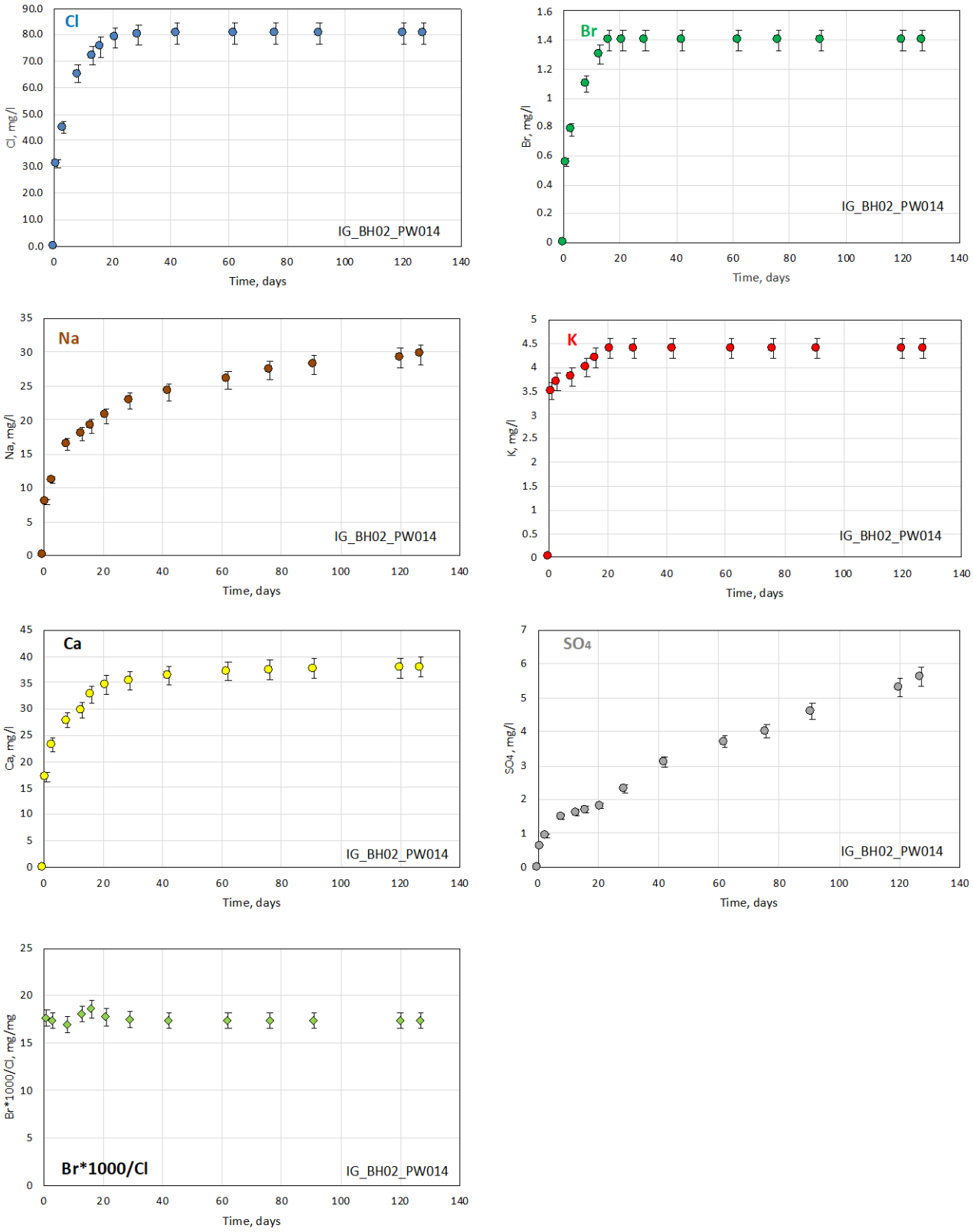


Figure 21 continued

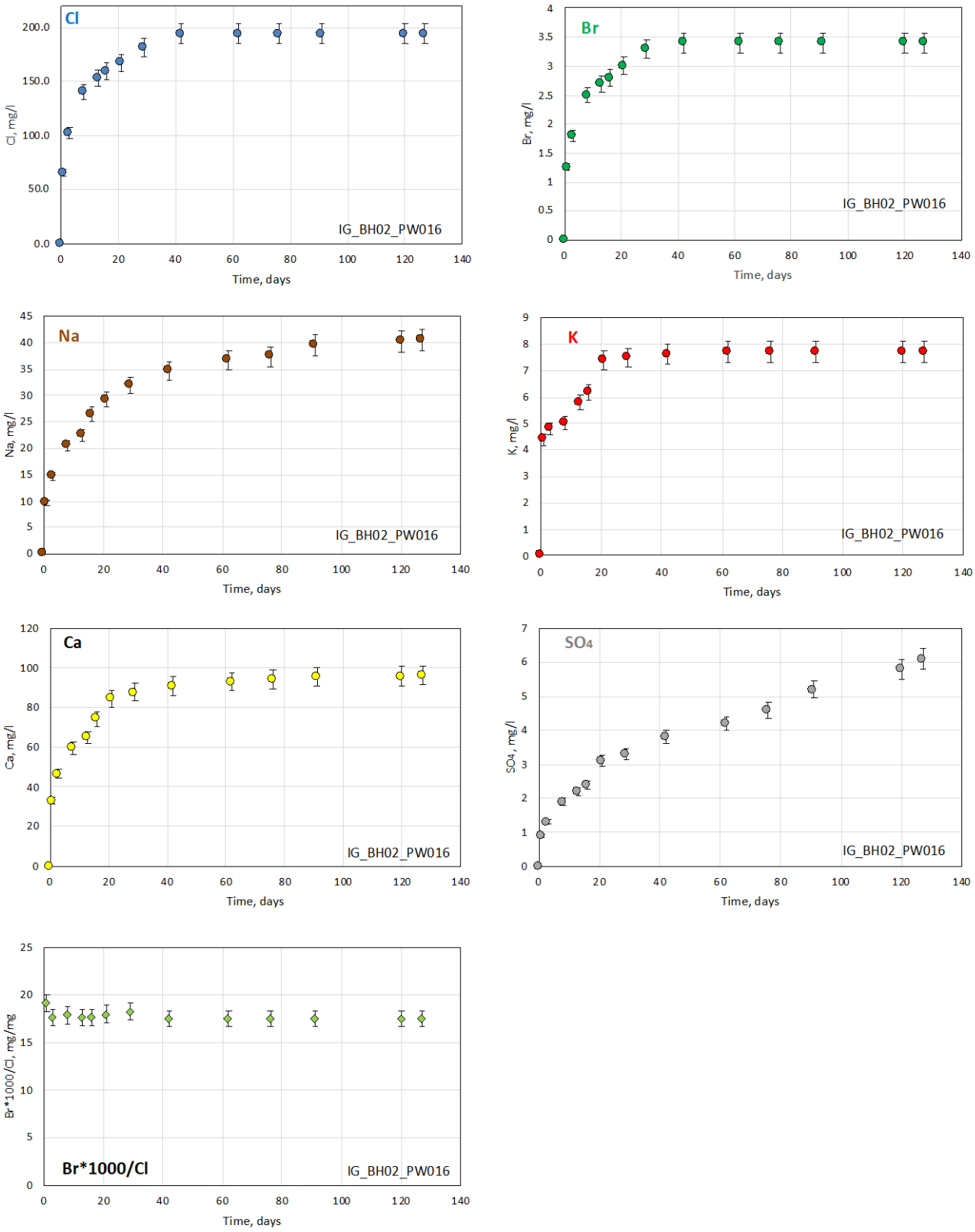


Figure 21 continued

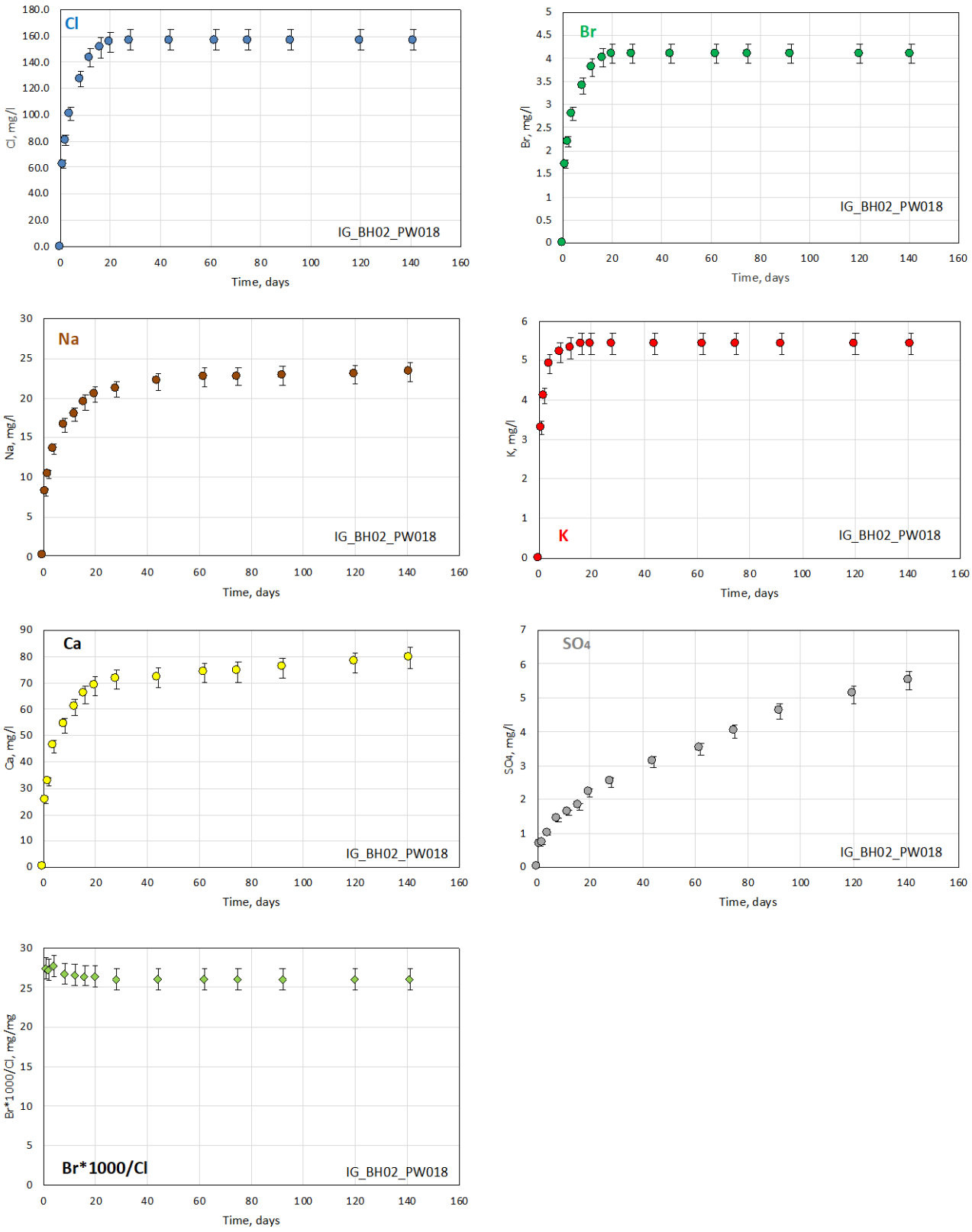


Figure 21 continued

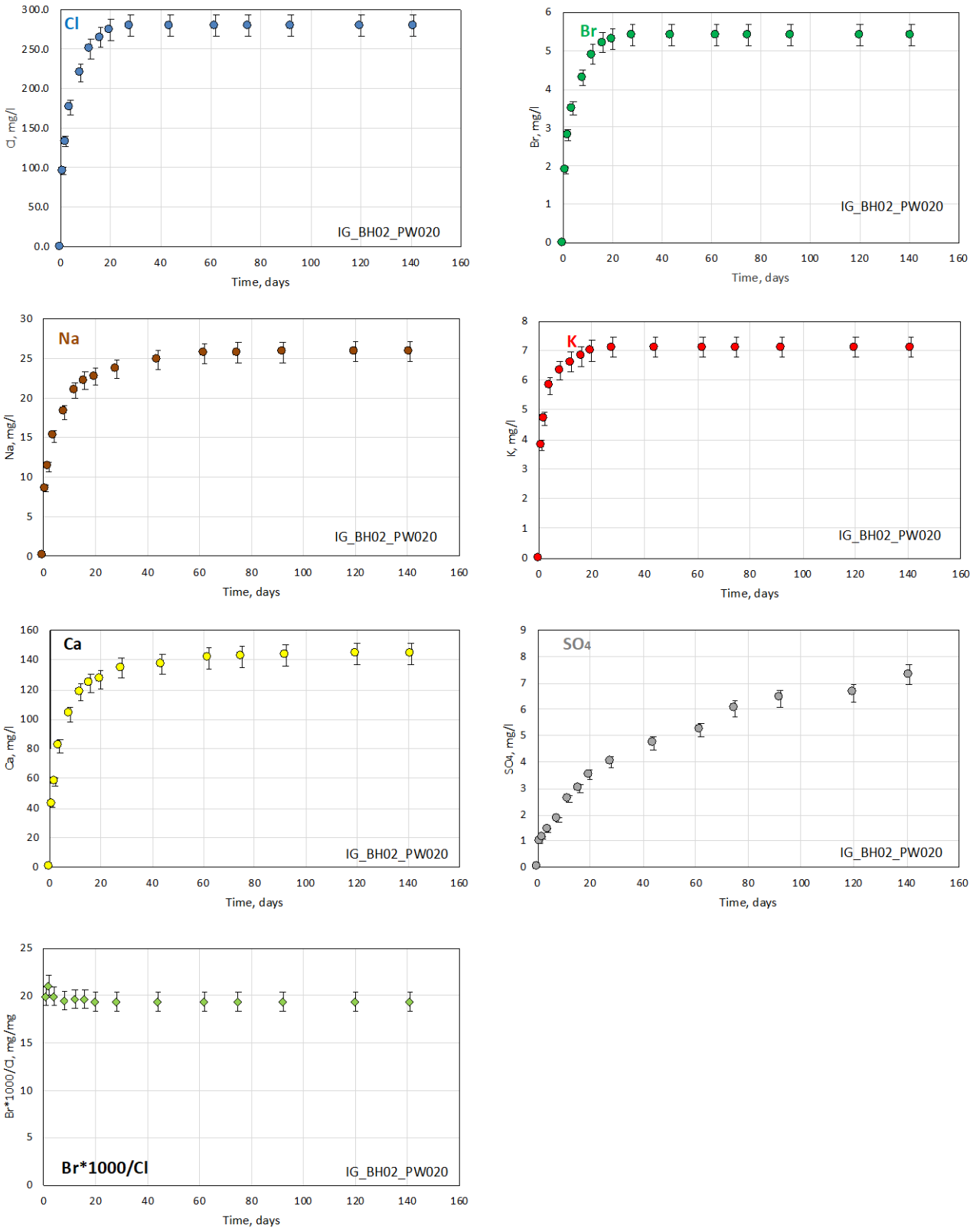


Figure 21 continued

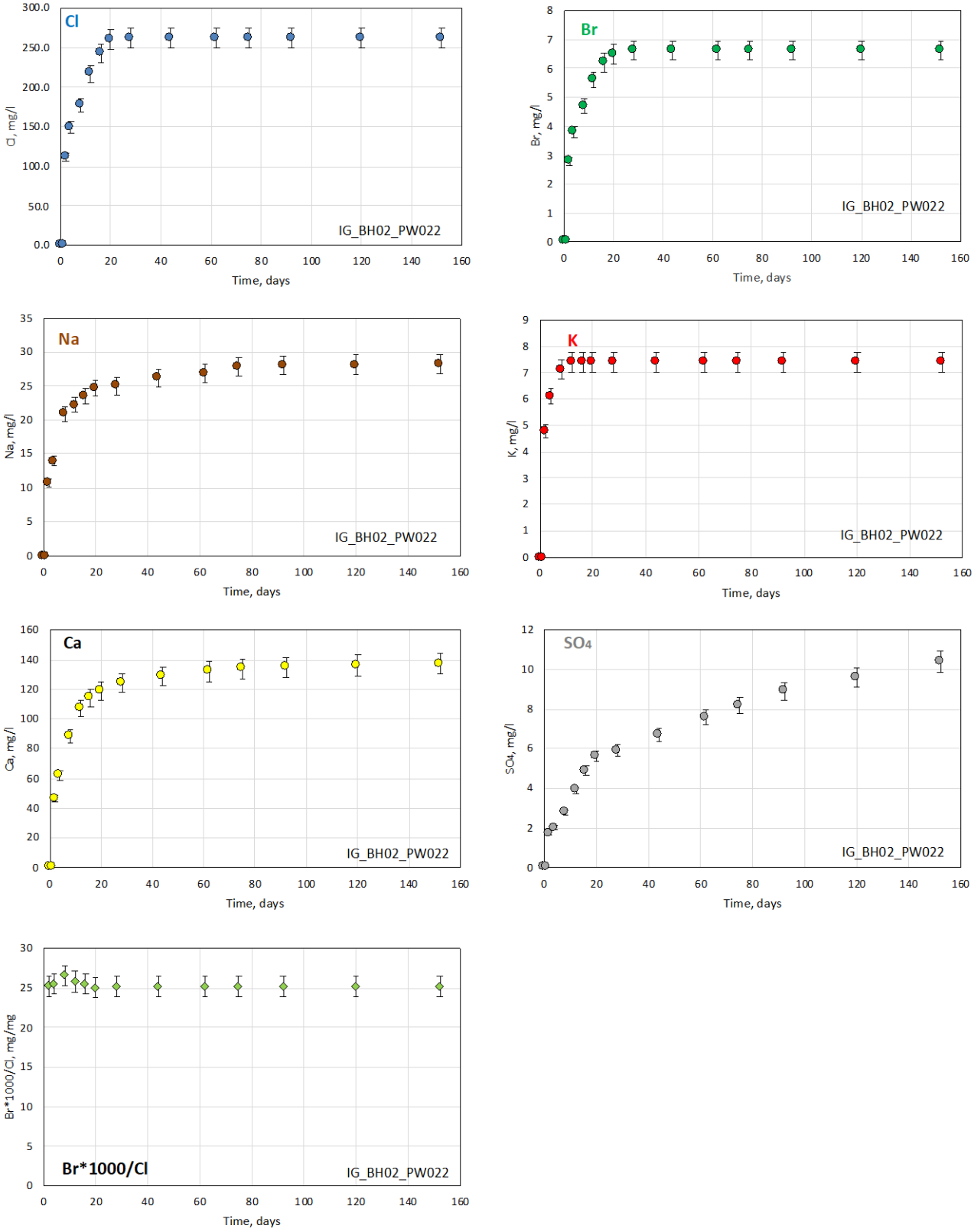


Figure 21 continued

7.2 Modelling of pore diffusion coefficients

Chloride pore diffusion coefficients were derived by modelling the chloride breakthrough curves obtained from the out-diffusion experiments of all 13 samples from borehole IG_BH02. The chloride breakthrough curves are deduced from the Cl contents in the small-sized subsamples that were collected periodically during the out-diffusion experiments (cf. Section 3.3.2, 7.1). The pore diffusion coefficient is obtained by fitting the observed data with an analytical solution for one-dimensional radial diffusion out of the cylinder into a well-mixed solution reservoir (Crank 1975). The applied model (T. Gimmi, RWI, University of Bern) is restricted to homogeneous hydraulic properties (porosity, diffusion coefficient) across the core cylinder, and cannot consider heterogeneous properties due to rock anisotropy or induced effects, such as a drilling disturbed zone and/or stress release (Meier et al., 2015).

The pore diffusion coefficient, D_p, of a solute in a geological media mainly depends on the shape and size of water conducting pores (constrictivity) and on the pathways given by the connected pore network (tortuosity, cf. e.g., Ohlsson and Neretnieks 1995). It can be defined as:

$$D_p = D_w \frac{\delta_D}{\tau^2} \qquad \text{Eq. 8}$$

where D_P = pore-diffusion coefficient in m^2/s; D_W = diffusion coefficient in pure water in m^2/s; δ_D = constrictivity; τ = tortuosity; the term δ_D/τ^2 is called the geometry factor. In a first assumption the pore diffusion coefficient of a given species, D_P, can be converted to the effective diffusion coefficient of this species, D_e, according to:

$$D_e = D_p \Phi_{WC} \qquad \text{Eq. 9}$$

where D_e is the effective diffusion coefficient in m^2/s and Φ_{WC} the species-accessible porosity.

The shape of the Cl elution curves obtained for all core samples from borehole IG_BH02 suggests a heterogeneous transport system from the rim to the centre of the core (Figure 22). The initial slopes are steep (in the transient state) during the first five to ten days of out-diffusion, and become more moderate later in the experiment.

The quality of the D_P fits is controlled by the difference ($\Delta_{meas\text{-}mod}$) of the measured and modelled Cl concentration at equal time and shown graphically by logarithmic plots (Figure 22). To determine the lowest $\Delta_{meas\text{-}mod}$ values, a stepwise adjustment of the single points was conducted and the $\Delta_{meas\text{-}mod}$ values were calculated for every measured point. The determination of the best fits per sampling point indicates a gradual decrease of the modelled pore diffusion coefficients as diffusion progresses deeper into the cores.

The modelled D_P values, which were determined at 45 °C, are additionally converted to 10 °C and 25 °C by the Stoke-Einstein equation (Lide 1994). For the investigated core samples, the influence of the disturbed zone results in a pore diffusion coefficient that is a factor 1.7 to 4.0 higher than that of the inner core (Table 12, Figure 10). The average pore diffusion coefficients (D_P) of the 13 crystalline core samples vary between 1.0 and $1.6*10^{-10}$ m^2/s (10 °C), resulting in effective diffusion coefficients (D_e) between 0.4 and $0.9*10^{-12}$ m^2/s (10 °C, Table 12, Figure 11.)

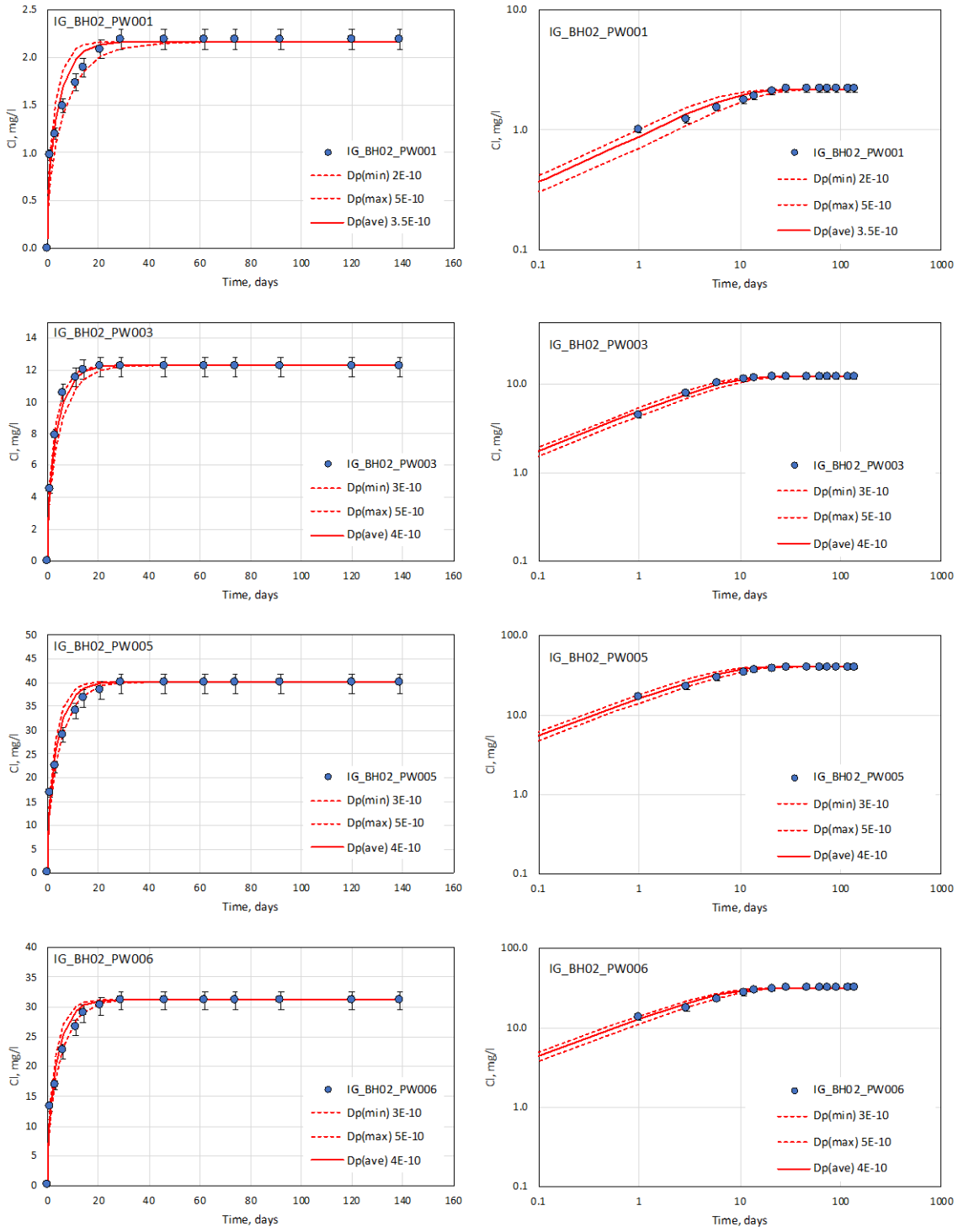


Figure 22: Maximum (Dp(max)) and minimum (Dp(min)) pore diffusion coefficients (45 °C) determined by a best fit of Cl elution curves in linear and logarithmic time and concentration scale; the solid lines mark the average diffusion coefficients (45 °C, Dp(ave))

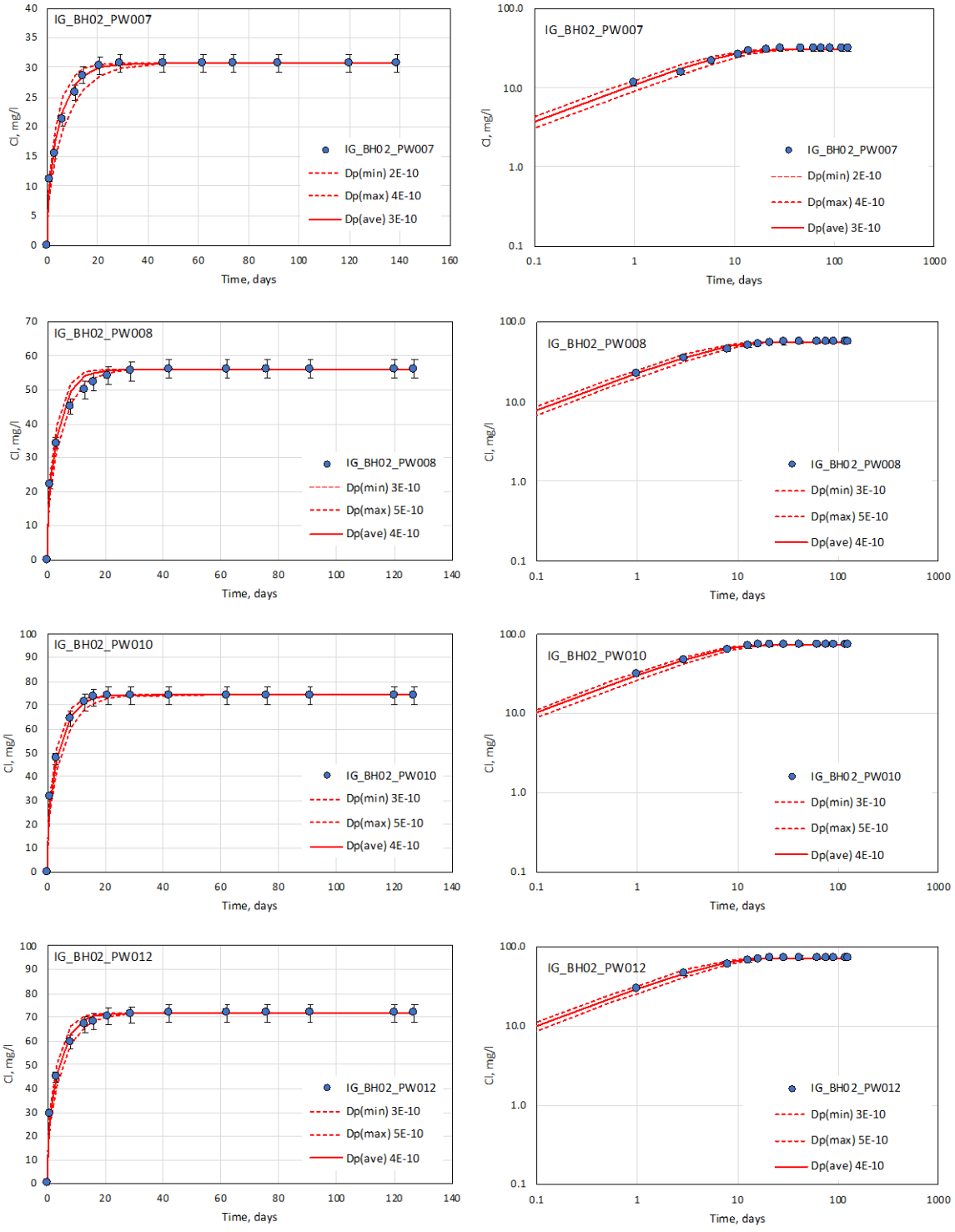


Figure 22 continued

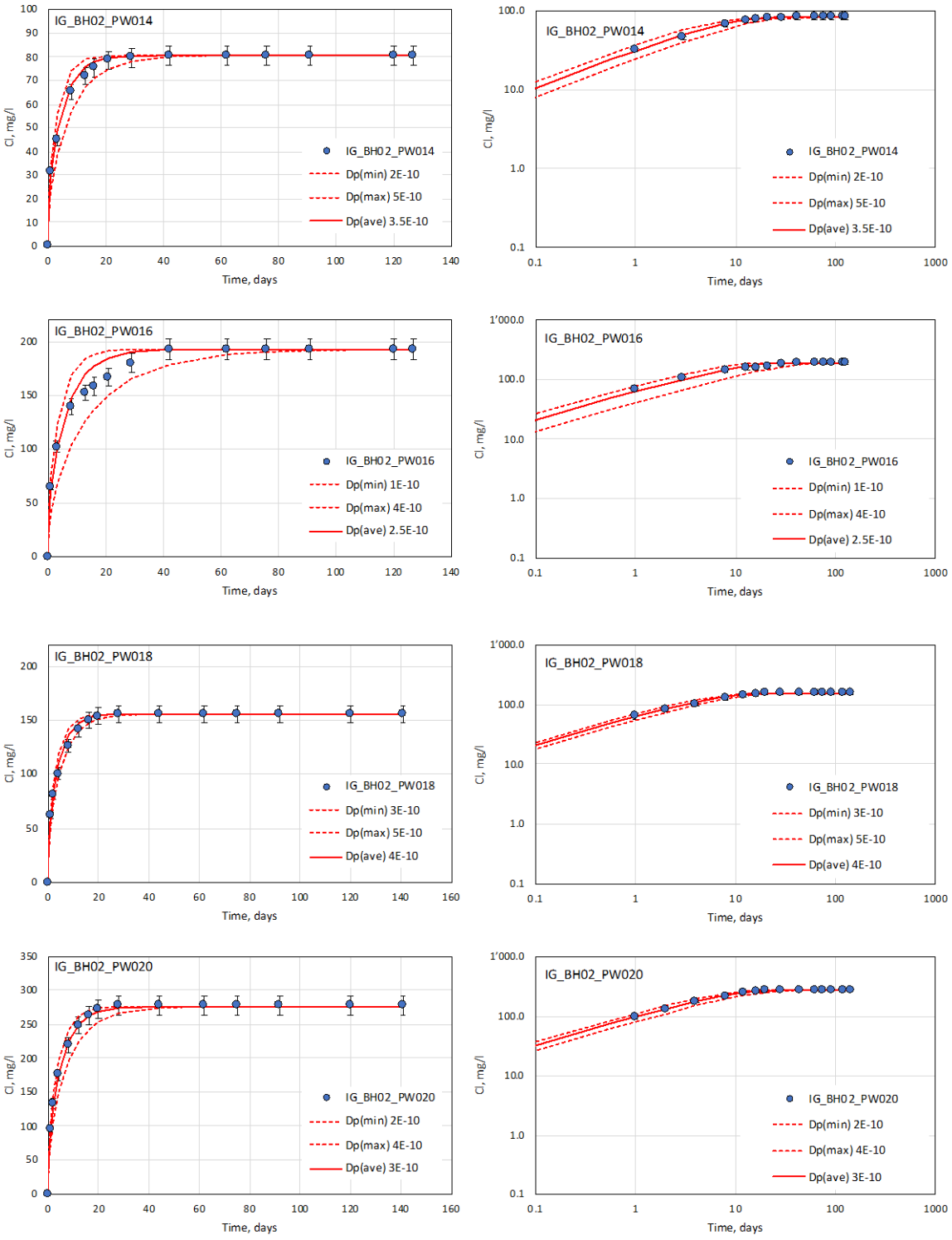


Figure 22 continued

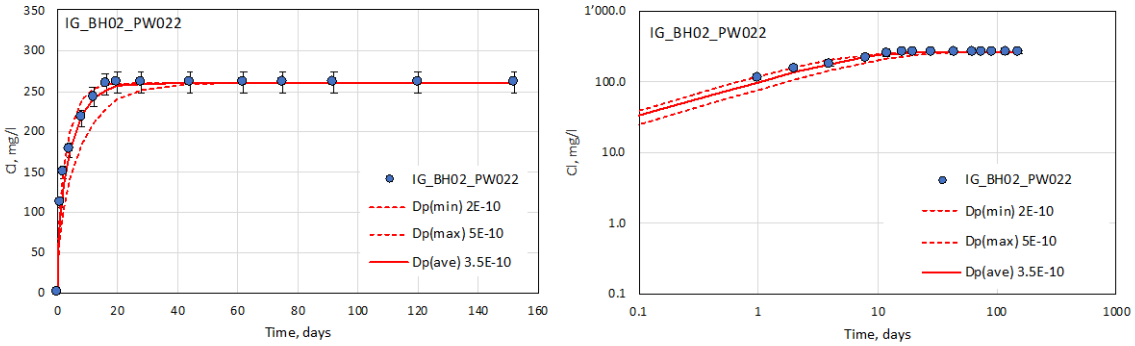


Figure 22 continued

Table 17: Minimum (min), maximum (max) and average (ave) pore and effective diffusion coefficients determined by 1-dimensional modelling of Cl-elution curves of out-diffusion experiments conducted on core samples from borehole IG_BH02 at 45 °C and calculated by the Stoke-Einstein equation for 10 °C and 25°C

Sample	Depth	WL-Porosity	D_P*10^{-10} (45°C)				D_P*10^{-10} (10°C)				D_e*10^{-12} (10°C)				D_P*10^{-10} (25°C)				D_e*10^{-12} (25°C)		
			max	min	ave		max	min	ave		max	min	ave		max	min	ave		max	min	ave
	mbgs*	Vol.%	m^2/s	m^2/s	m^2/s		m^2/s	m^2/s	m^2/s		m^2/s	m^2/s	m^2/s		m^2/s	m^2/s	m^2/s		m^2/s	m^2/s	m^2/s
IG_BH02_PW001	240.0	0.52	5	2	3.5		2.0	0.8	1.4		1.1	0.4	0.7		3.1	1.3	2.2		1.6	0.7	1.2
IG_BH02_PW003	348.0	0.43	5	3	4.0		2.0	1.2	1.6		0.9	0.5	0.7		3.1	1.9	2.5		1.3	0.8	1.1
IG_BH02_PW005	378.1	0.28	5	3	4.0		2.0	1.2	1.6		0.6	0.3	0.4		3.1	1.9	2.5		0.9	0.5	0.7
IG_BH02_PW006	381.7	0.44	5	3	4.0		2.0	1.2	1.6		0.9	0.5	0.7		3.1	1.9	2.5		1.4	0.8	1.1
IG_BH02_PW007	383.0	0.46	4	2	3.0		1.6	0.8	1.2		0.7	0.4	0.6		2.5	1.3	1.9		1.1	0.6	0.9
IG_BH02_PW008	455.2	0.56	5	3	4.0		2.0	1.2	1.6		1.1	0.7	0.9		3.1	1.9	2.5		1.8	1.1	1.4
IG_BH02_PW010	502.8	0.56	5	3	4.0		2.0	1.2	1.6		1.1	0.7	0.9		3.1	1.9	2.5		1.8	1.1	1.4
IG_BH02_PW012	555.7	0.51	5	3	4.0		2.0	1.2	1.6		1.0	0.6	0.8		3.1	1.9	2.5		1.6	1.0	1.3
IG_BH02_PW014	611.2	0.44	5	2	3.5		2.0	0.8	1.4		0.9	0.4	0.6		3.1	1.3	2.2		1.4	0.6	1.0
IG_BH02_PW016	665.8	0.52	4	1	2.5		1.6	0.4	1.0		0.8	0.2	0.5		2.5	0.6	1.6		1.3	0.3	0.8
IG_BH02_PW018	770.6	0.49	5	3	4.0		2.0	1.2	1.6		1.0	0.6	0.8		3.1	1.9	2.5		1.5	0.9	1.2
IG_BH02_PW020	878.8	0.47	4	2	3.0		1.6	0.8	1.2		0.8	0.4	0.6		2.5	1.3	1.9		1.2	0.6	0.9
IG_BH02_PW022	984.2	0.53	5	2	3.5		2.0	0.8	1.4		1.1	0.4	0.8		3.1	1.3	2.2		1.7	0.7	1.2

* mbgs (down hole)

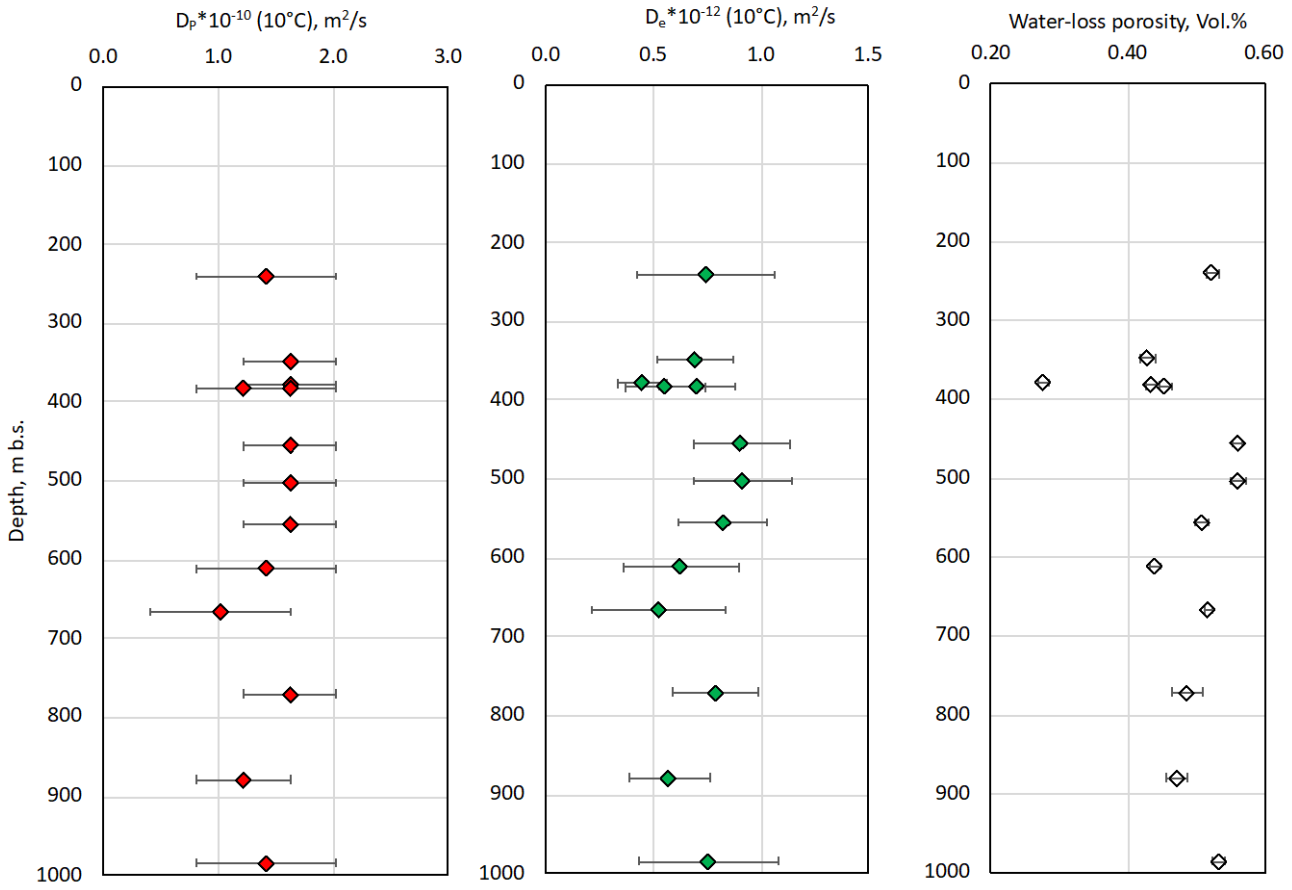


Figure 23: Average pore (left) and effective (middle) diffusion coefficients (10 °C) for chloride and the corresponding WL-porosity (right) of core samples from borehole IG_BH02 versus depth; the errors are the difference between the average and maximum/minimum values (depths are in mbgs (down hole))

8.0 CHLORIDE, BROMIDE AND CHLORIDE ISOTOPES IN POREWATER OF BOREHOLE IG_BH02

Chloride and bromide concentrations of porewater were determined by aqueous extraction (cf. Section 3.3.1) and out-diffusion experiments (cf. Section 3.3.2). Aqueous extraction experiments were conducted prior to the other longer lasting out-diffusion and isotope diffusive exchange experiments in order to obtain rough estimations of porewater salinities.

8.1 Porewater chloride concentrations estimated by aqueous extraction experiments

Aqueous extraction experiments were conducted on 12 core samples from the individual sampled depth intervals. Approximate estimates of porewater Cl concentrations were calculated according to Equation 3 (cf. Section 3.3.1). During crushing of the rock samples, saline fluids from fluid inclusions in quartz and feldspar are released, which contribute to the Cl and Br inventory of the samples. This means that the chloride concentrations determined by aqueous extraction overestimate the actual porewater Cl concentrations, especially for the samples from the upper bedrock zone, which have low porewater Cl-concentrations.

Estimated porewater Cl concentrations for core samples from borehole IG_BH02 determined by aqueous extraction vary between 2.05 and 14.9 g/kg H_2O (Table 18). Estimated porewater Cl concentrations determined by aqueous extraction are 1.1 to 23 times higher than those determined by out-diffusion (Table 13). The differences in porewater Cl concentrations determined by the two methods decreases with increasing depth and increasing porewater Cl concentrations (Table 18), indicating that porewater is the main Cl source in the deeper, higher salinity samples.

Based on the Cl-concentration range of porewater in core samples taken from borehole IG_BH02 (2.05 - 14.9 g/kg H_2O = 0.06 - 0.43 mol), the salinity of isotope diffusive exchange experiments was defined as 0.3 mol NaCl.

8.2 Porewater chloride and bromide concentrations and δ^{37}Cl isotope ratios determined by out-diffusion experiments

The conservative behaviour of chloride and bromide, the absence of Cl and Br bearing minerals in the rock, and the non-destructive character of the out-diffusion method make the porewater the only source for dissolved Cl and Br in the experimental solution. This allows calculation of the Cl and Br concentration in the porewater using mass balance according to Equation 4 (Section 3.3.2), given that equilibrium in the out-diffusion experiments is achieved. As shown by their chloride and bromide elution curves, this latter condition is fulfilled for all samples (cf. Section 7.1).

The mass ratio of the two conservative elements, Cl and Br, serves as tracer of the origin of Cl and Br in porewater (and also in fracture groundwaters). The δ^{37}Cl ratio measured for the experiment solutions directly corresponds to the porewater Cl isotope signature. This is because the attained equilibrium in the out-diffusion experiment with respect to total Cl is also expected to result in equilibrium with respect to the Cl isotopes (Gimmi and Waber 2004).

Chloride concentrations of porewater taken between 240 mbgs and 984 mbgs from borehole IG_BH02 vary between 91 and 14,168 mg/kg H_2O (Table 18, Figure 24). Considering the depth profile, the porewater chloride concentrations increase continuously from 91 mg/kg H_2O at 240 mbgs (down hole) to 14’168 mg/kg H_2O at

984 mbgs (down hole) (Table 18, Figure 24). The porewater Cl-concentrations show a sharp increase between 611 and 665 mbgs (down hole) from 4235 mg/kg H_2O to 8780 mg/kg H_2O and between 770 and 879 mbgs from 7439 mg/kg H_2O to 14168 mg/kg H_2O (Figure 12, Table 13). In the interval between 378 and 383 mbgs (down hole) three samples were taken. The porewater Cl-concentrations show a sharp decrease between 378.1 and 381.7 mbgs (down hole) from 3342 mg/kg H_2O to 1630 mg/kg H_2O and remain almost constant down to 383.0 mbgs (1588 mg/kg H_2O, Table 13, Figure 12).

Porewater bromide concentrations of core samples from borehole IG_BH02 vary between 30.3 and 307 mg/kg H_2O (Table 18, Figure 24). Along the depth profile porewater Br concentrations increase almost continuously from 31.1 mg/kg at 240 mbgs (down hole) to 73.3 mg/kg H_2O at 611mbgs (down hole) and display a steep increase to 154 mg/kg H_2O at 665 mbgs (down hole) and continuously increase to 307 mg/kg H_2O at 984 mbgs (down hole) (Figure 24). In the zone between 378.1 and 383 mbgs (down hole), porewater Br-concentrations show the same trend as Cl. They decrease sharply from 61.7 mg/kg H_2O at 378.1 mbgs to 30.8 mbgs at 381.7 mbgs (done hole) and remain constant to 383.0 mbgs (down hole) (30.3 mg/kg H_2O, Table 13, Figure 12).

The Br*1000/Cl mass ratios (=Br/Cl ratio) of porewater from borehole IG_BH02 vary over a wide range between 17 and 341 (Table 18, Figure 24). From 240 to 378 mbgs (down hole) porewater Br/Cl ratios decrease from 341 to 18 and stay almost constant between 17 and 21 to a depth of 665 mbgs (down hole). In the deep zone between 770 and 984 mbgs (down hole) the Br/Cl ratios vary between 19 and 26 (Table 18, Figure 24).In the zone between 378 and 383 mbgs (down hole) the Br/Cl ratios of the three taken samples are similar, between 18 and 19 (Table 13).

In the bromide versus chloride diagram, porewaters extracted from borehole IG_BH02 cores plot significantly above the seawater dilution line (Br*1000/Cl mass ratio of seawater = 3.4, Figure 25).

Porewater $\delta^{37}Cl$ isotope signatures vary between -0.20 ± 0.20 ‰ and 0.81 ± 0.44 ‰ SMOC along the depth profile between 348 and 984 mbgs (down hole) (Figure 24, Table 18). Porewater stable chlorine isotope signatures do not show a trend with porewater Cl-concentrations (Figure 26). The chloride isotope signatures of porewater of the three core samples taken between 378 and 383 mbgs (down hole) are in the same range (0.03 ‰ to 0.12 ‰ SMOC).

Table 18: Porewater Cl and Br concentrations and Br*1000/Cl mass ratios and $\delta^{37}Cl$ isotope signatures. Cl concentrations are determined by out-diffusion (o.d.) and estimated using aqueous extraction experiments (aq.ex.); the errors of porewater (o.d.) Br concentrations and Br*1000/Cl mass ratios are calculated by Gaussian error propagation (Appendix III); the errors of $\delta^{37}Cl$ values are the standard deviation of triplicate analyses

Sample	Depth	Cl_{PW} (o.d.)	Estimated Cl_{PW}(aq.ex.)	Br_{PW}	Br*1000/Cl	$\delta^{37}Cl$
	mbgs*	mg/kgH_2O	mg/kgH_2O	mg/kgH2O	mg/mg	‰ SMOC
IG_BH02_PW001	240.0	91±5		31.1±1.7	341±27	**
IG_BH02_PW003	348.0	641±45		78.2±5.4	122±12	-0.20±0.20
IG_BH02_PW005	378.1	3342±247		61.7±4.6	18±2	0.12±0.20
IG_BH02_PW006	381.7	1630±99		30.8±1.9	19±2	0.03±0.33
IG_BH02_PW007	383.0	1588±83		30.3±1.6	19±1	0.09±0.50
IG_BH02_PW008	455.2	2570±138		54.7±2.9	21±2	0.81±0.44

Sample	Depth	Cl_{PW} (o.d.)	Estimated Cl_{PW}(aq.ex.)	Br_{PW}	Br*1000/Cl	$\delta^{37}Cl$
	mbgs*	mg/kgH_2O	mg/kgH_2O	mg/kgH2O	mg/mg	‰ SMOC
IG_BH02_PW010	502.8	3255±204		61.2±3.8	19±2	0.04±0.49
IG_BH02_PW012	555.7	3781±228		68.3±4.1	18±2	0.23±0.22
IG_BH02_PW014	611.2	4235±240		73.3±4.2	17±1	0.13±0.20
IG_BH02_PW016	665.8	8780±474		154±8	18±1	0.04±0.20
IG_BH02_PW018	770.6	7439±837		194±22	26±4	0.41±0.29
IG_BH02_PW020	878.8	14168±1238		274±24	19±2	0.60±0.20
IG_BH02_PW022	984.2	12192±764		307±19	25±2	0.09±0.31
IG_BH02_AQ001	240.2		2048	132	65	
IG_BH02_AQ002	348.5		2289	186	81	
IG_BH02_AQ003	379.6		4312	67	15	
IG_BH02_AQ004	382.0		4106	56	14	
IG_BH02_AQ005	455.5		4456	68	15	
IG_BH02_AQ006	530.8		4959	150	30	
IG_BH02_AQ007	555.1		6739	85	13	
IG_BH02_AQ008	611.4		8420	115	14	
IG_BH02_AQ009	666.1		4422	59	13	
IG_BH02_AQ010	771.4		10252	327	32	
IG_BH02_AQ011	879.0		14941	391	26	
IG_BH02_AQ012	984.5		14074	494	35	

* mbgs (down hole)

** Cl-concentrations in out-diffusion test solutions were too low for the determination of chloride isotope signatures

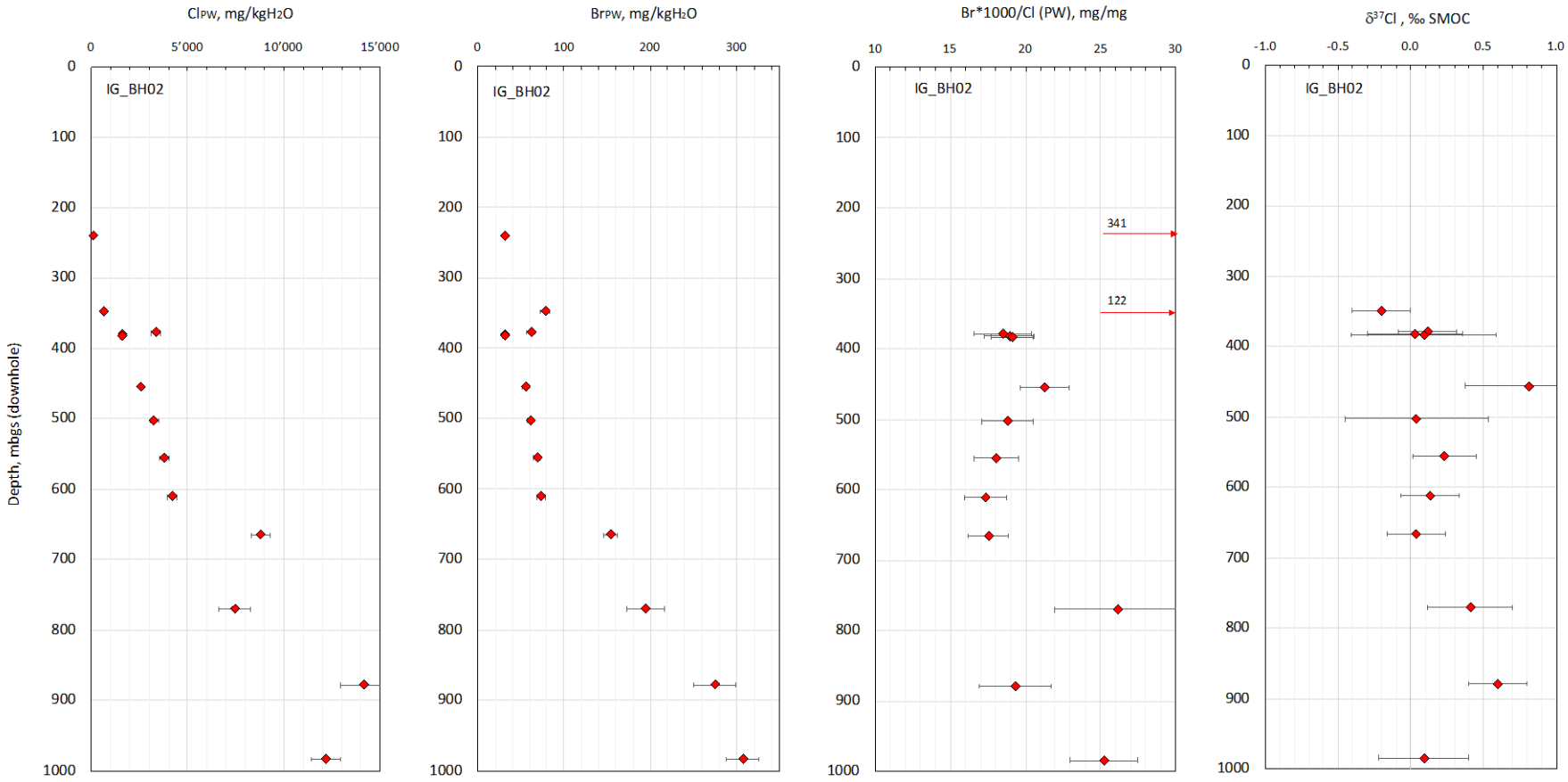


Figure 24: Porewater chloride and bromide concentrations (out-diffusion only), Br*1000/Cl mass ratios and $\delta^{37}Cl$ porewater signatures extracted from borehole IG_BH02 cores as function of depth (depth in mbgs (down hole))

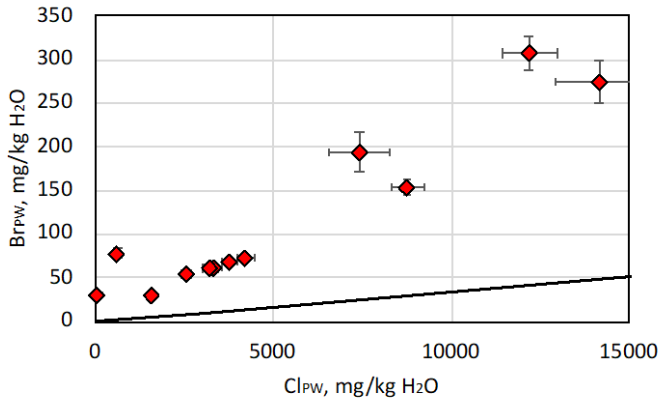


Figure 25: Chloride versus bromide concentrations of porewater from cores from borehole IG_BH02; the blue line indicates the seawater dilution line

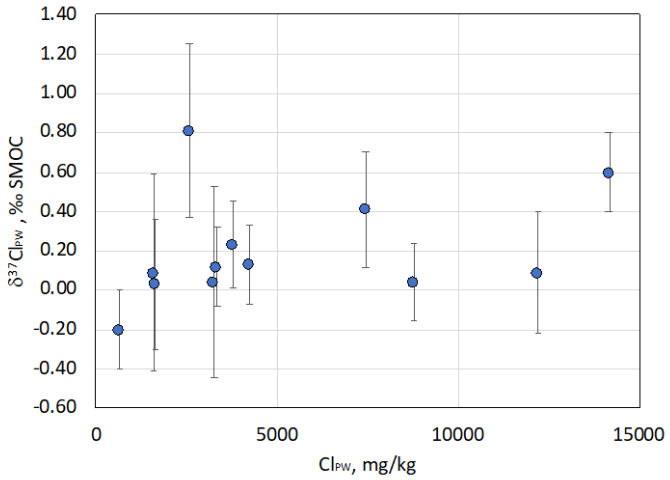


Figure 26: Porewater $\delta^{37}Cl$ isotope signatures versus porewater Cl-concentrations

9.0 $\delta^{18}O$ AND $\delta^{2}H$ OF POREWATER OF CORE SAMPLES FROM BOREHOLE IG_BH02

Isotope diffusive exchange experiments have been carried out on 13 core samples (26 individual experiments) from borehole IG_BH02. The $\delta^{18}O$ and $\delta^{2}H$ values of porewater are calculated according to Equation 7 (cf. Section 3.3.3), expressed relative to the standard V-SMOW, and are listed in Table 19 and graphically shown in Figure 27 and Figure 28. The calculated porewater isotope signatures, which are based on the isotope analyses of the test waters, are carefully evaluated for potential artefacts, mainly due to evaporation of test water during the experiment, and during test water storage and handling. Evaporation of porewater during storage and handling was minimized by careful handling of the core samples (cf. Section 3.3.3). These processes might result in large discrepancies between the gravimetric water content and that calculated from isotope mass balance or isotope signatures that are out of any natural range and/or a large error on the calculated porewater isotope signatures. Such differences were not observed in this study (cf. Section 5.1.2).

Evaporation within the experiment was monitored by keeping track of all individual weights before and after the experiments. None of the experiments suffered evaporation > 2 % of the total water mass in the experiments (= mass of porewater determined gravimetrically + mass of test water) during the time of equilibration.

The maximum Cl concentration determined by aqueous extraction prior to the set-up of the isotope diffusive exchange experiments is 14.9 g/kg H_2O, which relates to 0.46 mol $NaCl_{eq}$. Out-diffusion experiments showed a maximum Cl concentration of 14.2 g/kg H_2O, which relates to 0.44 mol $NaCl_{eq}$. Based on the aqueous extraction results, it was decided to adjust the salinity of the test solutions to 0.3 mol NaCl to prevent mass transfer from the test water reservoir to the rocks.

Stable oxygen and hydrogen isotope signatures of porewater extracted from core samples from borehole IG_BH02 vary between -10.88 and -7.40 ‰ for $\delta^{18}O$ and -83.3 and -61.3 ‰ for $\delta^{2}H$ (Table 19, Figure 27). Along the depth profile encountered by borehole IG_BH02, stable water isotope signatures are almost constant within the error range between 242 and 772 mbgs (down hole) become generally slightly enriched in ^{18}O and ^{2}H with increasing depth from 240 mbgs (down hole) ($\delta^{18}O$ = -10.82 ‰, $\delta^{2}H$ = -83.3 ‰) to 611 mbgs ($\delta^{18}O$ = -8.76 ‰, $\delta^{2}H$ = -68.8 ‰). Between 770 and 984 mbgs (down hole) the stable isotope signatures are more enriched in heavy isotopes than in the upper zones at almost constant signatures between -7.90 ‰ and -7.40 ‰ for $\delta^{18}O$, and between -65.0 ‰ and -61.3 ‰ for $\delta^{2}H$.

Porewaters from borehole IG_BH02 of core samples taken between 240 and 984 mbgs (down hole) plot on or slightly to the right of the global meteoric water line (GMWL) on the $\delta^{18}O$-$\delta^{2}H$ diagram (Figure 28).

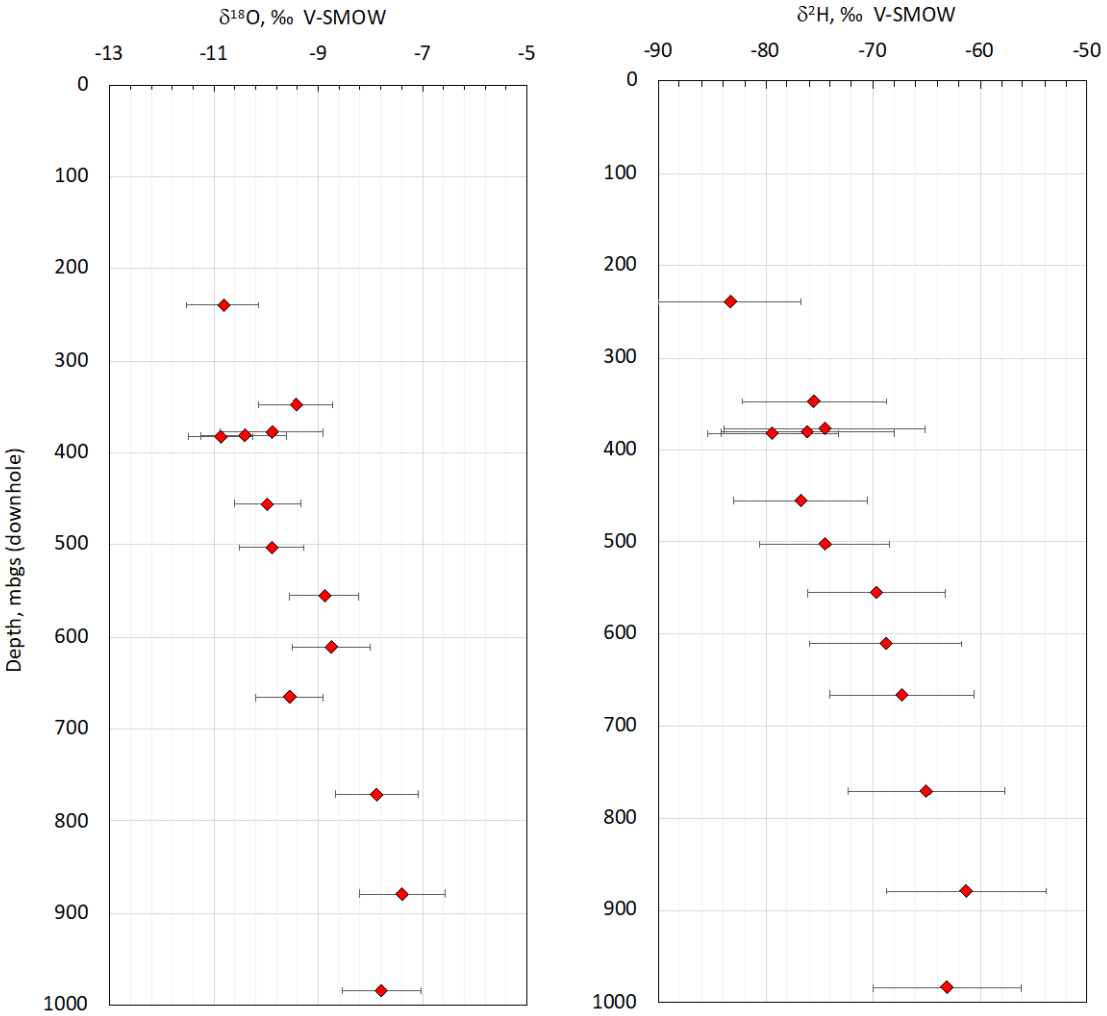


Figure 27: $\delta^{18}O$ and $\delta^{2}H$ porewater signatures as function of depth along borehole IG_BH02; errors are calculated by Gaussian error propagation (depth in mbgs (down hole))

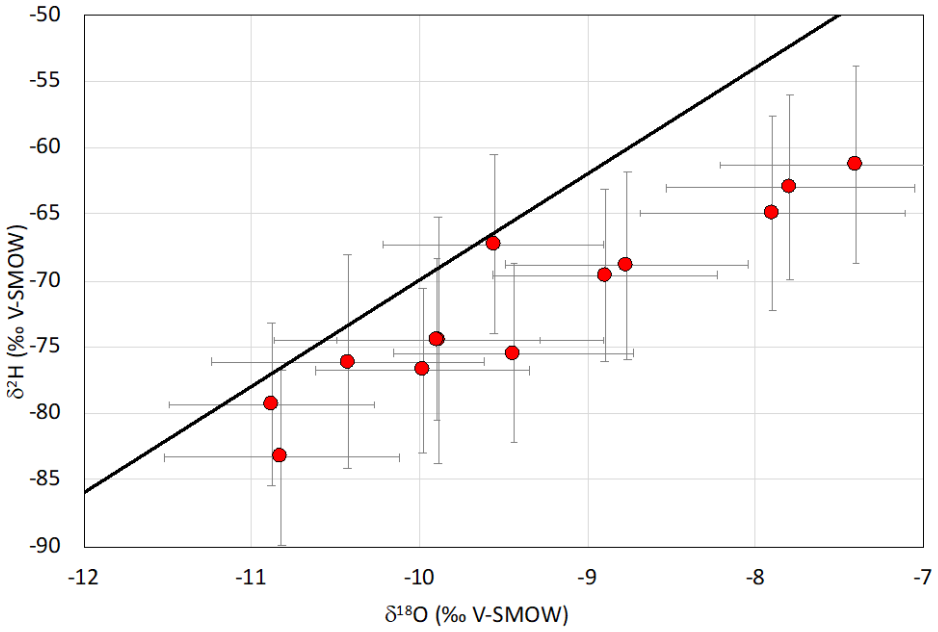


Figure 28: $\delta^{18}O$ versus $\delta^{2}H$ values of porewater; the blue line marks the global meteoric water line; the errors of the stable isotope ratios are calculated by Gaussian error propagation

Table 19: $\delta^{18}O$ and $\delta^{2}H$ values of porewater of core samples from borehole IG_BH02; the errors are calculated by Gaussian error propagation

Sample	Depth	$\delta^{18}O$	Error $\delta^{18}O$	$\delta^{2}H$	Error $\delta^{2}H$
	mbgs*	‰ V-SMOW	‰ V-SMOW	‰ V-SMOW	‰ V-SMOW
IG_BH02_PW001	240.0	-10.82	0.70	-83.3	6.6
IG_BH02_PW003	348.0	-9.44	0.71	-75.5	6.8
IG_BH02_PW005	378.1	-9.89	0.98	-74.5	9.3
IG_BH02_PW006	381.7	-10.43	0.81	-76.1	8.1
IG_BH02_PW007	383.0	-10.88	0.61	-79.3	6.1
IG_BH02_PW008	455.2	-9.98	0.63	-76.8	6.2
IG_BH02_PW010	502.8	-9.89	0.61	-74.5	6.1
IG_BH02_PW012	555.7	-8.90	0.67	-69.6	6.5
IG_BH02_PW014	611.2	-8.76	0.73	-68.8	7.1
IG_BH02_PW016	665.8	-9.56	0.65	-67.3	6.7
IG_BH02_PW018	770.6	-7.90	0.78	-65.0	7.3
IG_BH02_PW020	878.8	-7.40	0.81	-61.3	7.4
IG_BH02_PW022	984.2	-7.79	0.74	-63.0	6.9

*mbgs (down hole)

10.0 SUMMARY

Porewater investigations applying different indirect methods were successfully conducted on crystalline core samples taken between 240 and 984 mbgs (down hole) from borehole IG_BH02 drilled in the Revell batholith (RE-B at Ignace, Ontario).

Potential major sampling-, preservation-, preparation-, experimental- and analytical artefacts, were carefully monitored during the investigation, and none were observed.

The investigated core samples consisted of macroscopically homogeneous, equigranular granodiorite and tonalite with quartz, plagioclase and biotite as main components, with variable degrees of alteration.

The gravimetrically determined water contents (weighted for the entire core sample) vary along the depth profile between 0.15 and 0.29 wt.%, corresponding to water-loss porosities between 0.39 and 0.77 Vol.%. Gravimetrically determined water contents agreed well with those determined by isotope diffusive exchange experiments. The bulk, wet density values are between 2.62 and 2.70 g/cm^3.

Out-diffusion experiments ran for more than 150 days. The analyses of time series samples showed that all experiments were in equilibrium with respect to Cl before they were terminated. Test water chemistries are mainly dominated by sodium, calcium, potassium, hydrogen carbonate and chloride in varying proportions and concentrations.

Pore diffusion coefficients were determined by 1-dimensional diffusion modelling based on the fitting of Cl-elution curves, set up by taking periodic sub-samples from out-diffusion experiments. Elution curves could not be fitted by a single pore diffusion coefficient. All cores showed a faster diffusion in the outer rim of the cores and a slower diffusion in the inner parts. The average pore diffusion coefficients (10 °C) vary between $1.0*10^{-10}$ and $1.6*10^{-10}$ m^2/s, corresponding to effective diffusion coefficients between $0.4*10^{-12}$ and $0.9*10^{-12}$ m^2/s.

Aqueous extraction experiments were conducted prior to the set-up of the long-term experiments to obtain first information about porewater salinities, which are necessary for the applied test water concentrations for isotope diffusive exchange experiments.

Porewater Cl and Br concentrations were calculated using out-diffusion concentrations and the gravimetrically determined mass of porewater. They vary between 91 and 14,168 mg/kg H_2O for Cl, and 31 and 307 mg/kg H_2O for Br, resulting in Br*1000/Cl mass ratios between 17 and 341.

Chlorine isotope signatures of porewater vary along the profile between 0.20 and 0.81 ‰ SMOC and show no correlation to porewater Cl concentrations.

Porewater stable water isotope signatures were determined by isotope diffusive exchange experiments. Along the depth profile encountered by borehole IG_BH02, porewater $\delta^{18}O$ signatures vary between -10.88 and -7.40 ‰ V-SMOW, and δ^2H signatures between -83.3 and -61.3 ‰ V-SMOW.

11.0 REFERENCES

Bas, M.J., Streckeisen, A.L., 1991. The IUGS Systematic of Igneous Rocks. Journal of the Geological Society, London.

Blackburn, C.E. and Hinz, P., 1996. Gold and base metal potential of the northwest part of the Raleigh Lake greenstone belt, northwestern Ontario-Kenora Resident Geologist's District; in Summary of Field Work and Other Activities 1996, Ontario Geological Survey, Miscellaneous Paper 166, p.113-115.

Crank, J., 1975. The Mathematics of Diffusion; Oxford Science Publications; Oxford.

DesRoches, A., Sykes, M., Parmenter, A. and Sykes, E., 2018. Lineament Interpretation of the Revell Batholith and Surrounding Greenstone Belts. Nuclear Waste Management Organization. NWMO Report Number: NWMO-TR-2018-19.

Eichinger, F.L., Waber, H.N., Smellie, J.A.T., 2006. Characterisation of Matrix Porewater at the Olkiluoto Investigation Site, Finland. Posiva Working Report 2006-103, Posiva OY, Olkiluoto Finland.

Golder (Golder Associates Ltd.) and PGW (Paterson Grant and Watson Ltd.), 2017. Phase 2 Geoscientific Preliminary Assessment, Geological Mapping, Township of Ignace and Area, Ontario: APM-REP-01332-0225.

Gimmi, T. and Waber, H.N., 2004. Modelling of Tracer Profiles in Pore Water of Argillaceous Rocks in the Benken Borehole: Stable Water Isotopes, Chloride, and Chlorine Isotopes; Nagra Tech. Rep. 2004-05, Nagra, Wettingen, Switzerland.

Jäckli, H., 1970. Kriterien zur Klassifikation von Grundwasservorkommen. Ecologae geol. Helv., 63 (2), 389-434.

Le Maitre, R.W. (ed.), 2002. IGNEOUS ROCKS A classification and Glossary of Terms. Cambridge University Press, Cambridge, UK.

Lide, D.R., 1994. CRC Handbook of chemistry and physics. 75th ed., CRC Press, Boca Raton, USA.

Meier, D.B., Waber, H.N., Gimmi, T., Eichinger, F., Diamond, L.W., 2015. Reconstruction of in-situ porosity and porewater compositions of low-permeability crystalline rocks: Magnitude of artefacts induced by drilling and sample recovery. Journal of Contaminant Hydrology, 183, 55-71.

OGS (Ontario Geological Survey), 2011. 1:250 000 scale bedrock geology of Ontario, Ontario Geological Survey, Miscellaneous Release Data 126 - Revision 1.

Ohlsson, Y. and Neretnieks, I., 1995. Literature survey of matrix diffusion theory and of experiments and data including natural analogues; SKB Tech. Rep. 95-12, Svensk Kärnbränslehantering AB, Stockholm, Sweden.

Parmenter, A., Waffle, L. and DesRoches, A., 2020. An updated bedrock geology map and geological database for the northern portion of the Revell batholith. Nuclear Waste Management Organization. NWMO Report Number: NWMO-TR-2020-08.

Rogge, T., 1997. Eine molekular-diffusive Methode zur Bestimmung des Porenwassergehaltes und der Zusammensetzung von stabilen Isotopen im Porenwasser von Gestein; unveröffentlichte Diplomarbeit; Heidelberg.

Rübel, A.P., Sonntag, Ch., Lippmann, J., Pearson, F.J. and Gautschi, A., 2002. Solute transport in formations of very low permeability: Profiles of stable isotope and dissolved noble gas contents of pore water in the Opalinus Clay. Mont Terri, Switzerland; Geochim. Cosmochim. Acta, 66, 1311-1321.

Schmid, R., Douglas, Fettes D., Harte, B., Davis, E., Desmons, J., 2007. How to Name a Metamorphic Rock. Recommendations by the IUGS Subcomission on the Systematics of Metamorphic Rocks.

SGL (Sander Geophysics Limited), 2015. Phase 2 Geoscientific Preliminary Assessment, Acquisition, Processing and Interpretation of High-Resolution Airborne Geophysical Data, Township of Ignace, Ontario. NWMO Report Number: APM-REP-06145-0002.

Siivola, J., Schmid, R., 2007. List of Mineral Abbreviations. Recommendations by the IUGS Subcomission on the Systematics of Metamorphic Rocks.

SRK (SRK Consulting, Inc.) and Golder, 2015. Phase 2 Geoscientific Preliminary Assessment, Observation of General Geological Features, Township of Ignace, Ontario. NWMO Report Number: APM-REP-06145-0004.

Streckeisen A.L.,1974. Classification and Nomenclature of Plutonic Rocks. Recommendations of the IUGS Subcommission on the Systematics of Igneous Rocks. International Journal of Earth Sciences 63, 2, 773-786.

Stone, D., 2009. Geology of the Bending Lake Area, Northwestern Ontario; *in* Summary of Field Work and Other Activities 2009. Ontario Geological Survey. Open File Report 6240.

Stone, D., 2010a. Geology of the Stormy Lake Area, Northwestern Ontario; *in* Summary of Field Work and Other Activities 2010. Ontario Geological Survey, Open File Report 6260.

Stone, D., 2010b. Precambrian geology of the central Wabigoon Subprovince area, northwestern Ontario. Ontario Geological Survey, Open File Report 5422.

Stone, D., Halle, J. and Chaloux, E., 1998. Geology of the Ignace and Pekagoning Lake Areas, Central Wabigoon Subprovince; *in* Summary of Field Work and Other Activities 1998, Ontario Geological Survey, Misc. Paper 169.

Stone, D., Davis, D.W., Hamilton, M.A. and Falcon, A., 2010. Interpretation of 2009 Geochronology in the Central Wabigoon Subprovince and Bending Lake Areas, Northwestern Ontario, *in* Summary of Field Work and Other Activities 2010, Ontario Geological Survey, Open File Report 6260.

Waber, H.N. and Smellie, J.A.T., 2005. SKB Site Investigations Forsmark – Borehole KFM06: Characterisation of porewater. Part I: Diffusion experiments; SKB P-Rep. P-05-196, Svensk Kärnbränslehantering AB, Stockholm, Sweden.

Waber, H.N. and Smellie, J.A.T., 2006. Oskarshamn site investigations. Borehole KLX03: Characterisation of porewater. Part 2: Rock properties and diffusion experiments; SKB P-Report P-06-77. Svensk Kärnbränslehantering AB, Stockholm, Sweden.

APPENDIX I

Photo Documentation

Figure A-1: On site documentation of core samples for porewater characterization sent to Hydroisotop (photos provided by Golder); Core samples are packed in the first evacuated and sealed plastic bag (depths are in mbgs (down hole))



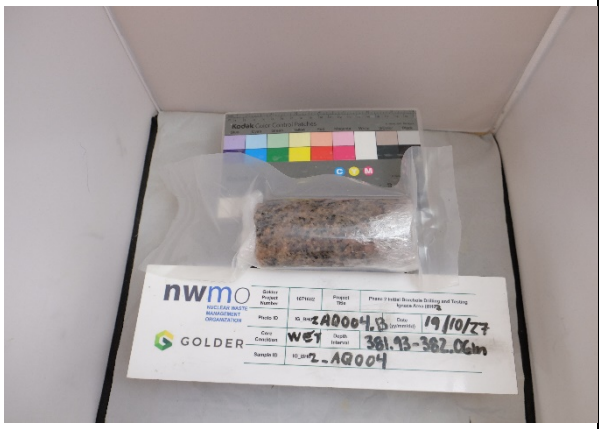
IG_BH02_AQ001: 240.14-240.25 m



IG_BH02_AQ002: 348.44-348.60 m



IG_BH02_AQ003: 379.51-379.69 m



IG_BH02_AQ004: 381.93-382.06 m



IG_BH02_AQ005: 455.39-455.54 m



IG_BH02_AQ006: 503.76-503.89 m

		
IG_BH02_AQ007: 555.04-555.18 m	IG_BH02_AQ008: 611.35-611.48 m	IG_BH02_AQ009: 666.01-666.16 m
		
IG_BH02_AQ010: 771.38-771.51 m	IG_BH02_AQ011: 878.96-879.11 m	IG_BH02_AQ012: 984.40-984.53 m



IG_BH02_PW001: 239.79-240.14 m



IG_BH02_PW002: 243.09-243.46 m



IG_BH02_PW003: 347.77-348.13 m



IG_BH02_PW004: 351.52-351.90 m



IG_BH02_PW005: 377.96-378.31 m



IG_BH02_PW006: 381.56-381.93 m



IG_BH02_PW007: 382.76-383.16 m



IG_BH02_PW008: 454.98-455.39 m



IG_BH02_PW009: 460.56-460.93 m



IG_BH02_PW010: 502.57-502.94 m



IG_BH02_PW011: 507.54-507.88 m



IG_BH02_PW012: 555.55-555.94 m

		
IG_BH02_PW013: 558.09-558.44 m	IG_BH02_PW014: 610.98-611.35 m	IG_BH02_PW015: 613.66-614.04 m
		
IG_BH02_PW016: 665.64-666.01 m	IG_BH02_PW017: 667.32-667.54 m	IG_BH02_PW018: 770.41-770.78 m



IG_BH02_PW019: 772.88-773.29 m



IG_BH02_PW020: 878.60-878.96 m



IG_BH02_PW021: 885.41-885.80 m

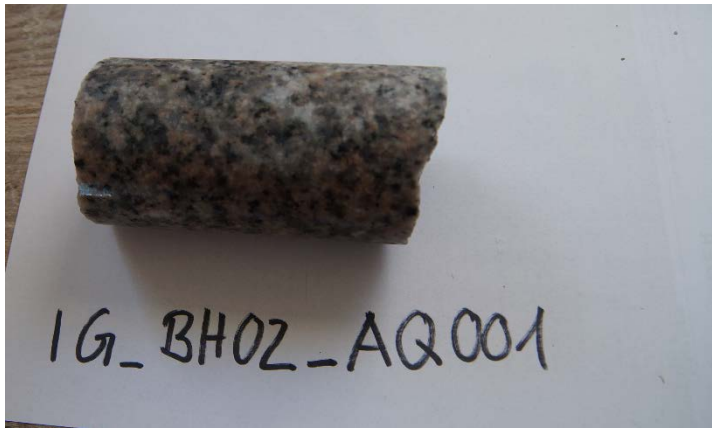


IG_BH02_PW022: 984.02-984.40 m

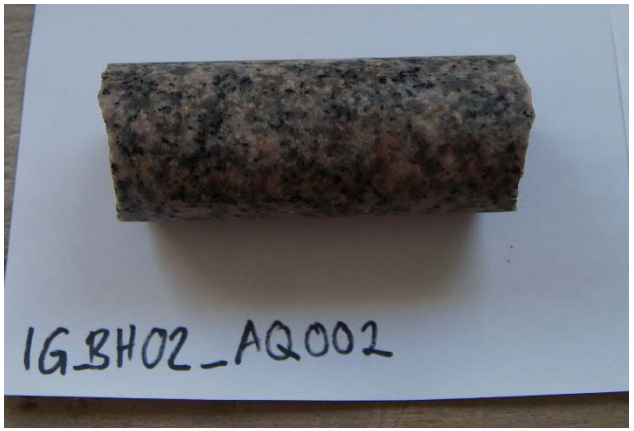


IG_BH02_PW022: 985.74-986.12 m

Figure A-2: Laboratory documentation of core samples for porewater characterization sent to Hydroisotop; photos were taken right after unpacking (depths are in mbgs (down hole))



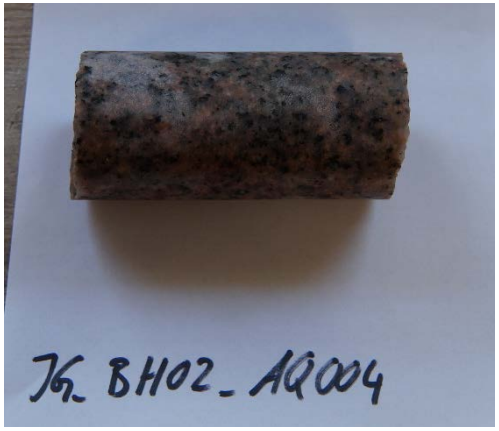
IG_BH02_AQ001: 240.14-240.25 m



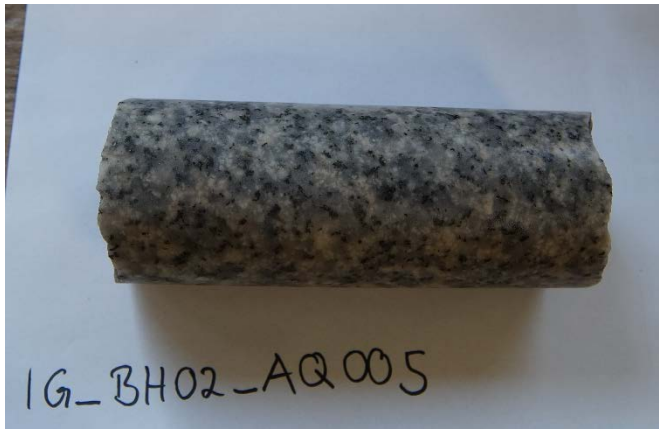
IG_BH02_AQ002: 348.44-348.60 m



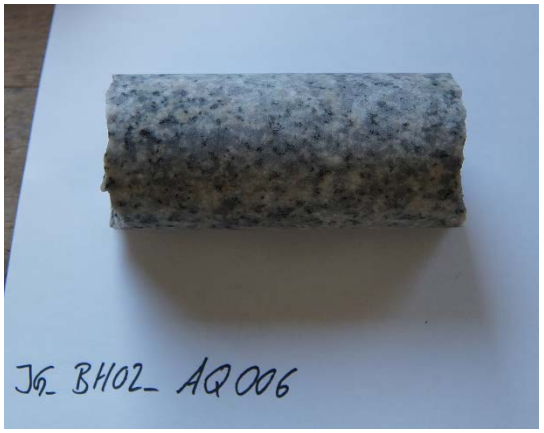
IG_BH02_AQ003: 379.51-379.69 m



IG_BH02_AQ004: 381.93-382.06 m



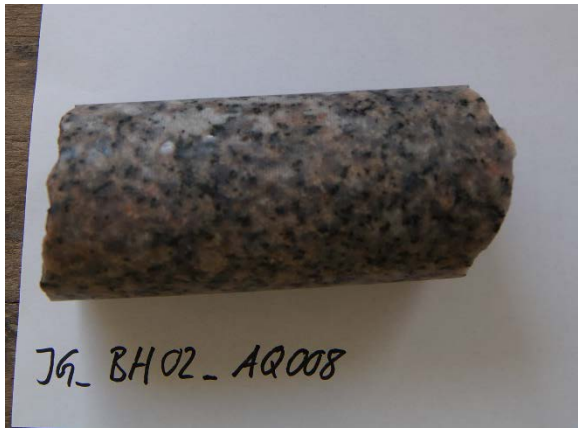
IG_BH02_AQ005: 455.34-455.54 m



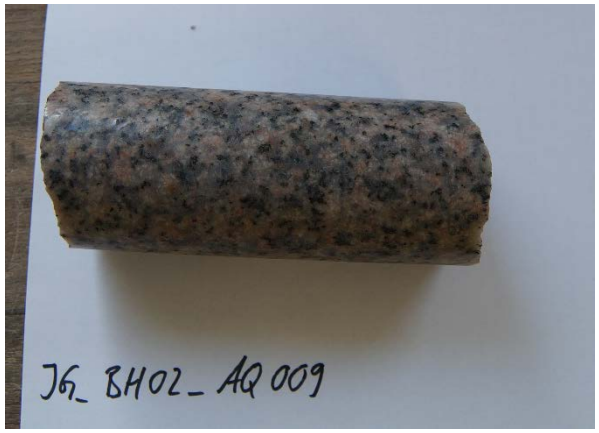
IG_BH02_AQ006: 503.76-503.89 m



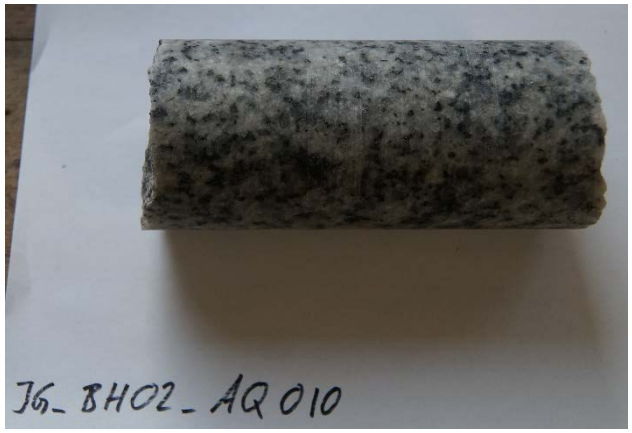
IG_BH02_AQ007: 555.04-555.18 m



IG_BH02_AQ008: 611.35-611.48 m



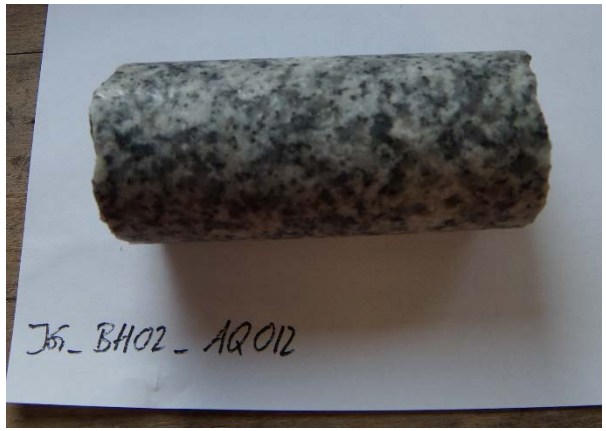
IG_BH02_AQ009: 666.01-666.16 m



IG_BH02_AQ010: 771.38-771.38 m



IG_BH02_AQ011: 878.96-879.11 m



IG_BH02_AQ012: 984.40-984.53 m



IG_BH02_PW001: 239.79-240.14 m



IG_BH02_PW003: 347.77-348.13 m



IG_BH02_PW005: 377.96-378.31 m



IG_BH02_PW006: 381.56-381.93 m



IG_BH02_PW007: 382.76-383.16 m



IG_BH02_PW008: 454.98-455.39 m



IG_BH02_PW010: 502.57-502.94 m



IG_BH02_PW012: 555.55-555.94 m



IG_BH02_PW014: 610.98-611.35 m



IG_BH02_PW016: 665.64-666.01 m



IG_BH02_PW018: 770.41-770.78 m



IG_BH02_PW020: 878.60-878.96 m



IG_BH02_PW022: 985.74-986.12 m

APPENDIX II

Analytical Raw Data

APPENDIX II-1

Calculation of Water Content Values: Raw Data

Table A-1: Determination of gravimetric water content; sample weights, drying times and calculated water contents of core pieces used for aqueous extraction experiments

Sample	Date prepared	Drying times	m (cryst.dish)	m (cryst+ rock)	14.11.2019	02.12.2019	12.12.2019	07.01.2020	22.01.2020	04.02.2020		Sample	m(rock, wet)	m (rock, dry)
			g	g	g	g	g	g	g	g			g	g
IG_BH02_AQ001	07.11.2019	89	92,286	418,123	417,58	417,564	417,573	417,559	417,569	417,57		IG_BH02_AQ001	325,837	325,273
IG_BH02_AQ002	07.11.2019	76	86,343	443,124	442,566	442,547	442,561	442,526	442,526			IG_BH02_AQ002	356,781	356,183
IG_BH02_AQ003	07.11.2019	89	86,232	505,695	504,652	504,549	504,576	504,512	504,526	504,527		IG_BH02_AQ003	419,463	418,280
IG_BH02_AQ004	07.11.2019	89	86,253	403,807	403,317	403,296	403,307	403,278	403,295	403,296		IG_BH02_AQ004	317,554	317,025
					27.11.2019	**12.12.2019**	**07.01.2020**	**22.01.2020**						
IG_BH02_AQ005	19.11.2019	64	85,727	469,710	468,817	468,84	468,828	468,830				IG_BH02_AQ005	383,983	383,101
IG_BH02_AQ006	19.11.2019	64	94,264	400,950	400,263	400,287	400,276	400,277				IG_BH02_AQ006	306,686	306,012
IG_BH02_AQ007	19.11.2019	64	89,008	423,460	422,814	422,790	422,780	422,780				IG_BH02_AQ007	334,452	333,772
IG_BH02_AQ008	19.11.2019	64	85,352	367,989	367,632	367,530	367,517	367,519				IG_BH02_AQ008	282,637	282,165
IG_BH02_AQ009	19.11.2019	64	90,616	403,858	403,350	403,337	403,318	403,320				IG_BH02_AQ009	313,242	312,702
					18.12.2019	**07.01.2020**	**23.01.2020**							
IG_BH02_AQ010	11.12.2019	43	85,978	320,025	319,701	319,685	319,685					IG_BH02_AQ010	234,047	233,707
IG_BH02_AQ011	11.12.2019	43	84,290	445,756	445,194	445,160	445,158					IG_BH02_AQ011	361,466	360,868
IG_BH02_AQ012	11.12.2019	43	90,878	384,540	384,083	384,057	384,055					IG_BH02_AQ012	293,662	293,177
			m (wet surf)		**14.11.2019**	**28.11.2019**	**12.12.2019**	**07.01.2020**	**23.01.2020**					
IG_BH02_AQ001-A	07.11.2019	77	87,403		87,210	87,195	87,179	87,175	87,175			IG_BH02_AQ001-A	87,403	87,175
IG_BH02_AQ002-A	07.11.2019	35	102,630		102,473	102,464	102,466					IG_BH02_AQ002-A	102,630	102,464
IG_BH02_AQ003-A	07.11.2019	77	209,448		209,028	208,94	208,916	208,886	208,886			IG_BH02_AQ003-A	209,448	208,886
IG_BH02_AQ004-A	07.11.2019	35	120,944		120,734	120,722	120,722					IG_BH02_AQ004-A	120,944	120,722
IG_BH02_AQ001-B	07.11.2019	35	84,545		84,384	84,371	84,372					IG_BH02_AQ001-B	84,545	84,371
IG_BH02_AQ002-B	07.11.2019	35	187,235		186,923	186,911	186,912					IG_BH02_AQ002-B	187,235	186,911
IG_BH02_AQ003-B	07.11.2019	35	161,917		161,445	161,363	161,365					IG_BH02_AQ003-B	161,917	161,363
IG_BH02_AQ004-B	07.11.2019	77	126,180		125,960	125,947	125,942	125,934	125,936			IG_BH02_AQ004-B	126,180	125,934
					27.11.2019	**10.12.2019**	**07.01.2020**	**23.01.2020**						
IG_BH02_AQ005-A	19.11.2019	65	121,263		120,973	120,958	120,952	120,952				IG_BH02_AQ005-A	121,263	120,952
IG_BH02_AQ006-A	19.11.2019	65	126,122		125,839	125,827	125,818	125,819				IG_BH02_AQ006-A	126,122	125,818
IG_BH02_AQ007-A	19.11.2019	65	176,308		175,959	175,955	175,947	175,947				IG_BH02_AQ007-A	176,308	175,947
IG_BH02_AQ008-A	19.11.2019	65	116,821		116,617	116,603	116,597	116,595				IG_BH02_AQ008-A	116,821	116,595
IG_BH02_AQ009-A	19.11.2019	65	137,373		137,090	137,064	137,056	137,054				IG_BH02_AQ009-A	137,373	137,054
IG_BH02_AQ005-B	19.11.2019	65	136,255		135,838	135,824	135,817	135,818				IG_BH02_AQ005-B	136,255	135,817
IG_BH02_AQ006-B	19.11.2019	65	131,690		131,362	131,342	131,336	131,336				IG_BH02_AQ006-B	131,690	131,336
IG_BH02_AQ007-B	19.11.2019	65	170,674		170,337	170,330	170,323	170,323				IG_BH02_AQ007-B	170,674	170,323
IG_BH02_AQ008-B	19.11.2019	65	171,795		171,504	171,490	171,481	171,483				IG_BH02_AQ008-B	171,795	171,481
IG_BH02_AQ009-B	19.11.2019	65	166,304		165,982	165,981	165,972	165,973				IG_BH02_AQ009-B	166,304	165,972
					18.12.2019	**07.01.2020**	**23.01.2020**	**04.02.2020**						
IG_BH02_AQ010-A	11.12.2019	55	137,383		137,166	137,155	137,153					IG_BH02_AQ010-A	137,383	137,153
IG_BH02_AQ011-A	11.12.2019	55	146,036		145,806	145,790	145,790					IG_BH02_AQ011-A	146,036	145,79
IG_BH02_AQ012-A	11.12.2019	55	112,007		111,805	111,792	111,793					IG_BH02_AQ012-A	112,007	111,792
IG_BH02_AQ010-B	11.12.2019	55	132,786		132,586	132,569	132,567					IG_BH02_AQ010-B	132,786	132,567
IG_BH02_AQ011-B	11.12.2019	55	155,510		155,259	155,244	155,239	155,239				IG_BH02_AQ011-B	155,510	155,239
IG_BH02_AQ012-B	11.12.2019	55	125,184		124,950	124,940	124,934	124,936				IG_BH02_AQ012-B	125,184	124,934

Table A-2: Determination of gravimetric water content; sample weights, drying times and calculated water contents of rim core pieces of samples used for out-diffusion and isotope diffusive exchange experiments

Sample	Set-up date	Drying times	m (ini)	14.11.2019	28.11.2019	12.12.2019	07.01.2020	21.01.2020		Sample	m wet	m dry
			g	g	g	g	g	g			g	g
IG_BH02_PW001-A	07.11.2019	75	151.766	151.503	151.424	151.488	151.481	151.481		IG_BH02_PW001-A	151.766	151.424
IG_BH02_PW001-B	07.11.2019	35	183.550	183.176	183.147	183.146				IG_BH02_PW001-B	183.550	183.146
IG_BH02_PW003-A	07.11.2019	75	154.123	153.889	153.877	153.869	153.862	153.860		IG_BH02_PW003-A	154.123	153.86
IG_BH02_PW003-B	07.11.2019	75	283.256	282.793	282.771	282.757	282.745	282.743		IG_BH02_PW003-B	283.256	282.743
IG_BH02_PW005-A	07.11.2019	35	228.249	227.748	227.689	227.691				IG_BH02_PW005-A	228.249	227.689
IG_BH02_PW005-B	07.11.2019	75	306.670	305.975	305.809	305.798	305.744	305.746		IG_BH02_PW005-B	306.670	305.744
IG_BH02_PW006-A	07.11.2019	75	181.845	181.454	181.431	181.424	181.408	181.410		IG_BH02_PW006-A	181.845	181.408
IG_BH02_PW006-B	07.11.2019	35	170.046	169.779	169.764	169.763				IG_BH02_PW006-B	170.046	169.763
IG_BH02_PW007-A	07.11.2019	75	143.169	142.886	142.879	142.874	152.868	142.866		IG_BH02_PW007-A	143.169	142.866
IG_BH02_PW007-B	07.11.2019	35	218.097	217.38	217.356	217.358				IG_BH02_PW007-B	218.097	217.356
				27.11.2019	**10.12.2019**	**07.01.2020**	**21.01.2020**	**04.02.2020**				
IG_BH02_PW008-A	19.11.2019	63	176.447	175.89	175.883	175.876	175.875			IG_BH02_PW008-A	176.447	175.875
IG_BH02_PW008-B	19.11.2019	63	150.358	150.04	150.036	150.031	150.029			IG_BH02_PW008-B	150.358	150.029
IG_BH02_PW010-A	19.11.2019	63	167.347	167.025	167.016	167.011	167.009			IG_BH02_PW010-A	167.347	167.009
IG_BH02_PW010-B	19.11.2019	63	323.688	322.963	322.951	322.939	322.939			IG_BH02_PW010-B	323.688	322.939
IG_BH02_PW012-A	19.11.2019	63	229.802	229.374	229.338	229.328	229.327			IG_BH02_PW012-A	229.802	229.327
IG_BH02_PW012-B	19.11.2019	63	198.822	198.434	198.426	198.414	198.413			IG_BH02_PW012-B	198.822	198.413
IG_BH02_PW014-A	19.11.2019	77	203.275	202.835	202.824	202.815	202.804	202.804		IG_BH02_PW014-A	203.275	202.804
IG_BH02_PW014-B	19.11.2019	63	249.561	249.091	249.078	249.068	249.066			IG_BH02_PW014-B	249.561	249.066
IG_BH02_PW016-A	19.11.2019	63	244.387	243.931	243.929	243.919	243.918			IG_BH02_PW016-A	244.387	243.918
IG_BH02_PW016-B	19.11.2019	63	190.497	190.120	190.117	190.111	190.109			IG_BH02_PW016-B	190.497	190.109
				18.12.2019	**07.01.2020**	**21.01.2020**	**04.02.2020**					
IG_BH02_PW018-A	11.12.2019	41	242.715	242.31	242.296	242.295				IG_BH02_PW018-A	242.715	242.295
IG_BH02_PW018-B	11.12.2019	41	173.952	173.682	173.668	173.667				IG_BH02_PW018-B	173.952	173.667
IG_BH02_PW020-A	11.12.2019	41	182.918	182.648	182.631	182.629				IG_BH02_PW020-A	182.918	182.629
IG_BH02_PW020-B	11.12.2019	41	158.711	158.479	158.455	158.453				IG_BH02_PW020-B	158.711	158.453
IG_BH02_PW022-A	11.12.2019	55	162.355	162.029	162.013	162.007	162.005			IG_BH02_PW022-A	162.355	162.005
IG_BH02_PW022-B	11.12.2019	55	282.622	282.077	282.039	282.034	282.036			IG_BH02_PW022-B	282.622	282.034

Table A-3: Determination of gravimetric water content; sample weights, drying times and calculated water contents of core pieces used for isotope diffusive exchange experiments

Sample	Date start drying	Drying time	m (cryst.dish)	m (cryst+ rock	17.01.2020	04.02.2020	14.02.2020	21.02.2020	28.02.2020	06.03.2020		Mass dry	m rock wet	m rock dry
			g	g	g	g	g	g	g	g		g	g	g
IG_BH02_PW001 LAB	10.01.2020	56	89,130	423,461	422,976	422,985	422,984	422,974	422,953	422,955		422,953	334,331	333,823
IG_BH02_PW001 ICE	10.01.2020	56	87,606	422,245	421,735	421,747	421,740	421,742	421,729	421,731		421,729	334,639	334,123
IG_BH02_PW003 LAB	10.01.2020	49	88,640	458,582	458,158	458,158	458,153	458,141	458,14			458,140	369,942	369,500
IG_BH02_PW003 ICE	10.01.2020	49	92,810	465,322	464,928	464,934	464,928	464,918	464,916			464,916	372,512	372,106
IG_BH02_PW005 LAB	10.01.2020	49	91,205	366,375	366,022	366,030	366,019	366,013	366,011			366,011	275,170	274,806
IG_BH02_PW005 ICE	10.01.2020	49	89,553	364,945	364,590	364,596	364,589	364,582	364,581			364,581	275,392	275,028
IG_BH02_PW006 LAB	10.01.2020	56	88,405	391,908	391,460	391,470	391,463	391,458	391,431	361,433		361,433	303,503	273,028
IG_BH02_PW006 ICE	10.01.2020	49	90,690	398,219	397,776	397,786	397,780	397,775	397,775			397,775	307,529	307,085
IG_BH02_PW007 LAB	10.01.2020	56	83,825	481,803	481,213	481,226	481,211	481,197	481,192	481,193		481,192	397,978	397,367
IG_BH02_PW007 ICE	10.01.2020	56	90,925	487,247	486,63	486,642	486,632	786,635	486,615	486,616		486,615	396,322	395,690
Sample	**Date start drying**		**m (cryst.dish)**	**m (cryst+ rock**	**19.02.2020**	**04.03.2020**	**18.03.2020**	**31.03.2020**	**14.04.2020**					
IG_BH02_PW008 LAB	07.02.2020	40	89,941	473,723	473,103	473,095	473,094					473,094	383,782	383,153
IG_BH02_PW008 ICE	07.02.2020	53	88,829	465,593	464,936	464,932	464,918	464,920				464,918	376,764	376,089
IG_BH02_PW010 LAB	07.02.2020	53	81,094	470,602	470,042	470,035	470,025	470,023				470,023	389,508	388,929
IG_BH02_PW010 ICE	07.02.2020	40	92,224	478,061	477,484	477,477	477,475					477,475	385,837	385,251
IG_BH02_PW012 LAB	07.02.2020	53	90,816	501,131	500,604	500,594	500,585	500,583				500,583	410,315	409,767
IG_BH02_PW012 ICE	07.02.2020	67	81,812	512,356	511,738	511,727	511,716	511,708	511,710			511,708	430,544	429,896
IG_BH02_PW014 LAB	07.02.2020	67	90,404	470,967	470,428	470,418	470,413	470,405	470,408			470,405	380,563	380,001
IG_BH02_PW014 ICE	07.02.2020	40	89,050	470,766	470,238	470,226	470,224					470,224	381,716	381,174
IG_BH02_PW016 LAB	07.02.2020	67	91,363	459,932	459,218	459,212	459,203	459,194	459,200			459,194	368,569	367,831
IG_BH02_PW016 ICE	07.02.2020	53	86,482	450,872	450,168	450,157	450,148	450,148				450,148	364,390	363,666
Sample	**Date start drying**		**m (cryst.dish)**	**m (cryst+ rock**	**18.02.2020**	**03.03.2020**	**17.03.2020**	**31.03.2020**	**14.04.2020**					
IG_BH02_PW018 LAB	08.02.2020	52	87,836	462,720	462,124	462,119	462,105	462,107				462,105	374,884	374,269
IG_BH02_PW018 ICE	08.02.2020	52	89,354	443,603	443,034	443,028	443,024	443,026				443,024	354,249	353,670
IG_BH02_PW020 LAB	08.02.2020	66	81,566	482,703	482,027	482,015	482,005	482,000	482,000			482,000	401,137	400,434
IG_BH02_PW020 ICE	08.02.2020	52	91,292	479,485	478,807	478,803	478,784	478,782				478,782	388,193	387,490
IG_BH02_PW022 LAB	08.02.2020	66	91,403	474,528	473,773	473,759	473,748	473,741	473,743			473,741	383,125	382,338
IG_BH02_PW022 ICE	08.02.2020	52	93,666	455,181	454,493	454,475	454,461	454,463				454,461	361,515	360,795

Table A-4: Determination of gravimetric water content; sample weights, drying times and calculated water contents of core pieces used for out-diffusion experiments

			before experiment (b.e.)		after experiment (a.e.)																	
Sample	Date start drying	Drying time	m (core,wet surf.)	m (core, dry surf.)	m (core,wet surf.)	m (core, 2min)	m (core,dry surf)	08.04.2020	21.04.2020	06.05.2020	14.05.2020	20.05.2020	26.05.2020	28.05.2020	03.06.2020	10.06.2020	17.06.2020	24.06.2020	08.07.2020	22.07.2020	05.08.2020	18.08.2020
			g	g	g	g	g	g	g	g	g	g	g	g	g	g	g	g	g	g	g	g
IG_BH02_PW001	25.03.2020	84	1477,481	1477,468	1477,710	1477,490	1477,466	1474,551	1474,551	1474,544		1474,538			1474,553		1474,578					
IG_BH02_PW003	25.03.2020	56	1473,680	1473,575	1474,065	1473,832	1473,680	1471,319	1471,314	1471,297		1471,299										
IG_BH02_PW005	25.03.2020	70	1450,162	1450,139	1450,226	1450,084	1450,077	1448,749	1448,662	1448,598		1448,589			1448,591							
IG_BH02_PW006	25.03.2020	56	1428,804	1428,741	1428,862	1428,678	1428,665	1426,354	1426,313	1426,288		1426,289										
IG_BH02_PW007	25.03.2020	84	1437,354	1437,323	1437,540	1437,382	1437,312	1434,856	1434,855	1434,838		1434,834			1434,851		1434,880					
IG_BH02_PW008	25.03.2020	84	1407,866	1407,760	1408,085	1407,869	1407,724	1404,746	1404,731	1404,717		1404,712			1404,724		1404,747					
IG_BH02_PW010	25.03.2020	84	1460,517	1460,395	1460,936	1460,722	1460,505	1457,378	1457,375	1457,370		1457,364			1457,386		1457,403					
IG_BH02_PW012	25.03.2020	56	1411,965	1411,850	1412,185	1411,964	1411,845	1409,142	1409,131	1409,108		1409,106										
IG_BH02_PW014	25.03.2020	56	1450,576	1450,400	1450,560	1450,366	1450,344	1447,949	1447,942	1447,923		1447,922										
IG_BH02_PW016	25.03.2020	56	1462,464	1462,393	1462,586	1462,393	1462,355	1459,514	1459,520	1459,489		1459,491										
IG_BH02_PW018	30.04.2020	55	1450,299	1450,160	1450,710	1450,556	1450,430				1447,773			1447,747		1447,750		1447,752				
IG_BH02_PW020	30.04.2020	55	1448,958	1448,892	1449,391	1448,169	1449,060				1446,500			1446,471		1446,464		1446,466				
IG_BH02_PW022	12.05.2020	98	1441,788	1441,711	1442,235	1441,930	1441,810						1439,010					1438,988	1438,981	1438,973	1438,968	1438,970

				WC wet weight		WC dry weight	
m (dry)	m(PW) b.e.	m(PW) a.e.	Δm(PW) a.e.-b.e.	WC dry surf b.e.	WC dry surf a.e.	WC dry surf b.e.	WC dry surf a.e.
g	g	g	g	wt.%	wt.%	wt.%	wt.%
1474,538	2,930	2,928	-0,002	0,20	0,20	0,20	0,20
1471,297	2,278	2,383	0,105	0,15	0,16	0,15	0,16
1448,589	1,550	1,488	-0,062	0,11	0,10	0,11	0,10
1426,288	2,453	2,377	-0,076	0,17	0,17	0,17	0,17
1434,834	2,489	2,478	-0,011	0,17	0,17	0,17	0,17
1404,712	3,048	3,012	-0,036	0,22	0,21	0,22	0,21
1457,364	3,031	3,141	0,110	0,21	0,22	0,21	0,22
1409,106	2,744	2,739	-0,005	0,19	0,19	0,19	0,19
1447,922	2,478	2,422	-0,056	0,17	0,17	0,17	0,17
1459,489	2,904	2,866	-0,038	0,20	0,20	0,20	0,20
1447,747	2,413	2,683	0,270	0,17	0,18	0,17	0,19
1446,464	2,428	2,596	0,168	0,17	0,18	0,17	0,18
1438,968	2,743	2,842	0,099	0,20	0,20	0,20	0,20

APPENDIX II-2

Determination of Bulk Wet and Dry Density: Raw Data

Table A-5: Determination of bulk wet and dry density; sample dimensions, weights and density results

Sample	m (core) wet	diameter core	height core	Volume core	bulk, wet density	error, wet density
	g	cm	cm	ccm	g/ccm	g/ccm
IG_BH02_AQ001	353,067	6,12	4,57	134,43	2,63	0,08
IG_BH02_AQ002	371,920	6,12	4,79	140,91	2,64	0,08
IG_BH02_AQ003	451,944	6,1	5,81	169,80	2,66	0,11
IG_BH02_AQ004	332,641	6,09	4,3	125,25	2,66	0,09
IG_BH02_AQ005	433,851	6,03	5,73	163,64	2,65	0,08
IG_BH02_AQ006	326,352	6,09	4,32	125,84	2,59	0,11
IG_BH02_AQ007	316,847	6,04	4,16	119,19	2,66	0,13
IG_BH02_AQ008	321,120	6,09	4,18	121,76	2,64	0,09
IG_BH02_AQ009	390,985	6,08	5,09	147,78	2,65	0,08
IG_BH02_AQ010	350,569	6,09	4,58	133,41	2,63	0,07
IG_BH02_AQ011	371,220	6,10	4,79	139,99	2,65	0,08
IG_BH02_AQ012	386,760	6,09	5,05	147,10	2,63	0,06

Sample	m (core a.e.) wet	m (core) dry	diameter core	height core	Volume core	bulk, wet density	error, wet density	bulk, dry density	error, dry density
	g	g	cm	cm	ccm	g/ccm	g/ccm	g/ccm	g/ccm
IG_BH02_PW001	1477,466	1474,538	6,12	18,97	558,03	2,65	0,02	2,64	0,02
IG_BH02_PW003	1473,680	1471,297	6,13	18,85	556,32	2,65	0,02	2,64	0,02
IG_BH02_PW005	1450,077	1448,589	6,11	18,35	538,03	2,70	0,01	2,69	0,01
IG_BH02_PW006	1428,665	1426,288	6,12	18,55	545,68	2,62	0,02	2,61	0,02
IG_BH02_PW007	1437,312	1434,834	6,11	18,57	544,48	2,64	0,02	2,64	0,02
IG_BH02_PW008	1407,724	1404,712	6,05	18,67	536,72	2,62	0,02	2,62	0,02
IG_BH02_PW010	1460,505	1457,364	6,06	19,35	558,11	2,62	0,02	2,61	0,02
IG_BH02_PW012	1411,845	1409,106	6,08	18,55	538,57	2,62	0,02	2,62	0,02
IG_BH02_PW014	1450,344	1447,922	6,11	18,75	549,76	2,64	0,02	2,63	0,02
IG_BH02_PW016	1462,355	1459,489	6,11	18,9	554,16	2,64	0,02	2,63	0,02
IG_BH02_PW018	1450,430	1447,747	6,12	18,75	551,56	2,63	0,02	2,62	0,02
IG_BH02_PW020	1449,060	1446,464	6,11	18,71	548,59	2,64	0,02	2,64	0,02
IG_BH02_PW022	1441,810	1438,968	6,08	18,63	540,89	2,67	0,02	2,66	0,02

APPENDIX II-3

Aqueous Extraction Experiments: Raw Data

Table A-6: Experimental data of aqueous extraction experiments (depths are in mbgs (down hole))

Sample	Depth	m (bottle)	m (bottle + rock)	m (rock)	m (H2O)	water:rock
	m a.b.	g	g	g	g	
IG_BH02_AQ001	240,2	18,722	112,292	93,570	77,458	0,83
IG_BH02_AQ002	348,5	17,984	106,073	88,089	78,904	0,90
IG_BH02_AQ003	379,6	18,028	112,292	94,264	79,295	0,84
IG_BH02_AQ004	382,0	18,698	115,735	97,037	68,972	0,71
IG_BH02_AQ005	455,5	18,007	105,279	87,272	75,469	0,86
IG_BH02_AQ006	530,8	17,952	105,286	87,334	77,413	0,89
IG_BH02_AQ007	555,1	17,963	96,838	78,875	80,431	1,02
IG_BH02_AQ008	611,4	17,963	101,865	83,902	85,139	1,01
IG_BH02_AQ009	666,1	18,684	104,793	86,109	81,673	0,95
IG_BH02_AQ010	771,4	18,225	121,376	103,151	61,287	0,59
IG_BH02_AQ011	879,0	18,336	115,061	96,725	66,224	0,68
IG_BH02_AQ012	984,5	18,127	115,859	97,732	71,972	0,74

APPENDIX II-4

Isotope Diffusive Exchange Experiments: Raw Data

Table A-7: Experimental data of isotope diffusive exchange experiments

Sample		Date Experiment Start	Date Experiment End	Standard	Weight container	Weight container and rock	Cryst. dish	Cryst Dish + H2O	Total weight container	Weight rock	Weight test solution	Total weight container after experiment	Weight test solution after experiment	Weight container and rock after experiment	Weight test solution after experiment	Weight rock after experiment	mass (PW)	mass TW+PW after exp.	Δ total weight before & after	Δ weight rock before & after	Δ weight test solution before & after	Δ weight rock and test solution	Δ weight rock and test solution - Δ total weight before and after	Δ weight rock and test solution	Δ water loss (total weight)	remaining water fraction
					g	g	g	g	g	g	g	g	g	g	g	g	g	g	g	g	g	g	g	% of TW	% of TW+PW	
IG_BH02_PW001	LAB	07.11.2019	08.01.2020	IG01-LAB	525,813	860,370	14,434	16,221	876,588	334,557	1,787	876,539	16,221	860,327	1,787	334,514	0,508	2,295	-0,049	-0,043	0,000	-0,043	0,006	2,4	2,1	0,98
IG_BH02_PW003	LAB	07.11.2019	08.01.2020	Lab Nr.	526,064	896,272	13,581	15,397	911,652	370,208	1,816	911,605	15,440	896,179	1,859	370,115	0,442	2,301	-0,047	-0,093	0,043	-0,050	-0,003	2,8	2,0	0,98
IG_BH02_PW005	LAB	07.11.2019	08.01.2020	0.3 n NaCl	522,243	797,464	14,268	16,105	813,563	275,221	1,837	813,513	16,004	797,516	1,736	275,273	0,364	2,100	-0,050	0,052	-0,101	-0,049	0,001	2,7	2,4	0,98
IG_BH02_PW006	LAB	07.11.2019	08.01.2020		525,283	828,867	12,322	14,155	843,018	303,584	1,833	842,978	14,090	828,892	1,768	303,609	30,475	32,243	-0,040	0,025	-0,065	-0,040	0,000	2,2	0,1	1,00
IG_BH02_PW007	LAB	07.11.2019	08.01.2020		523,010	921,101	14,119	15,948	937,042	398,091	1,829	936,997	15,885	921,114	1,766	398,104	0,611	2,377	-0,045	0,013	-0,063	-0,050	-0,005	2,7	1,9	0,98
IG_BH02_PW008	LAB	19.11.2019	16.01.2020		524,132	908,414	14,913	16,728	925,120	384,282	1,815	925,099	16,672	908,424	1,759	384,292	0,629	2,388	-0,021	0,010	-0,056	-0,046	-0,025	2,5	0,9	0,99
IG_BH02_PW010	LAB	19.11.2019	16.01.2020		524,670	914,831	13,565	15,484	930,301	390,161	1,919	930,271	15,486	914,783	1,921	390,113	0,579	2,500	-0,030	-0,048	0,002	-0,046	-0,016	2,4	1,2	0,99
IG_BH02_PW012	LAB	19.11.2019	16.01.2020		522,934	950,628	12,966	14,783	965,404	427,694	1,817	965,382	14,780	950,597	1,814	427,663	0,548	2,362	-0,022	-0,031	-0,003	-0,034	-0,012	1,9	0,9	0,99
IG_BH02_PW014	LAB	19.11.2019	16.01.2020		525,781	909,022	14,483	16,297	925,313	383,241	1,814	925,286	16,214	909,065	1,731	383,284	0,562	2,293	-0,027	0,043	-0,083	-0,040	-0,013	2,2	1,2	0,99
IG_BH02_PW016	LAB	19.11.2019	16.01.2020		524,874	894,005	13,856	15,682	909,675	369,131	1,826	909,660	15,499	894,156	1,643	369,282	0,738	2,381	-0,015	0,151	-0,183	-0,032	-0,017	1,8	0,6	0,99
IG_BH02_PW018	LAB	11.12.2019	08.02.2020		521,650	900,701	14,822	16,640	917,336	379,051	1,818	917,313	16,540	900,770	1,718	379,120	0,615	2,333	-0,023	0,069	-0,100	-0,031	-0,008	1,7	1,0	0,99
IG_BH02_PW020	LAB	11.12.2019	08.02.2020		524,038	932,359	14,293	16,101	948,445	408,321	1,808	948,419	15,931	932,481	1,638	408,443	0,703	2,341	-0,026	0,122	-0,170	-0,048	-0,022	2,7	1,1	0,99
IG_BH02_PW022	LAB	11.12.2019	08.02.2020		523,717	906,891	13,274	15,098	921,983	383,174	1,824	921,955	14,913	907,046	1,639	383,329	0,787	2,426	-0,028	0,155	-0,185	-0,030	-0,002	1,6	1,2	0,99
IG_BH02_PW001	ICE	07.11.2019	08.01.2020	IG01-ICE	527,010	861,876	15,063	16,878	878,742	334,866	1,815	878,700	16,887	861,816	1,824	334,806	0,516	2,340	-0,042	-0,060	0,009	-0,051	-0,009	2,8	1,8	0,98
IG_BH02_PW003	ICE	07.11.2019	08.01.2020	Lab Nr.	522,414	895,194	15,003	16,829	912,018	372,780	1,826	911,970	16,895	895,084	1,892	372,670	0,406	2,298	-0,048	-0,110	0,066	-0,044	0,004	2,4	2,1	0,98
IG_BH02_PW005	ICE	07.11.2019	08.01.2020	0.3 n NaCl	526,991	802,394	14,831	16,644	819,014	275,403	1,813	818,980	16,533	802,454	1,702	275,463	0,364	2,066	-0,034	0,060	-0,111	-0,051	-0,017	2,8	1,6	0,98
IG_BH02_PW006	ICE	07.11.2019	08.01.2020		524,093	831,706	14,788	16,605	848,313	307,613	1,817	848,264	16,541	831,726	1,753	307,633	0,444	2,197	-0,049	0,020	-0,064	-0,044	0,005	2,4	2,2	0,98
IG_BH02_PW007	ICE	07.11.2019	08.01.2020		523,258	919,703	15,733	17,540	937,233	396,445	1,807	937,188	17,488	919,706	1,755	396,448	0,632	2,387	-0,045	0,003	-0,052	-0,049	-0,004	2,7	1,9	0,98
IG_BH02_PW008	ICE	19.11.2019	16.01.2020		525,908	911,040	13,571	15,392	926,424	385,132	1,821	926,406	15,336	911,068	1,765	385,160	0,675	2,440	-0,018	0,028	-0,056	-0,028	-0,010	1,5	0,7	0,99
IG_BH02_PW010	ICE	19.11.2019	16.01.2020		525,742	912,261	13,234	15,055	927,299	386,519	1,821	927,278	15,109	912,166	1,875	386,424	0,586	2,461	-0,021	-0,095	0,054	-0,041	-0,020	2,3	0,9	0,99
IG_BH02_PW012	ICE	19.11.2019	16.01.2020		524,030	955,955	15,272	17,089	973,036	431,925	1,817	973,010	17,060	955,950	1,788	431,920	0,648	2,436	-0,026	-0,005	-0,029	-0,034	-0,008	1,9	1,1	0,99
IG_BH02_PW014	ICE	19.11.2019	16.01.2020		523,318	905,662	13,799	15,686	921,332	382,344	1,887	921,302	15,613	905,687	1,814	382,369	0,542	2,356	-0,030	0,025	-0,073	-0,048	-0,018	2,5	1,3	0,99
IG_BH02_PW016	ICE	19.11.2019	16.01.2020		523,472	898,290	13,888	15,812	914,083	374,818	1,924	914,067	15,613	898,450	1,725	374,978	0,724	2,449	-0,016	0,160	-0,199	-0,039	-0,023	2,0	0,7	0,99
IG_BH02_PW018	ICE	11.12.2019	08.02.2020		525,314	901,239	14,274	16,099	917,332	375,925	1,825	917,306	15,997	901,309	1,723	375,995	0,579	2,302	-0,026	0,07	-0,102	-0,032	-0,006	1,8	1,1	0,99
IG_BH02_PW020	ICE	11.12.2019	08.02.2020		523,523	934,907	14,805	16,611	951,514	411,384	1,806	951,485	16,417	935,065	1,612	411,542	0,703	2,315	-0,029	0,158	-0,194	-0,036	-0,007	2,0	1,3	0,99
IG_BH02_PW022	ICE	11.12.2019	08.02.2020		521,332	908,222	14,744	16,509	924,718	386,89	1,765	924,693	16,319	908,374	1,575	387,042	0,72	2,295	-0,025	0,152	-0,19	-0,038	-0,013	2,2	1,1	0,99

Table A-8: Analytical raw data of isotope diffusive exchange experiments

		Initial $\delta^{18}O$ TW	Initial $\delta^{2}H$ TW	Final $\delta^{18}O$ TW	Final $\delta^{2}H$ TW
		‰ VSMOW	‰ VSMOW	‰ VSMOW	‰ VSMOW
IG_BH02_PW001	LAB	-10,15	-72,6	-10,33	-75,4
IG_BH02_PW003	LAB	-10,15	-72,6	-9,96	-73,4
IG_BH02_PW005	LAB	-10,15	-72,6	-10,10	-73,0
IG_BH02_PW006	LAB	-10,15	-72,6	-10,22	-73,4
IG_BH02_PW007	LAB	-10,15	-72,6	-10,37	-74,6
IG_BH02_PW008	LAB	-10,29	-73,3	-10,20	-74,3
IG_BH02_PW010	LAB	-10,29	-73,3	-10,17	-73,6
IG_BH02_PW012	LAB	-10,29	-73,3	-9,89	-72,2
IG_BH02_PW014	LAB	-10,29	-73,3	-9,87	-72,1
IG_BH02_PW016	LAB	-10,29	-73,3	-10,08	-71,6
IG_BH02_PW018	LAB	-10,30	-73,3	-9,66	-71,1
IG_BH02_PW020	LAB	-10,30	-73,3	-9,55	-70,1
IG_BH02_PW022	LAB	-10,30	-73,3	-9,60	-70,4
IG_BH02_PW001	ICE	-31,68	-246,1	-26,32	-203,6
IG_BH02_PW003	ICE	-31,68	-246,1	-25,70	-200,1
IG_BH02_PW005	ICE	-31,68	-246,1	-27,32	-210,8
IG_BH02_PW006	ICE	-31,68	-246,1	-26,75	-206,8
IG_BH02_PW007	ICE	-31,68	-246,1	-25,58	-197,3
IG_BH02_PW008	ICE	-31,62	-245,1	-25,26	-196,5
IG_BH02_PW010	ICE	-31,62	-245,1	-24,71	-192,1
IG_BH02_PW012	ICE	-31,62	-245,1	-24,93	-194,1
IG_BH02_PW014	ICE	-31,62	-245,1	-25,53	-199,0
IG_BH02_PW016	ICE	-31,62	-245,1	-25,44	-196,6
IG_BH02_PW018	ICE	-31,77	-245,2	-25,45	-197,4
IG_BH02_PW020	ICE	-31,77	-245,2	-25,37	-195,9
IG_BH02_PW022	ICE	-31,77	-245,2	-24,89	-192,5

APPENDIX II-5

Out-diffusion Experiments: Raw Data

Table A-9: Experimental data of out-diffusion experiments (depths are in mbgs (down hole))

Sample		IG_BH02_PW001	IG_BH02_PW003	IG_BH02_PW005	IG_BH02_PW006	IG_BH02_PW007	IG_BH02_PW008	IG_BH02_PW010	IG_BH02_PW012	IG_BH02_PW014	IG_BH02_PW016	IG_BH02_PW018	IG_BH02_PW020	IG_BH02_PW022
Depth	m	240,0	348,0	378,1	381,7	383,0	455,2	502,8	555,7	611,2	665,8	770,6	878,8	984,2
start experiment		07.11.2019	07.11.2019	07.11.2019	07.11.2019	07.11.2019	07.11.2019	19.11.2019	19.11.2019	19.11.2019	19.11.2019	11.12.2019	11.12.2019	11.12.2019
Initial Rock Mass (as received, +/- mountain wet)	g	1477,481	1473,680	1450,162	1428,804	1437,354	1407,866	1460,517	1411,965	1450,576	1462,464	1450,299	1448,958	1441,788
Initial Rock Mass (start experiment)	g	1477,468	1473,575	1450,139	1428,741	1437,323	1407,760	1460,395	1411,850	1450,400	1462,393	1450,160	1448,892	1441,711
Final Rock Mass (resaturated)	g	1477,466	1473,680	1450,077	1428,665	1437,312	1407,724	1460,505	1411,845	1450,344	1462,355	1450,430	1449,060	1441,810
Uptake of water	g	-0,02	0,00	-0,09	-0,14	-0,04	-0,14	-0,01	-0,12	-0,23	-0,11	0,13	0,10	0,02
Saturation	%	100,001	100,000	100,006	100,010	100,003	100,010	100,001	100,008	100,016	100,007	99,991	99,993	99,998
Core Diametre	cm	6,12	6,13	6,11	6,12	6,11	6,05	6,06	6,08	6,11	6,11	6,12	6,11	6,08
Core Length	cm	18,97	18,85	18,35	18,55	18,57	18,67	19,35	18,55	18,75	18,9	18,75	18,71	18,63
Volume of Rock Sample	cm3	558,03	556,32	538,03	545,68	544,48	536,72	558,11	538,57	549,76	554,16	551,56	548,59	540,89
Wet Density (calculated from volume & mass)	g/cm3	2,65	2,65	2,70	2,62	2,64	2,62	2,62	2,62	2,64	2,64	2,63	2,64	2,67
Mass of Rock (calculated from volume and density)		1477,48	1473,68	1450,16	1428,80	1437,35	1407,87	1460,52	1411,97	1450,58	1462,46	1450,30	1448,96	1441,79
Masses before experiment														
Mass cylinder	g	362,763	361,739	362,663	362,420	362,294	231,176	380,466	359,636	379,806	382,108	376,194	359,939	381,959
Mass cylinder + core	g	1840,235	1835,303	1812,824	1791,173	1799,665	1766,932	1840,574	1771,427	1830,252	1844,294	1826,337	1808,844	1823,666
Mass cylinder + core + H2O	g	1965,212	1958,972	1936,431	1914,159	1925,784	1902,132	1975,433	1913,369	1955,518	1972,211	1951,852	1939,086	1953,919
Mass tot start	g	1965,197	1958,959	1936,405	1914,132	1925,751	1902,095	1975,424	1913,357	1955,400	1972,115	1951,816	1939,066	1953,91
Initial Water Mass	ml	124,977	123,669	123,607	122,986	126,119	135,200	134,859	141,942	125,266	127,917	125,515	130,242	130,253
Ratio Exp.Water : Rock		0,085	0,084	0,085	0,086	0,088	0,096	0,092	0,101	0,086	0,087			
End Experiment		25.03.2020	25.03.2020	25.03.2020	25.03.2020	25.03.2020	25.03.2020	25.03.2020	25.03.2020	25.03.2020	25.03.2020	30.04.2020	30.04.2020	12.05.2020
Final Water Mass (measured, not all recoverable)	ml	115,49	112,46	113,37	112,91	116,17	125,14	124,85	127,66	115,01	118,18	114,78	116,54	120,07
Time Experiment	days	139	139	139	139	139	139	127	127	127	127	141	141	153
Volume of samples for Cl-measurements														
sample A	ml	0,5	0,8	0,5	0,5	0,5	0,5	0,5	0,5	0,5	0,5	0,5	0,5	0,5
sample B	ml	0,5	0,5	0,5	0,5	0,5	0,5	0,5	0,5	0,5	0,5	0,7	0,5	0,5
sample C	ml	0,5	0,5	0,5	0,5	0,5	0,5	0,5	0,5	0,5	0,5	0,5	0,5	0,5
sample D	ml	0,5	0,5	0,5	0,5	0,5	0,5	0,5	0,5	0,5	0,5	0,5	0,5	0,5
sample E	ml	0,5	0,5	0,5	0,5	0,5	0,5	0,5	0,5	0,5	0,5	0,5	0,5	0,5
sample F	ml	0,5	0,5	0,5	0,5	0,5	0,5	0,5	0,5	0,5	0,5	0,5	0,5	0,5
sample G	ml	0,5	0,5	0,5	0,5	0,5	0,5	0,5	0,5	0,5	0,5	0,5	0,5	0,5
sample H	ml	0,5	0,5	0,5	0,5	0,5	0,5	0,5	0,5	0,5	0,7	0,5	0,5	0,5
sample I	ml	0,5	0,5	0,5	0,5	0,5	0,5	0,5	0,5	0,7	0,5	0,5	0,5	0,5
sample K	ml	0,5	0,5	0,5	0,5	0,5	0,5	0,5	0,6	0,7	0,5	0,5	0,5	0,5
sample L	ml	0,5	0,5	0,5	0,5	0,5	0,5	0,5	0,5	0,5	0,5	0,5	0,5	0,5
sample M	ml	0,5	0,5	0,5	0,5	0,5	0,5	0,5	0,5	0,5	0,5	0,5	0,5	0,5
sample N	ml											0,5	0,5	0,5
sample O	ml													
sample P	ml													
sample Q	ml													
sample R	ml													
sample S	ml													
total volume subsamples		6,0	6,3	6,0	6,0	6,0	6,0	6,0	6,1	6,4	6,2	6,7	6,5	6,5
Mass of cylinder wet + core	g	1842,165	1838,374	n.m.	1794,377	1802,704	1770,205	1843,706	1775,152	1833,291	1846,892	1829,192	1812,178	1826,651
m (H2O) in cyl		1,93	3,07		3,20	3,04	3,27	3,13	3,73	3,04	2,60	2,86	3,33	2,99
Final Mass of Experiment-Solution (calculated)	g	118,98	117,37	117,61	116,99	120,12	129,20	128,86	135,84	118,87	121,72	118,82	123,74	123,75
Final Mass of Experiment-Solution (measured)	g	117,42	115,53	113,37	116,12	119,21	128,41	127,98	131,38	118,05	120,78	117,63	119,87	123,05
Difference in water mass	Dif (ml)	1,56	1,84	4,24	0,87	0,91	0,79	0,88	4,46	0,82	0,94	1,18	3,87	0,70
Water loss in % of ini water mass	Dif (%)	1,3	1,6	3,6	0,7	0,8	0,6	0,7	3,3	0,7	0,8	1,0	3,1	0,6

Table A-10: Chemical composition of time series samples taken during out-diffusion experiments

Sample			IG_BH02_PW001											IG_BH02_PW003										
Sub-samples	Time	Date	Na	K	Ca	Mg	Sr	F	Cl	SO4	NO3	Br	Br/Cl	Na	K	Ca	Mg	Sr	F	Cl	SO4	NO3	Br	Br/Cl
	days		mg/l	mg/l	mg/l	mg/l	mg/l	mg/l	mg/l	mg/l	mg/l	mg/l		mg/l	mg/l	mg/l	mg/l	mg/l	mg/l	mg/l	mg/l	mg/l	mg/l	
Preparation		07.11.2019																						
A	1	08.11.2019	6,3	1,67	5,5	<0,2	<1	<1	0,98	0,39	0,26	0,32	327	6,9	1,5	5,5	<0,2	<1	<1	4,5	0,51	0,41	0,47	104
B	3	10.11.2019	8,7	1,75	5,6	<0,2	<1	<1	1,2	0,41	0,2	0,36	300	10,6	1,7	5,9	<0,2	<1	<1	7,9	0,68	0,36	0,82	104
C	6	13.11.2019	11,7	1,86	5,8	<0,2	<1	<1	1,5	0,5	0,22	0,43	287	14,2	2,1	6,1	<0,1	<1	<1	10,6	1,04	0,36	1,2	113
D	11	18.11.2019	13,8	1,95	6,3	<0,2	<1	<1	1,74	0,55	0,17	0,58	333	17	2,2	6,4	<0,2	<1	<1	11,6	1,2	<0,2	1,4	121
E	14	21.11.2019	14,8	2	6,8	<0,2	<1	<1	1,9	0,66	0,2	0,68	358	18,1	2,2	6,9	<0,2	<1	<1	12,1	1,5	<0,2	1,5	124
F	21	28.11.2019	16,7	2	7,3	0,26	<1	<1	2,1	0,85	<0,2	0,74	352	20,2	2,2	8,3	<0,2	<1	<1	12,3	2	<0,2	1,5	122
G	29	06.12.2019	18,9	2	7,5	<0,2	<1	<1	2,2	0,94	<0,2	0,75	341	22,3	2,2	10	<0,2	<1	<1	12,3	2,2	<0,2	1,5	122
H	46	23.12.2019	22,8	2	7,6	<0,2	<1	<1	2,2	1,6	<0,2	0,75	341	26,1	2,2	11,7	<0,2	<1	<1	12,3	2,8	<0,2	1,5	122
I	62	08.01.2020	26,2	2	7,8	<0,2	<1	<1	2,2	2,1	<0,2	0,75	341	29,2	2,3	12	<0,2	<1	1,9	12,3	3,7	0,22	1,5	122
K	74	20.01.2020	26,5	2	7,9	0,26	<1	1,5	2,2	2,4	<0,2	0,75	341	29,6	2,3	12,3	<0,2	<1	2,2	12,3	3,9	<0,2	1,5	122
L	92	07.02.2020	26,6	2	8	<0,2	<1	1,8	2,2	2,7	<0,2	0,75	341	29,8	2,3	12,4	0,37	<1	2,5	12,3	4,4	<0,2	1,5	122
M	120	06.03.2020	26,7	2	8,1	<0,2	<1	2	2,2	3,4	<0,2	0,75	341	29,9	2,3	12,5	<0,2	<1	2,6	12,3	5,1	<0,2	1,5	122
Final	139	25.03.2020	26,8	2	8,2	<0,2	0,05	2	2,2	4	<0,2	0,75	341	30	2,3	12,6	<0,2	0,19	2,6	12,3	5,8	<0,2	1,5	122
Sample			IG_BH02_PW005											IG_BH02_PW006										
Sub-samples	Time	Date	Na	K	Ca	Mg	Sr	F	Cl	SO4	NO3	Br	Br/Cl	Na	K	Ca	Mg	Sr	F	Cl	SO4	NO3	Br	Br/Cl
	days		mg/l	mg/l	mg/l	mg/l	mg/l	mg/l	mg/l	mg/l	mg/l	mg/l		mg/l	mg/l	mg/l	mg/l	mg/l	mg/l	mg/l	mg/l	mg/l	mg/l	
Preparation		07.11.2019																						
A	1	08.11.2019	6,8	2,6	11,3	0,18	<1	<1	16,8	0,38	0,44	0,29	17	5,2	2,2	11	0,25	<1	<1	13,2	0,4	0,28	0,24	18
B	3	10.11.2019	9,6	3	13,1	0,18	<1	<1	22,3	0,52	0,42	0,37	17	7,1	2,5	12,2	0,26	<1	<1	16,9	0,55	0,33	0,35	21
C	6	13.11.2019	12,6	4,1	14,6	0,13	<1	<1	29	0,69	0,34	0,43	15	9,5	2,9	13,7	<0,2	<1	<1	22,6	0,65	0,33	0,42	19
D	11	18.11.2019	15,5	5,2	18,1	0,15	<1	<1	34,1	0,91	<0,2	0,57	17	11,8	4	17,1	0,2	<1	<1	26,6	0,85	0,35	0,49	18
E	14	21.11.2019	16,4	5,6	20,9	0,32	<1	<1	36,8	1	<0,2	0,64	17	12,4	4,1	20,3	0,56	<1	<1	29	1,1	<0,2	0,51	18
F	21	28.11.2019	18,8	6	25	0,61	<1	<1	38,5	1,2	<0,2	0,69	18	13,8	4,4	23,4	0,69	<1	<1	30,4	1,3	<0,2	0,54	18
G	29	06.12.2019	21,7	6,2	26,5	0,42	<1	<1	40,1	1,7	<0,2	0,72	18	15,7	4,8	26	0,7	<1	<1	31,2	1,5	<0,2	0,56	18
H	46	23.12.2019	25	6,2	30,7	0,69	<1	<1	40,1	2,4	<0,2	0,77	19	18,9	5,4	29,2	0,89	<1	<1	31,2	2,3	<0,2	0,59	19
I	62	08.01.2020	27,4	6,2	32,3	0,7	<1	<1	40,1	3,3	<0,2	0,77	19	21,1	5,8	32,6	1,2	<1	<1	31,2	3,4	<0,2	0,59	19
K	74	20.01.2020	28,7	6,2	33,3	0,64	<1	<1	40,1	3,8	<0,2	0,77	19	22,5	6	33,7	1,1	<1	<1	31,2	3,9	<0,2	0,59	19
L	92	07.02.2020	30,5	6,2	34,5	0,81	<1	<1	40,1	4,3	<0,2	0,77	19	24,2	6	35,7	1,4	<1	<1	31,2	4,7	<0,2	0,59	19
M	120	06.03.2020	31,6	6,2	34,7	0,76	<1	<1	40,1	5,3	<0,2	0,77	19	25,5	6	35,9	1,4	<1	<1	31,2	6,3	<0,2	0,59	19
Final	139	25.03.2020	32,7	6,2	34,9	0,8	0,75	1	40,1	6,2	<0,2	0,77	19	27	6	36	1,5	0,77	0,92	31,2	7,4	<0,2	0,59	19
Sample			IG_BH02_PW007																					
Sub-samples	Time	Date	Na	K	Ca	Mg	Sr	F	Cl	SO4	NO3	Br	Br/Cl											
	days		mg/l	mg/l	mg/l	mg/l	mg/l	mg/l	mg/l	mg/l	mg/l	mg/l												
Preparation		07.11.2019																						
A	1	08.11.2019	5,2	2,5	15,1	<0,1	<1	<1	11,2	2,2	0,57	0,14	13											
B	3	10.11.2019	6,9	2,7	15,8	<0,1	<1	<1	15,4	2,4	0,5	0,26	17											
C	6	13.11.2019	9,1	3	16,1	<0,1	<1	<1	21,3	2,7	0,49	0,36	17											
D	11	18.11.2019	11,2	3	16,4	<0,1	<1	<1	25,8	2,9	0,54	0,43	17											
E	14	21.11.2019	11,5	3	16,9	0,1	<1	<1	28,8	3,1	0,58	0,47	16											
F	21	28.11.2019	12,8	3	17,5	0,11	<1	<1	30,4	3,3	0,61	0,5	16											
G	29	06.12.2019	14,4	3	17,8	0,1	<1	<1	30,9	3,4	0,57	0,54	17											
H	46	23.12.2019	16,5	3	18,1	0,2	<1	<1	30,9	3,9	0,6	0,59	19											
I	62	08.01.2020	18	3	18,7	0,24	<1	<1	30,9	4,3	0,51	0,59	19											
K	74	20.01.2020	19,4	3	19,8	0,23	<1	<1	30,9	4,6	<0,2	0,59	19											
L	92	07.02.2020	20,3	3	21,2	0,41	<1	1	30,9	4,9	0,92	0,59	19											
M	120	06.03.2020	21,6	3	22,4	0,55	<1	1,2	30,9	5,5	<0,2	0,59	19											
Final	139	25.03.2020	22	3	22,8	0,61	0,42	1,4	30,9	5,9	0,3	0,59	19											

Table A-10: continued

Sample			IG_BH02_PW008											IG_BH02_PW010										
Sub-samples	Time	Date	Na	K	Ca	Mg	Sr	F	Cl	SO4	NO3	Br	Br/Cl	Na	K	Ca	Mg	Sr	F	Cl	SO4	NO3	Br	Br/Cl
	days		mg/l	mg/l	mg/l	mg/l	mg/l	mg/l	mg/l	mg/l	mg/l	mg/l		mg/l	mg/l	mg/l	mg/l	mg/l	mg/l	mg/l	mg/l	mg/l	mg/l	
Preparation		19.11.2019																						
A	1	20.11.2019	9,1	2,9	12,5	<0,2	<1	<1	22,1	0,41	<0,2	0,44	20	10,4	3,6	15,6	<0,2	<1	<1	31,5	0,49	<0,2	0,65	21
B	3	22.11.2019	13,8	2,95	16,9	<0,2	<1	<1	34,4	0,46	0,21	0,65	19	15,5	3,7	20,8	<0,2	<1	<1	47,5	0,65	<0,2	0,9	19
C	8	27.11.2019	18,3	3,15	18,5	<0,2	<1	<1	45,3	0,57	<0,2	0,8	18	21	4	23,7	<0,2	<1	<1	64,3	0,99	<0,2	1,3	20
D	13	02.12.2019	20	3,3	19,3	<0,2	<1	<1	50,2	0,75	<0,2	0,92	18	22,9	4,3	25,6	<0,2	<1	<1	71,5	1,1	<0,2	1,4	20
E	16	05.12.2019	21,7	3,7	20,1	<0,2	<1	<1	52,4	0,86	<0,2	1	19	24,6	4,6	27	<0,2	<1	<1	73,5	1,2	<0,2	1,4	19
F	21	10.12.2019	23,5	4	23,5	<0,2	<1	<1	54,5	0,99	<0,2	1,05	19	26,1	4,7	29,4	<0,2	<1	<1	74,2	1,4	<0,2	1,4	19
G	29	18.12.2019	25,2	4	25,2	0,24	<1	<1	55,8	1,3	<0,2	1,1	20	27,8	4,7	31,9	<0,2	<1	<1	74,5	1,7	<0,2	1,4	19
H	42	31.12.2019	27,2	4	26,1	<0,2	<1	<1	56,4	1,6	<0,2	1,2	21	29,6	4,7	33,1	<0,2	<1	<1	74,5	2,1	<0,2	1,4	19
I	62	20.01.2020	29,3	4	26,8	0,25	<1	1,3	56,4	2,1	<0,2	1,2	21	31,7	4,7	34,9	0,25	<1	1,4	74,5	2,6	<0,2	1,4	19
K	76	03.02.2020	30,2	4	27,3	0,33	<1	1,4	56,4	2,3	<0,2	1,2	21	31,7	4,7	35,7	0,33	<1	1,6	74,5	2,8	<0,2	1,4	19
L	91	18.02.2020	30,9	4	27,5	0,37	<1	1,6	56,4	2,6	<0,2	1,2	21	32	4,7	36	0,33	<1	1,9	74,5	3	<0,2	1,4	19
M	120	18.03.2020	31,3	4	27,6	0,36	<1	1,8	56,4	3,1	<0,2	1,2	21	32,6	4,7	36,1	0,36	<1	2	74,5	3,6	<0,2	1,4	19
Final	127	25.03.2020	31,5	4	27,7	0,4	0,44	1,9	56,4	3,3	<0,2	1,2	21	32,8	4,7	36,2	0,38	0,6	2,1	74,5	3,8	<0,2	1,4	19
Sample			IG_BH02_PW012											IG_BH02_PW014										
Sub-samples	Time	Date	Na	K	Ca	Mg	Sr	F	Cl	SO4	NO3	Br	Br/Cl	Na	K	Ca	Mg	Sr	F	Cl	SO4	NO3	Br	Br/Cl
	days		mg/l	mg/l	mg/l	mg/l	mg/l	mg/l	mg/l	mg/l	mg/l	mg/l		mg/l	mg/l	mg/l	mg/l	mg/l	mg/l	mg/l	mg/l	mg/l	mg/l	
Preparation		19.11.2019																						
A	1	20.11.2019	10,6	3,3	14,5	<0,2	<1	<1	29,4	0,44	<0,2	0,57	19	7,8	3,5	17,1	<0,2	<1	<1	31,2	0,64	<0,2	0,55	18
B	3	22.11.2019	15,6	3,4	17,2	<0,2	<1	<1	44,8	0,6	<0,2	0,8	18	11,1	3,7	23,2	<0,2	<1	<1	44,9	0,92	<0,2	0,78	17
C	8	27.11.2019	21	3,5	22,4	<0,2	<1	<1	59,6	0,76	<0,2	1	17	16,4	3,8	27,8	0,25	<1	<1	65,1	1,5	0,26	1,1	17
D	13	02.12.2019	22,6	3,7	23,3	<0,2	<1	<1	67,2	0,93	<0,2	1,1	16	17,9	4	29,7	<0,2	<1	<1	72	1,6	<0,2	1,3	18
E	16	05.12.2019	24,1	3,8	24,8	<0,2	<1	<1	68,4	1	<0,2	1,2	18	19,1	4,2	32,7	<0,2	<1	<1	75,5	1,7	<0,2	1,4	19
F	21	10.12.2019	25,6	4,5	26,5	<0,2	<1	<1	70,4	1,15	<0,2	1,25	18	20,6	4,4	34,5	<0,2	<1	<1	78,9	1,8	<0,2	1,4	18
G	29	18.12.2019	27,2	4,6	32,1	<0,2	<1	<1	71,4	1,4	<0,2	1,3	18	22,8	4,4	35,4	<0,2	<1	<1	79,9	2,3	<0,2	1,4	18
H	42	31.12.2019	29	4,6	33	<0,2	<1	<1	72	2	<0,2	1,3	18	24,1	4,4	36,4	<0,2	<1	<1	80,9	3,1	<0,2	1,4	17
I	62	20.01.2020	30,5	4,6	35,3	0,22	<1	1,1	72	3,7	<0,2	1,3	18	25,9	4,4	37,1	<0,2	<1	<1	80,9	3,7	<0,2	1,4	17
K	76	03.02.2020	31,2	4,6	37,6	0,3	<1	1,2	72	4,2	<0,2	1,3	18	27,3	4,4	37,4	0,23	<1	<1	80,9	4	<0,2	1,4	17
L	91	18.02.2020	32,1	4,6	38	0,33	<1	1,5	72	5	<0,2	1,3	18	28,1	4,4	37,7	0,22	<1	1	80,9	4,6	<0,2	1,4	17
M	120	18.03.2020	32,6	4,6	38,2	0,31	<1	1,6	72	6,6	<0,2	1,3	18	29,2	4,4	37,8	0,21	<1	1,1	80,9	5,3	<0,2	1,4	17
Final	127	25.03.2020	32,7	4,6	38,4	0,33	0,64	1,7	72	6,9	<0,2	1,3	18	29,6	4,4	37,9	0,21	0,79	1,2	80,9	5,6	<0,2	1,4	17
Sample			IG_BH02_PW016																					
Sub-samples	Time	Date	Na	K	Ca	Mg	Sr	F	Cl	SO4	NO3	Br	Br/Cl											
	days		mg/l	mg/l	mg/l	mg/l	mg/l	mg/l	mg/l	mg/l	mg/l	mg/l												
Preparation		19.11.2019																						
A	1	20.11.2019	9,6	4,4	33	0,24	<2	<1	65,4	0,89	0,2	1,25	19											
B	3	22.11.2019	14,7	4,8	46,5	0,16	<2	<1	102	1,3	<0,2	1,8	18											
C	8	27.11.2019	20,4	5	59,6	0,28	<2	<1	140	1,9	<0,2	2,5	18											
D	13	02.12.2019	22,4	5,8	65	0,2	<2	<1	153	2,2	<0,2	2,7	18											
E	16	05.12.2019	26,4	6,2	74,5	0,18	<2	<1	159	2,4	0,22	2,8	18											
F	21	10.12.2019	29,2	7,4	84,5	0,4	<2	<1	167	3,1	<0,2	3	18											
G	29	18.12.2019	31,9	7,5	87,8	0,22	<2	<1	181	3,3	<0,2	3,3	18											
H	42	31.12.2019	34,7	7,6	91	0,34	<2	<1	194	3,8	<0,2	3,4	18											
I	62	20.01.2020	36,7	7,7	93,2	0,31	<2	<1	194	4,2	<0,2	3,4	18											
K	76	03.02.2020	37,3	7,7	94,2	0,39	<2	1	194	4,6	0,22	3,4	18											
L	91	18.02.2020	39,4	7,7	95,8	0,42	<2	1,1	194	5,2	0,26	3,4	18											
M	120	18.03.2020	40,2	7,7	95,9	0,4	<2	1,3	194	5,8	<0,2	3,4	18											
Final	127	25.03.2020	40,4	7,7	96	0,41	1,6	1,4	194	6,1	0,21	3,4	18											

Table A-10: continued

Sample			IG_BH02_PW0018											IG_BH02_PW020										
Sub-samples	Time	Date	Na	K	Ca	Mg	Sr	F	Cl	SO4	NO3	Br	Br/Cl	Na	K	Ca	Mg	Sr	F	Cl	SO4	NO3	Br	Br/Cl
	days		mg/l	mg/l	mg/l	mg/l	mg/l	mg/l	mg/l	mg/l	mg/l	mg/l		mg/l	mg/l	mg/l	mg/l	mg/l	mg/l	mg/l	mg/l	mg/l	mg/l	
Preparation		11.12.2019																						
A	1	12.12.2019	8,1	3,3	25,4	<0,2	<1	<1	62,1	0,66	<0,2	1,7	27	8,5	3,8	42,3	<0,1	<2	<1	95,7	0,94	<0,2	1,9	20
B	2	13.12.2019	10,4	4,1	32,5	<0,2	<1	<1	80,9	0,72	<0,2	2,2	27	11,3	4,7	57,7	<0,1	<2	<1	133	1,1	<0,2	2,8	21
C	4	15.12.2019	13,6	4,9	46	0,2	<1	<1	101	1	0,34	2,8	28	15,2	5,8	81,8	0,12	<2	<1	176	1,4	0,25	3,5	20
D	8	19.12.2019	16,6	5,2	54	<0,2	<1	<1	127	1,4	0,21	3,4	27	18,2	6,3	103	0,16	<2	<1	220	1,8	<0,2	4,3	20
E	12	23.12.2019	17,9	5,3	60,9	<0,2	<1	<1	143	1,6	<0,2	3,8	27	20,9	6,6	118	0,25	<2	<1	250	2,6	<0,2	4,9	20
F	16	27.12.2019	19,4	5,4	65,7	<0,2	<1	<1	151	1,8	<0,2	4	26	22,2	6,8	124	0,29	<2	<1	265	3	<0,2	5,2	20
G	20	31.12.2019	20,4	5,4	68,8	<0,2	<1	<1	155	2,2	<0,2	4,1	26	22,7	7	127	0,19	<2	<1	274	3,5	<0,2	5,3	19
H	28	08.01.2020	21,1	5,4	71,5	0,27	<1	<1	157	2,5	0,22	4,1	26	23,7	7,1	134	0,21	<2	<1	279	4	0,75	5,4	19
I	44	24.01.2020	22,1	5,4	72	0,25	<1	<1	157	3,1	<0,2	4,1	26	24,8	7,1	137	0,31	<2	<1	279	4,7	<0,2	5,4	19
K	62	11.02.2020	22,6	5,4	73,8	0,26	<1	<1	157	3,5	<0,2	4,1	26	25,6	7,1	141	0,38	<2	<1	279	5,2	0,31	5,4	19
L	75	24.02.2020	22,7	5,4	74,2	0,24	<1	1	157	4	<0,2	4,1	26	25,7	7,1	142	0,35	<2	<1	279	6	<0,2	5,4	19
M	92	12.03.2020	22,8	5,4	75,6	0,26	<1	1,2	157	4,6	<0,2	4,1	26	25,8	7,1	143	0,36	<2	<1	279	6,4	<0,2	5,4	19
N	120	09.04.2020	23	5,4	77,7	0,37	<1	1,3	157	5,1	<0,2	4,1	26	25,9	7,1	144	0,29	<2	<1	279	6,6	<0,2	5,4	19
Final	141	30.04.2020	23,3	5,4	79,5	0,31	1	1,3	157	5,5	<0,2	4,1	26	25,9	7,1	144	0,37	1,5	0,85	279	7,3	<0,2	5,4	19
Sample			IG_BH02_PW022																					
Sub-samples	Time	Date	Na	K	Ca	Mg	Sr	F	Cl	SO4	NO3	Br	Br/Cl											
	days		mg/l	mg/l	mg/l	mg/l	mg/l	mg/l	mg/l	mg/l	mg/l	mg/l												
Preparation		11.12.2019																						
A	1	12.12.2019	10,7	4,8	46,5	<0,2	<2	<1	111	1,7	<0,2	2,8	25											
B	2	13.12.2019	13,9	6,1	62,1	<0,2	<2	<1	149	2	<0,2	3,8	26											
C	4	15.12.2019	20,9	7,1	88,2	<0,2	<2	<1	177	2,8	<0,2	4,7	27											
D	8	19.12.2019	22,2	7,4	107	<0,2	<2	<1	217	3,9	<0,2	5,6	26											
E	12	23.12.2019	23,6	7,4	114	<0,2	<2	<1	243	4,9	<0,2	6,2	26											
F	16	27.12.2019	24,7	7,4	119	<0,2	<2	<1	260	5,6	<0,2	6,5	25											
G	20	31.12.2019	25	7,4	124	<0,2	<2	<1	262	5,9	<0,2	6,6	25											
H	28	08.01.2020	26,2	7,4	129	<0,2	<2	<1	262	6,7	<0,2	6,6	25											
I	44	24.01.2020	26,9	7,4	132	<0,2	<2	<1	262	7,6	<0,2	6,6	25											
K	62	11.02.2020	27,8	7,4	134	0,21	<2	<1	262	8,2	0,39	6,6	25											
L	75	24.02.2020	28	7,4	135	<0,2	<2	<1	262	8,9	<0,2	6,6	25											
M	92	12.03.2020	28,1	7,4	136	<0,2	<2	<1	262	9,6	<0,2	6,6	25											
N	120	09.04.2020	28,2	7,4	137	<0,2	<2	<1	262	10,4	<0,2	6,6	25											
Final	152	11.05.2020	28,5	7,4	139	0,24	0,96	0,86	262	11,6	<0,2	6,6	25											

APPENDIX III

Error Calculations

APPENDIX III-1

Gravimetric Water Content

The water content is calculated according to $WC_{grav} = \frac{m_{pw}}{m_{core,wet}}$

Where WC_{grav} = gravimetric water content, m_{pw} = mass of pore water, $m_{core,wet}$ = mass of the wet core sample

Error calculation after Gaussian error propagation

$$\sigma(WC_{grav}) = \sqrt{\left(dWC_{grav}dm_{PW} \times \sigma(m_{PW})\right)^2 + \left(dWC_{grav}dm_{core,wet} \times \sigma(m_{core,wet})\right)^2}$$

Analytical errors (error of measurement)

$s(m_{pw})$ = difference between $m_{core,dry\ surface}$ before and after drying + 0.05 g (=variations at end of drying); The constant of 0.05 g is the empirically derived uncertainty associated to the drying process of the surface, i.e. loss of water from the core surface.

$s(m_{core,wet})$ = difference between $m_{core,dry\ surface}$ before and after experiment

Both uncertainties include the mass difference of the individual cores before and after the experiments (cf. Appendix II).

Derivations

$$dWC_{grav}dm_{pw} = \frac{100}{m_{core,wet}}$$

$$dWC_{grav}dm_{core,wet} = \frac{-100 \times m_{pw}}{(m_{core,wet})^2}$$

APPENDIX III-2

Water Loss Porosity

The water-loss (connected porosity), ϕ_{WL}, is calculated according to

$$\phi_{WL} = WC_{wet} \times \frac{\rho_{bulk,wet}}{\rho_{water}}$$

where WC_{wet} is the water content based on the wet weight of the rock sample and $\rho_{bulk,wet}$ the bulk wet density of the rock. The density of water, ρ_{water}, is assumed to be 1 g/cm^3.

The conversion of the formula leads to

$$\phi_{WL} = \frac{m_{pw} \times 100}{r^2 \times h \times \pi \times \rho_{water}}$$

where r = radius of the core pieces, h = height of the core.

Error calculation after Gaussian error propagation

$$\sigma(\phi_{WL}) = \sqrt{\left(d\phi_{WL}dm_{PW} \times \sigma(m_{PW})\right)^2 + \left(d\phi_{WL}dr \times \sigma(r)\right)^2 + \left(d\phi_{WL}dh \times \sigma(h)\right)^2 + \left(d\phi_{WL}d\rho_{water} \times \sigma(\rho_{water})\right)^2}$$

Analytical errors (error of measurement)

s(m_{pw}) = difference between $m_{core,dry\ surface}$ before and after drying + 0.05 g (=variations at end of drying)

s(r) = 0.02 cm

s(h) = 0.2 cm

s(r_{water}) = 0.03 g/cm^3

Derivations

$$d\phi dm_{pw} = \frac{100}{r^2 \times h \times \pi \times \rho_{water}}$$

$$d\phi dr = \frac{-m_{pw} \times 100 \times 2r \times h \times \pi \times \rho_{water}}{(r^2 \times h \times \pi \times \rho_{water})^2}$$

$$d\phi dh = \frac{-m_{pw} \times 100 \times r^2 \times \pi \times \rho_{water}}{(r^2 \times h \times \pi \times \rho_{water})^2}$$

$$d\phi dh = \frac{-m_{pw} \times 100 \times r^2 \times \pi \times h}{(r^2 \times h \times \pi \times \rho_{water})^2}$$

APPENDIX III-3

Porewater Cl- and Br Concentration

Calculations

$$C_{PW} = \frac{(m_{PW} + m_{TWi} - \sum^{n} m_s) \times C_{TW\infty} - (m_{TWi} \times C_{TWi}) + \sum^{n} m_s \times C_s}{m_{PW}}$$

where C_{pw} = porewater concentration; m_{pw} = mass of porewater; m_{TWi} = initial mass of test water; C_{TWi} = initial Cl-concentration of test water; m_s = mass of sub sample used for time series; C_s = Cl concentration of sub sample used for time series.

Error calculation after Gaussian error propagation

$$\sigma(C_{PW}) = \sqrt{\begin{aligned}&\left(dC_{PW}dm_{PW} \times \sigma(m_{PW})\right)^2 + \left(dC_{PW}dm_{TWi} \times \sigma(m_{TWi})\right)^2 + \\ &+\left(dC_{PW}dC_{TW\infty} \times \sigma(C_{TW\infty})\right)^2 + \left(dC_{PW}dC_{TWi} \times \sigma(C_{TWi})\right)^2 + \\ &(\sigma(\sum m_S))^2 + (\sigma(\sum m_S \times c_S))^2\end{aligned}}$$

Analytical errors (error of measurement)

$\sigma(m_{PW})$ = difference between $m_{core,dry\ surface}$ before and after drying + 0.05 g (=variations at end of drying

$\sigma(m_{TWi})$ = difference between $m_{TWi} – m_S$-$m_{TW\infty}$-2ml (2 ml = remaining water in the cylinder

$\sigma(C_{TWi})$ = 5% (Cl) and 10 % (Br) of the analysed concentration

$\sigma(C_{TW\infty})$ = 5% (Cl) and 10 % (Br) of the analysed concentration

$\sigma(m_S)$ = 0.05 ml

$\sigma(C_S)$ = 5% (Cl) and 10 % (Br) of the analysed concentration

Derivations

$$dC_{PW}dm_{PW} = \frac{C_{TW\infty} * m_{PW} - \left[C_{TW\infty} * (m_{PW} + m_{TWi}) - C_{TW} * m_{TWi}\right]}{m_{PW}^{\ 2}}$$

$$dC_{PW}dm_{TWi} = \frac{(C_{TW\infty} - C_{TWi}) * m_{PW}}{m_{PW}^{\ 2}}$$

$$dC_{PW}dC_{TW\infty} = \frac{(m_{PW} - m_{TWi}) * m_{PW}}{m_{PW}^{\ 2}}$$

$$dC_{PW}dC_{TWi} = \frac{-m_{TWi} * m_{PW}}{m_{PW}^{\ 2}}$$

$$\sigma\left(\sum(m_s)\right) = \left(Nr_S \times \sigma(m_S)\right)$$

$$\sigma\left(\sum(m_S \times C_S)\right) = \left(Nr_S \times C_{S,ave} \times \sigma(m_S)\right) + \left(Nr_S \times m_S \times \sigma(C_S)\right)$$

APPENDIX III-4

Br*1000/Cl Mass Ratio of Porewater

Br*1000/Cl porewater mass ratio = R

Error calculation after Gaussian error propagation

$$\sigma(R) = \sqrt{\left(dRdC_{Br} \times \sigma(C_{Br})\right)^2 + \left(dRdC_{Cl} \times \sigma(C_{Cl})\right)^2}$$

Analytical errors (error of measurement)

$\sigma(C_{Cl})$ = Error of porewater Cl concentration calculated according to AIII-3

$\sigma(C_{Br})$ = Error of porewater Br concentration calculated according to AIII-3

Derivations

$$dRdC_{Br} = \frac{1000}{C_{Cl}}$$

$$dRdC_{Cl} = \frac{-1000 \times C_{Br}}{C_{Cl}^2}$$

APPENDIX III-5

Calculation of Isotopic Signatures of Matrix Porewater

Calculation

$$C_{PW} = \frac{C_{TW\infty(Std1)} \times m_{TW(Std2)} \times m_{Rock(Std1)} \times (C_{TW\infty(Std2)} - C_{TW^0(Std2)}) - C_{TW\infty(Std2)} \times m_{TW(Std1)} \times m_{Rock(Std2)} \times (C_{TW\infty(Std1)} - C_{TW^0(Std1)})}{m_{TW(Std2)} \times m_{Rock(Std1)} \times (C_{TW\infty(Std2)} - C_{TW^0(Std2)}) - m_{TW(Std1)} \times m_{Rock(Std2)} \times (C_{TW\infty(Std1)} - C_{TW^0(Std1)})}$$

m_{PW} = mass of porewater (g)

m_{TW} = mass of test water (g)

C_{TW} = isotopic signature of test water at the beginning of the experiment (‰)

$C_{TW\infty}$ = isotopic signature of test water after equilibration (‰)

Std 1 = Experiment 1 applying standard 1

Std 2 = Experiment 2 applying standard 2

Error calculation after Gaussian error propagation

$$\sigma(C_{PW}) = \sqrt{\begin{aligned}&\left(dC_{PW}dm_{TW(Std1)} \times \sigma(m_{TW(Std1)})\right)^2 + \left(dC_{PW}dm_{TW(Std2)} \times \sigma(m_{TW(Std2)})\right)^2 + \\ &+\left(dC_{PW}dC_{TW(Std1)} \times \sigma(C_{TW(Std1)})\right)^2 + \left(dC_{PW}dC_{TW(Std2)} \times \sigma(C_{TW(Std2)})\right)^2 + \\ &+\left(dC_{PW}dC_{TW\infty(Std1)} \times \sigma(C_{TW\infty(Std1)})\right)^2 + \left(dC_{PW}dC_{TW\infty(Std2)} \times \sigma(C_{TW\infty(Std2)})\right)^2\end{aligned}}$$

Analytical errors (error of measurement)

$\sigma(m_{TW(Std1)})$ = 0.002 g

$\sigma(m_{TW(Std2)})$ = 0.002 g

$\sigma(C_{TW(Std1)})$ = 0.1 ‰ for ^{18}O and 1.0‰ for ^{2}H

$\sigma(C_{TW(Std2)})$ = 0.1 ‰ for ^{18}O and 1.0‰ for ^{2}H

$\sigma(C_{TW\infty(Std1)})$ = 0.1 ‰ for ^{18}O and 1.0‰ for ^{2}H

$\sigma(C_{TW\infty(Std2)})$ = 0.1 ‰ for ^{18}O and 1.0‰ for ^{2}H

Derivations

$$dC_{PW}dm_{TW(Std1)} = \frac{\left(C_{TW(Std1)} - C_{TW\infty(Std1)}\right) \times C_{TW\infty(Std2)}}{\left(m_{TW(Std1)} \times \left(C_{TW(Std1)} - C_{TW\infty(Std1)}\right) - \left(C_{TW(Std2)} - C_{TW\infty(Std2)}\right) \times m_{TW(Std2)}\right)} -$$

$$- \frac{\left(\left(C_{TW(Std1)} - C_{TW\infty(Std1)}\right) \times C_{TW\infty(Std2)} \times m_{TW(Std1)} - \left(C_{TW(Std2)} - C_{TW\infty(Std2)}\right) \times C_{TW\infty(Std1)} \times m_{TW(Std2)}\right) \times \left(C_{TW(Std1)} - C_{TW\infty(Std1)}\right)}{\left(m_{TW(Std1)} \times \left(C_{TW(Std1)} - C_{TW\infty(Std1)}\right) - \left(C_{TW(Std2)} - C_{TW\infty(Std2)}\right) \times m_{TW(Std2)}\right)^2}$$

$$dC_{PW}dm_{TW(Std2)} = \frac{-\left(C_{TW(Std2)} - C_{TW\infty(Std2)}\right) \times C_{TW\infty(Std1)}}{\left(m_{TW(Std1)} \times \left(C_{TW(Std1)} - C_{TW\infty(Std1)}\right) - \left(C_{TW(Std2)} - C_{TW\infty(Std2)}\right) \times m_{TW(Std2)}\right)} +$$

$$+ \frac{\left(\left(C_{TW(Std1)} - C_{TW\infty(Std1)}\right) \times C_{TW\infty(Std2)} \times m_{TW(Std1)} - \left(C_{TW(Std2)} - C_{TW\infty(Std2)}\right) \times C_{TW\infty(Std1)} \times m_{TW(Std2)}\right) \times \left(C_{TW(Std2)} - C_{TW\infty(Std2)}\right)}{\left(m_{TW(Std1)} \times \left(C_{TW(Std1)} - C_{TW\infty(Std1)}\right) - \left(C_{TW(Std2)} - C_{TW\infty(Std2)}\right) \times m_{TW(Std2)}\right)^2}$$

$$dC_{PW}\,dC_{TW(Std1)} = \frac{C_{TW\infty(Std2)} \times m_{TW(Std1)}}{\left(m_{TW(Std1)} \times \left(C_{TW(Std1)} - C_{TW\infty(Std1)}\right) - \left(C_{TW(Std2)} - C_{TW\infty(Std2)}\right) \times m_{TW(Std2)}\right)} -$$
$$- \frac{\left(\left(C_{TW(Std1)} - C_{TW\infty(Std1)}\right) \times C_{TW\infty(Std2)} \times m_{TW(Std1)} - \left(C_{TW(Std2)} - C_{TW\infty(Std2)}\right) \times C_{TW\infty(Std1)} \times m_{TW(Std2)}\right) \times m_{TW(Std1)}}{\left(m_{TW(Std1)} \times \left(C_{TW(Std1)} - C_{TW\infty(Std1)}\right) - \left(C_{TW(Std2)} - C_{TW\infty(Std2)}\right) \times m_{TW(Std2)}\right)^2}$$

$$dC_{PW}\,dC_{TW(Std2)} = \frac{-C_{TW\infty(Std1)} \times m_{TW(Std2)}}{\left(m_{TW(Std1)} \times \left(C_{TW(Std1)} - C_{TW\infty(Std1)}\right) - \left(C_{TW(Std2)} - C_{TW\infty(Std2)}\right) \times m_{TW(Std2)}\right)} +$$
$$+ \frac{\left(\left(C_{TW(Std1)} - C_{TW\infty(Std1)}\right) \times C_{TW\infty(Std2)} \times m_{TW(Std1)} - \left(C_{TW(Std2)} - C_{TW\infty(Std2)}\right) \times C_{TW\infty(Std1)} \times m_{TW(Std2)}\right) \times m_{TW(Std2)}}{\left(m_{TW(Std1)} \times \left(C_{TW(Std1)} - C_{TW\infty(Std1)}\right) - \left(C_{TW(Std2)} - C_{TW\infty(Std2)}\right) \times m_{TW(Std2)}\right)^2}$$

$$dC_{PW}\,dC_{TW\infty(Std1)} = \frac{-\left(C_{TW\infty(Std2)} \times m_{TW(Std1)} + \left(C_{TW(Std2)} - C_{TW\infty(Std2)}\right) \times m_{TW(Std2)}\right)}{\left(m_{TW(Std1)} \times \left(C_{TW(Std1)} - C_{TW\infty(Std1)}\right) - \left(C_{TW(Std2)} - C_{TW\infty(Std2)}\right) \times m_{TW(Std2)}\right)} +$$
$$+ \frac{\left(\left(C_{TW(Std1)} - C_{TW\infty(Std1)}\right) \times C_{TW\infty(Std2)} \times m_{TW(Std1)} - \left(C_{TW(Std2)} - C_{TW\infty(Std2)}\right) \times C_{TW\infty(Std1)} \times m_{TW(Std2)}\right) \times m_{TW(Std1)}}{\left(m_{TW(Std1)} \times \left(C_{TW(Std1)} - C_{TW\infty(Std1)}\right) - \left(C_{TW(Std2)} - C_{TW\infty(Std2)}\right) \times m_{TW(Std2)}\right)^2}$$

$$dC_{PW}\,dC_{TW\infty(Std1)} = \frac{-\left(C_{TW\infty(Std2)} \times m_{TW(Std1)} + \left(C_{TW(Std2)} - C_{TW\infty(Std2)}\right) \times m_{TW(Std2)}\right)}{\left(m_{TW(Std1)} \times \left(C_{TW(Std1)} - C_{TW\infty(Std1)}\right) - \left(C_{TW(Std2)} - C_{TW\infty(Std2)}\right) \times m_{TW(Std2)}\right)} +$$
$$+ \frac{\left(\left(C_{TW(Std1)} - C_{TW\infty(Std1)}\right) \times C_{TW\infty(Std2)} \times m_{TW(Std1)} - \left(C_{TW(Std2)} - C_{TW\infty(Std2)}\right) \times C_{TW\infty(Std1)} \times m_{TW(Std2)}\right) \times m_{TW(Std1)}}{\left(m_{TW(Std1)} \times \left(C_{TW(Std1)} - C_{TW\infty(Std1)}\right) - \left(C_{TW(Std2)} - C_{TW\infty(Std2)}\right) \times m_{TW(Std2)}\right)^2}$$

$$dC_{PW}\,dC_{TW\infty(Std2)} = \frac{\left(m_{TW(Std1)} \times \left(C_{TW(Std1)} - C_{TW\infty(Std1)}\right) + C_{TW\infty(Std1)} \times m_{TW(Std2)}\right)}{\left(m_{TW(Std1)} \times \left(C_{TW(Std1)} - C_{TW\infty(Std1)}\right) - \left(C_{TW(Std2)} - C_{TW\infty(Std2)}\right) \times m_{TW(Std2)}\right)} -$$
$$- \frac{\left(\left(C_{TW(Std1)} - C_{TW\infty(Std1)}\right) \times C_{TW\infty(Std2)} \times m_{TW(Std1)} - \left(C_{TW(Std2)} - C_{TW\infty(Std2)}\right) \times C_{TW\infty(Std1)} \times m_{TW(Std2)}\right) \times m_{TW(Std2)}}{\left(m_{TW(Std1)} \times \left(C_{TW(Std1)} - C_{TW\infty(Std1)}\right) - \left(C_{TW(Std2)} - C_{TW\infty(Std2)}\right) \times m_{TW(Std2)}\right)^2}$$

APPENDIX III-6

Calculation of Mass of Porewater by Isotope Diffusive Exchange Technique

Calculation

$$WC_{IsoEx} = \left[\frac{m_{TW(Std\,2)} \times m_{Rock(Std1)} \times (C_{TW^0(Std\,2)} - C_{TW\infty(Std\,2)}) + m_{TW(Std1)} \times m_{Rock(Std\,2)} \times (C_{TW\infty(Std1)} - C_{TW^0(Std1)})}{m_{Rock(Std1)} \times m_{Rock(Std\,2)} \times (C_{TW\infty(Std\,2)} - C_{TW\infty(Std1)})} \right] \times 100$$

m_{PW} = mass of porewater (g)

m_{TW} = mass of test water (g)

C_{TW} = isotopic signature of test water at the beginning of the experiment (‰)

$C_{TW\infty}$ = isotopic signature of test water after equilibration (‰)

Std 1 = Experiment 1 applying standard 1

Std 2 = Experiment 2 applying standard 2

Error calculation after Gaussian error propagation

$$\sigma(m_{PW}) = \sqrt{\begin{aligned} &\left(dm_{PW}\,dm_{TW(Std1)} \times \sigma(m_{TW(Std1)})\right)^2 + \left(dm_{PW}\,dm_{TW(Std\,2)} \times \sigma(m_{TW(Std\,2)})\right)^2 + \\ &+\left(dm_{PW}\,dC_{TW(Std1)} \times \sigma(C_{TW(Std1)})\right)^2 + \left(dm_{PW}\,dC_{TW(Std\,2)} \times \sigma(C_{TW(Std\,2)})\right)^2 + \\ &+\left(dm_{PW}\,dC_{TW\infty(Std1)} \times \sigma(C_{TW\infty(Std1)})\right)^2 + \left(dm_{PW}\,dC_{TW\infty(Std\,2)} \times \sigma(C_{TW\infty(Std\,2)})\right)^2 \end{aligned}}$$

Analytical errors (error of measurement)

$\sigma(m_{TW(Std1)})$ = 0.002 g

$\sigma(m_{TW(Std2)})$ = 0.002 g

$\sigma(C_{TW(Std1)})$ = 0.1 ‰ for ^{18}O and 1.0‰ for ^{2}H

$\sigma(C_{TW(Std2)})$ = 0.1 ‰ for ^{18}O and 1.0‰ for ^{2}H

$\sigma(C_{TW\infty(Std1)})$ = 0.1 ‰ for ^{18}O and 1.0‰ for ^{2}H

$\sigma(C_{TW\infty(Std2)})$ = 0.1 ‰ for ^{18}O and 1.0‰ for ^{2}H

Derivations

$$dm_{PW}\,dm_{TW(Std1)} = \frac{\left(C_{TW(Std1)} - C_{TW\infty(Std1)}\right)}{\left(C_{TW\infty(Std1)} - C_{TW\infty(Std\,2)}\right)}$$

$$dm_{PW}\,dm_{TW(Std\,2)} = \frac{-\left(C_{TW(Std\,2)} - C_{TW\infty(Std\,2)}\right)}{\left(C_{TW\infty(Std1)} - C_{TW\infty(Std\,2)}\right)}$$

$$dm_{PW}\,dC_{TW(Std1)} = \frac{m_{TW(Std1)}}{\left(C_{TW\infty(Std1)} - C_{TW\infty(Std\,2)}\right)}$$

$$dm_{PW}\,dC_{TW(Std\,2)} = \frac{-m_{TW(Std\,2)}}{\left(C_{TW\infty(Std1)} - C_{TW\infty(Std\,2)}\right)}$$

$$dm_{PW}\,dC_{TW\infty(Std1)} = \left(\frac{-1}{\left(C_{TW\infty(Std1)} - C_{TW\infty(Std\,2)}\right)} - \frac{\left(C_{TW(Std1)} - C_{TW\infty(Std1)}\right)}{\left(C_{TW\infty(Std1)} - C_{TW\infty(Std\,2)}\right)^2}\right) \times m_{TW(Std1)} + \left(C_{TW(Std\,2)} - C_{TW\infty(Std\,2)}\right) \times m_{TW(Std\,2)}$$

$$dm_{PW}\,dC_{TW\infty(Std\,2)} = \left(\frac{\left(C_{TW(Std1)} - C_{TW\infty(Std1)}\right) \times m_{TW(Std1)}}{\left(C_{TW\infty(Std1)} - C_{TW\infty(Std\,2)}\right)^2} + \frac{1}{\left(C_{TW\infty(Std1)} - C_{TW\infty(Std\,2)}\right)^2} - \frac{\left(C_{TW(Std\,2)} - C_{TW\infty(Std\,2)}\right)}{\left(C_{TW\infty(Std1)} - C_{TW\infty(Std\,2)}\right)^2}\right) \times m_{TW(Std\,2)}$$





golder.com